Dissertation zur Erlangung des Doktorgrades

der Fakultät für Chemie und Pharmazie

der Ludwig-Maximilians Universität München

Dissection of the ATM-dependent antiviral response

following DNA damage

Dennis Nagl

aus

Neuburg a. d. Donau, Deutschland

2021

Erklärung

Diese Dissertation wurde im Sinne von § 7 der Promotionsordnung vom 28. November 2011 von Herrn Prof. Dr. Veit Hornung betreut.

Eidesstattliche Versicherung

Diese Dissertation wurde eigenständig und ohne unerlaubte Hilfe erarbeitet.

Dennis Nagl
_____

München, den 26.04.2021

Dissertation eingereicht am 29.04.2021

1. Gutachter: Prof. Dr. Veit Hornung

2. Gutachter: Prof. Dr. Julian Stingele

Mündliche Prüfung am 21.06.2021

Table of content

1 Introduction

1.1 The immune system

Our organism is confronted daily with a broad spectrum of different threats ranging from exogenous (e.g. pathogens) to endogenous origin (e.g. DNA damage). To maintain their physiological function, organisms have developed a complex set of defence mechanisms that include various signalling cascades, cell types, and even whole organs: the immune system. This system serves to protect against infections ranging from pathogenic bacteria and viruses to fungi, parasitic worms and protozoa [1–6]. In addition, the immune system functions to remove toxic substances and contain aberrant cell growth. This system can generally be divided into two lines of defence. The first line of defence is represented by the innate immune system. Being the evolutionary older one, some form of innate immunity can be found throughout all living organisms, including unicellular forms of life. On the other hand, the second line of defence, the adaptive immune system, can only be found in vertebrates. While the innate immune system acts as the rapid response to infections within minutes to hours in vertebrates, the adaptive immune system offers a more refined but slower response [7].

The innate immune system consists of three different defence levels: anatomical barriers, the innate phase, and the induced innate response. At points of entry, anatomical barriers like the skin or mucosa protect the organism from pathogens entering the system. When pathogens succeed in breaking through one of the host's anatomical barriers, the innate immune system begins acting with a set of non-specific soluble molecules present in the blood, epithelial secretions, and extracellular fluids. This set of soluble molecules attempts to weaken or eliminate the pathogens during the innate phase and includes the complement system, antimicrobial enzymes and antimicrobial peptides. In the last phase, the induced cell-based innate response comes into play after approximately four hours. This rapid cell-based response is mediated by various specialized cells like macrophages, neutrophils, dendritic cells and monocytes. The induced innate response relies on the recognition of a limited number of specific microbial moieties instead of the detection of specific pathogens. These evolutionary conserved moieties, which are often essential for the survival of the pathogens, enable the immune cells to recognize foreign bodies and to discriminate between self and non-self [8]. These pathogen-associated molecular patterns (PAMPs) are recognized by a limited amount of germline-encoded receptors, so-called pattern recognition receptors (PRRs) [9]. In addition to PAMPs, mislocated endogenous structures can be detected by PRRs during stress conditions and cell damage. Therefore, these structures are often referred to as damage-associated molecular patterns (DAMPs) and were first proposed by Polly Matzinger in 1994 [10]. The following pathogen-independent inflammatory response is often referred to as sterile inflammation and mediated by PRRs, or non-PRR DAMP receptors [11,12]. The recognition of PAMPs or DAMPs leads to pro-inflammatory chemokine and cytokine production by the innate immune cells, which recruit more phagocytic cells, induce fever and the production of acute-phase proteins. Moreover, this leads to an attraction of antigen-presenting cells (APC), inducing the adaptive immune response. Thus the innate immune system offers a fast albeit non-specific response to pathogens and tissue or cellular damage signals [7].

When the innate immune system is unable to contain the infection, the adaptive immune system is activated. Although it is slower, it can target specific pathogens with greater effectiveness. After infection and activation, the adaptive immune response needs several days to be fully functional. In contrast to the innate immune response, the adaptive immune system is not germline-encoded or inherited and evolves over an organism's entire lifespan. This enables the potent mechanism of immunological memory, preventing reinfections with the same pathogens through long-term protective immunity. The effector cells of the adaptive immune system consist of B- and T-lymphocytes being able to detect a diverse array of moieties, also termed antigens, through their receptors. These antigen-binding receptors are generated de novo by somatic DNA recombination in each lymphocyte individually (clonal distribution). This yields a repertoire of approximately 10^{15} different antigen receptors without selection for non-self-recognition [13]. To avoid self-recognition and identify potentially helpful B- and T-cell clones, these clones must undergo a strict and long selection process. This selection occurs during B- and T-cell development, where receptors are tested for functionality and autoreactivity. B-cells produce antigen-binding proteins, also called immunoglobulins. These immunoglobulins are either membrane-bound, known as B-cell receptors (BCR) or are secreted and soluble called antibodies. These antibodies are produced and secreted by terminally differentiated B-cells. The repertoire of antigen receptors can be increased in B-cells after maturation by somatic hypermutation. BCRs are essential for the maturation, proliferation, and long-term survival of B-cells, whereas the antibodies promote B-cells' primary effector function. The main function of antibodies is to bind and, in some cases, neutralise pathogens or related detectable antigens and promote the recruitment of cells and molecules for pathogen elimination. On T-cells, the membrane-bound T-cell receptor (TCR) represents the antigen receptor protein. In contrast to the BCR and antibodies, it recognizes presented protein fragments from the host cells instead of directly binding the antigen. These presenting structures are known as major histocompatibility complex (MHC) molecules. Therefore, the TCR is specific for the antigen and the highly polymorphic MHC molecules. The two major MHC molecules, MHC class I and MHC class II, are expressed on different cell types and vary in their structure and function. T lymphocytes can be distinguished by two co-receptors, CD4 and CD8, determining their ability to bind to one of these two MHC molecules. While CD8 T-cells detect antigens presented by MHC class I molecules, CD4 T-cells recognize antigens bound to MHC class II molecules. MHC class II molecules are expressed by APCs like dendritic cells and display fragments of endocytosed antigens. Dendritic cells are part of the innate immune system and, after activation, travel to lymphoid tissues to interact with naïve B- and T-lymphocytes. In contrast, MHC class I molecules are expressed by most healthy cells and present cytosolic components on their surface. Following TCR binding to an antigen incorporated by an MHC class I receptor, CD8 cytotoxic T-cells (T_c) are activated and lead to the induced cell death of the presenting cell. In contrast, CD4 T-cells function as T-helper (T_h) cells and detect antigens presented by MHC class II molecules on APCs. Here, different types of T_h-cells have been reported to enhance and sustain the innate immune response to pathogens or aid during B-cell maturation. After infections, specific B- and T-lymphocytes remain in the body as memory cells to enable a fast response in case of reinfections [7].

To prevent auto-activation and improper functioning of the immune system, tight regulation of the innate and the adaptive immune system is applied. Therefore, PRRs are compartmentalized to avoid

self-recognition or T- and B-cells undergo a positive and negative selection process during their development. However, these control mechanisms sometimes fail or are improperly executed, leading to severe diseases. A misregulated innate immune response can cause autoinflammatory diseases triggering severe cases of chronic inflammation with associated tissue damage or even septic shock. Dysfunction of the T- or B-cell selection process on the other side can, for instance, provoke autoimmune diseases via the production of autoantibodies, the attack of healthy tissue or even the recognition of harmless structures causing allergies [7,14].

1.2 The innate immune system

The innate immune system can be divided into three layers, anatomical barriers, humoral components and a cell-based response. The first phase is the containment of pathogens using anatomical barriers. Therefore, several physical, chemical, and microbiological barriers from the external environment exist at possible entry points. All these barriers are built up by epithelial cells tightly connected by tight junctions, albeit varying in their mechanical and chemical defence mechanism. For instance, the epidermis, a highly specialized epithelial tissue of the skin, consists of multiple layers of keratinocytes. The basal layer comprises stem cells, followed by several layers of keratinocytes in different differentiation stages, and the *stratum corneum* as the top layer. Differentiated keratinocytes produce and secrete lamellar bodies with incorporated β-defensins and cathelicidins to the top layer as additional chemical barriers. The top layer itself is built up by cornified dead cells enabling a waterproof lipid layer. In contrast, the bronchial epithelium is ciliated and uses its cilia movement to generate a continuous mucus stream to remove pathogens. The mucus is produced by goblet cells, a mucosal epithelial cell type. Like the skin, the bronchial system uses chemical barriers such as α-defensin or cathelicidins. In the intestinal tract, specialized epithelial cells, so-called Paneth cells, create a toxic environment for most pathogens by generating a low pH and secreting several antimicrobial proteins. Similar means of pathogen containment exist for the eyes, nose and oral cavity. The organism's microbiota composed of commensal bacteria also serves as a defence mechanism by outcompeting harmful bacteria. In some cases, it even produces antimicrobial substances like lactic acid or antimicrobial peptides [7,15,16].

The second phase of the innate immune system acts directly after pathogens overcome the anatomical barriers and their associated chemical components and infect the organism. Here a pre-synthesized set of soluble antimicrobial proteins and enzymes including defensins, histatine, pentraxins, ficolins, collectins, lectins, and lysozyme awaits the pathogen [17]. These antimicrobial compounds are often secreted in an inactive state and require cleavage or binding of specific structures to be activated, representing the simplest form of pattern recognition receptors and effector molecules. Pathogens surviving this first line of antimicrobial peptides and enzymes encounter the complement system. The complement system was already discovered in normal plasma as a heat-labile substance in the 1890s by Jules Bordet and still composes a significant component of the innate immune system. The 30 distinct plasma proteins of the complement are mainly produced in the liver and circulate in the blood and bodily fluids in an inactive form. When encountering pathogens, the complement system can be activated by three different pathways. The classical and first discovered complement activation is triggered by antibodies and initiated by binding of the complement component C1 to a microbial surface or to antibodies bound to pathogens. The alternative pathway is independent of antibody

binding and relies on the spontaneous cleavage and binding of complement component C3 to a microbial surface. The third activation pathway, the so-called lectin pathway, is mediated by soluble carbohydrate-binding proteins like ficolins or mannose-binding lectin. All three pathways rely on proteolytic cleavage to form a C3 convertase cleaving the complement protein C3. This leads to the opsonization of the pathogen and preparation of phagocytosis of the pathogens. Phagocytes are recruited to the site of infections and promote inflammation. In addition, phagocytes bind and engulf the opsonized pathogens to eliminate them. Alternatively, a membrane-attack complex (MAC) can be formed by the complement cascade disrupting the cell membrane by creating a pore and leading to pathogen lysis. Several intermediates of the component cascade mediate inflammation and recruit immune cells to the location of infection [7,18–20].

The third phase of the innate immune response is cell-mediated and activated shortly after pathogens have crossed the epithelial barriers. These pathogens are mostly directly recognized by resident phagocytic cells or in later stages of infection by attracted effector and phagocytic cells. Here the main mechanism of pathogen clearance is the engulfment and destruction by a specific form of endocytosis, called phagocytosis. This is performed by phagocytes such as macrophages, dendritic cells, and neutrophils [7,21]. Besides its function in pathogen destruction, phagocytosis also plays an important role, for instance, during development and maintenance of tissue homeostasis. This mechanism was first discovered by Ilja Metschnikow in 1884 and was later recognized to be a critical component of the innate and adaptive immune system [21]. Phagocytosis relies on a wide variety of cell surface receptors detecting molecular pathogenic patterns, opsonic structures like antibodies or complement proteins bound to pathogens and apoptotic structures. For instance, Dectin-1 can recognize β-1,3-linked glucans, a typical structure of fungal cell walls, while the receptor CR3 can detect the complement component iC3b associated with opsonization [7,21]. Following the binding to one of the receptors, the pathogen is ingested by surrounding it with the phagocyte plasma membrane and engulfed by an actin-driven process in an enclosed endocytic vesicle called a phagosome. The engulfed pathogen is then destroyed by the fusion of the phagosome with lysosomes, forming a phagolysosome. During this process, the phagosome is enriched with hydrolytic enzymes and antimicrobial proteins, the pH is strongly reduced, and a highly oxidative environment is created. This oxidative environment is mediated by the production of reactive oxygen species (ROS) by the two enzymes nicotinamide adenine dinucleotide phosphate (NADPH) oxidase and superoxide dismutase (SOD) and nitric oxide (NO) by the inducible NO synthase (iNOS) [7,21,22]. Overall, while this creates a potent eradication mechanism for most pathogens, some pathogens have developed strategies to modify the phagosome maturation and use it for their own benefit [21].

Several classes of phagocytic cells have been described, including macrophages, monocytes, granulocytes and dendritic cells. The majority of phagocytes is represented by macrophages being resident in most tissues. Macrophages can arise from embryonic progenitor cells or circulating monocytes and are historically named differently in different tissues, like microglia cells in neural tissue [7,23]. Monocytes exist in two main populations: the classical and circulating monocytes, which can differentiate into macrophages, and the patrolling monocytes for injury surveillance in the endothelium. The second class of phagocytes is represented by granulocytes, including neutrophils, basophils and eosinophils. Neutrophils that contain granules with a reservoir for digestive and

hydrolytic enzymes are highly specialized for intracellular killing of pathogens [7,24]. Both granulocytes and macrophages can eliminate most pathogens without an adaptive immune response. The third class of phagocytes, the immature dendritic cells are similar to macrophages and granulocytes, however, they engulf and digest pathogens to produce antigens presented to naïve B- and T-cells in the lymph nodes. Two types of dendritic cells are distinguished, the conventional dendritic cells (cDCs) and the plasmacytoid dendritic cells (pDCs). While cDCs bridges the innate and adaptive immune system as antigen-presenting cells, pDCs are specialised in the production of cytokines like type I interferons (IFN) [7].

Another group of innate immune cells is represented by natural killer cells (NK cells). In contrast to the previously described cells of the innate immune system, these cells do not derive from myeloid progenitor cells but lymphoid progenitors. NK cells rely on inhibitory receptors instead of the clonal expression of somatically rearranged antigen receptors. These inhibitory receptors are essential for self and non-self-recognition as well as the development and maturation of NK cells [7,25]. Activation of NK cells is mainly dependant on the balance between inhibitory and activating signals. In the case of missing inhibitory signals from the MHC class I molecules, the induction of cell death is triggered by the release of cytoplasmic granules containing cytotoxic proteins. MHC class I molecule expression is often reduced during viral infections or on cancer cells giving NK cells an important role in cancer therapy research [7,25,26].

The elimination of infected cells by programmed cell death pathways is an effective host defence mechanism to contain pathogen infections [7]. Conceptually, cell death can occur as a last resort, cell-autonomous defence strategy to deprive pathogens of their replication niche. At the same time, cell death of infected cells can also be induced extrinsically, e.g. by NK cells or cytotoxic T cells. The first form of programmed cell death known as 'apoptosis' was defined in 1972 and described as an immunologically silent death [7,27]. Apoptosis can be subdivided into extrinsic and intrinsic apoptosis. While extrinsic apoptosis is receptor-based and needs an external signal to be activated, intrinsic apoptosis is initiated by mitochondrial outer membrane permeabilization (MOMP), resulting in the release of mitochondrial proteins [28]. Excluding apoptosis, programmed cell deaths usually trigger the recruitment of immune cells and an induced inflammatory response by releasing cellular content. Two examples are necroptosis, a programmed cell death leading to a controlled cell swelling and the subsequent loss of membrane integrity; and pyroptosis, an inflammatory cell death regulated by caspase-1, caspase-4 and caspase-5 in humans [28–32]. These cell death pathways require either a death or damage signal initiated by different mechanisms such as PRR activation, cytotoxic T-cell and NK cell interaction.

1.3   Pattern recognition receptors

The induction of phagocytosis or cell death requires the recognition of pathogenic or damage-related structures. Immune cells must also be able to respond precisely and efficiently to the respective pathogen. These detection processes were considered to be rather unspecific until Charles Janeway, Jr. in 1989 proposed a model of nonclonal, germline-encoded PRRs [9]. These PRRs were proposed to detect specific conserved and essential structures of pathogens, so-called PAMPs, and subsequently trigger innate and adaptive immune responses [9]. The experimental validation of this model came in

1996 when Jules Hoffmann and co-workers identified the Toll gene in *Drosophila melanogaster* as a mediator of antifungal response. One year later, a homolog of the fly's Toll protein was found in humans to regulate inflammatory cytokine expression[33]. This observation initiated the discovery of other so-called 'Toll-like receptors (TLRs)' with TLR4 and its ligand lipopolysaccharide (LPS) being the first identified and characterised receptor of this group by Bruce Beutler and co-workers in 1998 [34–36]. Besides TLRs, several other PRR families have been identified, such as nucleotide oligomerization domain (NOD)-like receptors (NLRs); retinoic acid-inducible gene (RIG)-I-like receptors (RLRs); C-type lectin receptors (CLRs); absent in melanoma 2 (AIM2)-like receptors (ALRs), and oligoadenylate synthase (OAS)-like second-messenger receptors (OLRs) [7,37–41]. PRRs can either induce direct effector mechanisms like the induction of cell death or indirectly through a transcriptional response [7]. An overview of PRRs, their respective ligands and downstream signalling cascades is depicted and described in Figure 1.1.
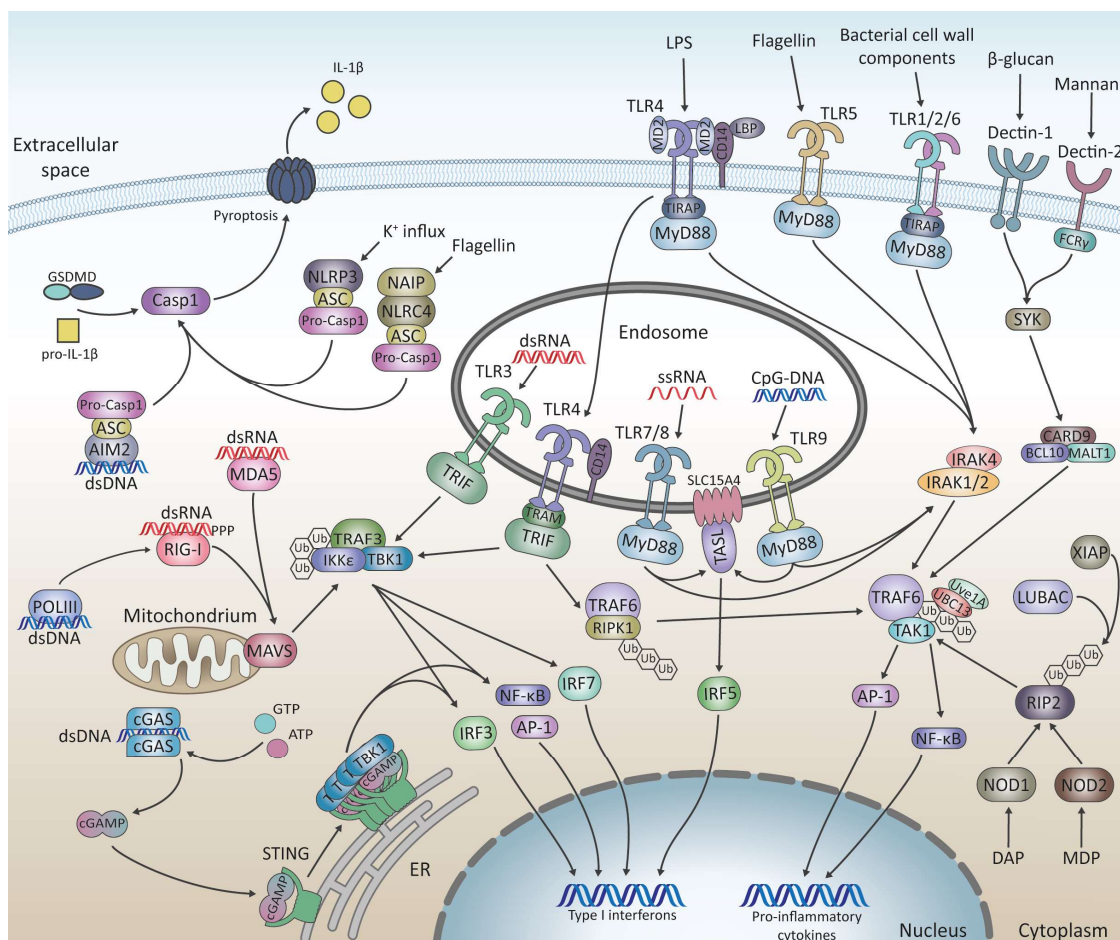
Figure 1.1 Pattern recognition receptors and their downstream signal transduction
Pattern recognition is mediated by different receptor families, some leading to an induction of type I IFNs or pro-inflammatory cytokines, while others mediate pyroptosis through inflammasome formation. NLR family members like NLRP3 and NLRC4 or the DNA sensor AIM2 form an inflammasome complex with ASC and pro-caspase 1 upon ligand binding leading to the cleavage of GSDMD and pro-IL-1β and to pyroptosis. RLRs, like RIG-I and MDA5, and cGAS recognize nucleic acids in the cytosol besides AIM2 and subsequently trigger a type I IFN response through STING or MAVS, respectively. TLRs signal through the adaptor proteins MyD88 or TRIF. While MyD88 triggers the induction of pro-inflammatory cytokines through the recruitment of TRAF6 and TAK1, TRIF

mediates a type I IFN response through TRAF3 and the kinases IKKε and TBK1. One exception is the signalling via TASL, which is mediated by TLR7/8 and TLR9 in combination with MyD88, leading to the activation of IRF5 and subsequently a type I IFN induction. Also, TLR4 can signal through MyD88 and TRIF, depending on its stage of activation, localisation and respective adaptor protein. CLRs like Dectin-1 trigger the activation of TRAF6 and NF-κB through SYK and a complex containing CARD9, BCL10 and MALT1. Two other NLR members, NOD1 and NOD2, also engage the activation of TAK1 via RIP2.

The TLR family represents the first described and best-characterised group of PRRs with ten distinct receptors in humans [7]. TLRs are located on the cell surface and in intracellular compartments, like lysosomes or endosomes [38]. TLRs are a conserved type I membrane glycoprotein family consisting of a leucine-rich-repeats (LRRs) domain, a transmembrane domain as well as a cytoplasmic Toll/IL-1 receptor (TIR) domain. The LRR domain is horseshoe-shaped and can detect ligands on both the convex and the concave surfaces [42,43]. Most TLRs form and function as homodimers, however, some TLRs can also form heterodimers. Two groups of TLRs exist based on their cellular localisation, the cell surface TLRs and the intracellular TLRs. While cell surface TLRs are specialized on microbial membrane components containing lipids, proteins and lipoproteins, intracellular TLRs instead recognize bacterial or viral nucleic acids as well as self-nucleic acids in distinct disease conditions. The cell surface TLRs include TLR1, TLR2, TLR4, TLR5, TLR6 and TLR10 [38]. Here, TLR2 is involved in sensing a variety of PAMPs, mainly lipopeptides from different pathogens, including bacteria, viruses, fungi and parasites [44]. This range of recognized patterns is based on the ability of TLR2 to form heterodimers with TLR1 and TLR6 and to collaborate with other receptors [45]. TLR5 is specialized in sensing the flagellin protein from flagellated bacteria [44]. The first described member of the TLR family, TLR4, recognizes the cell wall component LPS from gram-negative bacteria, as mentioned before [34]. However, for proper recognition, an accessory protein called myeloid differentiation factor 2 (MD-2), bound to the LRR domain, is necessary [46]. Besides MD-2, two other accessory proteins are needed for activation of TLR4. The LPS-binding protein (LBP) picks up LPS present in the blood during infections and delivers it to innate immune cells. Subsequently, LPS is transferred from the LBP to CD14. CD14 has two distinct roles in LPS sensing; on the one hand, it mediates phagocytosis when expressed on neutrophils or on the other hand, it acts as an accessory protein for TLR4 on macrophages and dendritic cells [47,48]. The intracellular TLR receptors, TLR3, TLR7, TLR8 and TLR9, require internalization via endolysosomes before signalling occurs [49]. TLR3 detects dsRNA produced during the replication cycle of single-stranded RNA (ssRNA) viruses as well as polyinosinic-polycytidylic acid (poly(I:C)), a synthetic double-stranded RNA (dsRNA) analogue, leading to its activation [45,50]. Upon activation, TLR3 initiates an antiviral immune response via inflammatory cytokine and type I IFN induction [45]. The rotational symmetry of TLRs creates in the homodimeric endosomal receptors TLR7 and TLR8 a set of two distinct ligand-binding pockets [51–53]. Both TLRs recognize breakdown products of viral or microbial RNA. TLR7 is activated by guanosines and uridine-containing ssRNA fragments binding to both distinct ligand pockets, while TLR8 binds uridine molecules and ssRNA fragments processed by RNase T2 [52–54]. TLR9 is specialized in detecting unmethylated DNA with CpG-motifs, which are underrepresented in mammalian cells [45,55]. All these TLRs dimerize or undergo conformational changes upon activation, subsequently recruiting their respective adaptor proteins containing a TIR domain [44,56]. This specific combination of adaptor protein and TLR enables a tailored immunological response to specific pathogens [57].

Four known adaptor proteins mediate these distinct downstream signalling cascades, Myeloid differentiation primary response 88 (MyD88); Toll/interleukin-1 receptor domain-containing adapter protein (TIRAP or MAL); TIR-domain-containing adapter-inducing interferon-β (TRIF); and Translocating chain-associated membrane protein (TRAM) [44,45]. While some TLRs only interact with one adaptor protein, others utilize a combination of different adaptor proteins [7]. TLRs classically signal through one of two main pathways, the MyD88-dependent and the TRIF-dependent pathway. Most of the TLRs, except TLR3, induce pro-inflammatory responses via the production of cytokines through MyD88 signalling upon activation by their respective PAMPs [45]. For that, MyD88 is recruited to the cytoplasmic part of the TLRs and interacts directly with the TLR TIR domains using its C-terminal TIR domain or requires the adaptor protein TIRAP to mediate the binding [58]. Subsequently, members of the Interleukin-1 receptor-associated kinase (IRAK) family associate with the N-terminal death domain (DD), leading to the formation of a multiprotein complex called the mydosome [59]. The mydosome is composed of six MyD88, four IRAK4 and four IRAK2 proteins, enabling close proximity between the serine-threonine kinase domains of the IRAK family members [60]. This leads to trans-autophosphorylation and activation of the IRAK proteins and the recruitment of the E3 ubiquitin ligase tumour necrosis factor receptor-associated factor 6 (TRAF6) [61,62]. TRAF6 associates with the E2 ubiquitin ligase ubiquitin-conjugating enzyme 13 (UBC13) and its cofactor ubiquitin-conjugating enzyme E2 variant 1A (Uve1A) via its N-terminal RING domain. This leads to the formation of polyubiquitins chains with K63 linkages on TRAF6 itself as well as on NF-κB essential modulator (NEMO) [63,64]. In contrast to K48 linkages, which mediate proteasomal degradation, the K63 linkage acts as a scaffold for signal transduction [65]. In the next step, the adaptor proteins TGF-β activated kinase-1 (TAK1) and MAP3K7-binding protein 1 (TAB1) and TAB2/3, and the serine-threonine kinase TAK1 are recruited and form a signalling complex [66,67]. After binding to the scaffold and being phosphorylated by the IRAK complex, TAK1 mediates further downstream signalling by phosphorylation of specific mitogen-activated protein kinases (MAPKs) and the IκB kinase (IKK) complex leading to the induction of pro-inflammatory cytokines [67,68]. In addition, nucleic-acid sensing TLRs have been described to activate interferon regulatory factor 5 (IRF5) and IRF7 through a complex containing IRAK proteins and TRAF6 in plasmacytoid DCs to induce type I IFNs against an antiviral infection [58,69–72]. However, as a potent activator of the adaptive immune response, IFNs must be tightly regulated to prevent malfunctions as well as autoimmunity [73]. The pLxIS motif mediates this regulation in adaptor proteins like TRIF, which needs to be phosphorylated as a control step before activating members of the IRF family [73]. Since MyD88 has no pLxIS motif, another mechanism for TLR7, TLR8 and TLR9 dependent IFN induction is needed to activate IRF5 [74]. Interaction of the pLxIS motif-containing protein TLR adaptor interacting with SCL15A4 on the lysosome (TASL) with the endolysosomal transporter SLC15A4 was recently proposed to be necessary to activate IRF5 [75]. However, this interaction was not required to activate pro-inflammatory cytokines by MAPK signalling and nuclear factor κB (NF-κB) activation via the IKK complex. Therefore, TASL is proposed to bind SLC15A4, which serves as a scaffold, upon TLR activation and subsequently is phosphorylated by IKKβ. IRF5 is then recruited and activated, leading to its dimerization. Upon entering the nucleus, IRF5 triggers a type I IFN transcription [75]. The TRIF-dependent pathway is only initiated by the activation of TLR3 and TLR4 [45]. TLR4 is an exception here since it can activate the signalling pathway of MyD88 with TIRAP and after endocytosis TRIF signalling in combination with TRAM and CD14 [76–79]. In contrast to MyD88, TRIF not only activates NF- κB through

TAK1 and the IKK complex but also induces type I IFNs by IRF3 [80]. For this, TRIF recruits TRAF6 and receptor-interacting serine/threonine-protein kinase 1 (RIPK1) to activate TAK1, similar to MyD88 [81,82]. However, TRIF also recruits TRAF3 and mediates IRF3 phosphorylation via its pLxIS motif by the noncanonical IKKs TANK-binding kinase 1 (TBK1) and IKKε. IRF3 phosphorylation and dimerization subsequently leads to an antiviral immune response through the induction of type I IFN transcription [45,80].

Another group of PRRs is represented by the NLR family with its 22 known NLR protein members in humans recognising microbial products and DAMPs [83]. All NLR proteins share a basic domain structure with an N-terminal interaction domain, a central nucleotide-binding and oligomerization (NACHT) domain and an LRR domain [84]. The N-terminal interaction domain is used to subdivide the family into four groups: NLRA; NLRB; NLRC; and NLRP [83,84]. Besides this, NLR proteins can be distinguished by their effector mechanisms. Some NLRs induce innate immune signalling by activation of IRFs, MAPKs or NF-κB, while other NLRs directly engage inflammatory caspases through the formation of inflammasomes leading to pyroptosis and maturation of inflammatory cytokines [85]. The NLRA subfamily is represented by only one protein, the class II major histocompatibility complex transactivator (CIITA), activating MHC class II antigen presentation and containing a C-terminal acidic transactivation domain [86]. The second small NLR subfamily is NLRB, with its multiple baculovirus inhibitor of apoptosis protein repeats domains. The only NLRB family member in humans, NAIP (NLR family, apoptosis inhibitory protein), serves as an inhibitor of apoptosis and acts as a sensor of NLRC4 [87–89]. One of the two most important NLR subfamilies, the subfamily NLRC, has an N-terminal caspase recruitment domain (CARD), allowing the interaction with CARD-containing proteins like pro-caspase1 or receptor-interacting serine/threonine kinase 2 (RIPK2) [90,91]. NOD1 and NOD2 represent the best-characterised members of the NLRC family. Both NOD1 and NOD2 oligomerize with their NACHT domain after recognising their respective bacterial peptidoglycan ligands in the cytosol. This complex, referred to as nodosome, induces inflammatory cytokines and antimicrobial effectors like nitric oxide [92–94]. The NLRP subfamily is characterized by an N-terminal pyrin domain (PYD). Some of the NLRPs can trigger the activation of an inflammasome complex, which culminates in the activation of caspase-1 [91,95]. The best-characterised member of the NLRP family, NLRP3, is involved in sensing plenty of different pathogens including bacteria, viruses, and fungi or DAMPs by a yet unknown mechanism, therefore, it can be seen as a sensor of cellular damage [96–99]. Upon activation, NLRP3 oligomerizes and recruits apoptosis-associated speck-like protein containing a CARD (ASC) via its pyrin domain [100]. The adaptor protein ASC with its N-terminal pyrin domain and its C-terminal CARD domain interacts subsequently with pro-caspase 1 using the CARD domain, forming the inflammasome complex [101,102]. Pro-caspase 1 undergoes autocleavage after binding to ASC, leading to its activation. Activated caspase-1 cleaves pro-inflammatory cytokines as well as gasdermin D (GSDMD), a pyroptosis inducer, into active mature proteins [103]. Besides caspase 1, pyroptosis can be activated by caspase 4 and caspase 5 in humans. Moreover, pyroptosis can also be mediated by other gasdermins like GSDME that are activated downstream of apoptotic caspases [104–106]. The variety of pathogens and DAMPs that can be recognized by NLRs reflect their critical role, for instance, in development and physiology as well as their influence on infectious and autoimmune diseases and their therapies [85].

CLRs are transmembrane proteins of the C-type lectin superfamily with over 1000 identified protein members subdivided into 17 groups, all sharing the characteristic C-type lectin domains (CTLDs) [107]. Besides transmembrane C-type lectin proteins, soluble forms exist and function, for instance, as opsonins, antimicrobial proteins, or growth factors [108]. CLR signalling is mediated through various pathways enabling a specific response to certain recognized ligands like glycans, proteins, lipids or inorganic molecules [109]. The best-characterised CLRs mediate their response through immunoreceptor tyrosine-based activation motifs (ITAMs), which can be part of the CLR or an associated adaptor protein [107]. For instance, the receptor Dectin-1 has an extracellular carbohydrate recognition domain (CRD), a stalk region, a transmembrane region and a signal transduction domain-containing ITAM. In contrast, Dectin-2 has the same domains except for the signal transduction domain and therefore requires the adaptor protein Fc receptor γ-chain (FcRγ). Upon activation by fungal components, Dectin-1, Dectin-2 and Dectin-3 initiate a fungicide immune response in myeloid cells, which is mediated through ITAM and leads to the recruitment of spleen recruitment tyrosine kinase (SYK) [107,110,111]. SYK induces downstream signalling and activation of NF-κB by assembling a complex consisting of caspase-recruitment domain protein 9 (CARD9), B cell lymphoma/leukaemia 10 (BCL-10) and mucosa-associated lymphoid tissue lymphoma translocation protein 1 (MALT1) [107,111]. Besides the activation of NF-κB, a variety of other signalling cascades involved in cell death, homeostasis, or cancer, are regulated or influenced by CLRs [107].

Four groups of PRRs are responsible for nucleic acid recognition depending on the localisation, the secondary structure, sequence and chemical modifications of the nucleic acids [112]. In contrast to the previously described nucleic acid-sensing through TLRs, the recognition through RLRs, OLRs, and ALRs occurs in the cytoplasm [113]. The RLR family members are specialized in RNA recognition of ssRNA and dsRNA viruses. In addition to RIG-I and melanoma differentiation-associated gene 5 (MDA5), the protein laboratory of genetics and physiology 2 (LGP2) is part of the family [113]. The C-terminal regulatory domain in RIG-I and MDA5 forms the binding platform for cytoplasmic RNAs, while the central DEAD-box helicase/ATPase domain and the two N-terminal CARD domains are needed for the downstream signalling [113,114]. RIG-I mediates an antiviral immune response upon recognition of short dsRNA strongly enhanced by the presence of a 5' triphosphate [115–118]. MDA5 recognizes long dsRNA and can be activated by poly(I:C) [119]. The last member of the RLR family, LGP2, might function in removing viral ribonucleoproteins or in unwinding complex RNA structures to enable RIG-I or MDA5 mediated detection of dsRNA [113,120]. Like TLRs, downstream signalling from RLRs also requires an adaptor protein, the mitochondrial antiviral signalling protein (MAVS) [121]. Along with TRIF, TASL and stimulator of interferon genes (STING), MAVS is one of four known proteins containing the pLxIS motif, which regulate the induction of IFNs via IRFs [73,75]. Upon activation of RLRs by viral RNA, RIG-I or MDA-5 bind to MAVS, which is located on the outer mitochondrial membrane, mitochondria-associated membranes and peroxisomes, through a CARD-CARD interaction [121–123]. This interaction leads to the recruitment of additional adaptor proteins, including TRAF3 and TRAF6, kinases like TBK-1 and IKKs, and transcription factors [121,124]. The signalling platform subsequently induces a pro-inflammatory cytokine and a type I IFN response [124].

The recognition of cytosolic non-self DNA is mediated through different proteins, including members of the ALR and OLR family [125]. The ALR family consists of four members in humans with AIM2 and IFN-

inducible protein 16 (IFI16) being the best-characterised members. All ALR family members contain an N-terminal pyrin domain like NLRP proteins but have a C-terminal H inversion (HIN) domain instead of the LRR domain [126]. AIM2 binds DNA with its HIN domain and subsequently associates with ASC and leads to the AIM2 inflammasome formation. This triggers the activation of NF-κB and pro-caspase 1, finally inducing pyroptotic cell death and resulting in the release of pro-inflammatory cytokine interleukin-1β (IL-1β) [127,128]. Unlike AIM2, IFI16 contains two HIN domains and has been proposed to act through STING, TBK1 and IRF3 upon activation by DNA recognition [129]. In addition to AIM2, the main PRR for cytosolic DNA with a broad-specificity is the cyclic guanosine monophosphate-adenosine monophosphate synthase (cGAS), a member of the OLR family [130]. After binding to DNA, cGAS produces the 2'-3'-linked cyclic dinucleotide second messenger 2'-3'-cyclic GMP-AMP (cGAMP) out of adenosine triphosphate (ATP) and guanosine triphosphate (GTP) [131–134]. cGAMP, as well as bacterial cyclic dinucleotides (CDNs), which are markers of intracellular infections, can be sensed by STING in the cytosol [134–136]. STING is anchored to the endoplasmic reticulum (ER) with multiple transmembrane regions and forms a homodimer with its cytoplasmic C-terminal domain. The binding of CDNs changes the STING conformation, allowing a side-by-side oligomerization and translocation of STING to the Golgi compartment [137,138]. During the translocation process, TBK1 binds STING adjacent to the pLxIS motif, IRF3 is then recruited and phosphorylated, leading to a type I IFN response [139–141]. In this context, cGAS has been proposed to be located in the cytosol to avoid recognition of self-DNA through different compartmentalization, however, several studies have revealed a nuclear localisation of cGAS in mitotic cells or during membrane rupture [142–144]. Indeed, recent publications have determined that cGAS is primarily located in the nucleus in an inactive state tightly controlled through the binding to chromatin [145–149]. Other proteins such as DExD/H box helicases (DEAD-Box Helicase 41 (DDX41), DExH-Box Helicase 9 (DHX9) and DEAH-Box Helicase 36 (DHX36)) or RNA polymerase III have also been described to be involved in cytosolic DNA or RNA sensing albeit in a cell-type or DNA-sequence specific manner [133,150–153].

1.4   Induction of antiviral and pro-inflammatory immune signalling

The recognition of pathogens through PRRs and their subsequent activation and recruitment of adaptor proteins is the initiation step for several signalling cascades leading to the induction of interferons or pro-inflammatory cytokines. While the pro-inflammatory immune response is mainly regulated by NF-κB and MAPK signalling, the antiviral immune response additionally relies on IRF signalling [154]. An overview of all three signalling cascades and their target gene expression is shown in Figure 1.2. One of the key mediators of the adaptive and innate immune responses are the NF-κB transcription factors [155]. The NF-κB transcription factor family was first discovered in 1986 in B-cells, and today, five members forming various homodimers and heterodimers have been described [156,157]. The five members, NF-κB1 (or p50), NF-κB2 (or p52), RelA (or p65), RelB and c-Rel, bind at the DNA element κB enhancer in their different combinations upon activation [158]. In contrast to RelA, RelB and c-Rel, the two family members NF-κB1 and NF-κB2, are not synthesized as mature proteins but arise from the two precursor proteins p105 and p100, respectively, and need to be cleaved post-translationally [157]. All five proteins have an N-terminal Rel homology domain (RHD) for DNA binding and recognition and protein dimerization followed by a nuclear localisation sequence (NLS). While RelA, RelB and c-Rel contain C-terminal transactivation domains (TADs), the two precursor proteins

p100 and p105 have C-terminal ankyrin repeats, which cover the NLS and are cleaved post-translationally [159]. The activation of NF-κB subsequently influences several responses upon bacterial or viral infections, DNA damage or oxidative stress, for instance, cell proliferation, apoptosis, cytokine expression, and cell migration and invasion [155,160]. Two main signalling pathways mediate the NF-κB activation, the canonical and the non-canonical pathway [161]. The canonical NF-κB pathway is induced by different receptors, including previously described PRRs, cytokine receptors, T- and B-cell-receptor [162]. All these receptors trigger an activation of the IKK complex, consisting classically of two kinases IKKα and IKKβ and the regulatory subunit IKKγ (NEMO) [157]. TAK1 mainly mediates this activation for the canonical NF-κB pathway, while the non-canonical pathway is induced by NF-κB-inducing kinase (NIK) downstream of RIP and TRAF proteins [163–166].
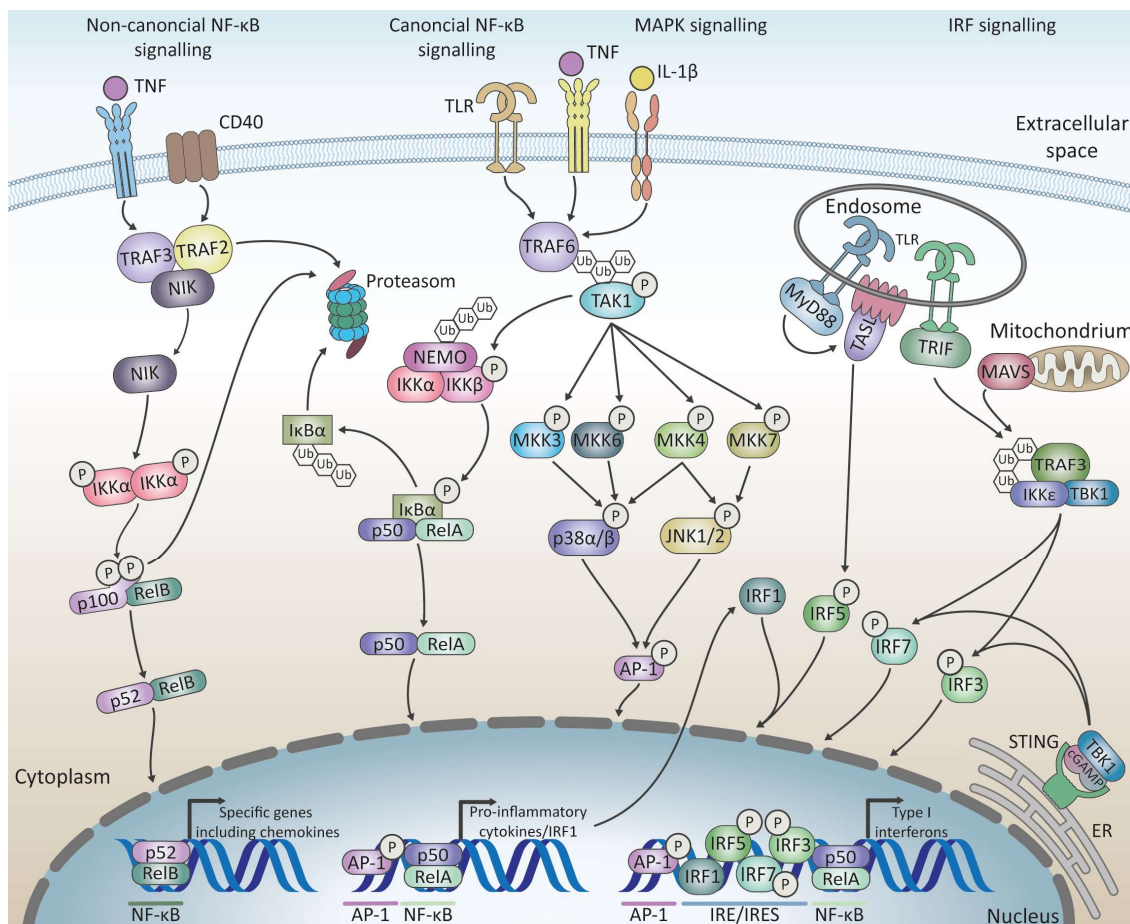
Figure 1.2 Induction of antiviral and pro-inflammatory cytokines via NF-κB, MAPK and IRF signalling
NF-κB activation is triggered by the canonical and non-canonical NF-κB signalling pathway. In the non-canonical NF-κB cascade, the stabilization of NIK through the degradation of the regulating TRAF complex is the key step for signal transduction upon receptor activation. NIK leads via IKKα to the activation and phosphorylation of p100, which is subsequently cleaved and forms the p52/RelB complex. This complex shuttles to the nucleus and induces target gene expression. The canonical NF-κB signalling is mediated by TAK1 and the scaffolding protein TRAF6. Upon receptor binding and TAK1 activation, the IKK complex is recruited and activated. IKKβ triggers the phosphorylation of the inhibitory protein IκBα and marks it for proteasomal degradation. The released RelA/p52 complex translocates to the nucleus and promotes pro-inflammatory cytokine and type I IFN expression. Besides the activation of the canonical NF-κB signalling, TAK1 also phosphorylates and activates the MAP2Ks leading to their activation and subsequent phosphorylation of the MAPK p38 and JNK. Both lead to the phosphorylation

and nuclear translocation of AP-1 transcription factors that trigger the activation of pro-inflammatory and antiviral gene expression. The activation of IRFs is mediated through the pLxIS motif-containing proteins TASL, TRIF, STING and MAVS. Some IRF transcription factors are phosphorylated, leading to their dimerization and nuclear translocation or are transcriptionally upregulated and thereby activated like IRF1. IRFs are necessary for the antiviral immune response, and together with AP-1 and NF-κB factors, they form the so-called enhanceosome for the type I IFN induction.

Active TAK1 is part of a multiprotein complex formed after activation of PRRs next to other proteins, including TRAF, TAB and IRAK proteins. This complex leads to the recruitment of the IKK complex and subsequent ubiquitination of IKKγ and phosphorylation of IKKβ [157,167]. The active IKK complex then phosphorylates the inhibitory IκB proteins and triggers their proteasomal degradation [168]. These inhibitory proteins containing an ankyrin repeats domain bind the NF-κB dimers to keep them in an inactive state in the cytosol by blocking their NLS [169]. After releasing NF-κB from its inhibitory proteins, it shuttles to the nucleus and induces target gene expression [157]. In contrast, the non-canonical pathway is induced by stabilization of NIK by removing a TRAF complex mediating its rapid proteasomal turnover [169]. NIK subsequently phosphorylates the IKKα homodimer leading to the phosphorylation of the cytoplasmic p100/RelB complex [157]. The p100 protein is subsequently cleaved at the C-terminal ankyrin repeats domain generating the p52/RelB complex, which translocates to the nucleus and triggers transcription of target genes like pro-inflammatory cytokines [170].

Besides the NF-κB signalling, all PRRs also trigger activation of MAPK signalling pathways to a certain extent [171,172]. Several of the 14 known human MAPKs have been described to play a role in innate immune signalling, including extracellular signal-regulated kinase 1 (ERK1), ERK2, Jun N-terminal kinase 1 (JNK1), JNK2 and p38α, p38β. The activation and phosphorylation of MAPKs generally follow the same pattern. Firstly, a MAP3K is activated and phosphorylated, leading to the phosphorylation and activation of a MAP2K. The MAP2Ks subsequently activate MAPKs, which trigger the activation of transcription factors or other kinases directly in the cytoplasm or after translocation into the nucleus [171]. One of the main MAP3Ks mediating innate immune signalling is TAK1 (also named MAP3K7), which triggers NF-κB signalling on the one hand and p38α and JNK1/2 signalling pathways on the other hand [67]. Other MAP3Ks have also been reported to impact immune signalling like apoptosis signal-regulating kinase 1 (ASK1), tumour progression locus 2 (TPL2) or MAPK/ERK kinase kinase 3 (MEKK3). However, many connections between the regulation of MAPK signalling and the corresponding MAP3K have to be further investigated [171]. The cascades following MAP3K activation are named according to the MAPKs, which are eventually activated. Therefore, the MAPK signalling is divided typically into four branches, the ERK1/2, the p38, the JNK and the ERK5 cascade [173].

The ERK1/2 signalling pathway is associated, for instance, with several pathologies ranging from neurodegenerative diseases to cancer due to its important role in proliferation, morphology determination, and apoptosis [173,174]. Several MAP3Ks like TPL2 lead to ERK1/2 signalling via the phosphorylation of MKK1 and MKK2 [171]. The ERK5 signalling pathway is mediated mainly by MEKK2/3 and involves MKK5 as the respective MAP2Ks. As the least researched MAPK cascade, it is still unknown how this cascade is activated. However, it has been already associated with several stimuli leading to stress or mitogenic signalling [173,175,176]. Even though ERK5 shares some similarities with ERK1/2 in their activation mechanism, both cascades have different substrates and upstream activators [173,177]. The last

two MAPK modules are both stress-induced and involved in pro-inflammatory cytokine expression and antiviral immune responses, as depicted in Figure 1.2 [178]. The first module, the JNK pathway, relies on the MAP2Ks MKK4 and MKK7 and includes the MAPKs JNK1, JNK2, and in some neuronal tissues JNK3 [171]. The second module, the p38 cascade, is mediated by the MAP2Ks MKK3, MKK6, and in some conditions MKK4 and includes the four members p38α, p38β, p38γ, and p38δ [173,174,179]. The proteins, p38α and p38β, are known to regulate inflammatory responses and exhibit similar functions, albeit p38α has been researched more extensively due to its higher expression levels [180]. The other two p38 kinases, p38γ and p38δ, differ in their substrate specificity, tissue-specific expression, and sensitivity to certain inhibitors and depict no distinct phenotypes in knockout mice [181–184]. The activation of JNK and p38 modules show several cross-talks and only slight differences, which are mainly in the usage of specific scaffold proteins, substrates or MAP3Ks [173,185–187].

Upon phosphorylation, all MAPK trigger the activation of several substrates, including cytoplasmic or nuclear kinases, so-called MAPK-activated protein kinases (MAPKAPKs), and transcription factors [171,180]. MAPKAPKs are subdivided into five groups MK2/3, MK5, MAPK interacting protein kinase 1/2 (MNK1/2), ribosomal s6 kinases (RSKs), and mitogen- and stress-activated kinases 1/2 (MSK1/2). While the first three subgroups contain one kinase domain, the RSK and MSK subfamilies contain a C-terminal (CTKD) and an N-terminal kinase domain (NTKD) [180,188]. RSK family members and partially MSK1/2 are activated by ERK1/2, while p38 cascades signal mainly over MK2/3 and MSK1/2 [180,189]. MK2 and MK3 are important kinases for cytokine and type I interferon production downstream of p38α/β [189–191]. MSK1 and MSK2 mainly regulate nuclear events due to their functional bipartite NLS leading to their strong localisation in the nucleus [192–194]. Both MSK family members have been described to act in the negative feedback regulation, leading to a reduction of the immune response upon TLR activation [195]. Besides the activation of MAPKAPKs, one important function of MAPK signalling in regulating immune responses is represented by the activation of AP-1 transcription factors. AP-1 transcription factors dimerize and bind to DNA upon activation through their basic domain and leucine-zipper motif [196,197]. The AP-1 transcription factor family consists of four subgroups, the activating transcription factor (ATF) family, the Jun family, the Fos family and the musculoaponeurotic fibrosarcoma (Maf) family [198]. AP-1 transcription factors form homo- or heterodimers and differ in their ability and effectiveness to transactivate AP-1 regulated genes [196]. The differential expression of these AP-1 family members in different tissues might determine the functions of the respective transcription factor complexes [199]. Overall, AP-1 plays an important role in several signalling cascades ranging from tumorigenesis over T-cell activation to PRR signalling and pro-inflammatory cytokine expression [196,199,200].

Besides AP-1 and NF-κB, the antiviral immune response relies on a third group of transcription factors, the IRF family [154]. The first IRF family member was described in 1988, and so far, a total number of nine IRF transcription factors have been identified in humans [201–203]. IRFs are either involved in the relay of induced immune responses, the differentiation of immune cells or immunomodulation. They share the same multi-domain structure with an N-terminal DNA binding domain (DBD) and a C-terminal activation domain (AD) with a linker region (LR) and an IRF-association domain (IAD) as depicted in Figure 1.3. However, some of the IRF family members also contain a C-terminal auto-inhibitory region (AR). The N-terminal DBD recognizes the IFN regulatory element (IRE) and the IFN-stimulated response element (ISRE) present in the regulatory regions of IFNs or IFN-stimulated genes. The IRF family is

subdivided into four subfamilies according to the phylogenetic relationship: the IRF1, the IRF3, the IRF4, and the IRF5 subfamily [203,204].

The IRF1 subfamily is comprised of the first two discovered IRFs, IRF1 and IRF2. IRF1 is transcriptionally regulated by NF-κB and signal transducers and activators of transcription 1 (STAT1) and gets strongly upregulated upon viral infections [205,206]. In addition, several post-translational modifications, including phosphorylation and ubiquitination, have been described to modify the stability and impact the regulation of the short-lived transcription factor [207]. IRF1, for instance, regulates antiviral gene expression, the induction of nitric oxide synthase in macrophages, and the development and function of T- and NK cell [203,206,208,209]. Moreover, IRF1 can form heterodimers with IRF2 or IRF8 to regulate target gene expression [203,210]. Here, the IRF1/IRF8 heterodimer, or IRF1/IRF8 regulome, has been shown to trigger an important antimicrobial defence mechanism upon tuberculosis infection [211]. The second family member IRF2 is regulated differently depending on its function as transcriptional activator or repressor. Besides several post-translational modifications, including acetylation, sumoylation, and phosphorylation, the activity of IRF2 has also been described to be modified by cleavage of its C-terminal region [212]. IRF2 was first described as an IRF1 antagonist and recently was shown to play a role in pyroptosis, IFN signalling, and MHC-I gene expression [213–215].
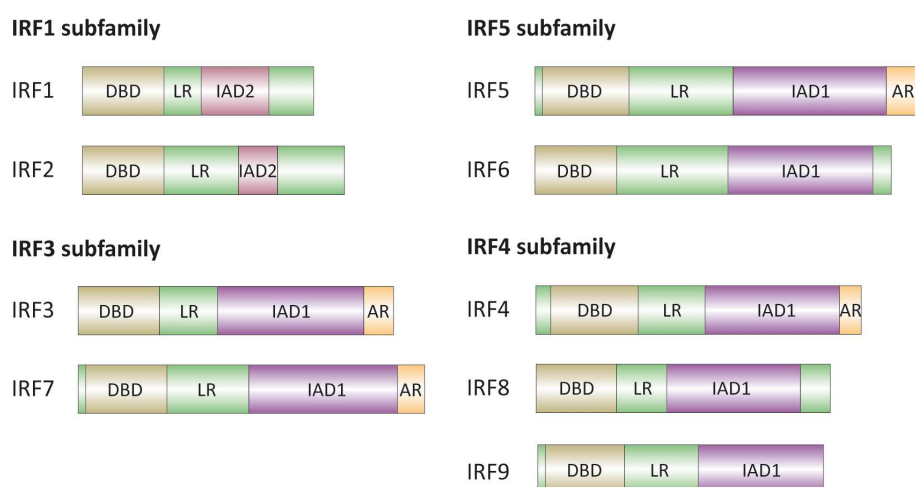
Figure 1.3 Overview of the domains of human IRF transcription factors
IRF transcription factors share a similar multi-domain structure with an N-terminal DNA-binding domain (DBD) and a C-terminal activation domain (AD) with the linker region (LR) and the IRF association domain (IAD). The IRF1 subfamily members contain an IAD type 2 (IAD2) domain, while all other IRFs have an IAD type 1 domain (IAD1). Some IRFs, including IRF3, IRF4, IRF5 and IRF7, also contain an auto-inhibitory region (AR). Adapted from Antonczyk et al., 2019 [203].

Among the IRF subfamilies, the IRF3 subfamily with the two members, IRF3 and IRF7, mainly regulates antibacterial or antiviral immune responses [203]. Phosphorylation at the C-terminal serine/threonine cluster triggers IRF3 and IRF7 activation and leads to conformational changes. These changes disable the auto-inhibitory mechanism and reveal the DBD enabling dimerization, translocation to the nucleus, and DNA interaction as depicted in Figure 1.2 [216,217]. IRF3 can form homodimers or heterodimers with IRF7 upon activation, which are important for IFNβ transcription and the subsequent activation of type I IFN signalling [218,219]. Besides the IRF3/IRF7 heterodimer, IRF7 can also form homodimers or

heterodimers with IRF5 and is important for type I interferon induction [220,221]. This variety of homo- and heterodimers and their differences in target gene expression point to the importance of specific IRF dimerization for tightly regulated differential regulation of gene expression [222]. The IRF5 subfamily consists out of IRF5 and IRF6. While the transcriptional activity of IRF5 is regulated by phosphorylation similar to IRF3 and IRF7, the regulation and function of IRF6 still remain unknown. IRF5 has been described to trigger the induction of antiviral gene expression upon nucleic acid sensing in the endolysosome [75]. The transcription factor IRF6 mediates keratinocyte proliferation and differentiation, and therefore, is involved in several severe developmental syndromes [203,223].

The last IRF subfamily is composed of IRF4, IRF8, and IRF9. Here, the expression of IRF4 and IRF8 is limited to immune cells from the lymphoid and myeloid lineages [224]. Both IRFs can form co-activating complexes with proteins like PU.1, enabling the binding to a variation of the classical ISRE motif [225–227]. In contrast to IRF8, IRF4 has been proposed to be in an auto-inhibited state mediated by the AR blocking the DBD, preventing binding to DNA. Therefore, the binding of an interaction partner, which leads to a conformational change unmasking the DBD and enabling interaction with DNA, is proposed to be necessary for IRF4 activation [204]. IRF4 and IRF8 have been described to be involved in the regulation of cytokine expression, T_h-cell differentiation and B-cell maturation [203]. The last member of the IRF4 subfamily, IRF9, forms the IFN stimulated gene factor 3 (ISGF3) complex with STAT1 and STAT2 [203,228]. This complex mediates type I and type III IFN-induced signalling and leads to the induction of ISGs [203].

1.5 Cytokines, chemokines, and interferons

The release and recognition of cytokines and subsequently induced signalling cascades are a central component of the innate immune response upon infection. Pattern recognition and downstream signalling via adaptor proteins leading to the activation of MAPK, NF-κB or IRF signalling all result in the expression of a specific subset of these molecules [7]. Besides growth factors, eicosanoids and complement factors, cytokines and their receptors are the main regulators of inflammation [229]. These small polypeptides or glycoproteins have a short half-life upon secretion and induce specific effects on different cell lines ranging from inflammatory or anti-inflammatory signals to growth and differentiation signals [230]. The short lifespan of cytokines in circulation allows only an autocrine or paracrine effect. However, some cytokines with increased stability can signal in an endocrine manner to affect distant cells [7,230]. Cytokines and their receptors are classically grouped into families by their structure. Cytokine receptors are grouped into: the homodimeric; heterodimeric with or without a common chain; tumour necrosis factor (TNF); and chemokine receptor family [7]. The IL-1 family with the two first discovered cytokines, IL-1α and IL-1β, consists of 11 members mediating pro- or anti- inflammatory responses and being expressed in numerous cell types [229,231]. IL-1 family members are mostly produced as precursor proteins. While some IL-1 family members like IL-1α are active in the precursor and processed form, other family members like IL-1β are produced in an inactive pro-form and must undergo cleavage or removal of an N-terminal peptide to create the mature and active cytokine or are already produced in their active form [7,229,232,233]. Depending on the cell type, mature IL-1α or IL-1β secreted during pyroptosis is sensed by a heterodimeric receptor without a common chain consisting of the two IL-1 family receptors, IL-1R1 and IL-1R2. Their accessory protein (IL-1RAP) promotes the recruitment of MyD88, which binds to the TIR domain of IL-1R [234]. Upon binding of

MyD88, MAPK and NF-κB signalling is activated leading to the expression of pro-inflammatory cytokines [229].

The TNF family consist of 30 TNF receptors and 19 associated ligands, with TNFα being the first discovered member in 1975 [229,235]. TNFα is produced in a similar manner to IL-1 family members as an inactive precursor protein, which subsequently needs to undergo several proteolytic cleavage events to be activated [236]. In contrast to IL-1, the precursor of TNFα is a transmembrane protein called mTNFα, which is transported to the cell surface via the endoplasmatic reticulum (ER), the Golgi network and the recycling endosome [237]. At the plasma membrane, a non-covalent TNFα trimer assembles and is subsequently cleaved by a disintegrin and metalloproteinase domain 17 (ADAM17), leading to the release of the soluble ectodomain sTNFα [229,238]. The remaining membrane-bound component of TNFα undergoes further cleavage to produce an intracellular domain that activates cell-intrinsic pro-inflammatory cytokine production after nuclear translocation [229]. The soluble ectodomain binds to TNF receptors and mediates, for instance, proliferation, inflammatory and antiviral effects or initiates cytolytic activity against tumour cells [229,238]. Secreted mainly from macrophages, the cytokine TNFα also triggers the non-canonical NF-κB signalling pathway through TNF receptor activation [169,229].

Another important cytokine family is the IL-6 family, whose members are all defined by their ability to signal through the receptor subunit glycoprotein 130 kDa (gp130) [239,240]. The family member IL-6 was discovered in 1986 and first associated with B-cell differentiation [241]. Several more functions ranging from B-cell maturation, antibody production, T-cell differentiation and regulation to haematopoiesis have been identified for IL-6 [242]. It is also important in a process called leukocyte switching. Here, IL-6 suppresses chemokines mediating the recruitment of neutrophils needed for the early inflammation while enhancing the expression of monocyte attracting chemokines [243,244]. There are two mechanisms for IL-6 mediated signalling. In the first mechanism, IL-6 binds to the membrane-bound IL-6 receptor (mbIL6R), leading to the recruitment of two gp130 proteins [244]. This subsequently initiates downstream signalling over Janus kinases (JAKs) in combination with the STAT transcription factor family, MAPKs and phosphoinositide 3-kinase (PI3K) [245,246]. In the second mechanism, IL-6 is recognized by the soluble IL-6 receptor (sIL6R), an mRNA splicing variant or product of ADAM proteases [244]. This IL-6/sIL6R complex binds in a process called trans-signalling to gp130 on cells not expressing mbIL6R. This enables signal transduction similar to the process in cells containing mbIL6R [244]. The IL-1, IL-6 and TNFα families mediate local and systemic effects to infections, including fever, lymphocyte activation, increased antibody and acute-phase protein productions [7].

Chemokines are a group of cytokines that are expressed very early after infection and recruit immune cells by inducing chemotaxis [7]. The family of chemokines includes more than 40 chemokines and over 20 chemokine receptors in humans [229]. Besides their function in guiding cellular migration by chemokine gradients, chemokines, for instance, also mediate DC maturation and interactions of immune cells [247]. These highly structural homologous chemokines are divided into four groups according to their first two cytosine residues [248]. The main two groups are CC chemokines and CXCL chemokines, while the C group and the CX3CL group only represent a minor number of chemokines [240]. All chemokines signal via seven-transmembrane, rhodopsin-like G-protein-coupled receptors and induce phosphorylation of heterotrimeric G protein upon activation. The activated G-protein subsequently mediates intracellular calcium release leading to the activation of protein kinase C (PKC),

induction of GTP-binding proteins and production of inositol triphosphate, enabling chemokines to trigger a variety of cellular signalling pathways [240,249].

The next important subgroup of cytokines is highly involved in antiviral immune signalling and are called interferons (IFN) [7]. IFNs are grouped into three different families: the type I IFN family, the type II IFN family, and the type III IFN family. They all have distinct receptors, signalling cascades, regulation, and activation mechanism [250]. The IFN receptors and the activated downstream signalling pathways with their respective gene targeting sequence are depicted in Figure 1.4. The type I IFNs were discovered in 1957 by Isaacs and Lindemann and were described to interfere with viral replication, hence they were named interferons [251,252]. Until recently, several members of the type I IFN family were discovered, including 13 isoforms of IFNα, IFNω, IFNε, IFNκ and IFNβ, the prototypical type I IFN [250,253]. Secreted type I IFNs are detected by the ubiquitously expressed heterodimeric interferon-α receptor (IFNAR) consisting of an IFNAR1 and an IFNAR2 chain [250]. The functions of type I IFNs range from immunomodulation and inhibition of proliferation to antiviral immune responses [253]. The Type II IFN family with its single member IFNγ is expressed mainly in NK and T-cells [254]. The transcript of IFNγ is constantly expressed, enabling a rapid production and secretion of the type III IFN upon infection [255,256]. Two pathways mediate the secretion, one of which is receptor-based and the other one cytokine-based. The receptor-regulated secretion is controlled by the NK cell-activating receptor or TCR in T-cells, while the cytokine-regulated secretion is controlled by IL-12 expressed by macrophages during infections [254]. The secreted and glycosylated IFNγ homodimer binds to two complexes, each consisting of one interferon-γ receptor 1 (IFNGR1) and one IFNGR2 protein. It is expressed in several tissues and initiates downstream signalling similar to type I and III IFNs [253,254]. Besides its role in orchestrating the innate and adaptive immune response, IFN-γ also has important regulatory functions in all stages of tumour immunoediting, including immune-stimulatory and immune-suppressive functions [254]. The most recently discovered IFN family is the type III IFN family with its four members IFNλ1, IFNλ2, IFNλ3, and IFNλ4 and was identified almost 50 years after the discovery of type I IFNs [257–259]. The dimeric receptor for the type III IFN consists of IFNLR1 and IL10R2, which is also part of the IL-10 receptor complex [257]. Due to IFNLR1 expression being limited to epithelial cells and a subset of immune cells, type III IFN is mainly associated with the epithelial antiviral host defence at mucosal surfaces [253,260,261]. Interestingly, even having no structural or sequence-specific relation, both type I and type III IFNs can mediate the activation of similar signalling pathways and cytokine expression patterns [262]. In addition, both IFNs are upregulated upon recognition of viral infections by PRR signalling. However, there are some differences in their activation and regulation of gene expression [262]. Upon RNA sensing by RLRs and the activation of MAVS, for instance, the localisation of MAVS is important for triggering type I or type III IFN signalling. While MAVS on peroxisomes induces type III IFN transcription, localisation in the mitochondria leads to additional MAPK activation and type I IFN transcription [262,263].

The mechanisms for gene regulation are highly divergent between the different types of IFNs. Here, IFNβ requires cooperative binding of three transcription factor families, AP-1, IRF3 or IRF7 and NF-κB, in close proximity to each other for enhanceosome assembly and transcriptional activation [264,265]. In contrast, transcriptional regulation of type III IFNs only relies on NF-κB or IRFs and can also be activated by IRF1 [266]. In addition, both transcription factors can induce transcription independently from one

another, leading to high inducibility of type III IFNs [262]. Type I and type III IFNs are secreted and mediate signalling in an autocrine and paracrine manner. Upon receptor binding, a ternary complex is formed, leading to conformational changes in the cytoplasmic parts of the receptor subunits and phosphorylation of the receptor through different associated JAK family members. This phosphorylation initiates the recruitment of STAT1 proteins, which in turn become phosphorylated and activated, leading to dimerization and ISGF3 complex formation [250,253].
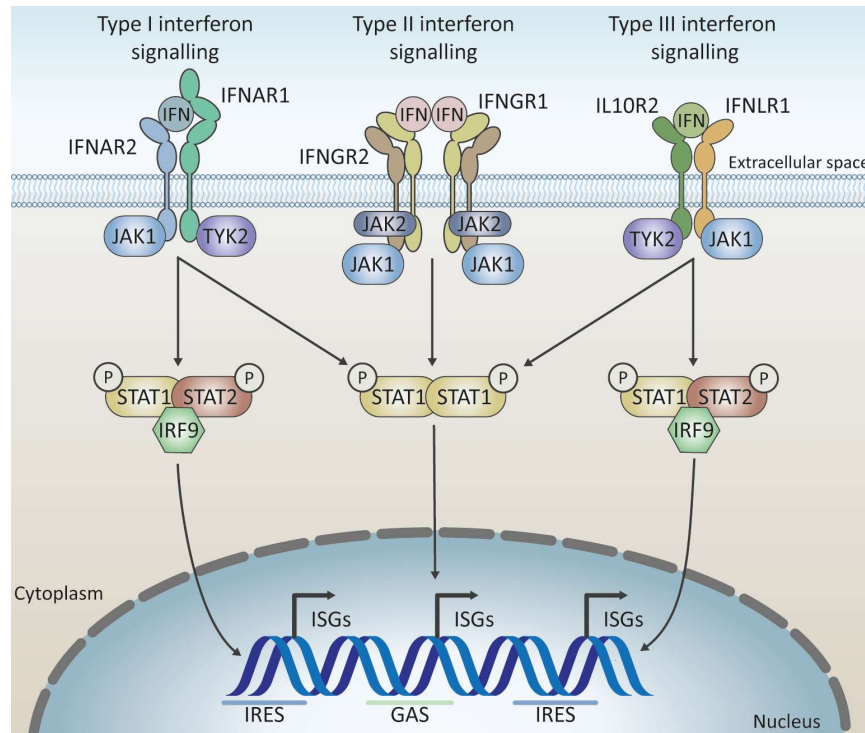
Figure 1.4 Interferon-induced JAK-STAT-signalling and activation of antiviral gene expression
Type I IFNs are detected and bound by the receptor IFNAR2, which subsequently leads to the recruitment of IFNAR1 and dimerization. The assembled IFNAR complex mediates the recruitment of JAK1 and TYK2. Both kinases phosphorylate IFNAR and create a signalling platform for STAT1 and STAT2 binding and activation. Upon phosphorylation, STAT1 forms a homo- or a heterodimer with STAT2 before translocating to the nucleus. In the case of the STAT1/STAT2 heterodimer, IRF9 is recruited to form the ISGF3 complex. In the nucleus, the ISGF3 complex triggers the activation of ISGs by binding to the ISRE promoter motif. The STAT1 homodimer leads to the induction of ISGs through its binding to the GAS motif in the target gene's promoter region. Like type I IFNs, type III IFNs trigger the activation of STAT1 and STAT2 through JAK1 and TYK2. Type III IFNs are detected by a heterodimeric receptor consisting of IL10R2 and IFNLR1. The last group of IFNs, type II IFNs, are secreted as homodimers primarily from NK and T-cells and are recognized by a heterodimer complex of IFNGR1 and IFNGR2. The receptor complex dimerizes and recruits JAK1 and JAK2. Both kinases subsequently trigger the phosphorylation of STAT1, which forms a homodimer and leads to the induction of GAS-mediated ISG expression.

IFNβ, which is secreted by several cell types, including macrophages and epithelial cells, is detected by the IFNAR heterodimeric complex consisting of IFNAR1 and IFNAR2. Unlike IFNAR2, IFNAR1 has a low binding affinity to IFN but is important for distinguishing between the different type I IFN subtypes [267–270]. Upon IFNβ binding to the IFNAR complex, the two kinases, tyrosine kinase 2 (TYK2) and JAK1, initiate the downstream signalling by phosphorylation of several target proteins like PI3K, MAPK, and STAT proteins. Activated MAPKs and the ISGF3 complex trigger ISRE-activated ISG transcription, while

activated STAT1 homodimers mediate γ-activated sequence (GAS)-mediated ISG-transcription [271]. Also, in the absence of infections, a constitutive expression of IFNβ at a low level is maintained and proposed to impact immune homeostasis, antiviral and antitumor immunity and prime cells for an efficient cytokine response. This constitutive expression depends on a homeostatic balance between transcription activators and suppressors [272]. While IRF3 and IRF7 are necessary for an antiviral immune response, the deletion of both does not impact the constitutive expression of IFNβ [272]. However, the two transcription factor families AP-1 and NF-κB appear to be essential for constitutive expression but not for the antiviral immune signalling [273,274]. Besides the positive effects of viral and bacterial infections, IFNs can also be harmful to the host in certain infections or when they are misregulated, leading to severe autoimmune diseases called interferonopathies or immune suppression [271,275].

1.6   DNA damage recognition and repair

Not only infections with pathogens pose a significant threat to cells and the whole organism, but other stresses and damaging factors must be addressed every day to safeguard survival and reproduction. Genomic integrity and DNA stability are especially essential, however, every cell in the human body is confronted with 10^5 lesions per day arising from exogenous or endogenous sources. While reactive molecules produced by mitochondrial respiration and replication errors are the primary sources for endogenous DNA damage, extrinsic DNA damage can be mediated by several triggers like ultraviolet (UV) light, ionizing radiation (IR), heavy metals or drugs [276–278]. The resulting lesions are often cytotoxic and mutagenic, leading to cell death, genomic instability, senescence or cancer depending on the damage severity, the cell type and differentiation stage [279]. The severity of DNA damage ranges from single base modifications to single or double-strand breaks. In order to overcome these dangers, cells have developed several coordinated pathways with specialized and tightly controlled mechanisms, also called DNA damage response (DDR) [280]. An overview of the various DNA repair pathways and their corresponding DNA damage types is depicted in Figure 1.5.

Several multistep DDR pathways are currently known, including DNA single-strand break (SSB) repair, DNA double-strand break (DSB) repair, mismatch repair (MMR), base excision repair (BER), DNA-Protein-crosslink (DPC) repair and nucleotide excision repair (NER) [281]. The importance of these repair mechanisms is well illustrated by the amount of ATP and single-use proteins cells must invest in maintaining their DNA sequence and genomic integrity. For instance, the enzyme O-6-methylguanine-DNA methyltransferase, one such single-use protein, promotes an error-free direct reversal of DNA lesions. During the repair of a single O-6-methylguanine lesion, the enzyme transfers a methyl group from guanine to one of its cysteine residues and therewith inactivates itself [279]. Besides the DDR, many repair proteins and mechanisms are also involved in other cellular processes like immune-receptor diversity, replication, telomere homeostasis and ageing [282].

A significant source of DNA damage is DNA base modifications caused by alkylation, deamination and oxidation by reactive oxygen species (ROS). Gamma rays and other sources of ionising radiation can also cause such modifications [280]. Over 100 different types of oxidative base modifications caused by ROS have been described [283]. A very common modification, for instance, is the oxidative modification of guanine to 8-oxo-dG, which can pair with cytosine and adenine, leading to G:C to A:T transversion mutations during replication [284,285]. Such transversion mutations also occur to a similar extent during

spontaneous deamination of bases generating inosine, uracil, or xanthosine residues [286,287]. To prevent mutations or mutant protein production, it is crucial to address these frequent events during all cell cycle stages [280,288]. Therefore, the BER uses a set of mono- and bifunctional glycosylases, each detecting specific DNA modifications. Upon detection, monofunctional glycosylases remove the modified base from the deoxyribose backbone leading to an abasic site, while bifunctional glycosylases directly create an SSB. The abasic site or the SSB is further processed by apurinic/apyrimidinic endonuclease 1 (APE1) [280,289,290]. Depending on the cell's differentiation state, the single strand site is subsequently filled up by DNA polymerase β in non-proliferating cells or DNA polymerase δ and ε in proliferating cells. The final ligation step is performed by DNA ligase I or a complex of DNA ligase III and X-ray repair cross-complementing protein 1 (XRCC1) [280,289].
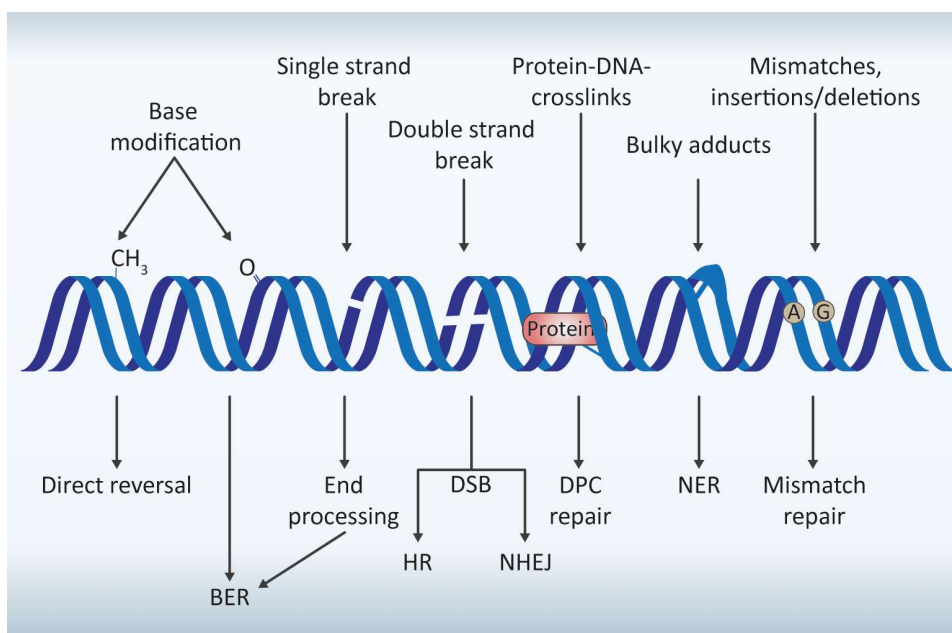
Figure 1.5 Overview of DNA damage kinds and their correlated repair mechanisms.
Base modifications are either directly reversed or are detected by glycosylases and repaired with the BER cascade. SSBs, with their variety of different strand ends, undergo end processing before being repaired by the BER pathway. DSBs can be repaired through HR or NHEJ, depending on the cell cycle. DNA-Protein-crosslink repair removes proteins bound to DNA. Bulky adducts or deformations of the DNA structure are detected and repaired by the NER. Mismatches and insertions or deletions trigger the mismatch repair pathway. Adapted from Lord and Ashworth, 2012 [291].

Besides single base modifications or abasic sites, more than one base can be damaged by crosslinking, formation of bulky adducts or mismatches during replication errors. These base-base mismatches and insertions-deletions-loops, which arise during DNA replication, are detected by the MMR pathway [280,289]. The MMR machinery removes non-complementary bases in three steps. In the first step, mismatches and insertions-deletions-loops are recognized by the MutS homolog 2 (MSH2) complexes leading to the recruitment of MutL homolog 1 (MHL1) alongside other factors. During the second step, the recruited exonuclease 1 (Exo1) removes the altered DNA segment. In the last step, this gap is filled up by DNA polymerase δ and ligated by DNA ligase I. The MMR pathway is associated with DNA replication and limited to the newly synthesized DNA strands [289,292,293].

Intrastrand crosslinks or bulky adducts induced by chemicals or UV-light leading to deformation of the normal helical duplex DNA structure are recognized and resolved by the NER [294]. Here, two NER pathways exist, the global genome NER and the transcription-coupled NER pathway. While a protein complex consisting of Xeroderma Pigmentosum, complementation group C (XPC), UV excision repair protein Radiation sensitive 23B (RAD23B) and Centrin2 (CETN2) scans for ssDNA segments formed by disrupted base pairing in the global-genome NER, the transcription-coupled NER mediated by RNA polymerase II detects modified nucleotides [289,295]. The detection of a damaged DNA site subsequently leads in both pathways to the assembly of further specific repair factors and the recruitment of endonucleases excision repair 1, endonuclease non-catalytic subunit (ERCC1)/ERCC4 and ERCC5, which subsequently cleave 3' and 5' of the modified bases and remove a short DNA fragment of 30 nucleotides. The arisen gap is filled by DNA polymerase δ, ε or κ and the final ligation step is carried out by the XRCC1/DNA ligase III complex or the flap endonuclease 1 (FEN1)/DNA ligase I complex [289,294,295]. Besides these two pathways, there is also the interstrand cross-link repair regulated by the Fanconi anaemia (FA) protein family; and the DPC repair mediated by tyrosyl-DNA phosphodiesterases (TDPs), the MRN complex and spartan (SPRTN) [289,296].

The most severe form of DNA damage is represented by DNA strand breaks, which can occur on only one strand or both strands simultaneously. The SSBs are often a product of oxidative DNA damage or abasic sites, which can also occur during other DNA repair mechanisms, the DNA replication process, and the malfunction of the enzyme topoisomerase I (TOP1) driving the DPC repair [297,298]. These different causes for SSBs are also reflected in the diversity of created SSB ends and can trigger, if remained unrepaired, blocking of transcription and inhibition of chromosome duplication [280]. SSBs arising from BER or disintegration of oxidized deoxyribose are detected by poly ADP-ribose-polymerase-1 (PARP1), which upon binding to DNA leads to the rapid modification with branched poly(ADP-ribose) chains on itself and other proteins [299,300]. After XRCC1 is recruited and interacts with PARP1 and PARP2, the variety of different SSB ends must be processed. This SSB end processing is mediated by several proteins depending on the type of damaged 3' and 5' end and includes polynucleotide kinase/phosphatase (PNKP), DNA polymerase β, APE1 and TDP1, besides others. After the end processing and the restoring of a classical hydroxyl 3' end, the DNA gap is filled by DNA polymerase β and sealed with DNA ligase I or III, similar to BER [289,299,301].

1.7 DNA double-strand break repair

DSBs represent a more severe threat to genome stability and can, for instance, lead to translocations, cancer, various disorders, or activate cell death signalling when left unrepaired [280]. DSBs arise endogenously during replication or by ROS or exogenously through IR or UV light [302]. Some commonly used chemotherapeutics like Doxorubicin or Etoposide also inhibit the cellular topoisomerase I or II activity leading to SSBs or DSBs. Topoisomerases are important for the topological surveillance of the DNA by resolving supercoiled or torsional tension, especially during replication and chromatin remodelling [303]. TOP1 inhibitors trigger SSBs by inhibiting the re-ligation of the cleaved DNA single strands [304]. In contrast, the inhibition of the re-ligation step of TOP2 drives DSBs by trapping TOP2 in a covalently-bound complex with the broken DNA strands [303]. While the chemotherapeutic drugs Doxorubicin and Etoposide inhibit the re-ligation and thus lead to DSBs, other TOP2 inhibitors like Aclarubicin or Merbarone block earlier steps and do not lead to DSBs [305]. On some occasions, DSBs and

the corresponding repair system are induced on purpose, mainly during meiosis and V(D)J recombination to trigger genetic diversity and to increase antibody diversification, respectively [280,306,307]. Two major DSB repair pathways have evolved, the homologous recombination (HR) and the non-homologous end joining (NHEJ). While HR relies on a homologous sister chromatid and therefore only acts during the S and G2 phase, the more error-prone NHEJ is applied independently of the cell cycle and in dividing or non-dividing cells [280]. As research tools, these two DSB repair mechanisms are used for genome editing or knockout generation using the clustered regularly interspaced palindromic repeats (CRISPR)/CRISPR associated protein 9 (Cas9) system[308,309]. Here, the NHEJ repair is used to obtain mutations of the targeted loci due to the error-prone repair and HR repair for creating point mutations by the integration of a co-transfected template oligo. Apart from these two main repair pathways, several minor repair pathways have been described, including single-strand annealing (SSA), alternative end joining (aEJ), microhomology-mediated end joining (MMEJ) and break-induced replication (BIR) [310].

During the G2 and S phase of the cell cycle, DSBs are mainly repaired by HR using the corresponding and intact sister chromatid as a repair template [280]. In HR, several alternative sub-pathways like BIR or synthesis-dependent strand annealing (SDSA) can be engaged during DSB repair [289]. For all these DSB repair pathways, the DSB is detected by the MRN complex, consisting of meiotic recombination 11 (MRE11), Nijmegen breakage syndrome 1 (NBS1) and RAD50 [280,311]. The MRN complex binds to the DSB and recruits the protein kinases ATR (ATM- and Rad3-Related) and ATM, which is named after the associated genetic disorder ataxia-telangiectasia (A-T) [312,313]. ATM interacts with NBS1 through its internal Huntington-elongation factor 3-protein phosphatase 2A-TOR1 (HEAT) repeats, while ATR binds to ATR interacting protein (ATRIP) through its HEAT repeats [314–316]. In humans, ATM and ATR are both inactive in the absence of DNA damage through the interaction of their FAK focal adhesion targeting (FAT) domain with their kinase domain. Upon recruitment to a DSB site and subsequent autophosphorylation of ATM or ATR, the interaction of the FAT domain with the kinase domain is disrupted, and the kinases are activated [313]. Once ATM is activated, it phosphorylates hundreds of targets, triggering the activation of several downstream cascades. This leads, for instance, to the activation of cell-cycle-checkpoint proteins, chromatin-remodelling factors, and DNA repair components, leading to DSB repair and cell cycle arrest [280,313]. The key step for HR cascade and chromatin remodelling is the phosphorylation of histone H2AX. This is initiated within minutes after the DNA damage occurred and propagates over chromatin areas flanking the DSBs [313,317]. Initiation of the HR repair requires resection of the DSB ends mediated by the endonuclease activity of the MRN complex in association with CtBP-interacting protein (CtIP) to form 3'-single-strand overhangs. In the next step, the exonuclease Exo1 together with DNA replication helicase/nuclease 2 (DNA2) mediates long-range resection with replication protein A (RPA) coating the 3'-single-strand overhangs [289]. RPA not only covers the ssDNA but also triggers the activation of ATR through ATRIP [280]. RPA is subsequently replaced by RAD51 mediated by RAD52 and breast cancer-associated gene 2 (BRCA2) [289,318]. RAD51 forms a nucleoprotein filament, which invades a nearby homologous dsDNA creating a D-loop. RAD51 is then removed by RAD54 and RAD54B, allowing the polymerases δ, κ and ν to initiate synthesis at the 3'-OH group [289]. Depending on the formed recombination synapse and the D-loop, different HR subpathways are initiated. While somatic cells, predominantly undergo SDSA, meiotic cells prefer the

formation of a double Holliday junction enabling cross-over. During SDSA, the DNA synthesis stops after a limited distance, the D loop is resolved by regulator of telomere length 1 (RTEL1) and the strands are ligated by DNA ligase I [289]. In case of failures during second strand engagement or nascent strand displacement, two error-prone HR pathways are initiated, the BIR and the long-tract gene conversion (LTGC) [310].

The second main DSB repair pathway, the NHEJ, is independent of end-resection, the presence of a homologous sister chromatid and the cell cycle [280]. Besides their functions during DSB repair, NHEJ proteins also mediate the V(D)J recombination for antibody diversity [306]. The NHEJ repair involves three different steps: the recognition of DSBs, DSB end processing, and the ligation of two suitable ends [280]. In the first step, the Ku70/Ku80 heterodimer detects and encircles the DSB ends to prevent end resection and forms a scaffold for further NHEJ protein recruitment. Subsequently, depending on the severity of the damage, several repair proteins, including DNA PK, SH3 Domain Binding Protein 1 (3BP1), non-homologous end-joining factor 1 (NHEJ1) and XRCC4, are recruited to the damage site [289]. DNA-PK binds to the opposing ends and forms a synaptic complex initiating its autophosphorylation and phosphorylation of other repair proteins [319]. Upon end stabilization and bridging, the endonuclease 'Artemis' with its associated proteins trigger DNA end resection to remove blocking groups and generate 3' and 5' overhangs to find complementary nucleotide sequences [289,320,321]. The remaining gaps are filled by polymerase μ or λ depending on template availability and in the final step ligated by DNA ligase IV [322–324]. Besides the two main DSB repair pathways also several minor pathways like a-EJ, MMEJ, and SSA are able to repair DSBs with different subsets of proteins [310].

1.8   DNA damage and innate immunity

Several human diseases and infections trigger the activation of DDR signalling components and cascades beside the activation of immune signalling pathways [325]. Over the past years, several examples of an interplay between the DDR and immune signalling in this context have been revealed [326]. Damaged DNA can lead to the release of DAMPs or can trigger immune responses induced by immune sensors like PRRs or DDR components. In addition, the innate immune signalling cascades can trigger the activation of DDR signalling components to mediate apoptosis and cell cycle arrest [326]. Here, IFNα/β signalling has been described to mediate the phosphorylation and activation of p53 through ATM during viral infections and tumour suppression in a ROS dependent manner leading to the induction of senescence or apoptosis [327,328].

DNA damage can lead to the activation of cell-autonomous immune responses by engaging PRR pathways. In the context of DNA damage, DNA can be released from the nucleus into the cytoplasm, where it can activate cytosolic PRR sensors, such as cGAS or AIM2. This can occur in the context of micronuclei formation or accumulation of cytosolic DNA [144]. Micronuclei are a result of DNA damage during the mitotic exit and are characterised by endogenous DNA fragments packaged in a nuclear envelope. These structures are highly fragile and rupture during interphase enabling the detection of fragmented dsDNA by cGAS [329–332]. The exact mechanism of micronuclei formation and defects of the micronuclei membrane leading to their rupture are not well understood yet [333,334]. In addition, nuclear DNA fragments or chromatin structures have been described to be released or even exported to the

cytosol during DNA damage or replication stress leading to increased cytosolic DNA. Cytosolic DNA subsequently triggers the activation of cGAS-STING or AIM2 signalling [335–338].

On the other hand, several DDR components themselves have been described to trigger cell-autonomous immune responses. In this context, the two NHEJ components Ku70 and DNA PK have been described to sense cytosolic DNA leading to the activation of IRF transcription factors and subsequent induction of an antiviral immune response by an unknown mechanism [339–341]. In addition, the MRN complex member RAD50 has been reported to form dsDNA-CARD9-RAD50 complexes upon DNA transfection or viral infections in the cytosol triggering NF-κB activation and pro-IL-1β induction [342]. Moreover, ATM, the main effector kinase of the HR repair pathway, has been shown to trigger NF-κB activation and type I IFN induction upon DNA damage by different signalling cascades depending on the cell type and the severity of the genotoxic stress [326,343,344]. For instance, ATM has been determined to mediate STING activation independent of cGAS through a complex containing IFI16, p53, PARP1, and TRAF6 in keratinocytes upon treatment with the TOP2 inhibitor Etoposide [345]. Additionally, the treatment of human macrophages with TOP2 inhibitors like Doxorubicin has been described to trigger the activation of type I IFN signalling and ISG production in an ATM-dependent manner [346]. This induction of type I IFN signalling is independent of nucleic-acid sensing PRRs and their adaptor proteins [346]. However, the exact mechanism of signal transduction could not be revealed.

Besides the activation of cell-autonomous immune signalling, DNA damage also mediates the induction of immune cascades in bystander cells through the release of DNA, DAMPs and alarmins. For example, the treatment of cells with UV-light or IR leads to the induction of several kinds of DNA damage and triggers immune responses in neighbouring cells. In this context, it has been reported that epidermal keratinocytes exposed to UV-light mediate the release of DAMPs like high mobility group box 1 (HMGB1), leading to the activation of inflammatory immune responses and triggering TRL4 signalling and recruitment of neutrophils [347]. In addition, DDR components can induce cell death leading to the release of DNA in the event of severe DNA damage. In this context, dead cells and extranuclear DNA can be engulfed, for instance, by macrophages and trigger the activation of cGAS-STING signalling in case of a perturbed phagocytic digestion [144,335,348].

The induction of innate immune responses upon DNA damage by PRRs or DDR components is important for several processes like tissue homeostasis, senescence, and direct or indirect recognition of pathogens. For tissue homeostasis, cells in an apoptotic or senescent state caused by persistent DNA damage need to be cleared by immune cells [349]. Here, for instance, the detection of DNA damage has been reported to mediate the recruitment of NK cells by the activation of natural killer group 2 member (NKG2D) and DNAX Accessory Molecule-1 (DNAM-1) in an ATM and ATR dependent manner [350,351]. In addition, the activation of a main DDR downstream effector and tumour suppressor, p53, initiates a cellular senescence program, the senescence-associated secretory phenotype (SASP), leading to the upregulation of inflammatory cytokine expression and the recruitment of immune cells [352–354]. This removal of apoptotic or senescent cells by the immune system is also used during tumour clearance. Besides the removal of apoptotic and senescent cells, interplays between the DDR and the immune signalling cascades are also beneficial for the detection of pathogens. DDR components can either directly detect pathogens by sensing foreign DNA structures or indirectly by effector-triggered immunity through the activation and production of cytokines upon pathogen-induced DNA damage [326].

1.9   BLaER1 transdifferentiation system and SMRV

Macrophages are relatively long-lived immune cells with different functions, resident in almost all tissues [7]. They emerge during embryonic development from either progenitor cells or at later points from circulating monocytes [7]. As one of the major phagocytic cell types, macrophages engulf and destroy invading pathogens in the early phase of infections and maintain tissue homeostasis. Moreover, macrophages orchestrate immune responses following infections by the production of pro-inflammatory cytokines, chemokines and interferons. Macrophages also serve as antigen-presenting cells, therefore, contributing to the activation of the adaptive immune response [7]. Due to their important functions in cytokine expression and clearing of pathogens, the investigation of macrophages and monocytes is of great interest for the further understanding of the innate immune system. Hence, most experiments are conducted using primary murine or human macrophages isolated from mouse or human blood, respectively, and subjected to genetic modifications. However, when large numbers of cells are required, 'immortalised' cell lines, e.g. THP-1 and U937 cells, are used to act as *in vitro* models for primary myeloid cells [355]. A recently described model to study human macrophages is the BLaER1 transdifferentiation system [356]. Here, B-cells containing a fusion of C/EBPα with an estrogen receptor hormone-binding domain can be cultivated in suspension or genetically modified using the CRISPR/Cas9 system. These cells are transdifferentiated into monocytes and macrophages using β-estradiol, human IL-3 and M-CSF, enabling the investigation of immune signalling cascades [357]. However, during the routine evaluation of BLaER1 supernatant for reverse transcriptase (RT) activity coupled to RNAseq data analysis, it was discovered that the cell line is infected with the squirrel monkey retrovirus (SMRV). The infection originated from the originally described parental cell line. In subsequent studies, SMRV infected BLaER1 cells were compared to other human myeloid cell lines and primary myeloid cells and no difference was observed in their response to different immunostimulatory treatments.

SMRV is a simian type D beta-retrovirus, first isolated from *Saimiri sciureus* (common squirrel monkey) and described in 1977 [358,359]. Beta-retroviruses exist in endogenous or exogenous forms [360]. Type D retroviruses represent a group of viruses, which are closely related to the Mason-Pfizer monkey virus (MPMV) and can cause an infectious immunodeficiency disease in certain macaque species [361]. Besides its prevalence in Old and New World monkeys, several infections with type D retroviruses of human cell lines were observed due to contaminations [361,362]. SMRV enters the cell over a yet unknown receptor [358]. To integrate into the host genome, the virus utilises Mg^{2+}-dependent reverse transcriptases (RT) and integrases [359]. Several publications identified contaminations with SMRV in cell lines like RPMI-8226, HLB and Namalwa [363]. In the Namalwa cell line, twelve integration sites of SMRV have been described [364]. SMRV, however, still remains poorly characterised, and its presence in cell lines, infectiousness and integration site preferences need to be further clarified.

2 Aim of the thesis

The recognition of pathogens during infections is crucial for the survival of the organism, however, also damaged DNA needs to be identified and repaired to protect the genomic integrity of cells. In recent years, several links between the DNA damage repair systems and the innate immune signalling cascades were identified. DNA damage has been shown to trigger PRR activation and innate immune signalling by the formation of micronuclei, the release of nucleic acid into the cytosol or the release of DAMPs like HMGB1 [347,365]. Several DDR repair proteins have also been described to mediate immune responses themselves by acting as sensors for DNA in the cytosol with varying effects in different tissues and cell lines. One of the most severe forms of DNA damage is represented by DSBs, leading to the activation of several different pathways. Besides the activation of repair and cell cycle arrest cascades, also an immune response is triggered, leading to type I IFN production. Since macrophages are important producers of cytokines during infections and modulate the innate and adaptive immune response, their role in sensing damaged self-DNA arising from viral integration, drug treatment, irradiation or ROS is important for a better understanding of the link between DNA damage and immune responses. Our lab previously revealed a considerable antiviral immune response in macrophages treated with chemotherapeutic drugs like the TOP2 inhibitor Doxorubicin leading to the formation of DSBs. This response was independent of any known PRR pathway yet dependent on the DDR sensor ATM. Since the IRF transcription factor family is crucial for type I IFN induction, also the role of several IRF molecules was already tested within this signalling cascade. However, their role in DSBs-mediated induction of type I IFN signalling downstream of ATM has remained elusive.

This study was conducted to dissect the mechanisms linking DSBs induced by chemotherapeutic drugs in human macrophages to type I IFN responses. To do so, I employed a hypothesis-driven knockout approach, in which the BLaER1 transdifferentiation system was mainly used to discover relevant protein components downstream of DNA damage. Further, given the serendipitous identification of BLaER1 cells being positive for the squirrel monkey retrovirus (SMRV), a BLaER1 cell line deficient for SMRV was generated and characterized.

3 Material and Methods

3.1 Material

All consumables used for sterile and non-sterile laboratory work were purchased from the following manufacturers: Bioplastic, Biorad, Biozym, Corning, Epoch Life Science, Greiner, Labomedic, Neolab, Sarstedt and VWR.

Whatmann Cellulose Blotting Papers, Grade GB005 and Amersham Protran 0.2 and 0.45 NC nitrocellulose Western blotting membranes came from GE Healthcare. All Novex^{TM} Tris-Glycine gels used (10 % and 12 % with 12 or 15-wells) were supplied by ThermoFisher Scientific.

3.1.1 Chemicals and reagents

Chemical/Reagent	Supplier
6x DNA Loading Dye	ThermoFisher Scientific
Acetic acid	Roth
Agarose powder	Biozym
Bromophenol blue	Roth
BSA	Roth
BSA (100 %)	New England BioLabs
$CaCl_2$	Roth
cOmplete^{TM} Protease Inhibitor Cocktail	Roche
DMSO	Roth
Gene Ruler DNA ladder (100 bp/1 kb)	ThermoFisher Scientific
DTT	Roth
EDTA (powder)	Roth
Ethanol	Roth
Glycerol	Roth
Glycine	Roth
Guanidine hydrochloride	Sigma-Aldrich
H_2O	Braun
HCl	Roth
IGEPAL	Sigma-Aldrich
Isopropanol	Roth
KCl	Roth
KH_2PO_4	Roth
LB	Roth
LB agar	Roth
Luminata Forte Western HRP substrate	Merck

MgCl$_2$	Roth
Milk powder	Roth
MS2 RNA	Sigma-Aldrich
Na$_2$CO$_3$	Roth
NaH$_2$PO$_4$	Roth
NaHCO$_3$	Roth
NaCl	Roth
NaN$_3$	Sigma-Aldrich
NaOH	Roth
(NH$_4$)$_2$SO$_4$	Roth
Novex^{TM} Tris-Glycine SDS Running buffer (10x)	Invitrogen
Nuclease-Free water	ThermoFisher Scientific
PageRuler^{TM} Prestained Protein Ladder	ThermoFisher Scientific
PEG8000	Sigma-Aldrich
PhosSTOP Phosphatase Inhibitors	Roche
Pierce ECL WB substrate	ThermoFisher Scientific
Ponceau S staining	Sigma-Aldrich
Potassium acetate	Roth
RLT buffer	Qiagen
RNase A	Life Technologies
SDS	Roth
Sodium acetate	Roth
Sodium deoxycholate	Sigma-Aldrich
SYBR^{TM} Green I Nucleic Acid Gel Stain 10000x	Invitrogen
SYBR® Safe DNA Gel Stain	ThermoFisher Scientific
Tris	Roth
Triton X 100	Roth
Tween 20	Roth

3.1.2 Enzymes and enzyme buffers

Enzyme/Buffer	Supplier
10x Fast Digest Green buffer	ThermoFisher Scientific
5x Phusion HF/GC buffer	ThermoFisher Scientific
CutSmart buffer (10x)	New England BioLabs
DNAse I	ThermoFisher Scientific
DNAse I buffer + MgCl$_2$ (10x)	ThermoFisher Scientific

dNTPs	ThermoFisher Scientific
FastAP (Alkaline phosphatase)	ThermoFisher Scientific
FastDigest restriction enzymes	ThermoFisher Scientific
FastDigest buffer (10x)	ThermoFisher Scientific
GoTaq DNA Polymerase	Promega
MseI	New England BioLabs
Phusion High-Fidelity DNA Polymerase (2 U/µl)	ThermoFisher Scientific
PowerUp Sybr Master Mix	ThermoFisher Scientific
Proteinase K	VWR
RevertAid Reverse Transcriptase (200 U/µl)	ThermoFisher Scientific
RiboLock RNase Inhibitor (40 U/µl)	ThermoFisher Scientific
RT buffer (5x)	ThermoFisher Scientific
T4 DNA ligase buffer (10x)	ThermoFisher Scientific
T4 DNA ligase	ThermoFisher Scientific

3.1.3 Kits

Kit	Supplier
Pierce^{TM} BCA Protein Assay kit	ThermoFisher Scientific
ELISA IP-10/IL-6	B&D Biosciences
MiSeq Reagent Kit v2 (300 cycles)	Illumina
PureLink HiPure Plasmid Filter Maxiprep Kit	Invitrogen
QIAamp DNA mini kit	Qiagen
QIAprep Spin Miniprep kit	Qiagen
QIAquick Gel Extraction kit	Qiagen
QIAquick PCR purification kit	Qiagen
Total RNA Purification Mini Spin kit	Genaxxon

3.1.4 Buffers and Solutions

All buffers and solutions were prepared with dH$_2$O, if not stated otherwise.

Buffer/Solution	Components
Coating buffer	0.1 M sodium carbonate/NaOH pH 9.5 7.13 g/l NaHCO$_3$ 1.59 g/l Na$_2$CO$_3$
Direct lysis buffer	10 mM Tris pH 7.5 3 mM MgCl$_2$ 1 mM EDTA 1 mM CaCl$_2$ 1 % (v/v) Triton X 100

	0.2 mg/ml Proteinase K
DISC buffer	30 mM Tris/HCl pH 7.5
	150 mM NaCl
	1 % (v/v) Triton X 100
	10 % (v/v) glycerol
	+ protease/phosphatase inhibitors
ELISA buffer	10 % (v/v) FCS in PBS
Freezing medium	10 % (v/v) DMSO
	in culture medium
Laemmli buffer (2x)	150 mM Tris/HCl pH 6.8
	200 mM DTT
	4 % (w/v) SDS
	0.02 % (v/v) bromophenol blue
	20 % (v/v) glycerol
Laemmli buffer (6x)	450 mM Tris/HCl pH 6.8
	600 mM DTT
	12 % SDS
	> 0.06 % bromophenol blue
	60 % glycerol
LB agar	20 g LB
	15 g Agar
	In 1 l H_2O
	Autoclaved before use
LB medium	20 g LB
	In 1 l H_2O
	Autoclaved before use
MACS buffer	0.5 % FCS
	2 mM EDTA
	in PBS
Miniprep buffer N3	4.2 M guanidine hydrochloride
	0.9 M potassium acetate
	pH = 4.8
Miniprep buffer P1	50 mM Tris pH = 8,0
	10 mM EDTA
	100 µg/ml RNase A
Miniprep buffer P2	200 mM NaOH
	1 % SDS
Miniprep buffer PE	10 mM Tris pH = 7,5
	80 % ethanol
PBS (10x, pH 7.4)	1.37 M NaCl
	26.8 mM KCl
	78.1 mM $Na_2HPO_4 \cdot 7\ H_2O$
	14.7 mM KH_2PO_4
PBS-T	100 ml 10x PBS
	500 µl Tween 20
	900 ml H_2O

10x PCR/dilution buffer	200 mM Tris/HCl (pH 8.3)
	200 mM KCl
	50 mM $(NH_4)_2SO_4$
2x Reaction buffer	1 ml 10x PCR/dilution buffer
	200 µl 100 % BSA
	1 µl 10000x SYBR Green
	10 mM $MgCl_2$
	400 µM each dNTP
	400 µl RT_Assay_fwd primer (50 µM)
	400 µl RT_Assay_rev primer (50 µM)
	1.5 µl MS2 RNA
	added up with dH_2O to 10 ml
RIPA buffer	50 mM Tris/HCl pH 8.0
	150 mM NaCl
	0.1 % (w/v) SDS
	1 % (v/v) Triton X 100
	0.5 % (w/v) sodium deoxycholate
	(+ protease and phosphatase inhibitors)
SG-PERT lysis buffer (2x)	100 mM Tris/HCl (pH 7.4)
	50 mM KCl
	40 % glycerol
	1 % Triton X 100
SPRI beads (22 % PEG)	1 M NaCl
	10 mM Tris/HCl (pH 8.0)
	1 mM EDTA
	22 % PEG8000
	0.01 % IGEPAL
	0.05 % NaN_3
	1 ml SPRI beads
	added up with dH_2O to 49 ml
TAE (50x)	2 M Tris
	68.025 g/l sodium acetate
	50 mM EDTA
	1 M acetic acid
TBS (10x)	1.5 M NaCl
	100 mM Tris pH 8.0
TBS-T	100 ml TBS (10x)
	1 ml Tween 20
	899 ml dH_2O
Tris-glycine buffer (10x)	250 mM Tris
	1.92 M glycine
Transfer buffer	100 ml Tris-glycine buffer (10x)
	200 ml ethanol
	700 ml H_2O
Western blot blocking buffer I	5 % (w/v) milk in PBS-T
Western blot blocking buffer II	5 % (w/v) BSA in TBS-T

3.1.5 Cell culture medium and reagents

Regent/medium	Supplier
Bovine pituitary extract (BPE)	ThermoFisher Scientific
Calcium chloride (CaCl$_2$)	Sigma-Aldrich
Deoxyribonucleic acid sodium salt from herring testes (HT DNA)	Sigma-Aldrich
DMEM with glutamine	Gibco
Doxorubicin	Sigma-Aldrich
DPBS	Gibco
EDTA (0.5 M, pH = 8)	Life Technologies
Epidermal growth factor (EGF)	MPI of Biochemistry, Martinsried
EpiLife defined growth supplement	ThermoFisher Scientific
Etoposide	Sigma-Aldrich
FCS	Gibco
GlutaMAX	ThermoFisher Scientific
Ham F12 medium	ThermoFisher Scientific
HEPES	Sigma-Aldrich
hIL-3	Peprotech
hM-CSF	Peprotech
IFNα	Miltenyi Biotec
Lipofectamine 2000	ThermoFisher Scientific
Lipopolysaccharide (LPS-EB ultrapure)	Invivogen
MDP	Invivogen
Non-essential amino acids	ThermoFisher Scientific
OptiMEM	Gibco
Penicillin/Streptomycin	Gibco
PMA (phorbol 12-myristate 13-acetate)	Enzo Life Sciences
R848 (Resiquimod)	Invivogen
RPMI-1640	Gibco
Sodium pyruvate (100x)	Gibco
Trypan Blue	Gibco
Trypsin EDTA	ThermoFisher Scientific
β-estradiol	Sigma-Aldrich

3.1.6 Western Blot Antibodies

Antibodies	Supplier	Organism	Dilution
α-rabbit IgG, HRP linked	Cell Signaling Technology	goat	1:3000
α-mouse IgG, HRP linked	Cell Signaling Technology	goat	1:3000
ATM	Cell Signaling Technology	rabbit	1:1000
IKKα	Cell Signaling Technology	rabbit	1:1000
IKKβ	Cell Signaling Technology	rabbit	1:1000
IRF1	Cell Signaling Technology	rabbit	1:1000
IRF4	Cell Signaling Technology	rabbit	1:1000
Phospho-JNK	Cell Signaling Technology	mouse	1:1000
NEMO (IKKγ)	Cell Signaling Technology	rabbit	1:1000
Phospho-p38	Cell Signaling Technology	rabbit	1:1000
STAT1	Cell Signaling Technology	mouse	1:1000
Phospho-STAT1	Cell Signaling Technology	rabbit	1:1000
TAK1	Cell Signaling Technology	rabbit	1:1000
TRAF3	Cell Signaling Technology	rabbit	1:1000
TRAF6	Cell Signaling Technology	rabbit	1:1000
β-Actin, HRP linked	Santa Cruz Biotechnology	mouse	1:3000

3.1.7 Primers

Name	Sequence (5' → 3')	Application
GAPDH_fwd	CTTTGTCAAGCTCATTTCCTGG	RT-qPCR
GAPDH_rev	TCTTCCTCTTGTGCTCTTGC	RT-qPCR
IFNβ_fwd	GGCACAACAGGTAGTAGGCG	RT-qPCR
IFNβ_rev	GTGGAGAAGCACAACAGGAGA	RT-qPCR
ATM_fwd	ACACTCTTTCCCTACACGACGctcttccgatctGGAAATCTAATGGAGGTGGAGGA	Genotyping
ATM_rev	TGACTGGAGTTCAGACGTGTGctcttccgatctGGAACAATCCTAAAAGGCTATAC	Genotyping
CGAS_fwd	ACACTCTTTCCCTACACGACGctcttccgatctCTTTTTGGCGCGGGCCCCAGTTG	Genotyping
CGAS_rev	TGACTGGAGTTCAGACGTGTGctcttccgatctAAGGCCATGCAGAGAGCTTCCGA	Genotyping
CHUK_fwd	ACACTCTTTCCCTACACGACGctcttccgatctGCAAAGACACCAAAGCTCAAGGA	Genotyping
CHUK_rev	TGACTGGAGTTCAGACGTGTGctcttccgatctGAGCATCAGAGTAGATTTGTACA	Genotyping
ERC1_fwd	ACACTCTTTCCCTACACGACGctcttccgatctATACTCACAGGAGGGAGGTGATG	Genotyping
ERC1_rev	TGACTGGAGTTCAGACGTGTGctcttccgatctGTGGCAGTGGGAAAACCCTTTCA	Genotyping
FOS_fwd	ACACTCTTTCCCTACACGACGctcttccgatctCCCTACTCATCTACTGGAGCGTC	Genotyping
FOS_rev	TGACTGGAGTTCAGACGTGTGctcttccgatctTTTGCCTAACCGCCACGATGATG	Genotyping
IFI16_fwd	ACACTCTTTCCCTACACGACGctcttccgatctTGCTTGTGGAGGGTGCAGGTGAA	Genotyping
IFI16_rev	TGACTGGAGTTCAGACGTGTGctcttccgatctGTCTTGTGACTGCTGGTCTCCTT	Genotyping
IKBKB_fwd	ACACTCTTTCCCTACACGACGctcttccgatctTTCAGGGGCATGCGGCATTTATC	Genotyping
IKBKB_rev	TGACTGGAGTTCAGACGTGTGctcttccgatctATGCAGAGTGTGCTCCTTTCCTC	Genotyping
IKBKG_fwd	ACACTCTTTCCCTACACGACGctcttccgatctAGATCAGGACGTACTGGGCGAAG	Genotyping

IKBKG_rev	TGACTGGAGTTCAGACGTGTGctcttccgatctTACTTCCTGAAACCAAGAGGGAG	Genotyping
IRF1_fwd	ACACTCTTTCCCTACACGACGctcttccgatctAGGTGAGGGGAGGGTAACTAAG	Genotyping
IRF1_rev	TGACTGGAGTTCAGACGTGTGctcttccgatctCCCTCCAGAAGTACATGGGTTA	Genotyping
IRF3_fwd	ACACTCTTTCCCTACACGACGctcttccgatctCTGGTCCATATGAAGTCTCCAGA	Genotyping
IRF3_rev	TGACTGGAGTTCAGACGTGTGctcttccgatctCAACAGCCGCTTCAGTGGGTTCT	Genotyping
IRF4_fwd	ACACTCTTTCCCTACACGACGctcttccgatctTTGTAGTCCTGCTTGCCCGCGTG	Genotyping
IRF4_rev	TGACTGGAGTTCAGACGTGTGctcttccgatctAGCTCTTCTCCCCGCAGTGCAGA	Genotyping
IRF5_fwd	ACACTCTTTCCCTACACGACGctcttccgatctAGCTTGACCTCTGAGTACCCTGT	Genotyping
IRF5_rev	TGACTGGAGTTCAGACGTGTGctcttccgatctTGTTATCTCCGTCCTGGCTGGGA	Genotyping
IRF7_fwd	ACACTCTTTCCCTACACGACGctcttccgatctTGCTTCCAGGGCACGCGGAAACA	Genotyping
IRF7_rev	TGACTGGAGTTCAGACGTGTGctcttccgatctTAACACCTGACCGCCACCTAACT	Genotyping
JUN_fwd	ACACTCTTTCCCTACACGACGctcttccgatctCCTTCTATGACGATGCCCTCAAC	Genotyping
JUN_rev	TGACTGGAGTTCAGACGTGTGctcttccgatctCCCGTTGCTGGACTGGATTATCA	Genotyping
LIColigo18mer	ggaaaggacgaaacaccgnnnnnnnnnnnnnnnnnngttttagagctagaaatagcaagttaaaataagg	LIC cloning
LIColigo20mer	ggaaaggacgaaacaccgnnnnnnnnnnnnnnnnnnnngttttagagctagaaatagcaagttaaaataagg	LIC cloning
LICsgRNA_rev	aacggactagccttattttaacttgctatttctagctctaaaac	LIC cloning
MAP2K3_fwd	ACACTCTTTCCCTACACGACGctcttccgatctAGCTCTACCCGCTCGTCAGGTGA	Genotyping
MAP2K3_rev	TGACTGGAGTTCAGACGTGTGctcttccgatctTAGATGCTCAGCAGCCAGTGAGA	Genotyping
MAP2K4_fwd	ACACTCTTTCCCTACACGACGctcttccgatctTCGGCTCTTCACTCCCAACAATG	Genotyping
MAP2K4_rev	TGACTGGAGTTCAGACGTGTGctcttccgatctTGCCGTGGCTTCCTCAGCCGGGT	Genotyping
MAP2K6_fwd	ACACTCTTTCCCTACACGACGctcttccgatctCTGGTTGACAATTGAGGTGGACA	Genotyping
MAP2K6_rev	TGACTGGAGTTCAGACGTGTGctcttccgatctACGAGATAGAGGATAATGTGCTC	Genotyping
MAP3K3_fwd	ACACTCTTTCCCTACACGACGctcttccgatctAAAGTCGAAGCAGAGCCACCTGA	Genotyping
MAP3K3_rev	TGACTGGAGTTCAGACGTGTGctcttccgatctAAATCTGCTTCCCCCACCTAATG	Genotyping
MAP3K7_fwd	ACACTCTTTCCCTACACGACGctcttccgatctGTGCTTGCATTCACATTGTGTCT	Genotyping
MAP3K7_rev	TGACTGGAGTTCAGACGTGTGctcttccgatctGTGAGAGTGAGAGAGAAGGAGGA	Genotyping
MAPK8_fwd	ACACTCTTTCCCTACACGACGctcttccgatctTTGTAGCCCATGCCAAGGATGAC	Genotyping
MAPK8_rev	TGACTGGAGTTCAGACGTGTGctcttccgatctCATGAATGTTTTGCAAGGGATAG	Genotyping
MAPK9_fwd	ACACTCTTTCCCTACACGACGctcttccgatctTGAATTATACCAGCTGAATGCAG	Genotyping
MAPK9_rev	TGACTGGAGTTCAGACGTGTGctcttccgatctCCAGTGCAGTGATTGGAAGTAAG	Genotyping
MAPK14_fwd	ACACTCTTTCCCTACACGACGctcttccgatctGGCCCCACAGGGCCACCTTCTTG	Genotyping
MAPK14_rev	TGACTGGAGTTCAGACGTGTGctcttccgatctAAATTCCTGCCACTTGACGCAAC	Genotyping
MRE11A_fwd	ACACTCTTTCCCTACACGACGctcttccgatctATGAAAGCTTTCGTTTGCACATC	Genotyping
MRE11A_rev	TGACTGGAGTTCAGACGTGTGctcttccgatctCAGAAGCTTTGTATGGCTTGGGT	Genotyping
NBN_fwd	ACACTCTTTCCCTACACGACGctcttccgatctACAGATGAAATCCCTGTATTGAC	Genotyping
NBN_rev	TGACTGGAGTTCAGACGTGTGctcttccgatctCCAATACTGTGCTAAGCAGGAAC	Genotyping
Oligo dT	TTTTTTTTTTTTTTTTTTTVN	cDNA
RAD50_fwd	ACACTCTTTCCCTACACGACGctcttccgatctTCAGCCATGTAAGCTATAGTGAG	Genotyping
RAD50_rev	TGACTGGAGTTCAGACGTGTGctcttccgatctATGTGGATGGCAAAATGGATTCA	Genotyping
RELA_fwd	ACACTCTTTCCCTACACGACGctcttccgatctTAATGGGGCTGCGGTGTCCCCTG	Genotyping
RELA_rev	TGACTGGAGTTCAGACGTGTGctcttccgatctCAGACATCCAAACCTGACTCCCA	Genotyping
RELB_fwd	ACACTCTTTCCCTACACGACGctcttccgatctGTGGGGCTTCCTTGGGATATTCT	Genotyping
RELB_rev	TGACTGGAGTTCAGACGTGTGctcttccgatctTGTCAGGAGAAAGCTGAGGTGGA	Genotyping
RPS6KA4_fwd	ACACTCTTTCCCTACACGACGctcttccgatctAAGAGTGAGCAGGCAGGAGGTCA	Genotyping
RPS6KA4_rev	TGACTGGAGTTCAGACGTGTGctcttccgatctTGGAGCTGCGGATCACAGAAGGT	Genotyping
RPS6KA5_fwd	ACACTCTTTCCCTACACGACGctcttccgatctTGTCACTTGTCATACTAGCTTGA	Genotyping

RPS6KA5_rev	TGACTGGAGTTCAGACGTGTGctcttccgatctCAATCAACACCAGAAAGACGGCT	Genotyping
RT_Assay_fwd	TCCTGCTCAACTTCCTGTCGAG	SG-PERT
RT_Assay_rev	CACAGGTCAAACCTCCTAGGAATG	SG-PERT
SMRV_env_fwd	GGCGGACCCCAAGATGCTGTG	SMRV test
SMRV_env_rev	TGGGCTAGGCTGGGGTTGGAGATA	SMRV test
SMRV_gag_fwd	TCAGAGCCCACCGAGCCTACCTAC	SMRV test
SMRV_gag_rev	CAGCGCAGCACGAGACAAGAAAA	SMRV test
SMRV_IVPin1	CATGTCTTGCCCGTGATCAG	Inverse PCR
SMRV_IVPin2	GTTCCCAACATCTCCTCCCT	Inverse PCR
SMRV_IVPout1	CCCGCTCCCCTCCCTATATA	Inverse PCR
SMRV_IVPout2	AGCTAAACACTCGTCTCCCA	Inverse PCR
STING1_fwd	ACACTCTTTCCCTACACGACGctcttccgatctTTCTACCTCCCCCTGTGTCATAC	Genotyping
STING1_rev	TGACTGGAGTTCAGACGTGTGctcttccgatctGTCTGGCTGTCACTCACAGGTAC	Genotyping
TAB1_fwd	ACACTCTTTCCCTACACGACGctcttccgatctTGTCGGCTGGGGAAATTACCTCT	Genotyping
TAB1_rev	TGACTGGAGTTCAGACGTGTGctcttccgatctAGGCAGGACTGACATGTGGAAAG	Genotyping
TRAF3_fwd	ACACTCTTTCCCTACACGACGctcttccgatctTCCCAATTAAGAACATTGAATGG	Genotyping
TRAF3_rev	TGACTGGAGTTCAGACGTGTGctcttccgatctGCCTGTGGAATGGGAGGAC	Genotyping
TRAF6_fwd	ACACTCTTTCCCTACACGACGctcttccgatctAGGGGTGGGTCAAACTCTACATC	Genotyping
TRAF6_rev	TGACTGGAGTTCAGACGTGTGctcttccgatctGGGGTGTGAGTGTGTGTGTTACT	Genotyping

3.1.8 Plasmids

Plasmid name	Application
pMini_U6_gRNA_CMV_BFP_T2A_Cas9	Knockout generation
pMini_U6_gRNA_CMV_mCherry_T2A_Cas9	Knockout generation
pRz_CMV_BFP_T2A_Cas9	Knockout generation
pLK0.1_gRNA_CMV_GFP	Knockout generation

3.1.9 sgRNAs

sgRNA oligos are composed of the LIColigo18mer or LIColigo20mer (listed in section 3.1.7) and the target sequence without the PAM sequence and their first nucleotide. The target sequence part in the LIColigomers is indicated by Ns. The PAM sequence is highlighted in bold in the following table.

Target gene	Target sequence (5' → 3')
ATM	GGAGAGAGCCAAAGTACCAT**AGG**
CGAS	GGCGCCCCTGGCATTCCGTG**CGG**
CHUK	TAGTTTAGTAGTAGAACCCA**TGG**
ERC1	GCAGTCATCCGAACACCGTA**AGG**
FOS	GGGCTCGCCTGTCAACGCGC**AGG**
IFI16	GACCAGCCCTATCAAGAAAG**AGG**
IKBKB	GAACCGAGAGCGGTGGTGCC**TGG**
IKBKG	GAGGAGAATCAAGAGCTCCG**AGG**
IRF1	CTCATGCGCATCCGAGTGAT**GGG**
IRF3	GGGGGTCCCGGATCTGGGAG**TGG**
IRF4	CTGATCGACCAGATCGACAG**CGG**
IRF5	GGGCTTCAGCCGCACGCGGC**GGG**
IRF7	GCAGCCCCACGCGTGCTGTT**CGG**

JUN	GGCTCCCCACTGGGTCGGCC**AGG**
MAP2K3	TCCGGGAGTCCAGGTTCCGG**GGG**
MAP2K4	GCCTGGCGCCGGGGACCCTA**CGG**
MAP2K6	GGGACGAGGTGCGTACGGGG**TGG**
MAP3K3	GGACATTCGTGATTTCCGGA**AGG**
MAP3K7	GTAAACACCAACTCATTGCG**TGG**
MAPK8	GAAGATTCTTGACTTCGGTC**TGG**
MAPK9	AATGGATGCTAACTTATGTC**AGG**
MAPK14	GACAGGTTCTGGTAACGCTC**GGG**
MRE11A	GTTTGCTGCGTATTAAAGGG**AGG**
NBN	TTCCCGAACTTTGAAGTCGG**GGG**
RAD50	GGATAGCCGAAAGAAGCAAA**TGG**
RELA	GCGCTTCCGCTACAAGTGCG**AGG**
RELB	GGAAACGGCGAGCGAGAGTG**AGG**
RPS6KA4	GCTCACCTTCTCCTCGTGCC**CGG**
RPS6KA5	GGCACCAGATATTGTCAGAG**GGG**
STING1	GCGGGCCGACCGCATTTGGG**AGG**
TAB1	GCTCCTCTCCACCACATCGA**AGG**
TRAF3	GGAGAAGGCGTGTAAATACC**GGG**
TRAF6	ATCTTTTGTTACAGCGCTAC**AGG**

3.1.10 Laboratory equipment

Instrument	Company
Biomek FXp liquid handler	Beckman Coulter
BD FACS Melody Cell Sorter	BD Biosciences
C1000 Touch Thermal Cycler	Bio-Rad
ChemiDoc Imaging system	Bio-Rad
CFX384 Touch Real-Time PCR Detection System	Bio-Rad
CFX96 Touch Real-Time PCR Detection System	Bio-Rad
Centrifuge 5420/5430	Eppendorf
Centrifuge 5810	Eppendorf
Epoch Microplate Spectrophotometer	BioTek
Fusion SL	Vilber Lourmat
Gene Pulser Xcell	Bio-Rad
HydroSpeed Microplate Washer	TECAN
MACS-Separators	Miltenyi Biotec
Mini Gel Tank	ThermoFisher Scientific
Mini Trans-Blot	Bio-Rad
NanoDrop	Peqlab
SH800S Cell Sorter	Sony
Spark 20m multimode Reader	TECAN
TC-20 Automated Cell Counter	Bio-Rad
Thermomixer C	Eppendorf
ThermoStat Plus	Eppendorf

3.1.11 Software

Software	Source
Biomek Software V5.0	Beckman Coulter
Illustrator	Adobe Creative Cloud
Gen5	BioTek
Prism 9.0.0	GraphPad
NanoDrop 1000 3.8.1	ThermoFisher Scientific
OutKnocker	GNU general public license
Pymol	Schrödinger
R 3.2.3	R Foundation for Statistical Computing
SPARK	TECAN
Snapgene 5.2	GSL Biotech
FUSION	Vilber

3.2   Cell biological methods

3.2.1   Cell lines

The following cell lines were used:

- BLaER1 (SCC165): a subclone of a human B-cell lymphoma cell line expressing C/EBPα for transdifferentiation into human monocytes [356]
- N/TERT-1 (RRID:CVCL_CW92/from J. Rheinwald): human telomerase immortalized keratinocyte cell line
- THP-1 (ATCCR TIB-202™): human monocytic cell line obtained from a patient with acute monocytic leukemia [366]
- HEK293T (ATCCRCRL-3216™): human embryonal kidney cell line stably expressing SV40 large antigen
- J774 (ATCCRTIB-67™): mouse macrophage cell line from ascites

3.2.2   Cell culture conditions

All cells were cultivated at 37 °C, 95 % humidity and 5 % CO_2. For THP-1 cells and BLaER1 cells RPMI1640 medium containing 10 % (v/v) FCS, 1 mM sodium pyruvate and 1 % (v/v) Penicillin/Streptomycin (5000 U/ml) (RPMI culture medium) was used. Both suspension cell lines were split after reaching a density of 1-2x 10^6 cells/ml by exchanging 90 % of the medium. HEK293T cells and J774 cells were cultured in DMEM medium containing 10 % (v/v) FCS, 1 mM sodium pyruvate and 1 % (v/v) Penicillin/Streptomycin (5000 U/ml) (DMEM culture medium). For splitting the two adherent cell lines, the medium was removed after reaching a confluence of 80 %. Cells were washed with PBS and detached from the surface with 2 mM EDTA in PBS (5 min, room temperature). Cells were spun down at 500 g for 5 min, the supernatant was discarded, and the cell pellet resuspended in 10 ml of DMEM culture medium. 1 ml was transferred back to the original culture plate or flask and topped up with 9 ml DMEM culture medium. N/TERT1 cells were cultured in 1:2 mix of Ham F12 and DMEM medium containing 1 % non-essential amino acids, 0.5 % EpiLife defined growth supplement, 25 µg/ml BPE, 20 ng/ml EGF, 10 mM

HEPES, 2 mM GlutaMax, 0.1 mM $CaCl_2$ and 1 % Penicillin/Streptomycin. All cell lines were split every 2-3 days depending on confluence or cell count.

BLaER1 cells were differentiated at a density of 90000 cells/well (96-well plate) or $1x\ 10^6$ cells/well (12-well plate) for 5 to 7 days in differentiation medium composed of RPMI culture medium with 10 ng/ml of hrIL-3, 10 ng/ml of M-CSF and 100 nM of β-estradiol. The differentiation medium was exchanged with fresh culture medium before stimulation. THP-1 cells were seeded at $3.3x\ 10^7$ cells/dish (15 cm dish) or $10x\ 10^6$ cell/dish (10 cm dish) and differentiated overnight with 100 ng/ml PMA. The differentiation medium was removed and cells were detached using 2 mM EDTA in PBS for 10 min on ice. PBS/cell suspension was spun down at 100 g for 10 min, PBS was removed, and fresh culture medium was added. For stimulation, these cells were plated with $1x\ 10^6$ cells/well (12-well plate) or $10x\ 10^6$ cells/dish (10 cm dish) and kept for 2 days in the incubator. The medium was exchanged one day before stimulation to RPMI1640 medium containing 1 % FCS, 1 % Penicillin/Streptomycin and 1 mM sodium pyruvate. Primary human monocytes were cultured in RPMI culture medium. By adding M-CSF at a final concentration of 100 ng/ml to the medium, monocytes were differentiated to monocyte-derived macrophages in 5 to 7 days. During the differentiation process, every 2-3 days new M-CSF was added to the culture medium.

3.2.3 Freezing and thawing of cells

For freezing cells, the medium was removed by centrifugation at 500 g for 5 min. The cells were washed once with PBS, and the pellet was resuspended in 250 µl freezing medium (10 % DMSO in culture medium). The cells were transferred to 1 ml barcoded cryotubes and frozen in a freezing container at -80 °C. After one day, the frozen cells were transferred into a -150 °C freezer for long term storage. For thawing, frozen cells were thawed quickly to room temperature and transferred to 15 ml falcon tube with 8 ml PBS. The cell suspension was centrifuged for 5 min at 500 g, and the supernatant was discarded. The cell pellet was resuspended in fresh culture medium and was transferred to a new culture flask.

3.2.4 Isolation of PBMCs and primary monocytes

Donated heparinized blood of informed consenting healthy volunteers was used for PBMC isolation. Therefore, blood samples were diluted with 0.9 % NaCl solution to a final volume of 100 ml. In a 50 ml falcon tube, 13 ml of Ficoll solution was placed at the bottom and gently overlaid with 35 ml of diluted blood by pipetting against the falcon's wall. Cell separation was conducted by centrifugation at 800 g for 15 min at room temperature with maximum acceleration and minimal brake force. The top layer containing white cells was collected in a separate falcon tube and diluted to 50 ml using 0.9 % NaCl solution. The cell suspension was centrifuged for 10 min at 500 g, and the supernatant was discarded. To lyse remaining erythrocytes, 10 ml of 1x BD Pharm lyse solution was added for 5 min, and the tube was subsequently filled up to 50 ml with ice-cold PBS. The cells were centrifuged for 7 min at 500 g at 4 °C (maximum acceleration and minimal break force), the supernatant was discarded, and cells were resuspended in ice-cold MACS buffer (0.5 % FCS, 2 mM EDTA in PBS). Monocytes were isolated using the CD14 positive selection method of MACS technology (Miltenyi) according to the manufacturer's protocol and cultured at $1x\ 10^5$ cells/well (96-well plate) or at $1x\ 10^6$ cells/well (12-well plate) as described in section 3.2.2.

3.2.5   Transfection of cells

Cells were transfected with HT DNA using lipofectamine 2000 as a transfection reagent according to the manufacturer's protocol. In brief, two mixtures containing either HT DNA or lipofectamine transfection reagent were prepared in OptiMEM. These mixtures were pre-incubated for 5 min and mixed and kept for 20 min at RT. After the incubation, the mix was added dropwise to the cells in a volume of 50 µl (96-well-plate) or 200 µl (12-well-plate). For Transfections in a 96-well format, 0.5 µl lipofectamine 2000 in 25 µl OptiMEM and 200 ng HT DNA in 25 µl OptiMEM per well were prepared. For 12-well plates, the amount of lipofectamine 2000 and HT DNA was scaled up according to the manufacturer's protocol.

3.2.6   Stimulation conditions

The different cell lines were cultivated as previously described and stimulated in 96-well and 12-well plates. The cell number per well of the different cell lines described is depicted in Table 3.1.

Table 3.1: Plating scheme for the different cell lines

Cell line	96-well format	12-well format
BLaER1	$9x\ 10^4$ cells/well	$1x\ 10^6$ cells/well
THP-1	$1x\ 10^5$ cells/well	$1x\ 10^6$ cells/well
J774	$1x\ 10^5$ cells/well	$1x\ 10^6$ cells/well
Primary monocytes	$1x\ 10^5$ cells/well	$1x\ 10^6$ cells/well
MDM	$1x\ 10^5$ cells/well	$1x\ 10^6$ cells/well
N/TERT1	$5x\ 10^4$ cells/well	$5x\ 10^5$ cells/well

Cells were stimulated with Doxorubicin at a final concentration of 2.0 µg/ml and Etoposide at a final concentration of 50 µM to induce DNA DSBs. In addition, cells were treated with 20 J/m^2 UV-C light for DSB induction. LPS, MDP, R848, IFNα, and HT DNA, were used as control stimulants. Transfection with HT DNA was used to induce cGAS-STING signalling. The stimulation of LPS, an activator of TLR4 signalling, and R848, a TLR7/8 agonist, were conducted with 200 ng/ml of LPS and 5 µM of R848. The stimulation with the NOD2 agonist MDP was performed with 4 µg/ml. As a control for IFN signalling, the stimulation with 6000 U/ml IFNα was used.

3.3   Molecular biological methods

3.3.1   Chemically competent bacteria

Chemically competent DH5α *E. coli* bacteria were generated according to the protocol in the Promega brochure "Subcloning Notebooks".

3.3.2   Polymerase chain reaction

Polymerase chain reactions (PCR) were conducted with Phusion or GoTaq DNA polymerases according to the manufacturer's protocols. In case of amplification from cDNA, a total volume of 20 µl was used for a 50 µl PCR reaction mix. For plasmid DNA, a final amount of 10 ng/reaction was applied, and for lysates, approximately $1x\ 10^6$ cells/150 µl lysis buffer was used. To assess the optimal annealing temperature, the TM-calculator tool of New England Biolabs was utilized. PCR amplicons were either

purified using the QIAquick PCR purification kit according to the manufacturer's protocol or analysed by agarose gel electrophoresis.

3.3.3 Agarose gel electrophoresis

For agarose gel electrophoresis, a 1-2 % agarose gel was prepared. The respective amount of agarose was melted in 1x TAE buffer with a microwave until a homogenous solution was achieved. This solution was shortly cooled before SYBR Safe was added in a dilution of 1:10000, and the solution was transferred into the gel tray with an inserted comb and left for polymerization. Before electrophoresis, the comb was removed, DNA samples mixed with 6x DNA loading dye were loaded, and the gel run was conducted in an electrophoresis chamber filled with 1x TAE at 100 to 120 V for 0.5 to 1 h. The gel was imaged with a Chemidoc system, and either discarded or PCR products were cut from the gel with a scalpel. The DNA fragment was purified using the QIAquick gel extraction kit following the manufacturer's protocol.

3.3.4 Restriction digest and cloning

Purified plasmids and PCR products were digested using specific restriction enzymes to integrate PCR products in the following step into the respective plasmids. After restriction digest, the products were analysed using agarose gel electrophoresis and subsequently extracted using a gel extraction kit according to the manufacturer's protocol. The purified digested product was used in 1:3 ratios from plasmid to insert for ligation. The ligation was conducted with T4 DNA ligase with the respective buffers according to the manufacturer's protocol. The final plasmid was transformed into chemically competent bacteria (DH5α *E. coli*).

3.3.5 LIC cloning for sgRNA expression plasmids

For CRISPR/Cas9 mediated knockout generation, two different sources for sgRNA expression plasmids were used. If the target gene was represented in our sgRNA library and the respective target sequence had a low off-target rate in addition to targeting an early exon of the gene, our ready to use sgRNA expression plasmids were utilized [367]. If the target gene was not present in our library or the target site was not suitable, the online tool ChopChop was used to find a specific target sequence and design the respective sgRNAs [368–370]. In this case, an oligo was designed as described in section 3.1.9 and ordered from IDT (Integrated DNA Technologies). These oligos were cloned into premade vectors using ligation independent cloning (LIC) as described in Schmidt et al., 2015 [371]. Subsequently, the cloned sgRNA expression plasmids were transformed into chemically competent bacteria (DH5α *E. coli*).

3.3.6 Transformation of chemically competent bacteria

Chemically competent DH5α *E. coli* bacteria were thawed on ice and mixed with 5 µl expression plasmid DNA. The mixture was incubated for at least 3 min on ice, and the transformation mix was heat-shocked at 42 °C for 45 s and directly transferred back on ice for another 3 min. Subsequently, 500 µl of LB medium was added, and the mixture was incubated for 30 min at 37 °C under constant shaking. After incubation, the mixture was centrifuged at 500 g for 5 min at RT, and the supernatant was discarded down to approximately 50 µl. The bacteria were resuspended in the remaining 50 µl and plated on LB$_{Amp}$ agar (100 µg/ml ampicillin) plates and kept overnight at 37 °C.

3.3.7 Plasmid DNA isolation from bacteria cultures

Grown colonies on the LB$_{Amp}$ agar plates were picked and transferred into 5 ml LB$_{Amp}$ (100 µg/ml ampicillin) medium. After incubation overnight at 37 °C, the plasmid DNA was isolated from the bacteria according to the QIAprep Spin Miniprep kit manual with homemade buffers and EconoSpin columns (Epoch Life Science). To screen for positive clones, a restriction digest was performed, or the correct plasmid sequence was validated by Sanger sequencing performed by Eurofins. Clones with a correct plasmid sequence were inoculated on 300 ml LB$_{Amp,}$ and after culturing overnight at 37 °C, the plasmid DNA was isolated using the PureLink Maxi Prep kit according to the manufacturer's protocol.

3.3.8 RNA isolation from human cells

RNA isolation was performed with the Total RNA Purification Mini Spin Kit (Genaxxon) according to the manufacturer's protocol or with SPRI beads (GE Healthcare) [372]. For RNA isolation with columns, 6x 10^5 BLaER1 cells were lysed with 360 µl RLys buffer overnight at -80 °C. The next day, 360 µl of 70 % ethanol were added to the lysate and mixed by pipetting. The mixture was applied to the provided RNA purification columns and centrifuged for 1 min at 12000 g. The column was washed once with 700 µl RW1 buffer, twice with 500 µl RW2 buffer. To remove the remaining ethanol, the collection tube was changed, and the column was centrifuged for 2 min at 12000 g. The column was placed in a fresh 1.5 ml tube, and 30 µl dH$_2$O was added. After 5 min incubation at RT, the column was centrifuged to elute the RNA at 8500 g for 2 min. For RNA extraction using SPRI beads, 4x 10^5 BLaER1 cells were washed once with PBS and lysed in 50 µl RLT lysis buffer per well overnight at -80 °C. The next day, the lysate was transferred to a 96-well PCR plate and 1 µl Proteinase K (20 mg/ml) and 0.5 µl EDTA (100 mM) were added. The mixture was incubated for 15 min at 50 °C, and Proteinase K was inactivated for 10 min at 80 °C. Subsequently, 100 µl beads (SPRI beads in 22 % PEG buffer with 0.5 µg beads/µl) were added, mixed and incubated for 5 min at RT. The plate was placed on a magnetic stand until the solution was clear and the supernatant was removed. The magnetic beads were washed twice with 100 µl 80 % ethanol and air-dried for 5 min. The beads were resuspended in 10 µl dH$_2$O and placed on the magnetic stand until the solution was clear. The nucleic acids were transferred to a fresh plate. The isolated nucleic acids from both isolation methods were stored at -80 °C until further usage.

3.3.9 DNAse I digestion

To remove remaining DNA from isolated RNA, the samples were digested using DNAse I in the following reaction mix:

Table 3.2: DNAse I reaction mix

Component	Volume
Isolated RNA sample	4 µl
DNAse I	0.5 µl
DNAse I buffer + MgCl$_2$ (10x)	0.5 µl

The reaction mix was incubated for 30 min at 37 °C. Inactivation of DNAse I was achieved by adding 0.5 µl EDTA (50 mM) to the reaction mix and incubation at 70 °C for 10 min. The RNA concentration was determined by photo-spectrometry.

3.3.10 cDNA synthesis

For the cDNA synthesis, the following mixture was added to the RNA samples after DNAse I digestion:

Table 3.3: cDNA synthesis mix

Component	Volume
Isolated RNA sample	5.5 µl
RT buffer (5x)	2 µl
dNTP mix	1 µl
RT	0.5 µl
RiboLock	0.5 µl
Oligo dT primer	0.5 µl

The reverse transcription mix was incubated for 1 h at 42 °C and enzyme inactivation another 10 min at 70 °C. The samples were transferred to a 96-well PCR plate, and 10 µl of SPRI beads in 22 % PEG were added (1 µg beads/µl). After 5 min incubation at RT, the plate was placed on a magnetic stand, and the supernatant was removed. The beads were washed twice with 100 µl 100 % ethanol and air-dried for 5 min at RT. The beads were resuspended in 30 to 100 µl dH$_2$O and kept on room temperature for 5 min to elute the cDNA. The plate was moved to a magnetic stand, and the cDNA was transferred into a fresh 96-well plate. The cDNA was further used as a PCR template or for quantitative real-time PCR or stored at -20 °C.

3.3.11 Quantitative real-time PCR

For quantification of the cDNA by qRT-PCR, the following reaction mix was prepared:

Table 3.4: qRT-PCR reaction mix

Component	Volume (96 well plate)	Volume (384 well plate)
cDNA	4 µl	2 µl
PowerUp SYBR Green Master mix	5 µl	2,5 µl
Gene-specific forward primer	0.5 µl	0.25 µl
Gene-specific reverse primer	0.5 µl	0.25 µl

The qPCR was performed according to the manufacturer's protocol using a CFX96 or CFX384 Touch Real-Time PCR detection system. Relative expression of target genes, quantified by cycle threshold (Ct), were normalized to GAPDH expression (ΔCt). The calculation for the relative gene expression using the ΔCt method was conducted according to the following equation:

$$\text{Relative gene expression} = 2^{(-(\text{Ct(target gene) - Ct(GAPDH)}))}$$

3.3.12 DNA isolation from human cells

The isolation of genomic DNA was performed using the QIAamp DNA mini kit and parts of the related protocol QIAamp Blood and Body Fluid Spin Protocol. In detail, 5x 10^6 BLaER1 cells were spun down, and the media was removed. The cells were resuspended in 200 µl PBS, and 20 µl Proteinase K (20 mg/ml) and 200 µl buffer AL were added. The sample was mixed by pulse-vortex for 15 s and was

incubated for 10 min at 56 °C. Subsequently, 200 µl 100 % ethanol was added, and the solution was pulse-vortexed again for 15 s. The mixture was applied to the QIAamp Mini spin column and centrifuged for 1 min at 6000 g. The flow-through was discarded, and the column washed once with 500 µl AW1 buffer (6000 g for 1 min) and once with 500 µl AW2 buffer (max. speed for 3 min). The column was placed in a fresh collection tube and centrifuged at 16000 g for 1 min to remove the remaining buffer. The column was placed in a 1.5 ml tube, and 200 µl dH$_2$O was applied to the column for elution. After 5 min incubation at RT, the column was centrifuged for 1 min at 6000 g, and the eluted DNA was stored at -20 °C.

3.3.13 Inverse PCR

The concentration of the isolated genomic DNA was analysed by photo-spectrometry and digested with the restriction enzyme MseI in the following reaction mix:

Table 3.5: MseI digestion mix

Component	Volume
Genomic DNA	4 µg
MseI	2.5 µl
CutSmart buffer	5 µl
dH$_2$O	to 50 µl

The restriction digest mix was incubated overnight at 37 °C and slight agitation. The DNA fragments were purified using the QIAquick PCR purification kit according to the manufacturer's protocol. The DNA concentration of the purified digested DNA was measured, and for each digestion, the following ligation mix was prepared.

Table 3.6: Ligation mix

Component	Volume
Purified DNA fragments	1 µg
T4 DNA Ligase	1 µl
T4 DNA ligase buffer (10x)	30 µl
dH$_2$O	to 300 µl

The ligation was performed overnight at RT. According to the manufacturer's protocol, the ligated DNA was purified using the QIAquick PCR purification kit and eluted in 60 µl dH$_2$O. The ligated DNA was used as a template for PCR reaction as described under 3.3.2. The product was loaded on a 2 % agarose gel, and the band pattern was analysed. In addition, the DNA amplicons were sequenced using primers suitable for Miseq from Illumina.

3.3.14 SG-PERT Assay

The SG-PERT Assay is used to identify viral RT activity in the medium of cultured cells. Therefore, it can be applied to assess the release of virus particles from cells previously infected with retroviruses or lentiviruses. This method uses the inert activity of the viral RT to transcribe a defined synthetic RNA template. The resulting cDNA is amplified in a quantitative real-time PCR [373].

Medium from cultured cells was centrifuged for 5 min at 500 g to remove remaining cells. The supernatant was transferred to a fresh tube, and for lysis, 20 µl of supernatant was mixed with 20 µl of 2x SG-PERT lysis buffer with 1:100 RiboLock and was incubated for 10 min at RT. The lysate was stored at -80 °C until further analysis. For the determination of RT activity, the standard was prepared in 1x PCR/dilution buffer. 1 µl of RT was added to 9 µl 1x PCR/dilution buffer and was subsequently diluted in 1:10 dilution steps. As non-targeting controls (NTC), only 1x PCR/dilution buffer without RT or supernatant of not infected cells were used. Standard and control samples were lysed in the same way as the test samples. The 2x reaction mix was supplemented with GoTaq Hot Start DNA Polymerase (1:100), and 10 µl per well were plated in a 96-well white qPCR plate. To the reaction mix, 10 µl of the standards, NTC and the samples were added and mixed. The SG-PERT analysis was performed after sealing the plate as described in Table 3.7 in a CFX96 Touch Real-Time PCR detection system (BioRad). Based on the RT activity of the standard, a standard curve was generated, which was used to calculate RT activity in the samples.

Table 3.7: Cycler program for the SG-PERT assay

Step	Temperature	Time
1. RT reaction	42 °C	20 min
2. Taq Activation	95 °C	2 min
3. Denaturation	95 °C	5 s
4. Annealing	60 °C	5 s
5. Elongation	72 °C	15 s
6. Acquisition	80°C	7 s
Repeat step 3 to 6 40x		
Melting curve 60°C → 95 °C in 0.5 °C steps		

3.3.15 SMRV stock generation from BLaER1 supernatant

Supernatant from BLaER1 cells (undifferentiated or differentiated) cultivated at high density was collected. The supernatant was centrifuged for 5 min at 600 g and filtered with a 0.45 µm filter to remove the remaining cells and cell debris.

3.3.16 Enzyme-linked immunosorbent assay – ELISA

Detection of cytokines, human IP-10 and human IL-6, in the supernatant of stimulated and unstimulated cells, was performed with the human IP-10/IL-6 ELISA set from BD Biosciences according to the manufacturer's protocol. In brief, 96-well plates with high binding affinity were coated with 50 µl/well capture antibody in the respective dilutions in coating buffer overnight at 4 °C. The coating solution was removed the next day, and plates were washed three times with PBS-T. Plates were blocked with 100 µl/well ELISA buffer for 1 h at RT. The standard was diluted in 1:2 dilution steps starting from 2 ng/ml, and test samples were diluted as determined previously. The blocking solution was removed, and 50 µl of the sample and standard were added for 2 h at RT. Plates were washed 5 times with PBS-T, and 50 µl/well of the detection antibody (respective dilutions) and HRP-enzyme reagent (1:500 in ELISA buffer) were applied. After 1 h incubation at RT, plates were washed 7 times, and 50 µl/well of the TMP solution from BD Bioscience were added until the colour changed to blue in

the fourth dilution of the standard. The reaction was stopped by adding 50 µl 1 M sulphuric acid (colour change from blue to yellow), and the absorbance was measured at 450 nm with the Gen5-Epoch microplate reader. For baseline correction, this value was subtracted by the measurement of 570 nm.

3.3.17 SDS-Page and Western Blotting

For lysate preparation, $1x 10^6$ cells of the respective cell line were detached after stimulation using 2 mM EDTA, spun down for 5 min at 500 g, and the supernatant was discarded. The cell pellet was lysed in 60 to 100 µl of DISC buffer with phosphatase and protease inhibitors overnight at -80 °C or 30 min on ice. The samples were thawed on ice if needed and centrifuged for 10 min at 16000 g to remove nucleic acids. The supernatant was transferred to a fresh 1.5 ml tube. A bicinchoninic acid assay (BCA) was performed for all lysates to adjust the loading in the following SDS gel electrophoresis. A 96-well plate with 1:2 dilutions of the lysates, 5 µl lysate plus 5 µl DISC buffer, and 10 µl of a BSA concentration row starting from 2 mg/ml with 1:2 dilution steps were prepared. A 1:50 mixture of reagent A to B from the Pierce BCA assay kit was prepared, and 90 µl were added to each sample. The reaction mix was incubated for 30 min at 37 °C, and the absorbance was measured at 562 nm. Linear regression was applied to the BSA concentration row absorbance values, and the absorbance values from the samples were interpolated to determine the protein concentration. The remaining lysate was mixed with 6x Laemmli buffer and boiled for 5 min at 95 °C. The samples were stored at -20 °C or directly loaded on an SDS polyacrylamide gel after short centrifugation at 10000 g. For the SDS PAGE, the lysates were loaded on a 10 % or 12 % Tris-Glycine gel (Novex). For this, the gel tank was set-up according to the manufacturer's protocol and was filled with 1x Tris-Glycine running buffer (Novex). As a protein marker, 4 µl of the PageRuler Prestained Protein Ladder were loaded next to the samples. The gel run was performed at 80 V for 30 min, followed by 140 V until the blue running front exited the gel. Proteins were blotted onto a nitrocellulose membrane (0.2 or 0.45 µm) by wet transfer for 1 h at 4 °C, and 100 V. Blots for non-phosphorylated proteins were blocked with 5 % (w/v) milk in PBS-T for 1 hour at 4 °C. For blocking blots for phosphorylated protein detection, 5 % BSA (w/v) in TBS-T was used. The blots were incubated with the respective primary antibody in 5 % BSA (w/v) in TBS-T overnight at 4 °C. Blots were washed the next day three times with PBS-T or TBS-T for 10 min and incubated with the respective HRP-labelled secondary antibodies in 5 % BSA (w/v) in TBS-T for 1 h at RT. After another three washing steps with PBS-T or TBS-T for 10 min each, Western Blot substrate was added on the blots, and the labelled proteins were detected via chemiluminescence imaging system (Fusion Fx, Vilber).

3.4   CRISPR/Cas9 mediated gene targeting

3.4.1   Electroporation

One day before electroporation, BLaER1 cells were seeded in 20 ml medium at a density of $2.5x 10^5$ cells/ml. For each electroporation, $5x 10^6$ cells were pelleted for 5 min at 500 g and washed with pre-warmed PBS. The cell pellet was resuspended in 250 µl pre-warmed OptiMEM. For gRNAs from our library, two plasmids were added, in detail 2.5 µg of pRz_CMV_BFP_T2A_Cas9 plasmid and 2.5 µg of pLK0.1_gRNA_CMV_GFP plasmid with the respective gRNA. For target sites designed by ChopChop, electroporation was performed with 5 µg of pMini_U6_gRNA_CMV_BFP_T2A_Cas9 or pMini_U6_gRNA_CMV_mCherry_T2A_Cas9 with the respective gRNA. The cell-DNA mixture was

incubated for 20 min at RT. BLaER1 cells were electroporated with a Gene Pulser Xcell electroporation device from Bio-Rad using an exponential decay protocol with 4 mm cuvettes and 265 V, 975 µF and 700 Ω were applied. Electroporated cells were transferred into 5 ml pre-warmed RPMI culture medium and cultivated for two days.

3.4.2 Flow cytometry sorting

Electroporated cells underwent flow cytometric cell sorting after 24 to 48 h for their expression of BFP, mCherry or GFP according to the plasmids used. Forward and side scatter was used to gate for intact cells, followed by double discrimination. Of the single cells, 5 to 10 % with the highest expression of the respective fluorescent protein was sorted for. Not electroporated cells served as a negative control. The sorting was performed with a Sony sorter SH800Z into 15 ml tubes containing 3 ml medium or a BD FACS Melody Sorter into 5 ml polypropylene tubes with 2 ml medium.

3.4.3 Limiting dilution plating

Sorted cells were plated in different dilutions into 96-well U-bottom plates. BLaER1 cells were seeded at a density of 1, 2 and 4 cell/well with three plates per density. The plates were incubated for 3 to 4 weeks at 37 °C, 95 % humidity and 5 % CO_2. Grown colonies were identified by eye or using absorbance measurement at 600 nm with the Spark 20m multimode Reader. Ninety-six identified clones were picked and transferred to one 96-well plate per knockout by hand or using the Biomek FX robot from Beckman Coulter. The plate was duplicated, one plate for further culture and one plate for lysis.

3.4.4 Genotyping – Miseq

After resuspension, 10 µl from the lysis plate were transferred to a 384-well PCR plate with 10 µl 2x direct lysis buffer with Proteinase K/well using the Biomek FX robot. After sealing the plate, it was incubated at 65 °C for 10 min, followed by incubation for 15 min at 95 °C for Proteinase K inactivation. The lysate was used as a template for PCR amplification of the sgRNA targeted region of interest. The amplified DNA was then subjected to Illumina sequencing. For this, two PCRs were conducted. The first PCR was performed with target site-specific primer pairs containing adaptor sequences for binding of barcode primers. The specific annealing temperatures were determined in advance using the TM-calculator tool from New England BioLabs. The master mix composition for the first PCR is in Table 3.8.

Table 3.8: Miseq PCR 1 reaction mix and respective cycler settings

First PCR		First PCR	
Component	Volume	Temperature	Time
5x HF or GC buffer	1.2 µl	95 °C	3 min
dNTPs (10 mM)	0.12 µl		
Primer forward (50 µM)	0.06 µl	95 °C	30 s
Primer reverse (50 µM)	0.06 µl	62 °C	30 s
Phusion polymerase	0.06 µl	72 °C	30 s
H₂O	3.5 µl	18 cycles	
Lysate	1.0 µl	72 °C	3 min
		12 °C	∞

The second PCR was applied to barcode the target-gene specific PCR fragments for their positions on the 96-well-plate. Therefore, barcode primers containing Illumina sequencing adaptors binding to the overhangs from PCR1 were used. The second PCR was conducted with the reaction mix shown in Table 3.9. For Primers containing a high GC-level, the 5x GC buffer was used otherwise, the 5x HF buffer was sufficient. A 2-step-PCR without the annealing step in addition to adding 3 % DMSO to the reaction mix was applied for primers and amplicons with a GC level over 65 %. After the second PCR, all PCR2 products having a unique combination of barcode primer and genomic region were pooled, and 5 µl of the first and second PCR were used for PCR validation. The amplicon size was determined and controlled by agarose gel electrophoresis as described in 3.3.3.

Table 3.9: Miseq PCR 2 reaction mix and respective cycler settings

Second PCR		Second PCR	
Component	Volume	Temperature	Time
5x HF or GC buffer	1.2 µl	95 °C	3 min
dNTPs (10 mM)	0.12 µl		
Phusion polymerase	0.06 µl	95 °C	30 s
H_2O	2.42 µl	62 °C	30 s
PCR 1 product	1.0 µl	72 °C	30 s
Barcode primer	1.5 µl	18 cycles	
		72 °C	7 min
		12 °C	∞

Another part of the pooled samples was loaded on an agarose gel and was purified. The nucleic acid was precipitated by mixing the purified samples with 0.1 sample volumes of 3 M sodium acetate (pH 5.2), and then the samples were diluted with 1.1 sample volumes of isopropanol. This mixture was incubated for 30 min at -20 °C and subsequently centrifuged at 14000 g for 15 min at 4 °C. The supernatant was removed, and the pellet was washed with ice-cold 70 % (v/v) ethanol. After a 5 min centrifugation at 14000 g at 4 °C, the pellet was air-dried and then resuspended in dH_2O. The DNA concentration was determined with a Nanodrop by measuring the absorbance at 260 nm. An Illumina Miseq platform with 300 bp length single read sequencing with the v2 chemistry was applied to perform the DNA sequencing. The sequencing files were analysed for frameshift mutations using the OutKnocker.org software [374]. The FastQ files were aligned to the reference WT amplicons, including the used target sequence and the number of reads was counted. The software so gives a read number of a certain sequence at their barcoded position in reference to the WT sequence. Clones with insertions/deletions leading to out of frame mutations are coloured in red/orange, while clones with in-frame mutations are coloured in dark and light blue. All found WT sequences are coloured in grey. All clones with exclusively out of frame mutation reads, especially the ones with two different out of frame mutations (one for each of both alleles), were considered as knockouts. This is shown in Figure 3.1 for the generation of TRAF6 knockouts in BLaER1 cells. These knockout clones were picked by hand, expanded and frozen or used directly for experiments. To further validate the knockouts, immunoblotting with the specific antibody was applied if possible, as shown in Figure 3.1.
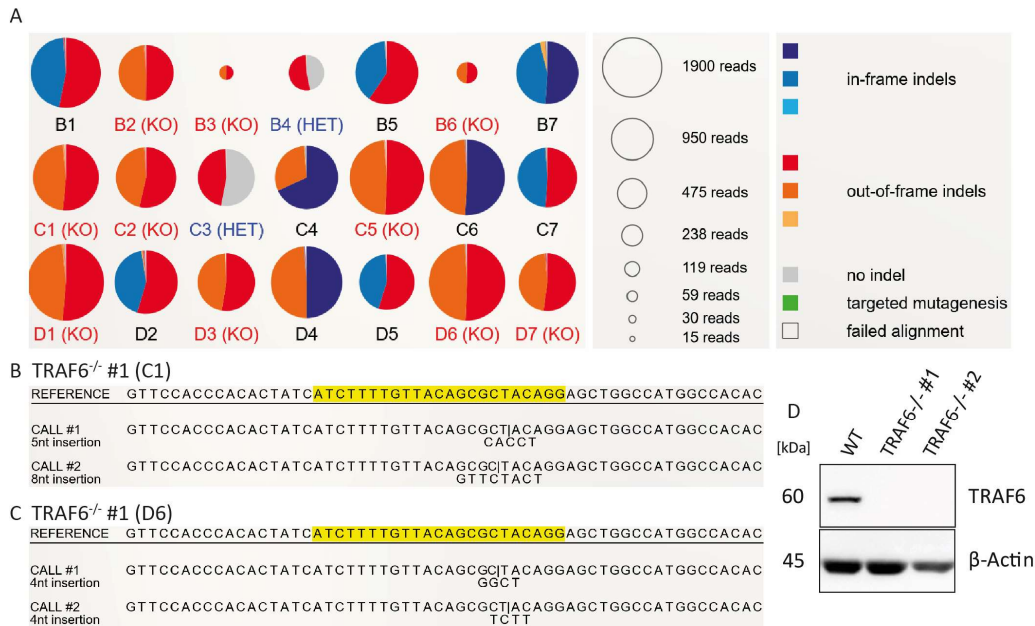
Figure 3.1: Validation and genotyping of TRAF6 BLaER1 knockout cells.

After electroporation of BLaER1 cells with Cas9-BFP and the CRISPR gRNA for TRAF6 targeting, the cells were sorted for BFP expression. BFP positive cells were seeded as single-cell clones by limiting dilution and analyzed by deep sequencing. **(A)** For visualization of the analysed single-cell clone genotypes, the Outknocker.org software was applied. The colours indicate wheater the clone has WT alleles or KO alleles. Therefore, WT alleles are marked with a grey colour, in-frame mutations are in different blue colours, and the out-of-frame mutations are in red to orange. **(B-C)** For the generation of knockouts, only out-of-frame mutations were used. So clones with two alleles with out-of-frame mutations were chosen. The reference, as well as the clonal sequences for both alleles of clone #1 (C1) **(B)** and clone #2 (D6) **(C)**, are shown. **(D)** Western Blot analysis of the picked clones #1 (C1) and #2 (D6).

3.5 Statistical analysis

Unless otherwise stated, all statistical tests were performed by using two-way ANOVA. If applicable, a post hoc correction for multiple comparisons was employed using Sidak's correction. * $p<0.05$, ** $p<0.01$, *** $p<0.001$. The GraphPad Prism 9.0.0 software was used for all statistical analyses.

4   Results

4.1   Topoisomerase II inhibitors induce an antiviral immune response in BLaER1 cells

Multiple links between DNA damage response pathways and the induction of innate immune signalling have been revealed so far. Several TOP2 inhibitors and small compounds with a related structure have been described to trigger the induction of a type I IFN response [375]. Here, our lab previously demonstrated that only TOP2 inhibitors, which trigger DNA damage by inhibition of the religation step, are capable of inducing an immune response, while catalytic inhibitors blocking TOP2 activity before DNA cleavage do not [346]. The induction of DNA damage by TOP2 inhibitors resulted in the production and release of IFNβ. This triggers auto- or paracrine signal transduction through IFNAR, which mediates the phosphorylation of STAT1 and subsequently leads to the production of ISGs like IP-10. As indirect readouts for the induction of a type I IFN response mediated by DNA DSBs, the phosphorylation of STAT1 was analysed by immunoblotting and the production and secretion of ISGs by ELISA. Further, IFNβ mRNA levels were determined by qPCR. Cells that were stimulated with LPS or R848 were used as a positive control for a type I IFN response.

To determine the capability of the TOP2 inhibitor Doxorubicin to induce an antiviral immune response and trigger pro-inflammatory cytokine expression, a time-course experiment was conducted in BLaER1 cells, which have also been used in the previous study. Here, the stimulation of differentiated BLaER1 WT cells with 2.0 µg/ml Doxorubicin resulted in an induction of STAT1 phosphorylation starting at four hours after stimulation and reaching a peak at seven to eight hours (Figure 4.1 A). Besides the phosphorylation of STAT1 also the p38 and JNK MAPK modules were activated. The phosphorylation of p38 was already detectable one to two hours after stimulation with Doxorubicin and became more pronounced over time, while the phosphorylation of JNK remained on a low level until six to seven hours' post-stimulation (Figure 4.1 A). Stimulation with LPS and R848 both triggered STAT1 and MAPK phosphorylation and were used as controls (Figure 4.1 A). To determine the optimal dosage of Doxorubicin, different concentrations were analysed for their capability to induce an IL-6 or IP-10 cytokine production and secretion. The secretion of both cytokines was determined by ELISA after 24 hours of stimulation with Doxorubicin. The secretion of IL-6 increased with the concentration of Doxorubicin until reaching a maximum at a concentration of 2.0 µg/ml. Higher concentration of Doxorubicin led to a decreased response due to the increasing cytotoxicity (Figure 4.1 B). A similar trend could be seen for the production and secretion of IP-10, which reached its maximum at a concentration of 1.0 and 2.0 µg/ml (Figure 4.1 D). This pattern was also validated by immunoblotting. The concentration of 1.0 and 2.0 µg/ml showed the strongest phosphorylation of STAT1 after eight hours of stimulation (Figure 4.1 C). However, higher concentrations resulted in more robust MAPK activation (Figure 4.1 C). Therefore, in the following experiments, Doxorubicin was applied at a concentration of 2.0 µg/ml for eight hours for immunoblotting or qPCR analysis and for 24 hours to detect cytokine production by ELISA.

Etoposide, another TOP2 inhibitor, blocks the religation step of TOP2 and therewith leads to DNA damage induction. Similar to Doxorubicin, it has been described to induce an antiviral immune response [376]. To address the ability of Etoposide to cause a type I IFN response in differentiated BLaER1 cells, these cells were treated with increasing concentrations of Etoposide for eight hours and analysed

by immunoblotting. The three highest concentrations of Etoposide were able to induce phosphorylation of STAT1 (Figure 4.1 E). However, the phosphorylation was significantly weaker in comparison to cells treated with Doxorubicin (Figure 4.1 E).
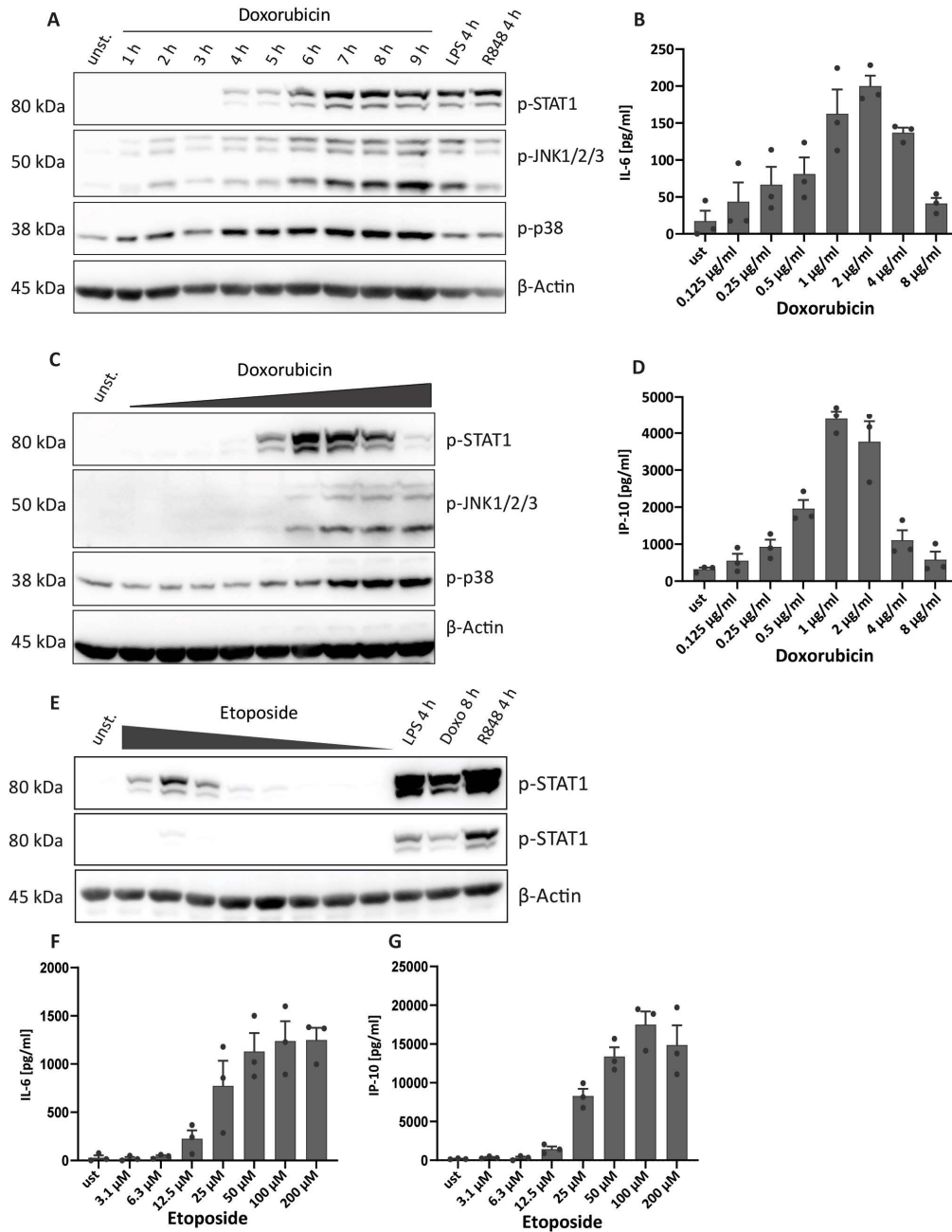

Figure 4.1 Doxorubicin induces an antiviral and pro-inflammatory immune response in BLaER1 cells
(A) Immunoblot analysis of BLaER1 WT cells stimulated with Doxorubicin at different time points between one to nine hours as indicated, with LPS and R848 for four hours, or remained unstimulated (unstim.). One representative experiment of three is depicted. **(B-D)** BLaER1 WT cells treated with increasing amounts of Doxorubicin starting from 0.0625 μg/ml until 8 μg/ml with duplication of the concentration every step was analysed by immunoblotting after eight hours of stimulation **(C)** or by ELISA for IL-6 **(B)** or IP-10 **(D)** in the supernatant after 24 hours of stimulation. **(E)** Immunoblot analysis of BLaER1 cells stimulated with Etoposide in declining concentrations (starting from 200 μM in 1:2 dilution steps) for eight hours, with LPS or R848 for four

hours, with Doxorubicin for eight hours or remained unstimulated. Depicted is one representative of three independent immunoblots. **(F and G)** Secreted IL-6 and IP-10 were detected via ELISA in the supernatant of cells stimulated with increasing concentrations of Etoposide. A representative immunoblot of three independent experiments is depicted **(A, C and E)**. ELISA data are depicted as mean + SEM of three independent experiments **(B, D, F and G)**.

In addition, the cytokine expression and secretion for Etoposide treated BLaER1 cells was analysed. Like the results obtained by immunoblotting, the three highest concentrations depicted the most robust cytokine production and secretion (Figure 4.1 F and G). In contrast to the stimulation with Doxorubicin, Etoposide-treated cells showed a plateau starting from 50 µM concentration instead of a distinct peak. Interestingly, in contrast to the phosphorylation of STAT1 analysed by immunoblotting, the production of cytokines and their secretion was increased by four to five-fold compared to the stimulation with Doxorubicin. In summary, these results depicted a robust type I IFN induction and subsequent phosphorylation of STAT1 for both TOP2 inhibitors and linked the induction of DNA damage, especially DSBs, with the induction of antiviral immune responses. Due to the low level of IL-6 production, cytokine production was analysed by IP-10 ELISA in further experiments.

4.2   Induction of antiviral immune signalling in different cell lines

To investigate whether the DSB mediated type I IFN induction observed in the BLaER1 system was also detectable in other human and mouse cell types, we analysed primary monocytes, primary monocyte-derived macrophages, N/TERT1 keratinocytes, J774, and THP-1 cells for their response to TOP2 inhibitor treatment. Besides stimulation with LPS, transfected DNA was used as a positive control for primary monocytes and keratinocytes to induce an antiviral immune response.
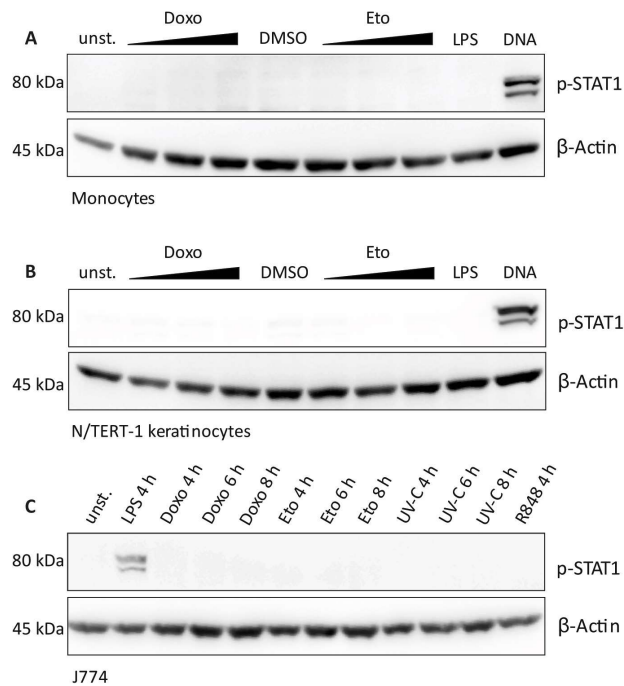

Figure 4.2 Cell lines tested for their induction of a type I interferon response upon induction of DSBs
(A-C) Immunoblot analysis of primary human monocytes **(A)** and N/TERT keratinocytes **(B)** treated with different concentrations of Doxorubicin or Etoposide for eight hours, with LPS for four hours or with transfected dsDNA for four hours. **(C)** J774 mouse macrophages were stimulated for different time points with Doxorubicin or

Etoposide or were irradiated with UV-C light. As controls, cells remained unstimulated or were stimulated with LPS or R848 for four hours. A representative immunoblot of two **(C)** or three **(A and B)** independent experiments is depicted.

Hence, primary human monocytes from three donors were isolated and stimulated with different concentrations of Etoposide (200 mM, 100 mM and 50 mM) and Doxorubicin (1.0 µg/ml, 2.0 µg/ml and 4.0 µg/ml) or were treated with LPS or transfected with dsDNA. Only monocytes transfected with dsDNA showed phosphorylation of STAT1, while LPS, Doxorubicin and Etoposide induced no STAT1 phosphorylation (Figure 4.2 A). Due to recent publications showing a type I IFN response in keratinocytes upon stimulation with Etoposide, N/TERT1 keratinocytes were analysed next. Unexpectedly, keratinocytes depicted no detectable phosphorylation of STAT1 upon stimulation with the TOP2 inhibitors (Figure 4.2 B). Only the transfection with dsDNA resulted in STAT1 phosphorylation (Figure 4.2 B). In addition, the mouse macrophage cell line J774 was analysed by immunoblotting. J774 cells were stimulated with both TOP2 inhibitors to induce DSB breaks and harvested four, six and eight hours post-treatment. In contrast to monocytes and keratinocytes, J774 cells were also irradiated with UV-C light to induce DSB breaks due to the later testing of this cell line. J774 cells stimulated with LPS depicted weak phosphorylation of STAT1 while all DSB inducing stimulations and R848 showed no STAT1 phosphorylation (Figure 4.2 C).

In addition to N/TERT1 keratinocytes, primary monocytes and J774 mouse macrophages, also differentiated THP-1 cells and monocyte-derived macrophages (MDMs) from human donors were analysed for their response to DSB induction. MDMs were treated with Doxorubicin and Etoposide for eight hours or kept in culture for eight hours after irradiation with UV-C light. Like BLaER1 cells, all donors showed robust phosphorylation of STAT1 upon treatment with Doxorubicin, while Etoposide and UV-C light led to a lower level of STAT1 phosphorylation (Figure 4.3 A). LPS and R848 also mediated phosphorylation of STAT1 (Figure 4.3 A). All DSB inducing treatments resulted in an activation of JNK and p38 modules with Doxorubicin leading to the strongest phosphorylation (Figure 4.3 A). The expression of IFNβ was detected by qPCR in MDMs from three donors stimulated with Doxorubicin or transfected with dsDNA. Both stimulations led to an induction of *IFNB1* (IFNβ) expression, however, Doxorubicin showed a weaker *IFNB1* induction than dsDNA (Figure 4.3 B). The production and secretion of IP-10 in MDMs stimulated with Doxorubicin or Etoposide were additionally analysed by ELISA. Similar to BLaER1 cells, Etoposide led to 6 times more potent induction and secretion of IP-10 than Doxorubicin (Figure 4.3 C). The induction mediated by Doxorubicin was only slightly elevated compared to the unstimulated control (Figure 4.3 C). Stimulation with LPS, transfected dsDNA and IFNα resulted in a robust secretion of IP-10 (Figure 4.3 D). Moreover, differentiated THP-1 cells were treated with Doxorubicin, Etoposide and UV-C light and analysed by immunoblotting. All stimulations led to a similar level of STAT1 phosphorylation, however, the unstimulated control indicated slight phosphorylation of STAT1 due to the differentiation of THP-1 cell with PMA (Figure 4.3 E). The supernatant of THP-1 cells treated with UV-C light, Doxorubicin and Etoposide was analysed for secreted IP-10 and showed a similar production of IP-10 as observed in MDMs (Figure 4.3 F). Here, UV-C light, Doxorubicin and Etoposide triggered the production and secretion of IP-10 with Etoposide displaying the most potent induction after 24 hours post-treatment (Figure 4.3 F). All control stimuli, including IFNα, LPS, and transfected dsDNA, induced the production and secretion of IP-10 in differentiated THP-1 cells (Figure 4.3 G).
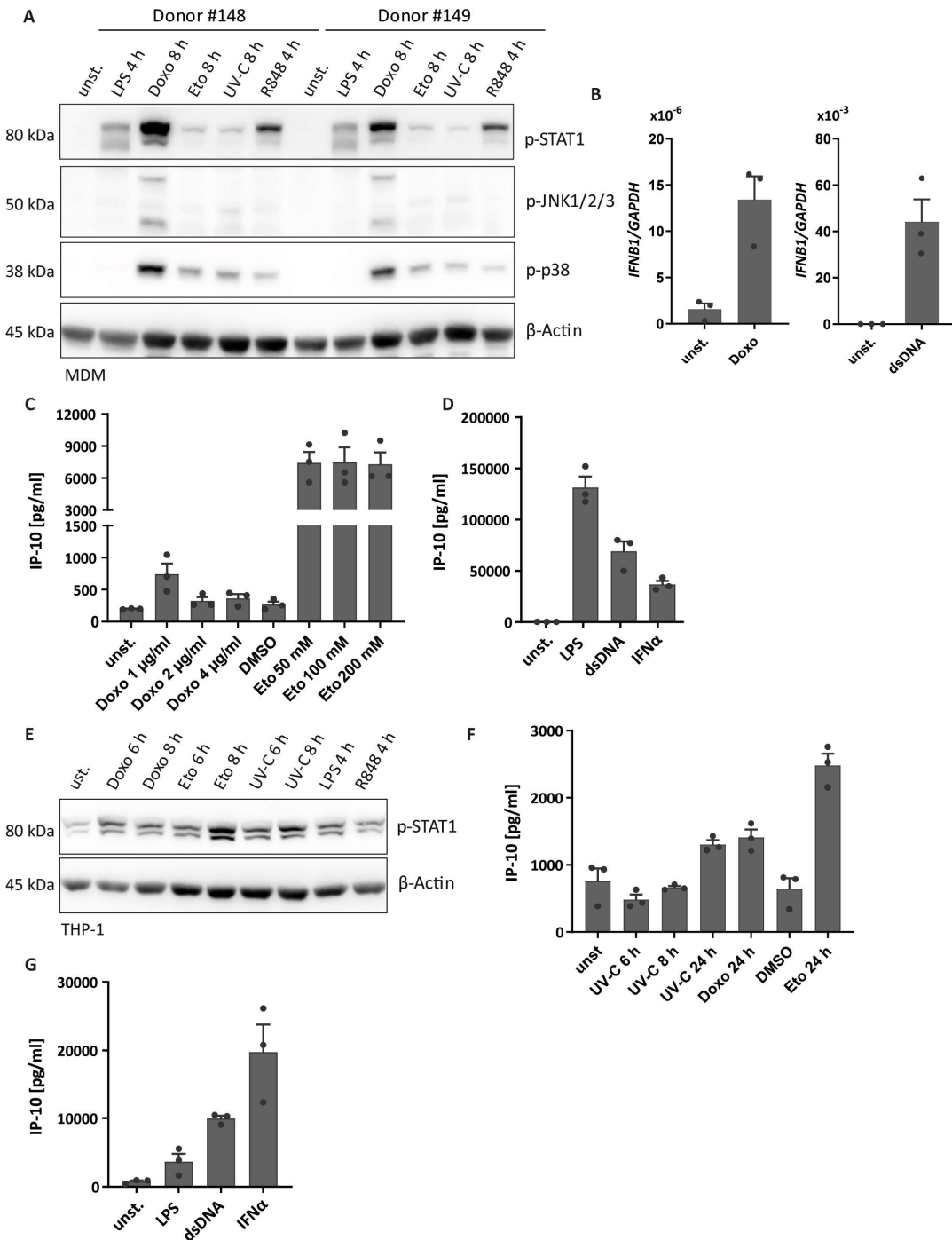
Figure 4.3 Cell lines tested for their induction of a type I interferon response upon induction of DSBs
(A) Monocyte-derived macrophages (MDMs) from two donors were treated with LPS, Doxorubicin, Etoposide and R848 or radiated with UV-C light as indicated and analysed by immunoblotting. Depicted are two of four independent experiments. **(B)** MDMs from three donors were treated with Doxorubicin for eight hours or with transfected dsDNA for six hours. The expression of *IFNB1* (IFNβ) was detected by RT-qPCR. **(C and D)** MDMs from three donors were stimulated for 24 hours with different concentration of Doxorubicin or Etoposide **(C)** as indicated or treated for six hours with transfected dsDNA and IFNα or 24 hours with LPS **(D)**. The secretion of IP-10 was determined by ELISA. **(E)** Differentiated THP-1 cells were stimulated for six or eight hours with Doxorubicin, Etoposide and UV-C light or for four hours with LPS and R848 as indicated and analysed by immunoblotting. A representative immunoblot of two independent experiments is depicted. **(F and G)** THP-1 cell

supernatant was analysed for its IP-10 secretion upon treatment with different stimuli as indicated. Data **(B, C, D, F and G)** are depicted as mean + SEM of three independent experiments.

Overall our results indicate a cell-type and differentiation stage-specific activation of DSB induced type I IFN expression. In addition, the data obtained from MDMs and THP-1 cells support the data generated in the BLaER1 system with regards to Etoposide and Doxorubicin stimulation. To genetically dissect the DSB induced antiviral immune signalling, we used the BLaER1 system for further studies due to its strong response to TOP2 inhibitors and its capacity to accept simple genetic modifications. In addition, the BLaER1 system accurately recapitulated the response obtained in MDMs.

4.3   The antiviral immune response is independent of cytosolic DNA sensors

DNA damage has been often reported to be associated with nucleic acid-sensing PRRs. Several studies have linked DNA damage to cGAS-STING, IFI16 or nucleic acid-sensing TLRs. Therefore, several TLRs and their adaptor proteins as well as cGAS and STING were previously investigated by our lab in the BLaER1 system and described not to impact the type I IFN response upon TOP2 inhibition by Doxorubicin [346].
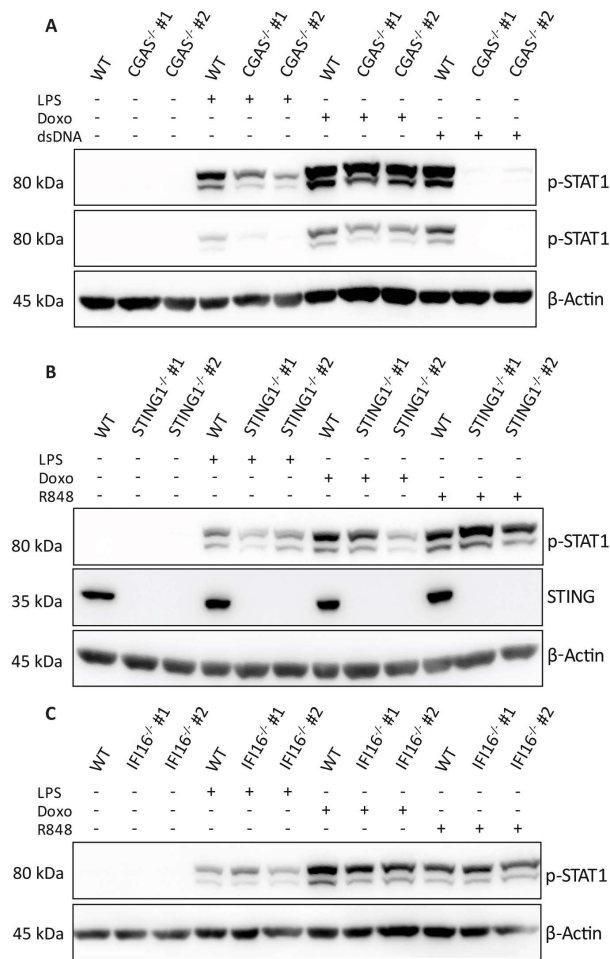

Figure 4.4 DDR induced type I IFN induction is independent of cGAS-STING and IFI16
(A-C) *CGAS$^{-/-}$* **(A)**, *STING1$^{-/-}$* **(B)**, and *IFI16$^{-/-}$* **(C)** were stimulated with Doxorubicin for eight hours and with LPS, R848 or transfected dsDNA for four hours. All samples were analysed using immunoblotting. A representative immunoblot of three independent experiments is depicted **(A-C)**.

To further investigate the link between the formation of DNA DSBs and the subsequent induction of a type I IFN response, knockouts for genes related to type I IFN signalling and DSB repair were generated in the BLaER1 system and analysed for their involvement in the signalling cascade. Cells deficient for cGAS or STING were tested by immunoblotting to validate previous findings on their influence on STAT1 phosphorylation upon DSB induction. While BLaER1 *CGAS*^{-/-} cells stimulated with Doxorubicin showed no reduction of STAT1 phosphorylation levels compared to WT cells, *STING1*^{-/-} cells depicted a slight decrease (Figure 4.4 A and B). The cGAS knockouts also displayed a complete loss of STAT1 phosphorylation upon stimulation with transfected DNA as expected, while LPS signalling was not impacted (Figure 4.4 B). The knockout of STING showed no impact on LPS or R848 signalling (Figure 4.4 B). Additionally, IFI16 was tested for its influence on the phosphorylation of STAT1 due to a recent publication linking IFI16 to STING and DDR signalling leading to the activation of type I IFN expression in HaCaT cells [345]. However, IFI16 knockout BLaER1 cells did not show reduced phosphorylation of STAT1 upon treatment with Doxorubicin, LPS or R848 compared to WT (Figure 4.4 C). Overall, these data indicate no role for the aforementioned nucleic acid-sensing PRRs or their adaptor proteins.

4.4 HR components mediating DSB induced antiviral immune signalling

Besides nucleic acid-sensing PRRs, DDR components have been described to sense damaged DNA structures and initiate downstream activation of innate immune responses. Therefore, known proteins related to DSB sensing like Ku70/Ku80, DNA-PK, the MRN complex or ATM were investigated. Previous work indicated that the NHEJ components are not involved in the induction of an antiviral immune response upon DSB induction by TOP2 inhibitors in THP-1 or BLaER1 cells [346].
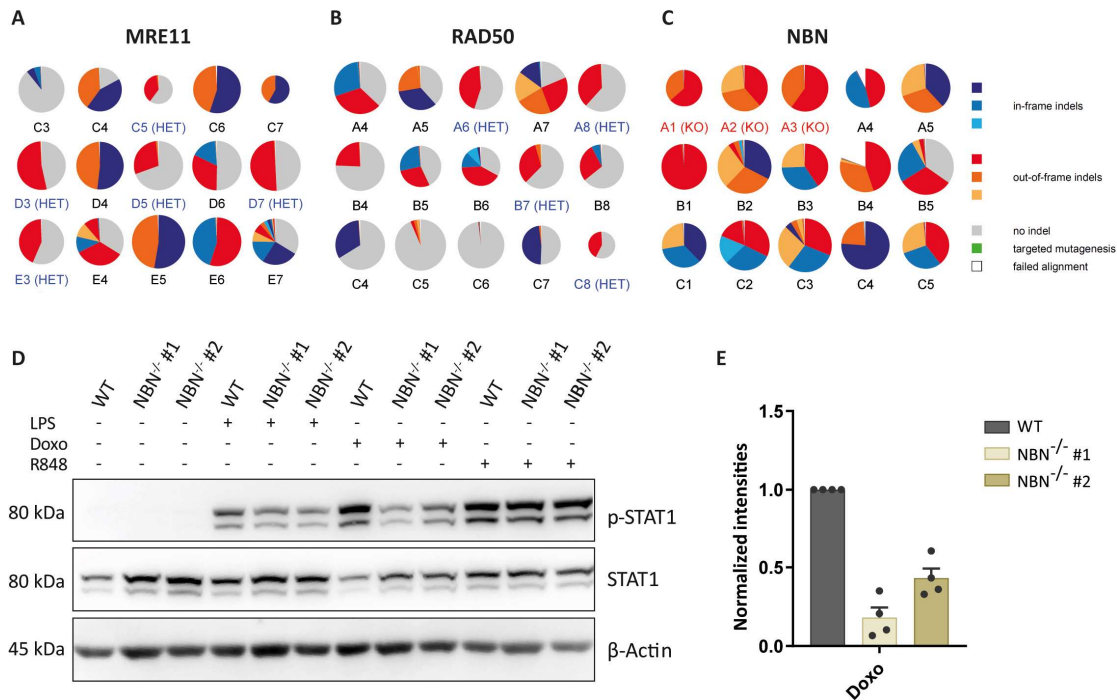

Figure 4.5 MRN complex in the induction of an antiviral immune response
(A-C) Overview of the knockout generation results of the MRN complex members MRE11 **(A)**, RAD50 **(B)** and NBS1 **(C)** after evaluation using the Outknocker software. Red and orange colours depict out of frame mutations while blue colours indicate in-frame mutations, and grey indicates WT reads. **(D)** Stimulated *NBN*^{-/-} cells were

analysed by immunoblotting upon stimulation with Doxorubicin for eight hours or with LPS and R848 for four hours. A representative immunoblot of three independent experiments is depicted. **(E)** Quantification of four independent *NBN⁻/⁻* (brown) immunoblots for the stimulation with Doxorubicin. All band intensities are normalized to the respective WT band and tested against the β-Actin control. The data depicted shows the mean and error bars represent the SEM of four analysed immunoblots.

Hence, knockout cell lines of HR components were generated and tested. However, the generation of knockout cell lines of MRN complex members proved to be difficult. Even when highly efficient gRNAs were used, the generation of MRE11 and RAD50 knockouts only resulted in WT or heterozygous knockouts displaying their essential role in cell survival (Figure 4.5 A and B). In contrast to the other two MRN complex members, the generation of *NBN⁻/⁻* knockout cell lines was successful. *NBN⁻/⁻* (NBS1) clones were analysed by immunoblotting for NBS1 function in the induction of DSB mediated antiviral immune signalling. Here, *NBN⁻/⁻* cells showed robust phosphorylation of STAT1 upon LPS or R848 treatment similar to WT cells (Figure 4.5 D). However, the phosphorylation of STAT1 upon stimulation with Doxorubicin was decreased (Figure 4.5 D). To validate the reduction of phosphorylated STAT1, the bands of phosphorylated STAT1 were analysed on four independent immunoblots and compared to the loading control β-Actin. The result of this quantification indicated a strong reduction in STAT1 phosphorylation in *NBN⁻/⁻* cells compared to WT cells after treatment with Doxorubicin (Figure 4.5 E). Because of the results obtained in *NBN⁻/⁻* cells and previous data, we next confirmed the role of the protein kinase ATM in this signalling pathway. ATM has also been described to interact with NBS1 and to be crucial for the type I IFN response upon Doxorubicin treatment in human macrophages [315,346].
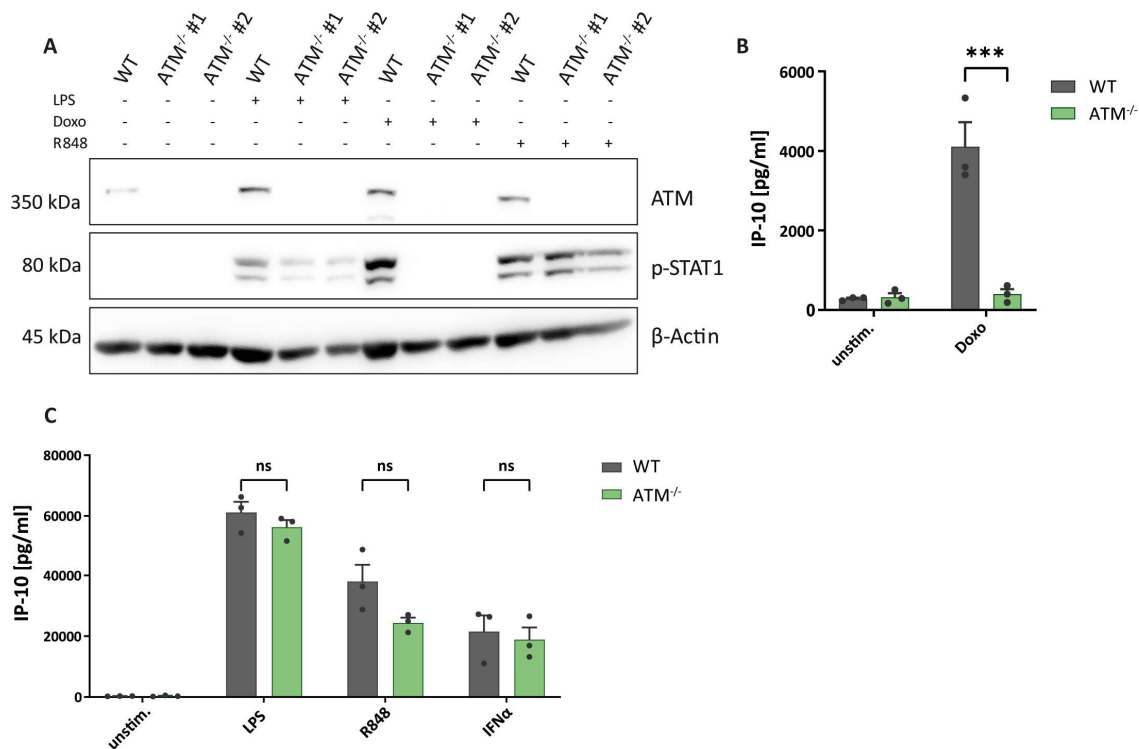

Figure 4.6 ATM-dependent STAT1 phosphorylation and IP-10 induction
(A) Immunoblot of BLaER1 WT and *ATM⁻/⁻* cells treated with LPS or R848 for four hours or Doxorubicin for eight hours. A representative immunoblot of three independent experiments is depicted. **(B and C)** Detection of IP-10 in the supernatant of treated BLaER1 WT (grey) and *ATM⁻/⁻* (light green) cells by ELISA. Cells were treated as

indicated for 24 hours with Doxorubicin and LPS or six hours with R848 and IFNα. The ELISA data depicted shows the mean and error bars represent the SEM of three independent experiments **(B and C)**. Statistical significance was calculated using two-way ANOVA. Sidak's correction was employed for multiple comparison testing. *** $p \leq 0.001$; ** $p \leq 0.01$; * $p \leq 0.05$; ns, not significant.

To this end, ATM deficient BLaER1 cells were generated by CRISPR/Cas9 mediated gene targeting and were analysed by ELISA and immunoblotting. Identity of the knockout was validated by immunoblotting (Figure 4.6 A). *ATM$^{-/-}$* cells showed a complete loss of STAT1 phosphorylation in the immunoblot when treated with Doxorubicin, while the stimulation of LPS and R848 was not decreased compared to WT cells (Figure 4.6 A). Furthermore, the production of IP-10 was measured by ELISA to validate the immunoblot result. Here *ATM$^{-/-}$* cells showed a significantly reduced IP-10 production compared to WT cells upon stimulation with Doxorubicin (Figure 4.6 B). The stimulation with LPS and R848 and with IFNα was not significantly reduced (Figure 4.6 C). In summary, these data indicate a recognition of DSBs through the MRN complex and further signal transduction by the protein kinase ATM.

4.5   TRAF6 is the scaffolding factor for downstream signalling

Different modes of NF-κB transcription factor activation by ATM involving members of the IKK complex as well as different scaffold proteins have been described previously in the literature. Therefore, a possible function for the three scaffold proteins TRAF3, TRAF6 and ELKS (ERC1) in the DSB induced antiviral immune response was investigated.

TRAF6 deficient BLaER1 cells were generated by CRISPR/Cas9 mediated gene targeting and were analysed by qPCR, ELISA and immunoblotting. The identities of the TRAF6 knockout and the TRAF3/6 double-knockout were validated by immunoblotting (Figure 4.7 A and C). While *TRAF6$^{-/-}$* cells displayed similar phosphorylation of STAT1 as WT cells for LPS treatment, both the stimulation with Doxorubicin and R848, led to decreased STAT1 phosphorylation in the immunoblot (Figure 4.7 A). The phosphorylation of STAT1 was completely ablated for R848 and strongly reduced for Doxorubicin (Figure 4.7 A). To validate this observation, the production of IP-10 in *TRAF6$^{-/-}$* cells was analysed by ELISA. TRAF6 deficient cells displayed a complete loss of IP-10 production upon stimulation with Doxorubicin (Figure 4.7 B). In line with these findings, the IFNβ mRNA levels were completely absent in *TRAF6$^{-/-}$* cells analysed by qPCR (Figure 4.7 C). This indicated an essential role of TRAF6 in the signal transduction leading to the type I IFN expression upon DSB formation. However, a residual activation and phosphorylation of STAT1 in TRAF6 deficient cells was still detectable by immunoblot. Therefore, a *TRAF3/6$^{-/-}$* cell line was generated and analysed for STAT1 phosphorylation by immunoblotting. TRAF3/6 deficient cells showed the same absence of STAT1 phosphorylation upon stimulation with R848 as TRAF6 deficient cells but also displayed a completely absent STAT1 phosphorylation upon LPS stimulation compared to WT cells as expected (Figure 4.7 D). Also, TRAF3/6 deficient cells showed a complete loss of STAT1 phosphorylation upon Doxorubicin treatment compared to WT cells (Figure 4.7 D). Further, a possible scaffolding function of ELKS was investigated. Here *ERC1$^{-/-}$* cells were generated and analysed by ELISA on their IP-10 production. *ERC1$^{-/-}$* showed no reduction in the production of IP-10 in Doxorubicin treated cells (Figure 4.7 E). Moreover, the treatment with LPS, R848 or IFNα resulted in no reduced IP-10 production (Figure 4.7 F). Thus, TRAF6 and TRAF3 might form a scaffold needed

for the further recruitment and activation of downstream factors while the signal transduction is independent of the scaffold factor ELKS.
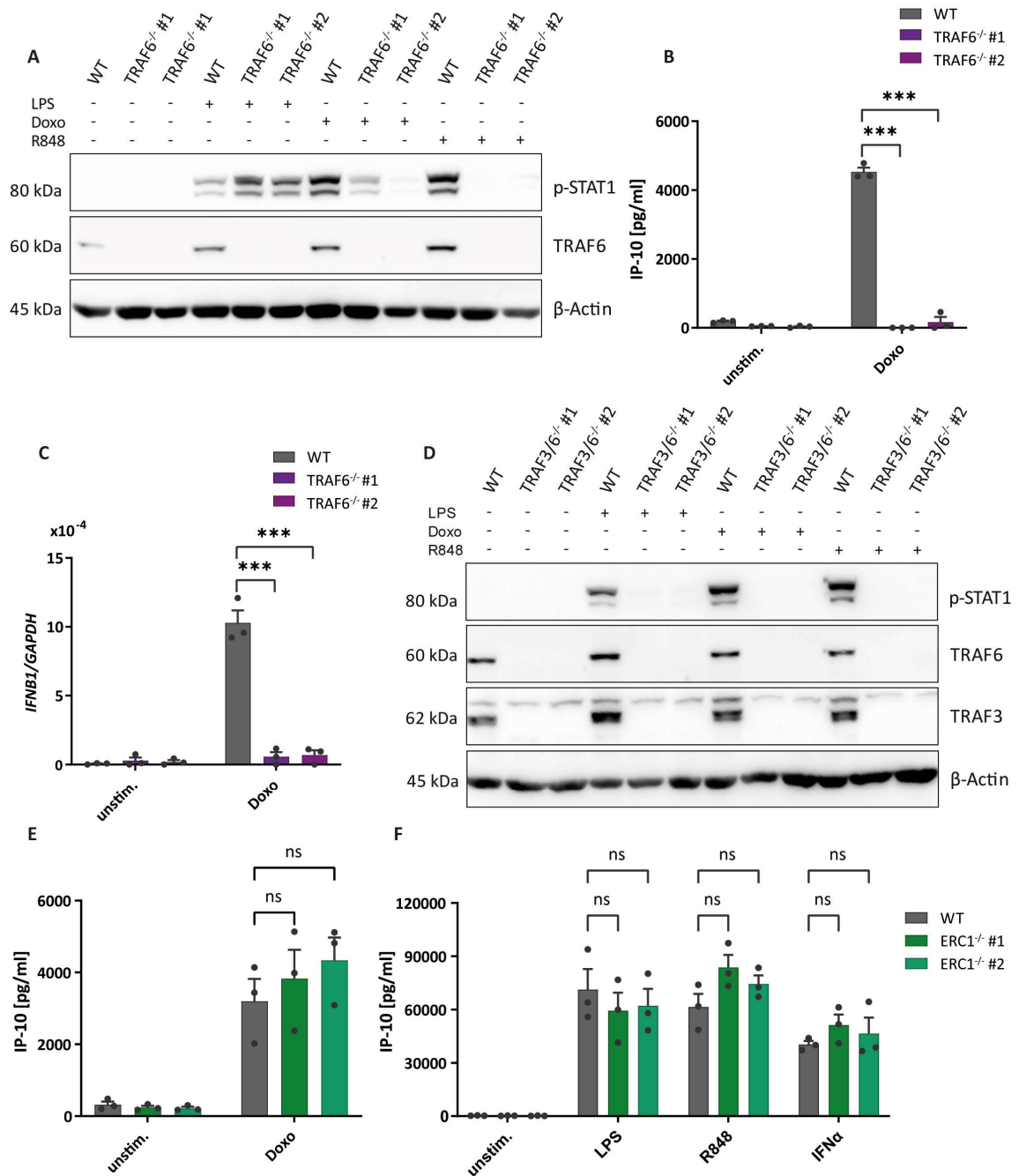

Figure 4.7 TRAF6 and TRAF3 are forming the scaffold for further downstream signalling
(A) Immunoblot of BLaER1 WT and *TRAF6*$^{-/-}$ cells treated with LPS or R848 for four hours or Doxorubicin for eight hours. **(B)** The supernatant of WT and *TRAF6*$^{-/-}$ cells (purple) stimulated with Doxorubicin for 24 hours was analysed by ELISA for secreted IP-10. **(C)** BLaER1 *TRAF6*$^{-/-}$ (purple) and WT cells were treated with or without Doxorubicin for eight hours and analysed by qPCR. **(D)** BLaER1 WT and *TRAF3/6*$^{-/-}$ cells were stimulated as described in (A) and analysed by immunoblotting. **(E and F)** Detection of IP-10 in the supernatant of treated BLaER1 WT and *ERC1*$^{-/-}$ cells (green) by ELISA. The stimulation was performed for six hours for R848 and IFNα and 24 hours for LPS and Doxorubicin. A representative immunoblot of three independent experiments is depicted **(A and D)**. The ELISA and qPCR data depicted shows the mean and error bars represent the SEM of three

independent experiments **(B, C, E and F)**. Statistical significance was calculated using two-way ANOVA. Sidak's correction was employed for multiple comparison testing. *** $p \leq 0.001$; ** $p \leq 0.01$; * $p \leq 0.05$; ns, not significant.

4.6 TAK1 is the central signalling mediator

The scaffold protein TRAF6 is known to form K63-linked polyubiquitin chains upon activation and to recruit the serine-threonine kinase TAK1 via its binding proteins TAB1 and TAB2/3 and other proteins. TAK1, also known as MAP3K7, is a major signal transducer in PRR signalling and is involved in the activation of MAPK and NF-κB signalling [164].
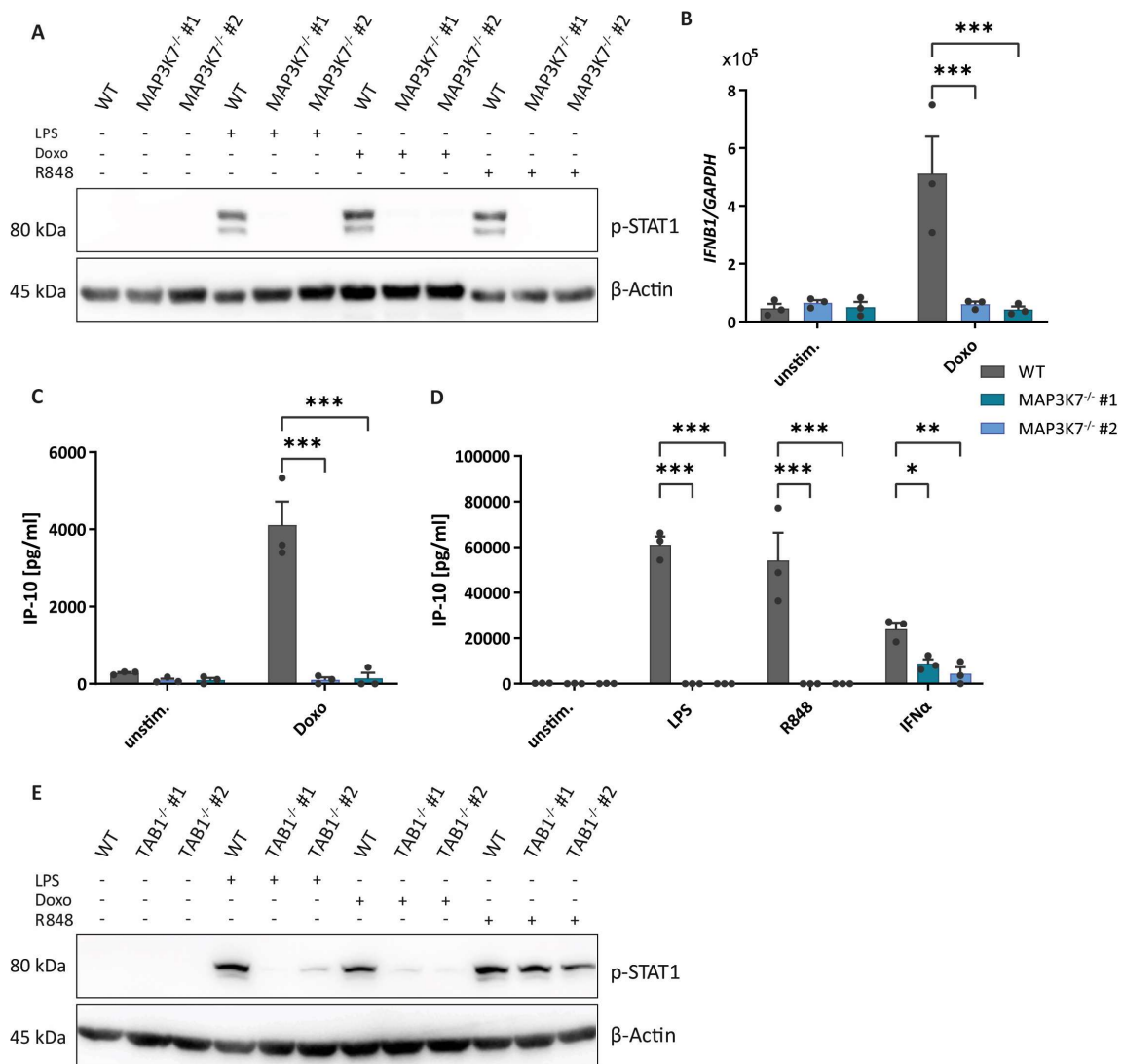

Figure 4.8 TAK1 is a central mediator of the DDR induced antiviral immune response
(A) Immunoblot of BLaER1 WT and *MAP3K7⁻/⁻* cells treated with LPS or R848 for four hours or Doxorubicin for eight hours. **(B)** BLaER1 *MAP3K7⁻/⁻* and WT cells were treated with or without Doxorubicin for eight hours and analysed by qPCR. **(C and D)** BLaER1 WT and *MAP3K7⁻/⁻* were treated for six hours for R848 and IFNα and 24 hours for LPS and Doxorubicin, and IP-10 was detected in the supernatant by ELISA. **(E)** BLaER1 WT and *TAB1⁻/⁻* cells were stimulated as described in **(A)** and analysed by immunoblotting. A representative immunoblot of three independent experiments is depicted **(A and E)**. The ELISA and qPCR depicted shows the mean and error bars represent the SEM of three independent experiments **(B-D)**. Statistical significance was calculated using two-way

MAP3K7$^{-/-}$ BLaER1 cells were generated and tested for their influence on DSB induced antiviral immune signalling by qPCR, ELISA and immunoblotting. MAP3K7 deficient cells showed a loss of STAT1 phosphorylation upon stimulation with LPS, R848 and Doxorubicin in the immunoblot (Figure 4.8 A). The expression levels of IFNβ mRNA were determined by qPCR. WT cells showed an induction of IFNβ mRNA levels, while MAP3K7 deficient cells did not show elevated levels of IFNβ mRNA upon Doxorubicin treatment (Figure 4.8 B). In addition, the production of IP-10 was analysed by ELISA. Similar to the immunoblotting observations, *MAP3K7*$^{-/-}$ cells showed no production of IP-10 upon stimulation with Doxorubicin (Figure 4.8 C), LPS or R848 (Figure 4.8 D). Interestingly, IP-10 production of *MAP3K7*$^{-/-}$ cells stimulated with IFNα was also reduced compared to WT cells production (Figure 4.8 D). It is conceivable that MAP3K7 activity is needed to induce IP-10, which is dependent on NF-κB activity. Immunoblotting was subsequently used to analyse the adaptor protein TAB1. *TAB1*$^{-/-}$ cells showed no phosphorylation of STAT1 upon stimulation with LPS or Doxorubicin (Figure 4.8 E). Surprisingly, the phosphorylation of STAT1 was not affected in cells stimulated with R848 (Figure 4.8 E). These results concur with the importance of MAP3K7 in signal transduction, followed by the activation of PRRs. Moreover, MAP3K7 and its adaptor protein TAB1 also represent an important link in the signalling cascade leading from DSBs to a type I IFN response.

4.7   NF-κB signalling cascade in the DDR response

MAP3K7 plays a central role in the activation of NF-κB transcription factors through the canonical NF-κB cascade. MAP3K7 has been described to phosphorylate and activate IKKβ, which is part of the IKK complex [377]. The IKK complex consists of three proteins, IKKα (*CHUK*), IKKβ (*IKBKB*) and IKKγ (*IKBKG*). IKKγ has been described as a regulatory subunit that is polyubiquitinated upon activation and forms a signalling scaffold. The two kinase subunits, IKKα and IKKβ, phosphorylate IκBα, subsequently activating the transcription factor NF-κB. In addition, IKKγ has been suggested to interact with ATM during genotoxic stress, subsequently mediating the downstream activation of NF-κB [344]. Thus, *IKBKG*$^{-/-}$, *CHUK*$^{-/-}$ and *IKBKB*$^{-/-}$ cells were generated and analysed for their involvement in DSB mediated type I IFN induction.

IKKγ deficient cells were stimulated with LPS, R848 and Doxorubicin and subsequently analysed by immunoblotting. The knockout of IKKγ was additionally validated by immunoblot (Figure 4.9 A). The deficiency of IKKγ was observed to lead to a complete loss of STAT1 phosphorylation for all three stimulants (Figure 4.9 A). However, a weak residual band for phosphorylated STAT1 was still visible for the stimulation with Doxorubicin (Figure 4.9 A). IKKα, IKKβ and IKKα/IKKβ deficient BLaER1 cells were generated by CRISPR/Cas9 mediated gene targeting and were analysed by immunoblotting. The knockouts were also validated by immunoblotting (Figure 4.9 C). IKKα, IKKβ and IKKα/IKKβ deficient cells were stimulated with LPS, R848 and Doxorubicin and analysed by immunoblotting for the phosphorylation of STAT1. The *CHUK*$^{-/-}$ cells showed increased phosphorylation of STAT1 when stimulated with LPS compared to WT cells, while for the *IKBKB*$^{-/-}$ cells and the double knockout cells a complete loss of STAT1 phosphorylation was observed (Figure 4.9 B). Similar to the LPS stimulation, STAT1 phosphorylation in *IKBKB*$^{-/-}$ and double knockout cells stimulated with R848 was completely absent (Figure 4.9 B). The *CHUK*$^{-/-}$ cells stimulated with R848 displayed STAT1 phosphorylation levels

similar to WT cells. In contrast to the stimulation with LPS and R848, *CHUK*⁻/⁻ cells and *IKBKB*⁻/⁻ cells stimulated with Doxorubicin displayed an equal reduction of STAT1 phosphorylation compared to WT cells, only double knockout cells depicted a complete loss of STAT1 phosphorylation (Figure 4.9 B). Overall, the DSB mediated type I IFN expression is dependent on all three factors of the IKK complex.
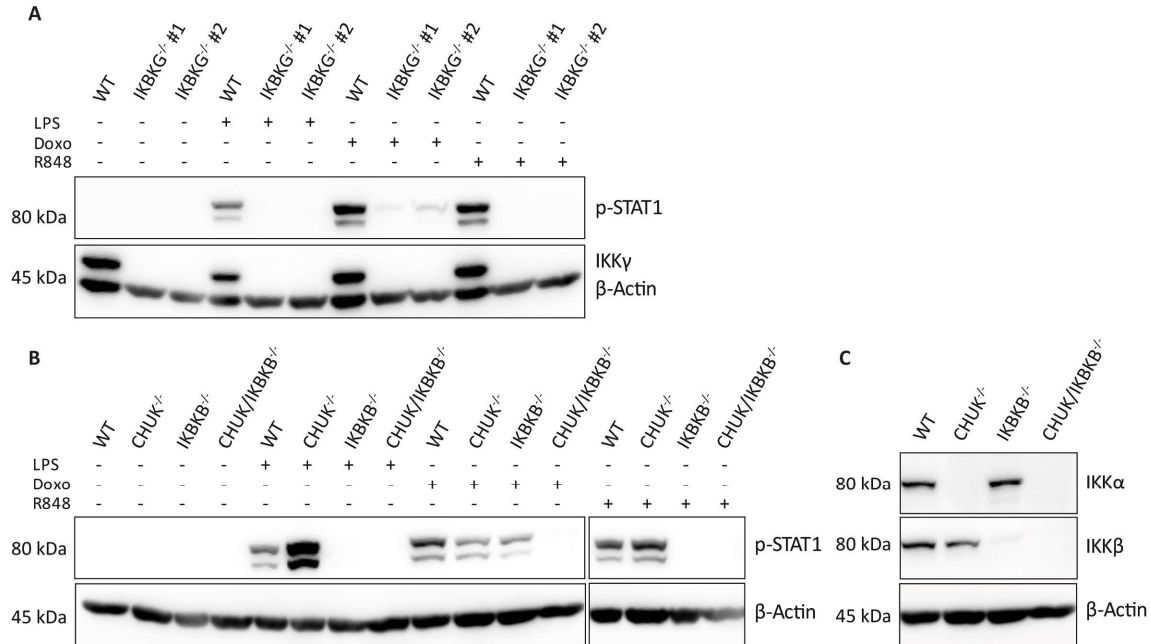

Figure 4.9 DDR dependent induction of an antiviral immune response is dependent on the IKK complex
(A) BLaER1 WT and *IKBKG*⁻/⁻ cells were treated with LPS or R848 for four hours or with Doxorubicin for eight hours and analysed by immunoblotting. **(B)** Immunoblot of BLaER1 WT and *CHUK*⁻/⁻, *IKBKB*⁻/⁻ or *CHUK/IKBKB*⁻/⁻ cells treated with LPS or R848 for four hours or Doxorubicin for eight hours. **(C)** BLaER1 *CHUK*⁻/⁻, *IKBKB*⁻/⁻ or *CHUK/IKBKB*⁻/⁻ cells were validated by immunoblotting after being selected by deep sequencing of the target region. A representative immunoblot of three independent experiments is depicted **(A-C)**.

The activation of the IKK complex and the dependence of the DSB induced type I IFN response on both IKKα and IKKβ hints at the activation of canonical or non-canonical NF-κB transcription factors. To evaluate the involvement of NF-κB transcription factors, RelA and RelB deficient BLaER1 cells were generated and tested by immunoblotting and qPCR. While RelA deficient cells depicted a complete loss of STAT1 phosphorylation upon treatment with LPS, Doxorubicin or R848 (Figure 4.10 A), RelB deficient cells showed similar levels of STAT1 phosphorylation as WT cells for all three stimuli (Figure 4.10 B). This observation was validated by the results obtained by qPCR for RelA and RelB deficient cells stimulated with Doxorubicin. *RELA*⁻/⁻ cells exhibited a significantly reduced induction of IFNβ mRNA levels compared to WT cells (Figure 4.10 C). In contrast, *RELB*⁻/⁻ cells showed no significant change for the IFNβ mRNA levels compared to WT cells (Figure 4.10 D). Overall, these experiments demonstrated the involvement of RelA in the induction of an antiviral immune response by DSBs, while indicating RelB is not crucial for this signalling cascade.
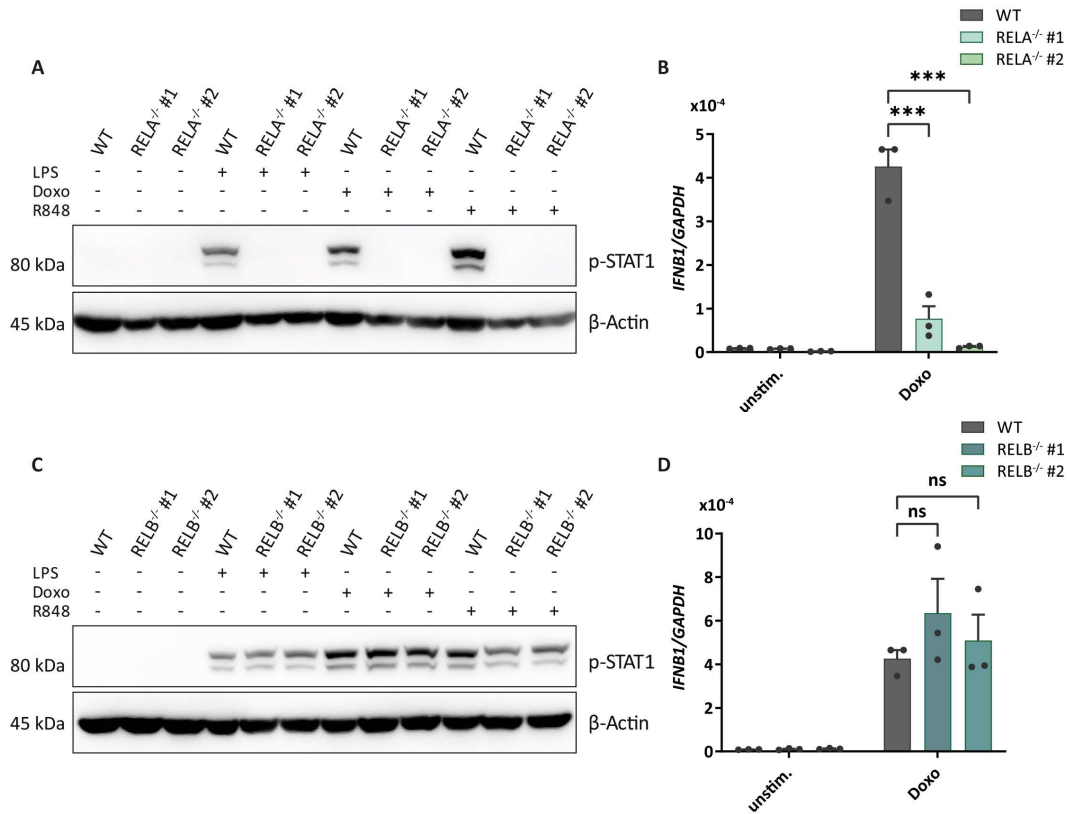
Figure 4.10 Dependency on the transcription factor p65 for the induction of an antiviral immune response
(A) Immunoblot of BLaER1 WT and *RELA*$^{-/-}$ cells treated with LPS or R848 for four hours or Doxorubicin for eight hours. **(B)** Two BLaER1 *RELA*$^{-/-}$ clones (turquoise) and WT cells were treated with or without Doxorubicin for eight hours and analysed by qPCR. **(C)** BLaER1 WT and *RELB*$^{-/-}$ cells were treated with LPS or R848 for four hours or with Doxorubicin for eight hours and analysed by immunoblotting. **(D)** BLaER1 *RELB*$^{-/-}$ (blue) and WT cells were treated with or without Doxorubicin for eight hours and analysed by qPCR. A representative immunoblot of three independent experiments is depicted **(A and C)**. The qPCR data depicted shows the mean and error bars represent the SEM of three independent experiments **(B and D)**. Statistical significance was calculated using two-way ANOVA. Sidak's correction was employed for multiple comparison testing. *** $p \leq 0.001$; ** $p \leq 0.01$; * $p \leq 0.05$; ns, not significant.

4.8 MAPK signalling in the context of DDR induced type I interferon induction

Besides the activation of NF-κB transcription factors, also AP-1 transcription factors, which are activated by MAPK signalling cascades, are important for the activation of a type I IFN response. During the time-course experiments, a phosphorylation and therewith an activation of the JNK and p38 MAPKs was detected. In this context, MAP3K7 has been described to activate both MAPK modules besides its role in priming the IKK complex for NF-κB activation [67]. However, additional MAP3Ks have been described to be involved in the activation of p38 and JNK MAPKs [171].

The MAP3K MAP3K3 (also known as MEKK3) has previously been described to act upstream of the IKK complex in response to certain stimuli and can mediate p38, JNK and ERK5 activation through their respective MAP2Ks [167,378,379]. Therefore, *MAP3K3*$^{-/-}$ cells were generated by CRISPR/Cas9 mediated gene targeting and were subsequently tested for their impact on the DSB mediated type I IFN response by immunoblotting and qPCR. In the immunoblot, MAP3K3 deficient cells showed a slightly reduced

phosphorylation of STAT1 upon stimulation with LPS, R848, and Doxorubicin compared to WT cells (Figure 4.11 A). In contrast to the STAT1 phosphorylation data, *MAP3K3$^{-/-}$* cells that underwent qPCR showed that the IFNβ mRNA levels of the knockout cells were significantly reduced compared to WT cells upon stimulation with Doxorubicin (Figure 4.11 B). Thus, induction of IFNβ mRNA levels by LPS or R848 stimulation was not impacted by MAP3K3 deficiency (Figure 4.11 C). In conclusion, MAP3K seems to impact the regulation of IFNβ, however, to a smaller extent than MAP3K7, which completely blunts type I IFN signalling as depicted in the STAT1 phosphorylation levels and IFNβ mRNA levels.
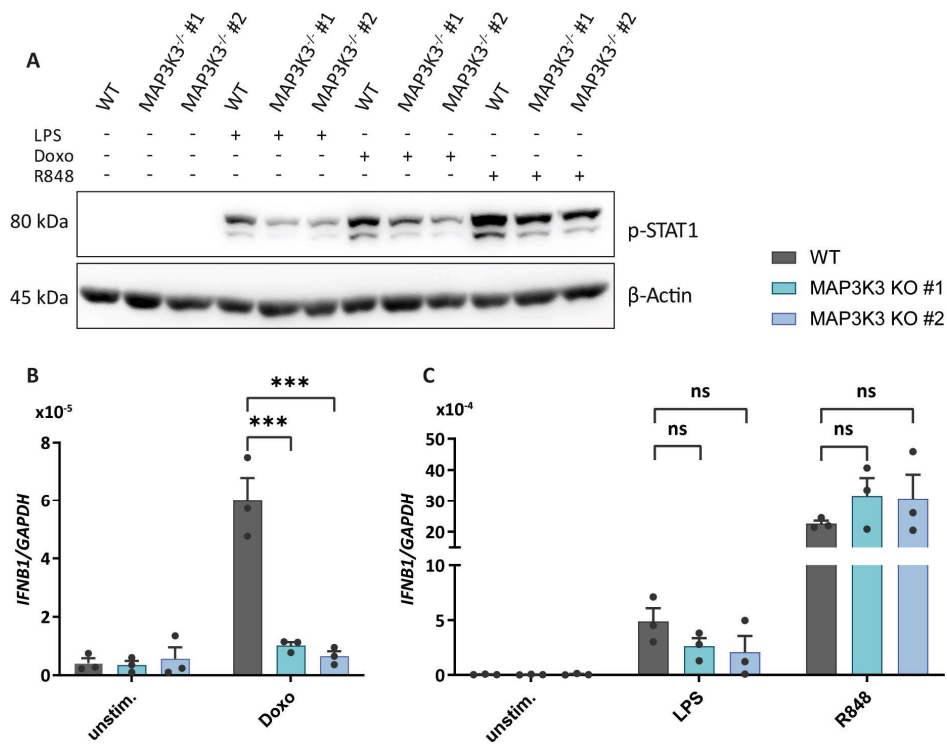

Figure 4.11 MEKK3 influences the expression of type I interferons
(A) Immunoblot of BLaER1 WT and *MAP3K3$^{-/-}$* cells treated with LPS or R848 for four hours or Doxorubicin for eight hours. A representative immunoblot of three independent experiments is depicted. **(B and C)** The IFNβ mRNA levels were determined in WT and *MAP3K3$^{-/-}$* cells upon stimulation with Doxorubicin or LPS for 8 hours or for 6 hours with R848 for six hours. The qPCR data depicted shows the mean and error bars represent the SEM of three independent experiments **(B and C)**. Statistical significance was calculated using two-way ANOVA. Sidak's correction was employed for multiple comparison testing. *** $p \leq 0.001$; ** $p \leq 0.01$; * $p \leq 0.05$; ns, not significant.

MAP3Ks activation mediates the activation of downstream MAP2Ks. Due to the function of MAP3K7 in both the JNK and the p38 module, four possible MAP2Ks for signal transduction were of interest. MKK3 (*MAP2K3*), MKK6 (*MAP2K6*) and MKK4 (*MAP2K4*) phosphorylate p38 MAPKs, while MKK4 and MKK7 (MAP2K7) phosphorylate JNK MAPKs (Fig. 1.2). Since the activation of JNKs appeared to occur concomitant or after the phosphorylation of STAT1 (Fig. 4.1) and Doxorubicin stimulated cells depicted very robust p38 phosphorylation compared to cells stimulated with LPS or R848, the focus was put on the three p38-phosphorylating MAP2Ks, MKK3, MKK4 and MKK6.

Firstly, *MAP2K3$^{-/-}$* BLaER1 cells were generated and analysed by immunoblotting. Stimulation with LPS in *MAP2K3$^{-/-}$* cells showed reduced STAT1 phosphorylation compared to WT cells, while R848 and

Doxorubicin stimulation did not differ between WT and KO cells (Figure 4.12 A). No difference in the phosphorylation of JNK and p38 was detectable between knockout and WT cells (Figure 4.12 A).
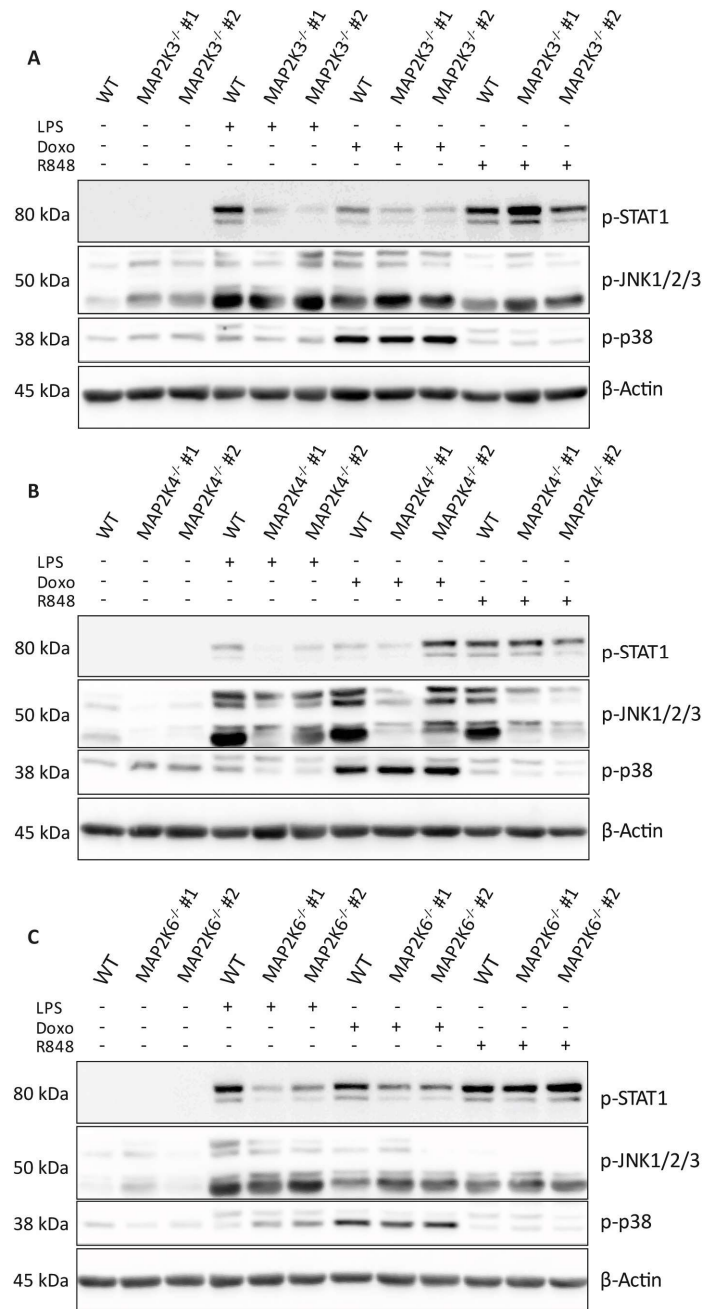

Figure 4.12 Single knockouts of MAP2Ks show no impact on type I interferon induction
(A-C) Immunoblot analysis of BLaER1 WT and different *MAP2K$^{-/-}$* cells as indicated. Cells were treated with LPS or R848 for four hours or Doxorubicin for eight hours. A representative immunoblot of three independent experiments is depicted **(A-C)**.

MAP2K4$^{-/-}$ cells displayed similar levels of STAT1 and p38 phosphorylation as WT cells in the immunoblot for all three stimuli (Figure 4.12 B). However, MKK4 deficient cells showed reduced JNKs activation (Figure 4.12 B). In MKK6 deficient BLaER1 cells, phosphorylation of STAT1 was slightly reduced in LPS and Doxorubicin treated cells, while R848 stimulation was unaffected (Figure 4.12 C).

65

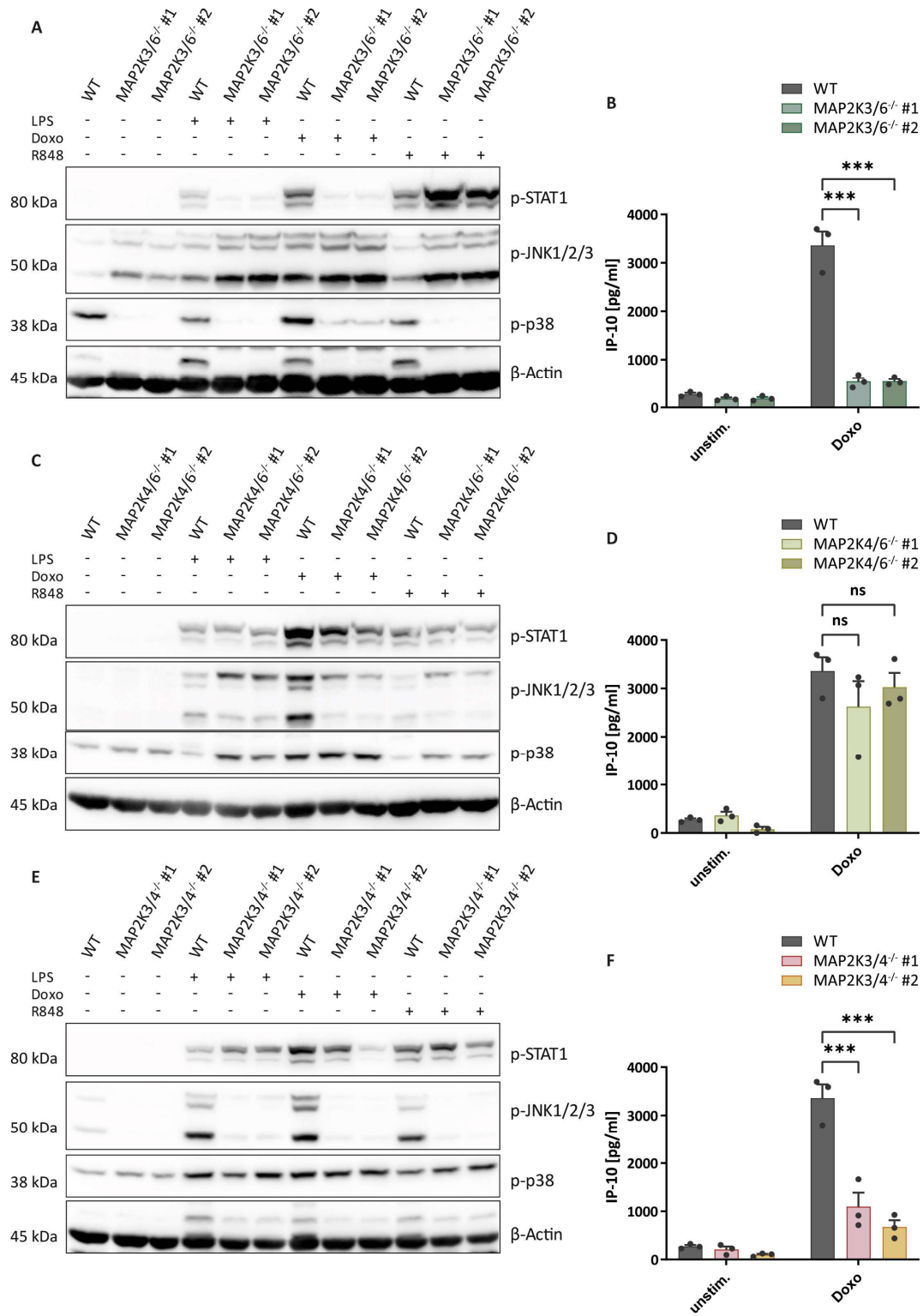MKK6 deficient cells displayed similar levels of JNK and p38 phosphorylation as WT cells (Figure 4.12 C).

Figure 4.13 MAP2Ks influences the expression of type I interferons upon DSB induction
(A) Immunoblot of BLaER1 WT and *MAP2K3/6⁻/⁻* cells treated with LPS or R848 for four hours or Doxorubicin for eight hours. **(B)** IP-10 secretion was determined after stimulation with or without Doxorubicin stimulation for 24

hours in BLaER1 WT and *MAP2K3/6$^{-/-}$* cells (green). **(C)** BLaER1 WT and *MAP2K4/6$^{-/-}$* cells treated with LPS or R848 for four hours or Doxorubicin for eight hours were analysed by immunoblotting. **(D)** The supernatant of BLaER1 WT and *MAP2K4/6$^{-/-}$* cells (olive) were analysed for secreted IP-10 by ELISA upon stimulation with or without Doxorubicin for 24 hours. **(E)** Immunoblot of BLaER1 WT and *MAP2K3/4$^{-/-}$* cells treated with LPS or R848 for four hours or Doxorubicin for eight hours. **(F)** IP-10 secretion was determined upon stimulation of BLaER1 WT and *MAP2K3/4$^{-/-}$* cells (red/orange) with or without Doxorubicin for 24 hours. A representative immunoblot of three independent experiments is displayed **(A, C and E)**. The ELISA data depicted shows the mean and error bars represent the SEM of three independent experiments **(B, D and F)**. Statistical significance was calculated using two-way ANOVA. Sidak's correction was employed for multiple comparison testing. *** $p \leq 0.001$; ** $p \leq 0.01$; * $p \leq 0.05$; ns, not significant.

Since many MAP2Ks share similar functions and are often redundant, double knockouts of the three tested MAP2Ks were generated using CRISPR/Cas9 mediated gene targeting. *MAP2K3$^{-/-}$/MAP2K6$^{-/-}$* cells were stimulated with LPS, Doxorubicin and R848 and analysed by immunoblotting. The double knockout exhibited almost no phosphorylation of STAT1 in LPS and Doxorubicin treated cells (Figure 4.13 A). Moreover, these cells displayed a complete loss of p38 phosphorylation when stimulated with LPS and R848, while phosphorylation of JNK was not affected (Figure 4.13 A). In cells stimulated with Doxorubicin, no change between WT and knockout cells was detectable in the phosphorylation of JNK, but the phosphorylation of p38 was strongly reduced (Figure 4.13 A). This observation was validated by ELISA for secreted IP-10. *MAP2K3$^{-/-}$/MAP2K6$^{-/-}$* cells displayed a complete loss of IP-10 production upon stimulation with Doxorubicin (Figure 4.13 B). Subsequently, *MAP2K4$^{-/-}$/MAP2K6$^{-/-}$* cells were tested by immunoblotting and IP-10 ELISA. This double knockout displayed a slight reduction in STAT1 phosphorylation levels when treated with Doxorubicin, but not when stimulated with R848 or LPS (Figure 4.13 C). Additionally, the JNK phosphorylation was strongly reduced when stimulated with Doxorubicin, while p38 phosphorylation was not affected (Figure 4.13 C). IP-10 production upon stimulation with Doxorubicin displayed no significant changes compared to WT cells (Figure 4.13 D). *MAP2K3$^{-/-}$/MAP2K4$^{-/-}$* cells in contrast, showed a more robust reduction in STAT1 phosphorylation levels than *MAP2K4$^{-/-}$/MAP2K6$^{-/-}$* cells (Figure 4.13 E). STAT1 phosphorylation was not affected if cells were stimulated with LPS or R848 (Figure 4.13 E). Interestingly, *MAP2K3$^{-/-}$/MAP2K4$^{-/-}$* cells completely lost JNK phosphorylation when stimulated with LPS, R848, and Doxorubicin, while p38 phosphorylation remained unaffected (Figure 4.13 E). The production of IP-10 was also significantly reduced in *MAP2K3$^{-/-}$/MAP2K4$^{-/-}$* cells compared to WT cells (Figure 4.13 F). All three MAP2Ks affect the DSB induced immune response, albeit in different ways. While MKK3 and MKK6 appears to mainly regulate p38 activation, the JNK response is largely MKK4-dependent following Doxorubicin treatment. In the context of DDR signalling STAT1 phosphorylation is only seen in the presence of an intact p38 response, while JNK activation seems to be dispensable. IP-10 production was nevertheless affected in cells, in which JNK signalling was perturbed, yet this could be attributable to the fact that IP-10 production requires additional input. LPS-dependent activation of STAT1 in the context of MAPK perturbation was largely congruent with the picture seen for the Doxorubicin response. However, R848 stimulation is independent of p38 activation.

MAP2Ks activation subsequently leads to MAPKs phosphorylation and activation. MKK3, MKK4 and MKK6 mainly regulate the activation of p38 and JNK MAPKs. Both groups consist of several protein members and isoforms. Due to their described role in stress and immune signalling and their expression profile in BLaER1 cells, MAPK8 (also known as JNK1), MAPK9 (also known as JNK2) and

MAPK14 (also known as p38α) were further investigated. MAPK8 deficient cells showed no reduction in STAT1 and p38 phosphorylation upon stimulation with LPS, Doxorubicin or R848 in the immunoblot (Figure 4.14 A). However, the JNK phosphorylation was reduced for all three tested stimulations due to the knockout of MAPK8 (JNK1) (Figure 4.14 A). The knockout of MAPK9 led to a slight reduction in phosphorylated STAT1, upon stimulation with LPS and Doxorubicin, while R848 stimulation was not impacted (Figure 4.14 B). The phosphorylation level of p38 was increased in MAPK9 deficient cells stimulated with Doxorubicin and slightly for LPS and R848 treated cells (Figure 4.14 B).
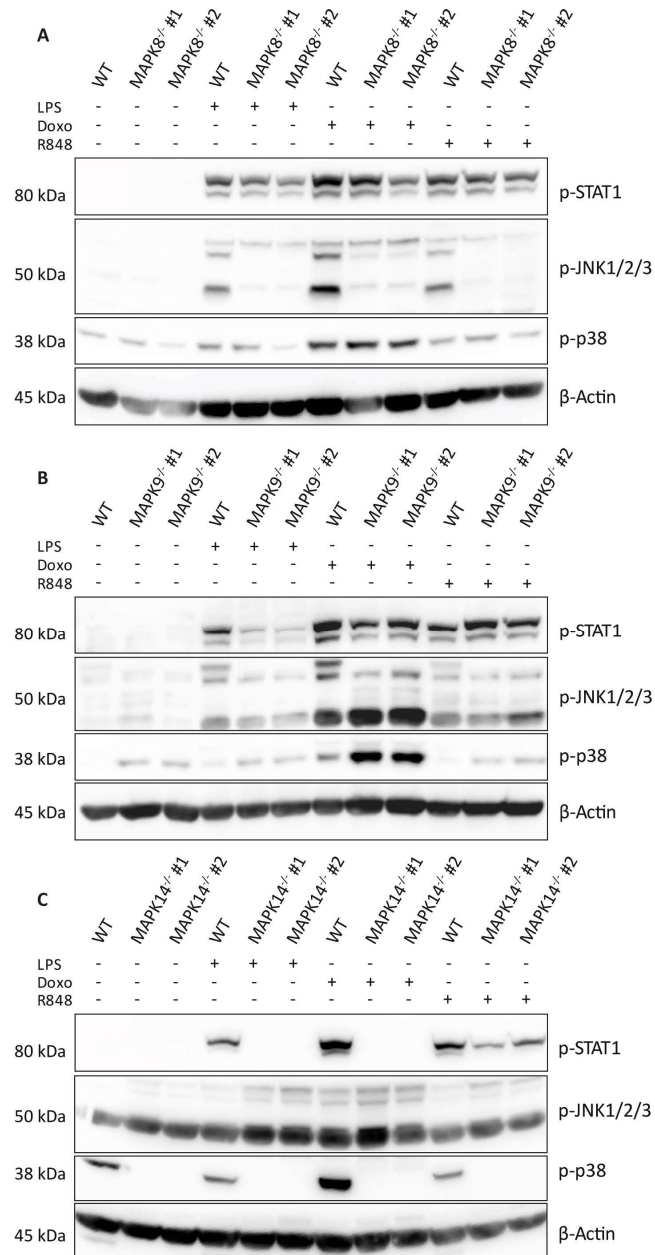

Figure 4.14 MAPK14 is important for DDR mediated type I interferon induction
(A-C) Immunoblot analysis of BLaER1 WT and *MAPK8⁻/⁻* (A), *MAPK9⁻/⁻* (B) or *MAPK14⁻/⁻* (C) cells as indicated. Cells were treated with LPS or R848 for four hours or Doxorubicin for eight hours. A representative immunoblot of three independent experiments is depicted (A-C).

In addition, a complete loss of the highest band of phosphorylated JNK was observed, indicating the knockout of MAPK9 (JNK2) (Figure 4.14 B). MAPK14 deficient cells exhibited a complete loss of STAT1 phosphorylation upon stimulation with LPS and Doxorubicin in the immunoblot, while R848 stimulation was only slightly reduced (Figure 4.14 C). Moreover, the MAPK14 deficient cells showed a complete loss of p38 phosphorylation, indicating that only the p38 family member MAPK14 (p38α) was activated and phosphorylated under the conditions studied (Figure 4.14 C). Phosphorylation of JNKs was not affected in MAPK14 deficient cells (Figure 4.14 C). Overall, all three MAPKs are activated upon stimulation with LPS, R848 and Doxorubicin and their respective knockouts are represented by the loss of specific phosphorylation bands in the immunoblot. However, only MAPK14 is able to completely prevent the induction of STAT1 phosphorylation upon Doxorubicin treatment, indicating that the later activated JNKs (Fig. 4.1) could be a part of a feedback response.
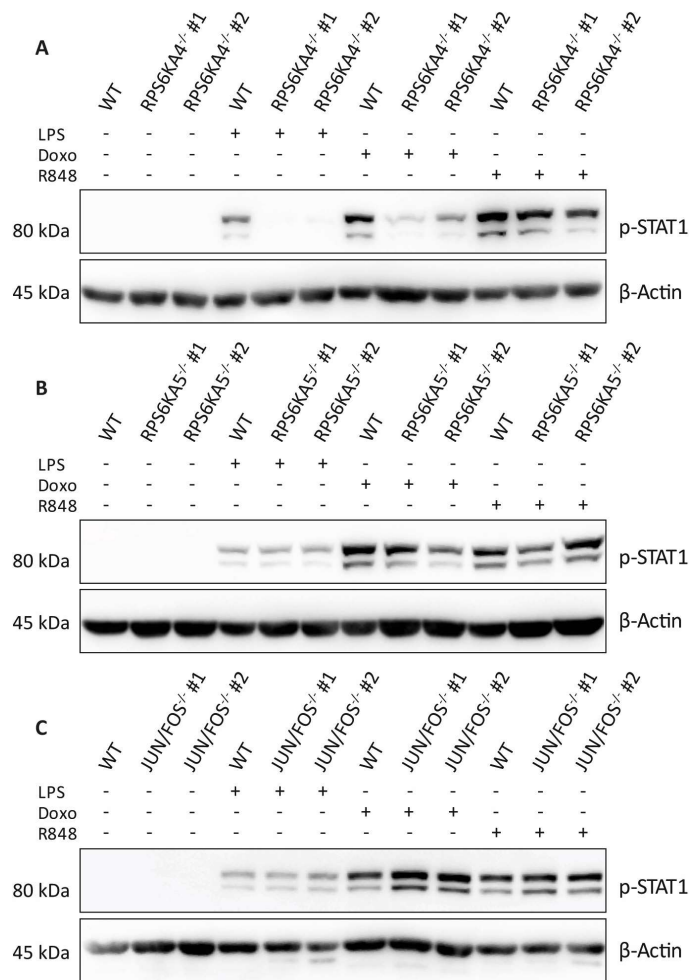

Figure 4.15 MSK2 triggers the type I interferon induction
(A-C) Immunoblot analysis of BLaER1 WT and *RPS6KA4*$^{-/-}$ **(A)**, *RPS6KA5*$^{-/-}$ **(B)** or *JUN/FOS*$^{-/-}$ **(C)** cells as indicated. Cells were treated with LPS or R848 for four hours or Doxorubicin for eight hours. A representative immunoblot of three independent experiments is depicted **(A-C)**.

MAPKs can activate AP-1 transcription factors directly or lead to the activation of MAPKAPKs, which promote further downstream signalling. Therefore, several knockout cell lines of MAPKAPKs, like MSK1 and MSK2, and AP-1 transcription factors, were generated and analysed. MSK2 (*RPS6KA4*) deficient

cells depicted a loss of STAT1 phosphorylation in the immunoblot upon stimulation with LPS (Figure 4.15 A). In addition, *RPS6KA4*^{-/-} cells showed reduced STAT1 phosphorylation compared to WT cells upon treatment with Doxorubicin, while STAT1 phosphorylation for R848 stimulation was not affected (Figure 4.15 A). MSK1 (*RPS6KA5*) deficient cells, in contrast, showed no reduction of STAT1 phosphorylation compared to WT cells upon stimulation with LPS, Doxorubicin or R848 (Figure 4.15 B). AP-1 transcription factors were subsequently analysed for their function in DSB induced type I IFN induction. Initially, two transcription factors, Jun and Fos, of the four AP-1 subfamilies were investigated since both have been reported to trigger type I IFN induction under certain conditions [272,380]. However, the double knockout of Jun and Fos resulted in no reduction of STAT1 phosphorylation levels in the immunoblot upon treatment with LPS, R848 or Doxorubicin (Figure 4.14 C). Overall, the MAPKAPK MSK2, which functions downstream of MAPK14, appears to be essential for signal transduction cascade of DSB-dependent type I IFN induction. Thus, a signalling cascade emanating from MAP3K7 (and to a minor extent from MAP3K3) to the activation of three MAP2Ks and further to the activation of MAPK14 and MSK2 appears the most likely. A decisive role for a specific AP-1 transcription factor downstream this signalling cascade could not be identified.

4.9 The IRF transcription factor family in the DSB induced antiviral immune signalling

The last group of transcription factors required for the induction of an antiviral immune response is the IRF transcription factor family. Especially, IRF3, IRF5 and IRF7 have been described to be activated upon PRR activation and to mediate a type I IFN response. The pLxIS motif-containing adaptor proteins represent one major regulatory step in the activation of these IRFs [73]. Several IRF family members were previously tested in our lab and showed no impact on the DSB induced type I IFN response [346].

To validate the previous results, quadruple- and penta-knockouts of IRF family members were generated and tested by immunoblotting. Cells deficient for IRF1, IRF3, IRF5 and IRF7 depicted a complete loss of STAT1 phosphorylation upon treatment with LPS or R848 (Figure 4.16 A). In contrast, upon stimulation with Doxorubicin, these cells displayed only a slightly reduced STAT1 phosphorylation compared to WT cells (Figure 4.16 A). In addition, cells deficient for IRF3, IRF4, IRF5 and IRF7 were analysed. This quadruple-knockout displayed, like the first one, a complete loss of STAT1 phosphorylation upon LPS and R848 treatment, while Doxorubicin treated cells behaved as the WT control (Figure 4.16 B). Interestingly, the penta-knockout of five IRFs, IRF1, IRF3, IRF4, IRF5 and IRF7, displayed a complete loss of STAT1 phosphorylation. This was true not only for the stimulation with LPS and R848 as observed in the quadruple-knockouts but also for the stimulation with Doxorubicin (Figure 4.16 C). This result suggested an important role for the two transcription factors IRF1 and IRF4, in the DSB mediated type I IFN response.

To this end, knockout cell lines for IRF1 and IRF4 were generated by CRISPR/Cas9 mediated gene targeting and analysed by immunoblotting on their function in the DSB induced antiviral immune response. IRF1 and IRF4 knockout identities were validated by immunoblotting (Figure 4.17 B and D). Here, IRF1 deficient cells were stimulated with LPS, R848 and Doxorubicin and subsequently analysed by immunoblotting. *IRF1*^{-/-} cells depicted reduced STAT1 phosphorylation upon stimulation with LPS or Doxorubicin compared to WT cells (Figure 4.17 A). The stimulation with R848 was not impacted by IRF1 deficiency (Figure 4.17 A). However, the stimulation of WT cells with LPS, Doxorubicin and R848 led to

elevated IRF1 protein levels compared to the unstimulated control indicating its activation (Figure 4.17 A). Like IRF1-deficient cells, IRF4-deficient cells exhibited reduced STAT1 phosphorylation upon treatment with LPS and Doxorubicin compared to the WT control, while R848 meditated type I IFN expression remained unchanged (Figure 4.17 C).
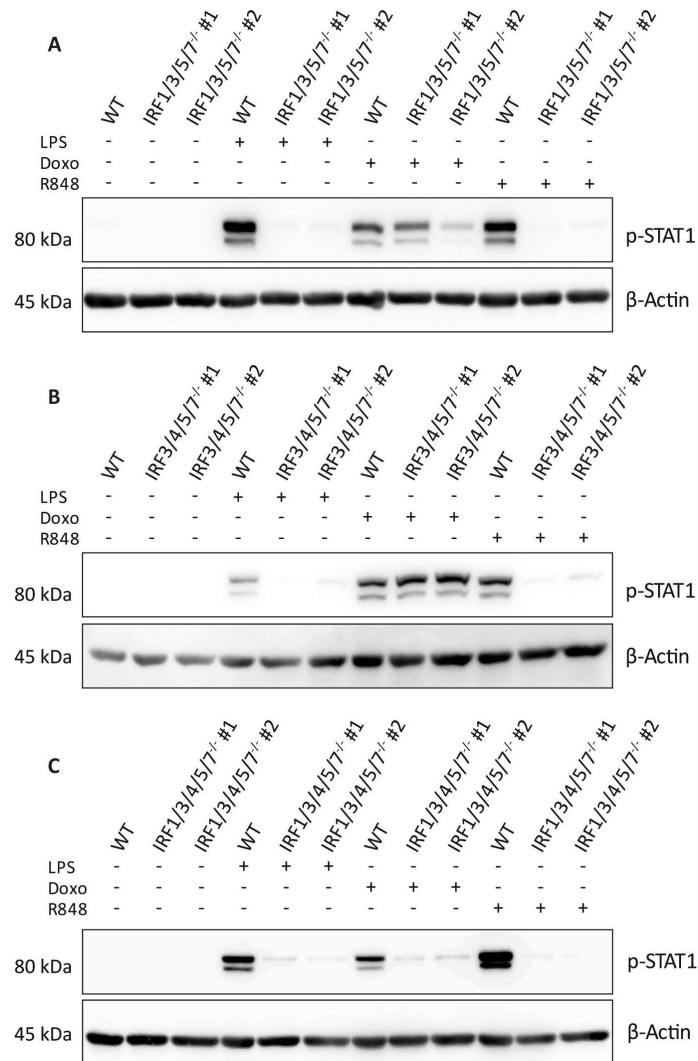

Figure 4.16 IRF1/3/4/5/7 triggers the type I interferon induction
(A-C) Immunoblot analysis of BLaER1 WT and *IRF1/3/5/7$^{-/-}$* **(A)**, *IRF3/4/5/7$^{-/-}$* **(B)** or *IRF1/3/4/5/7$^{-/-}$* **(C)** cells as indicated. Cells were treated with LPS or R848 for four hours or Doxorubicin for eight hours. A representative immunoblot of three independent experiments is depicted **(A-C)**.

Double-knockouts of IRF1 and IRF4 were then generated and analysed by immunoblotting. *IRF1$^{-/-}$* and *IRF4$^{-/-}$* cells showed an almost complete loss of STAT1 phosphorylation upon treatment with LPS or Doxorubicin, again the stimulation with R848 was not affected (Figure 4.17 E). These observations could be validated by testing all three knockouts side by side depicting the reduction of STAT1 phosphorylation in the single-knockouts in comparison to the double-knockout and WT cells upon stimulation with LPS and Doxorubicin. Here, *IRF1$^{-/-}$* or *IRF4$^{-/-}$* cells displayed only a slight reduction in STAT1 phosphorylation upon LPS and Doxorubicin, only the double-knockout completely eliminated

71

STAT1 phosphorylation (Figure 4.17 F). The transcription factor binding profiles of IRF1 and IRF4 are very similar as visualized in the position weight matrix obtained by JASPAR (Figure 4.17 G and H). The similarity of the binding profiles indicates the same binding site for IRF1 and IRF4 in the IFN promotor. Together, these data indicate that the regulation of DSB induced type I IFN expression is mediated by IRF1 and IRF4, while it is independent of IRF3, IRF5 and IRF7.
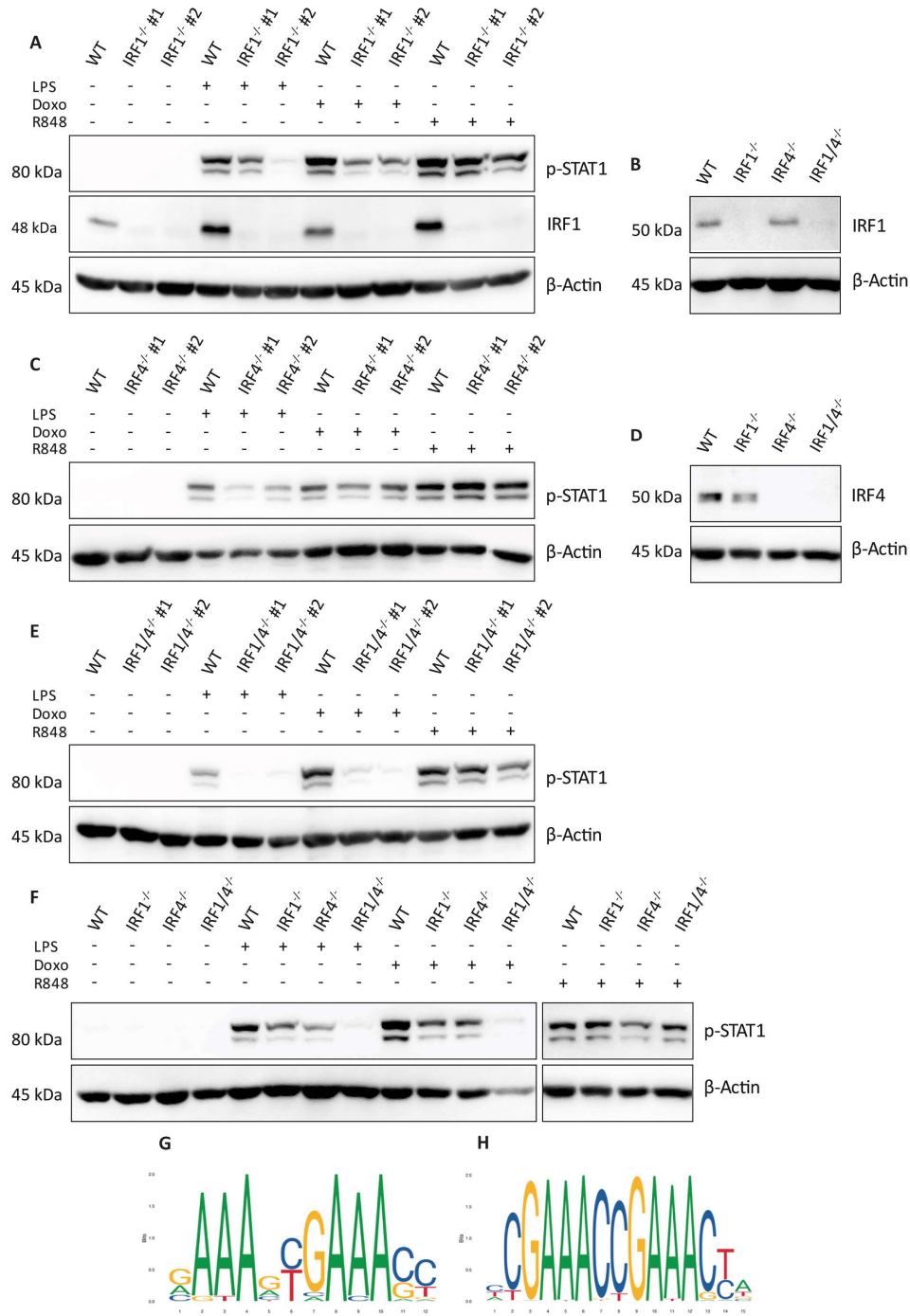
Figure 4.17 IRF1/4$^{-/-}$ blocks the type I interferon induction
(A, C, E and F) Immunoblot analysis of BLaER1 WT and *IRF1$^{-/-}$*, *IRF4$^{-/-}$* or *IRF1/4$^{-/-}$* cells as indicated. Cells were treated with LPS or R848 for four hours or Doxorubicin for eight hours. **(B and D)** BLaER1 *IRF1$^{-/-}$*, *IRF4$^{-/-}$* or *IRF1/4$^{-/-}$* cells were validated by immunoblotting after being selected by deep sequencing of the target region. A

representative immunoblot of three independent experiments is depicted **(A-F)**. **(G-H)** Transcription factor binding profiles for IRF1 (F) and IRF4 (G) visualized by a position weight matrix and obtained from JASPAR [381].

4.10 BLaER1 SMRV RT knockout generation

The BLaER1 transdifferentiation system is used as a model system of monocytes and macrophages. However, our lab's recent findings of testing the supernatant for RT activity and analysing RNA sequencing for viral sequences showed a contamination of the original cell line with SMRV. To restore and enable handling BLaER1 cells under biosafety 1 conditions, a knockout approach for the RT of the SMRV was conducted. A set of two gRNAs flanking the RT and primers widely spanning the target site were designed (Figure 4.18 A). BLaER1 cells were electroporated with two constructs containing either gRNA1 or gRNA2 and gRNA3 or gRNA4, FACS sorted and plated (Figure 4.18 A). Grown clones were picked after approximately four weeks of culture and subjected to testing by PCR. In the case of SMRV RT KO cells, a drop of around 600 bp in the amplicon size generated by PCR was visible (Figure 4.18 B). However, some samples displayed both the WT amplicon length and the RT KO amplicon length in different intensities, indicating polyclones or multiple insertions sites of SMRV in the BLaER1 genome. The KO efficiency in total was relatively low, with only 16 identified KOs out of 384 tested monoclones. The clones were subsequently tested for residual RT activity in the supernatant by SG-PERT assay. While BLaER1 WT cells depicted a strong RT activity in the supernatant, SMRV knockout cells displayed a complete loss of RT activity similar to not transduced HEK293T cells, which were used as a negative control (Figure 4.18 E).

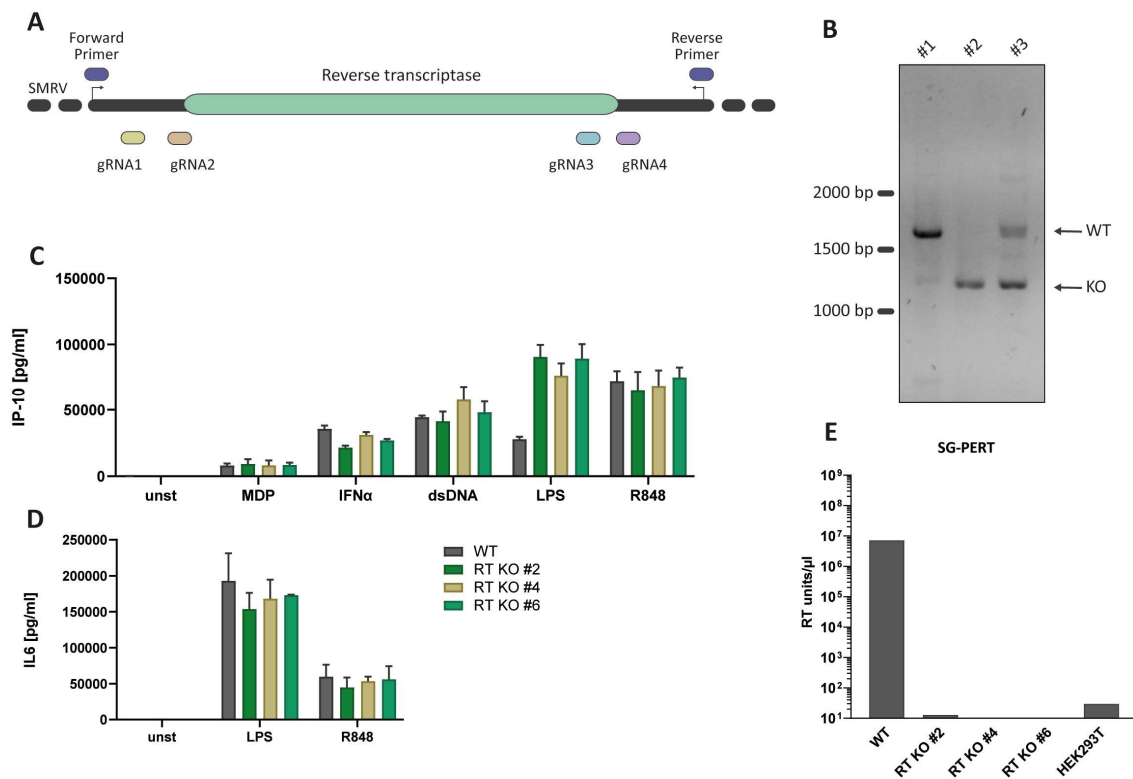**Figure 4.18 Reverse transcriptase KO in SMRV infected cells**
(A) Schematic of the RT KO generation with the gRNA target site locations and the respective primers for KO validation. **(B)** Representative agarose gel of the RT KO validation. **(C-D)** The supernatant of BLaER1 WT cells (grey) and three independent BLaER1 RT knockout cells were analysed by ELISA for cytokine expression upon

stimulation with MDP or LPS for 24 hours or with IFNα, R848 and transfected dsDNA for six hours. The data depicted shows the mean and error bars represent the SEM of three independent experiments. **(E)** SG-PERT Assay for BLaER1 WT and $RT^{-/-}$ cells.

The ability of the BLaER1 RT deficient cells to respond to different stimuli was tested by stimulating WT and RT deficient cells with LPS, MDP, IFNα, and R848 or transfecting them with dsDNA. Secreted IP-10 and IL-6 in the supernatant were quantified by ELISA. All stimulations showed similar responses in WT and all three RT KO cells except when stimulated with LPS (Figure 4.18 C and D). Here, LPS stimulation resulted in higher IP-10 production in all three RT deficient cells, while the IL-6 production was not elevated (Figure 4.18 C and D).

Next, the supernatant of BLaER1 WT and RT knockout cells were tested for their infectivity. Therefore, supernatant from BLaER1 WT and RT deficient cells was collected, and SMRV stocks were generated by removing cells and cell debris from the supernatant by centrifugation and subsequent filtration. The activity of RT in the supernatant of transdifferentiated and undifferentiated (suspension) cells was determined by SG-PERT assay. While BLaER1 WT cells in both states displayed an RT activity in the supernatant, all three RT deficient cells showed no RT activity (Figure 4.19 A). The supernatant of BLaER1 WT and knockout cells was transferred to HEK293T cells and incubated for one day. The RT activity in the supernatant was subsequently determined by SG-PERT assay after one, eight and sixteen days. While HEK293T cells incubated with the supernatant of BLaER1 WT cells showed an increase of RT activity over time, HEK293T cells incubated with supernatant from all three KO cell lines remained at the background level (Figure 4.19 B). Together, these results suggested a complete knockout of the RT in all three tested KO cell lines. In addition, supernatant of RT KO cells displayed no detectable infection and viral replication in transduced HEK293T cells.
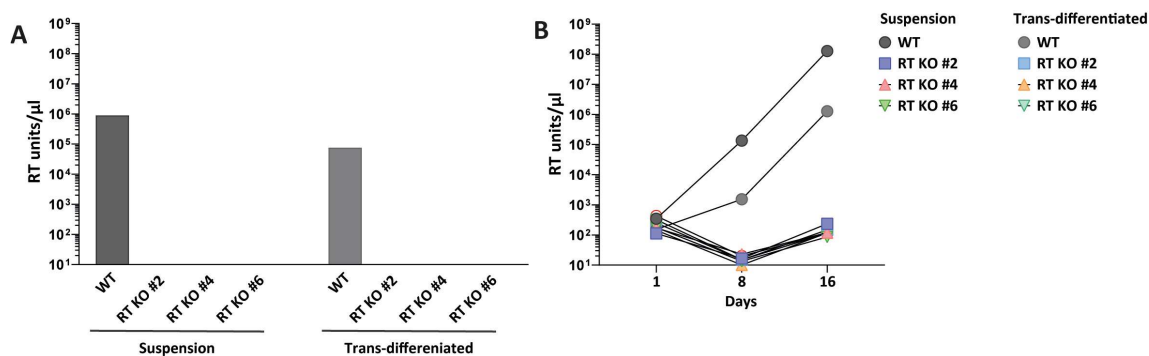
Figure 4.19 SMRV transduction studies with infected supernatants of WT and $RT^{-/-}$ cells
(A) SG-PERT analysis of suspension or transdifferentiated BLaER1 WT or $RT^{-/-}$ cells used for the transduction. **(B)** HEK293T cells transduced with the supernatant of BLaER1 WT or $RT^{-/-}$ cells. SG-PERT assay was performed one, eight and sixteen days after transduction.

4.11 SMRV integration site mapping in BLaER1 cells

During the RT knockout generation, several heterozygous knockouts next to WT cells were observed, indicating different proviral SMRV integration events. To identify these integration sites, an inverse PCR was performed. The whole BLaER1 genome was digested with a restriction enzyme, which does

not cut the terminal 3'-region of SMRV. The fragments were ligated, and a PCR with two sets of pre-designed primers was conducted and analysed by agarose gel electrophoresis (Figure 4.20 A).

Figure 4.20 Mapping of SMRV integration sites in BLaER1 WT cells
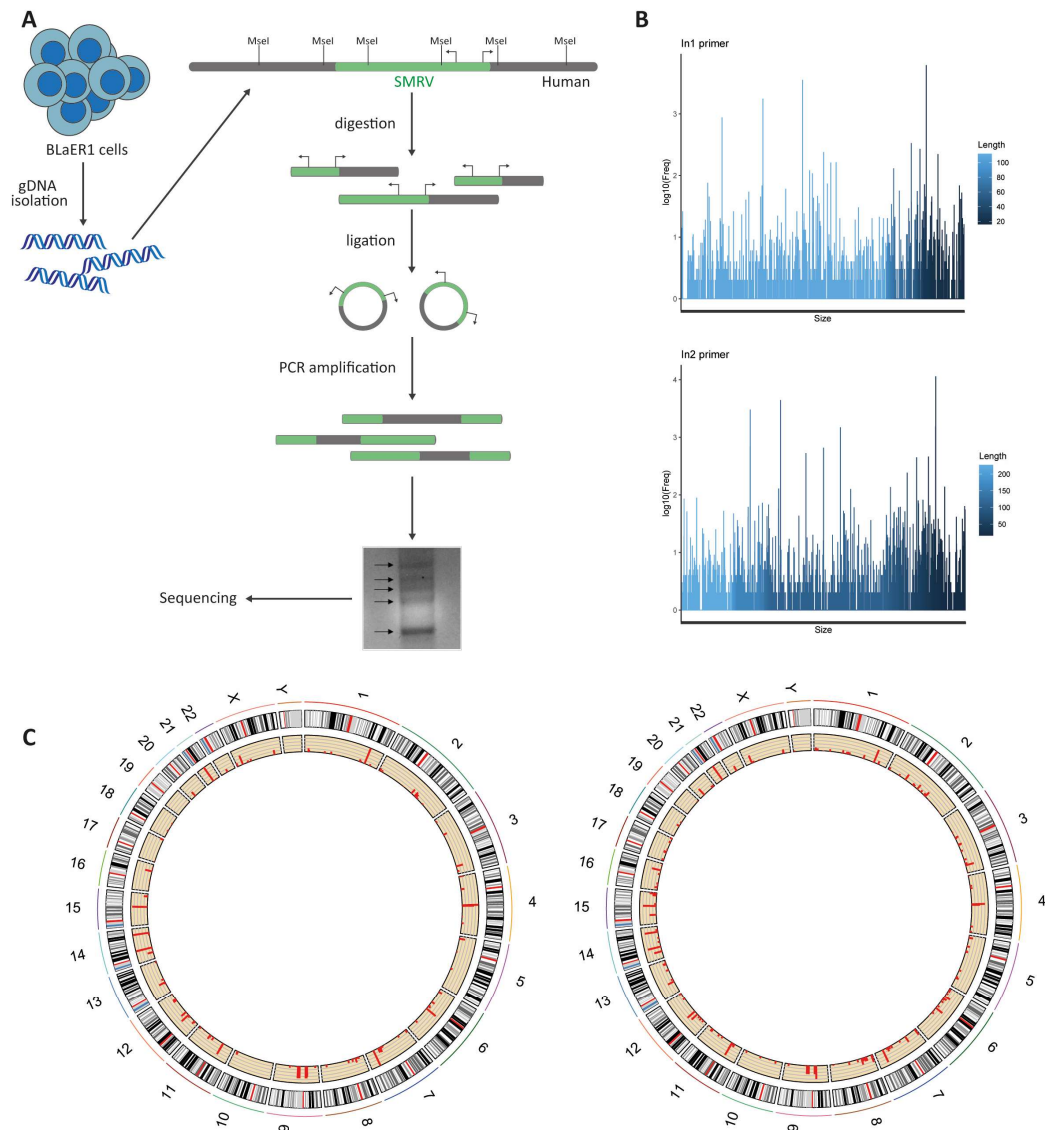**(A)** Inverse PCR setup and steps in a schematic overview. **(B)** Miseq results of the in1 and in2 primer of the inverse PCR plotted for their length and frequency. **(C)** Circos plots for in1 (left) and in2 (right) primers to visualize the hits after mapping. The two outer rings show human chromosomes 1-22 and XY followed by Giemsa stained karyogram with red bands for centromere, heterochromatin with darker bands and euchromatin with lighter bands. The inner ring bar plots depict viral integration sites (red) in the BLaER1 genome.

The obtained bands in the agarose gel were then subjected to Illumina sequencing. FastQ files were filtered, and viral sequence parts removed. The remaining cleaned-up sequences were mapped to the human genome (GRCh38) using STAR v.2.5 and plotted onto a polar coordinate graph. Heights correspond to the number of reads mapped (Figure 4.20 B). Both primers in1 and in2 displayed quite an even distribution in read lengths, as can be seen in the frequency plots. Since in1 was located further apart from a cutting site, the sequenced viral part was longer and therewith the length of the human

part shorter than for the in2 primer (Figure 4.20 B). The mapping results for both primers were plotted in R using the Rcircos package. The circos plots depict the integration sites in red in the most inner circle, while the outer ring represents a hypothetical karyogram (Figure 4.20 C). Most SMRV integration sites are in euchromatin regions (Figure 4.20 C). Overall, the integration site mapping delivered largely similar hits for both primer pairs. The detected integration sites of SMRV with more than 150 hits in the BLaER1 genome are depicted in Table 4.1.

Table 4.1: SMRV integration sites in the BLaER1 genome

Chromosome	Position	Hits (in1)	Hits (in2)	gene
Chr21	25331224	13065	6305	none
Chr11	36621711	5870	2266	C11orf74
Chr9	37126873	4428		ZCCHC7
Chr15	58882290	2015	4802	ADAM10
Chr11	36621713	837		C11orf74
Chr9	37126926	676	1133	ZCCHC7
Chr11	37302137	552	414	none
Chr16	67250090	181	313	LRRC29
Chr8	105111292	154	264	none
Chr13	38367680		293	TRPC4
Chr13	103318678	203		TPP2
Chr15	94131475		184	none

5 Discussion

5.1 DSB induced type I interferon response

In recent years, several links between genotoxic stress and subsequent induction of innate immune response have been revealed. These findings enabled a better understanding of the interplay of two important mechanisms, innate immune responses and DDR, which are both crucial for the survival of cells and organisms. These interplays also need to be considered for the development of medical treatments and drug design.

For both signalling pathways, different ways of cross-talks have already been described so far. DDR components have been shown to induce cell-autonomous innate immune responses upon DNA damage. In addition, DNA damage can lead to the production of PRR ligands by micronuclei formation or the release of nucleic acids to the cytosol, mediating cell-autonomous innate immune responses. Furthermore, DNA damage can trigger the release of DAMPs leading to the induction of innate immune signalling cascades in neighbouring cells. Here, we discovered an interplay between components of the HR DSB repair pathway and the induction of a type I IFN response in the monocyte/macrophage model BLaER1, which was also seen in THP-1 cells, as well as primary human monocyte-derived macrophages. In addition, we were able to identify major components of this pathway from TOP2 inhibitor-induced DSBs to the induction of ISGs. Figure 5.1 shows a schematic representation of this newly discovered pathway.

In a first step, the induction of DSBs through the inhibition of TOP2 triggers the recruitment of the MRN complex to the DNA damage site. The MRN complex leads to the recruitment of several repair proteins and effector kinases. The DSB induced type I IFN induction is partially dependent on the MRN complex member NBS1, while MRE11 and RAD50 could not be deleted due to the mutation being lethal. Upon binding of the MRN complex to the breakage site, NBS1 might interact with the effector kinase ATM and subsequently mediates the ATM autophosphorylation and activation. This leads to further signal transduction from the nucleus to the cytosol by an unknown mechanism. Several nucleic-acid sensing PRRs and their adaptor proteins that have been described to detect damaged DNA or formed micronuclei were tested and shown not to be involved in the sensing of DSBs in our setting. However, for the activation of NF-κB and MAPK signalling, which are necessary for a type I IFN response, a scaffold protein for signal transduction is needed. In the here-analysed signalling cascade, TRAF6 gets activated and ubiquitinated by an unknown protein and forms a scaffold for the recruitment of TAK1 and its adaptor protein TAB1. TAK1 subsequently triggers the activation of MAP2Ks and the IKK complex. The MAP2Ks, MKK3, MKK4 and MKK6, mediate the phosphorylation of p38α and, at a later time point, of JNK1 and JNK2. P38α mediates the activation of MSK2 and might trigger the activation of AP-1 transcription factors. The IKK complex leads to the phosphorylation of the inhibitory protein IκBα. IκBα is ubiquitinated and degraded by the proteasome. This leads to the nuclear translocation of a RelA containing NF-κB heterodimer. Besides the activation of NF-κB and AP-1 transcription factors, the signalling pathway was independent of classical type I IFN inducing IRFs like IRF3, IRF5 and IRF7. However, a dependency on IRF1 and IRF4 was found. The formation of DSBs leads to the upregulation and activation of IRF1 by a yet unknown mechanism. IRF4 activation has been described to be dependent on an interaction partner leading to its conformational change enabling DNA binding and

subsequent gene activation. This potential binding partner necessary for IRF4 activation still remains elusive. IFNβ is a secreted cytokine that activates IFNAR in an autocrine or paracrine manner. IFNβ binds to the IFNAR heterodimer and triggers the activation of JAK1 and TYK2. Both receptor-associated kinases can mediate the recruitment and activation of STAT1 and STAT2 subsequently. This leads to the activation and phosphorylation of STAT1, subsequently forming homodimers or the ISGF3 complex consisting of STAT1, STAT2 and IRF9. Both complexes translocate to the nucleus and activate the expression of ISGs.
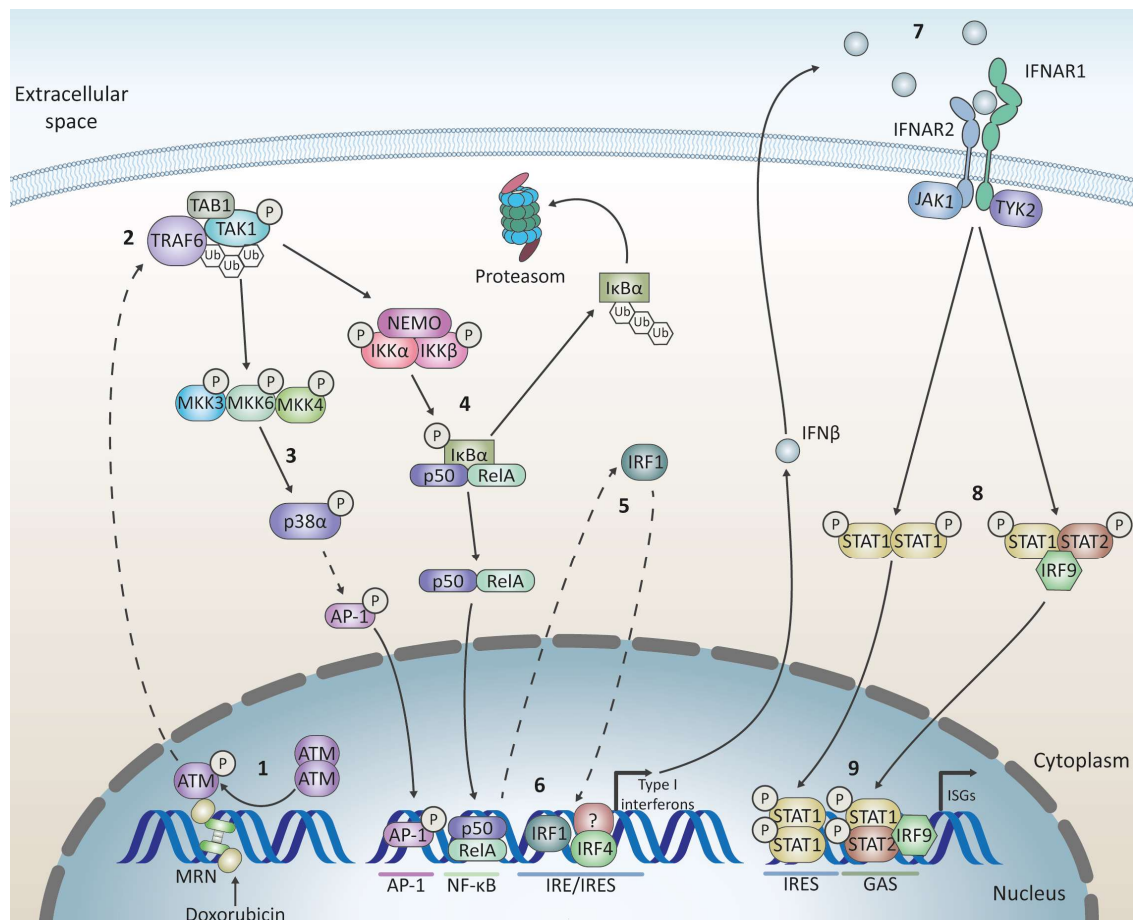

Figure 5.1 Mechanism for type I IFN and ISG induction mediated by TOP2 inhibitor induced DSBs
Mechanistic key steps are highlighted with bold numbers. **(1)** The induction of DSB by TOP2 inhibitors leads to the recruitment of HR components like the MRN complex. The MRN complex bridges the DSB and triggers the recruitment of further repair factors and the effector kinase ATM. Upon activation, ATM induces signal transduction by a yet unknown mechanism, which leads to the ubiquitination of TRAF6 and forms a scaffold for TAK1. **(2)** TAK1 and TAB1 are recruited to TRAF6 and subsequently activate the MAP2Ks MKK3, MKK4 and MKK6, and the IKK complex by phosphorylation. **(3)** Activated MAP2Ks trigger p38α (MAPK14) activation, leading to MSK2 and still unknown AP-1 transcription factor activation. **(4)** The activated IKK complex triggers the phosphorylation and subsequent ubiquitination as well as degradation of IκBα. NF-κB is activated and shuttles to the nucleus. **(5)** Besides activating the MAPK signalling cascade and the IKK complex, IRF1 is transcriptionally upregulated and activated by an unknown mechanism. **(6)** All three transcription factors shuttle to the nucleus and trigger a type I IFN response with the induction of IFNβ. While the possible induction of type I IFN signalling through IRF4 might be dependent on the interaction with co-activating transcription factors leading to a conformational change and the activation of IRF4. **(7)** IFNβ is produced and secreted and mediates an auto- or paracrine signal transduction. The IFNAR complex binds secreted IFNβ and leads to the activation of JAK1 and

TYK2. **(8)** These kinases activate and phosphorylate STAT1 and STAT2, leading to the formation and nuclear translocation of STAT1 homodimers or the ISGF3 complex. **(9)** Both transcription factor complexes lead to the production of ISGs.

Interestingly, this DSB mediated induction of type I IFN signalling was only observed in terminally differentiated macrophages, which were unable to proliferate further (Figure 4.3). However, the recognition and induction of the signalling cascade rely on the HR repair pathway factors, which classically depends upon the presence of a sister chromatid as a repair template during the S and G2 phase (Figure 4.5 and 4.6). Therefore, two questions need to be addressed to dissect further the role of the differentiation and cell cycle stages. Firstly, the recruitment of HR factors instead of NHEJ factors to the DSBs leading to the immune response in an ATM-dependent manner in terminally differentiated cells should be further investigated. Secondly, more cell lines, including BMDMs from mice, epithelial cells lines or other myeloid cells, need to be analysed to fully understand the role of differentiation and cycling stage in the DSB induced type I IFN response.

5.2   Detection of the damaged DNA

DNA damage is classically detected by DNA repair proteins, which subsequently trigger the recruitment of additional repair factors and effector kinases, leading to cell cycle arrest. However, damaged DNA is also known to trigger an immune response in several conditions. Cytosolic chromatin fragments, micronuclei formed during DNA damage or defective replication lead to the activation of the DNA sensor cGAS [144]. cGAS then mediates an antiviral immune response through the production of cGAMP and the subsequent activation of the ER-bound protein STING. Recent publications have shown that cGAS is not only localised in the cytosol but can be located at the plasma membrane or in the nucleus [142–144]. Due to tight regulation and the binding to chromatin, cGAS is not activated by DNA in the nucleus. During mitosis, the activity of cGAS has been shown to be selectively suppressed by hyperphosphorylation through mitotic kinases and its association with chromatin [382]. Besides cGAS, IFI16 has been described to mediate a STING dependent antiviral immune response downstream of DSB formation and ATM [345]. Using CRISPR/Cas9 mediated gene targeting, we could analyse the effect of nucleic-acid sensing PRRs and their downstream signalling proteins in the context of DSB induced type I IFN. Our group's previous work depicted an independence of the TOP2 inhibitor induced antiviral immune response of MyD88, TRIF, MAVS, TBK1, IKKε and several IRFs [346]. In addition, an independence of cGAS, STING and IFI16 could be shown (Figure 4.4).

Besides PRRs and their signal proteins, the DSB repair machinery proteins have been reported to interact with proteins of innate immune signalling pathways and regulate immune responses in certain conditions. The lack of the NHEJ effector kinase DNA-PK is known to reduce cytokine production upon stimulation with viral DNA in mice [340]. In addition, DNA-PK has been observed to trigger a STING-independent DNA sensing pathway upon stimulation with calf thymus DNA in HEK293T cells [383]. Upon stimulation with DNA, the DSB sensor subunit Ku70 mediates the IFNλ1 production in HEK293T cells. However, previously obtained data in our group excluded NHEJ factors from being involved in the DSB induced type I IFN response. Therefore, HR factors like the MRN complex members and ATM were further investigated since both have also been described to impact innate immune signalling. MRE11 and RAD50, two subunits of the MRN complex, have been reported in this context to detect cytosolic

dsDNA and mediate a STING and IRF3 dependent type I IFN response in cells from patients with AT-like disease while NBS1 was dispensable [384]. The knockout generation for RAD50 and MRE11 in BLaER1 cells resulted in only WT or heterozygous knockouts, indicating the essential function of both genes (Figure 4.5). To further analyse their influence on the DSB mediated type I IFN induction in human macrophages, known loss-of-function point mutations from patients with an AT-like disease would be an option. Nevertheless, the generation of $NBN^{-/-}$ was successful, and NBS1 deficient cells displayed a strong reduction of STAT1 phosphorylation upon stimulation with Doxorubicin in the immunoblot, while LPS and R848 stimulation led to unaltered STAT1 phosphorylation (Figure 4.5). This indicates the involvement of the MRN complex and hints towards an interaction of the C-terminus of NBS1 with the HEAT repeats of the effector kinase ATM (Figure 5.2 B) [385]. This interaction needs to be further validated by introducing C-terminally truncated NBS1 variants in the $NBN^{-/-}$ cells and subsequent analysis of STAT1 phosphorylation in the immunoblot and a co-immunoprecipitation of ATM and NBS1. ATM itself has been described to be involved in the activation of the innate immune system [386,387]. In line with these observations, the stimulation with Doxorubicin resulted in a complete loss of STAT1 phosphorylation and IP-10 production in $ATM^{-/-}$, while the stimulation with LPS or R848 was not affected (Figure 4.6). TOP2 inhibitor induced type I IFN induction might rely on the detection of DSBs through the MRN complex and subsequent ATM activation through NBS1. This induces a STING-independent downstream signalling, in contrast to other types of DNA damage, resulting in the activation of a STING-dependent type I IFN induction [331,332,376,388,389].

5.3 Signal transduction from the nucleus to the cytosol

The activation of ATM upon DSB detection is a nuclear event, while the signal transduction with the activation of MAPKs and the IKK complex occurs in the cytosol. Therefore, the signal must be transmitted from the nucleus to the cytosol. Several publications have suggested different possible mechanism for this setting. One set of mechanisms also involving IKKγ has been described by McCool and Miyamoto in 2012 [344]. Depending on the severity of the genotoxic stress, ATM is activated and translocates from the nucleus to the cytosol, dependent on different described interaction partners and posttranslational modifications. In the cytosol, ATM has been shown to interact with ELKS or RIPK1, which subsequently form a scaffold for TAK1 activation [344,390,391]. Alternatively, ATM has been described to translocate upon activation in a calcium-dependent manner to the cytosol, where it binds through its TRAF6-binding motif to TRAF6. The binding motif is a homolog of the classical TRAF6 binding motif PxExx with the sequence VKEVEE (2152-2157) [392,393]. The TRAF6 binding site is depicted in Figure 5.2 C in red for the inactive monomer (one part of the ATM homodimer depicted in Figure 5.2 A) and the active monomer. Upon activation, the VKEVEE motif gets more accessible through a conformational change in the protein structure and the monomerisation.

In our studies, activated ATM signals mainly via TRAF6 and via TRAF3. The $TRAF6^{-/-}$ cells depicted a complete loss of IFNβ mRNA level induction and production of IP-10 upon stimulation with Doxorubicin (Figure 4.7). However, the STAT1 phosphorylation in the TRAF6 deficient cells was only strongly reduced and not absent (Figure 4.7). An additional knockout of TRAF3 resulted in the complete loss of STAT1 phosphorylation, indicating another function of TRAF3 in the DSB induced type I IFN induction (Figure 4.7). The knockout of ELKS, in contrast, depicted no change in the production of IP-10 upon stimulation with Doxorubicin, LPS and R848 (Figure 4.7). Therefore, the interaction of ATM with TRAF6

via its TRAF6-binding motif might act as a platform for downstream signalling. This interaction leads to TRAF6 activation and K63-linked polyubiquitination of TRAF6 mediated by Ubc13 [393]. To prove this interaction, TRAF6 and ATM need to be investigated in a co-immunoprecipitation experiment for their cytosolic or nuclear binding. In addition, the shuttling of ATM from the cytosol to the nucleus needs to be validated by microscopy and nuclear extraction followed by immunoblotting. The ubiquitination of TRAF6 after stimulation with Doxorubicin also needs to be validated. Furthermore, the involvement of additional proteins and post-translational modifications in the export of ATM needs to be determined to completely understand the processes of ATM activation and shuttling.
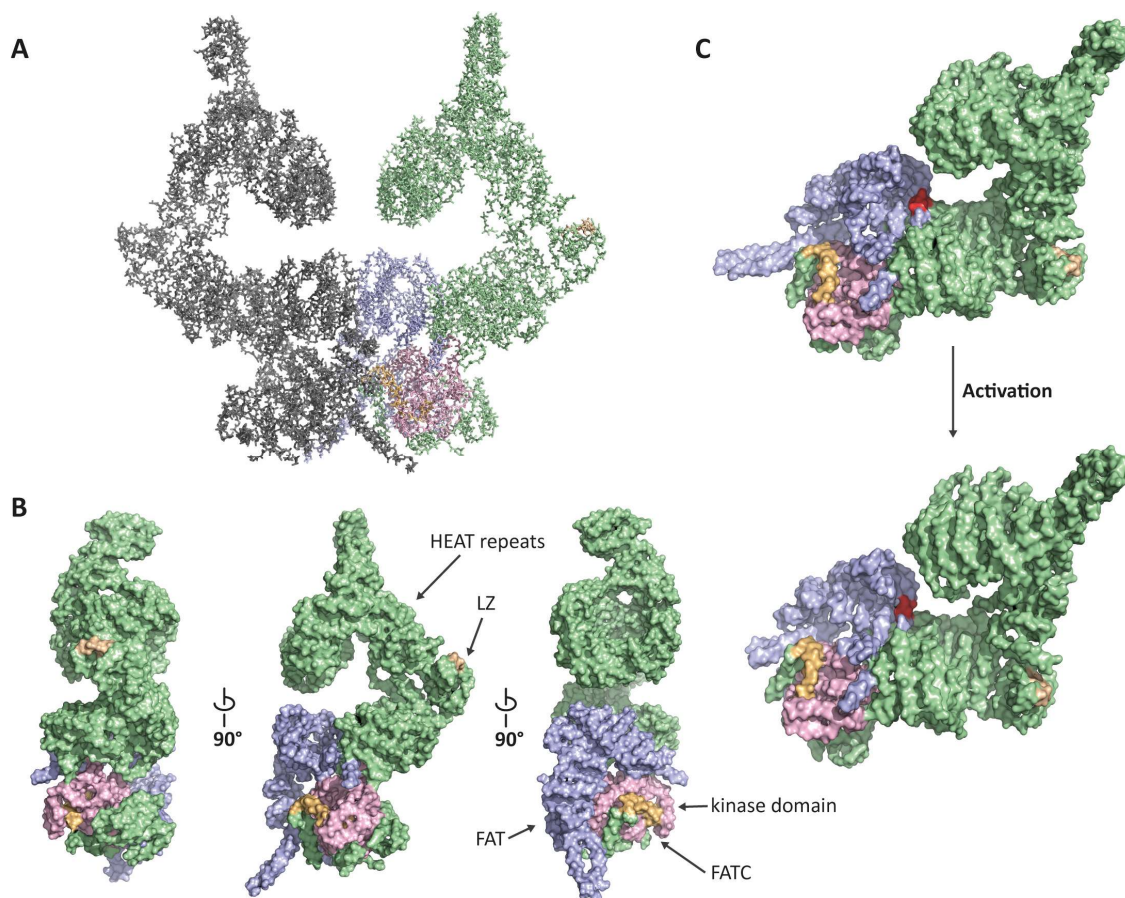

Figure 5.2 Structural analysis of ATM
Crystal structure (PDB 5NP0 and 5NP1) of inactive ATM dimer in the closed conformation and active ATM monomer [394]. **(A)** Inactive ATM dimer with one ATM monomer in grey and one monomer coloured according to its domains. **(B)** ATM monomer derived from the inactive closed conformation. The FAT domain (blue) binds to the second monomer and inhibits the kinase activity in the inactive ATM homodimer. The kinase domain (light pink) becomes activated and leads to autophosphorylation upon DNA damage and interaction with the C-terminal region of NBS1. NBS1 interacts with the HEAT repeats (green, not specifically defined), which are found around the leucine-zipper (LZ) motif (wheat), which is important for dimerization and ligand binding. The FATC domain (light orange) close to the kinase domain is important for the acetylation of ATM and for the activation of ATM [395]. **(C)** Tilted view of the inactive ATM monomer (one subunit of the homodimer on the left side) in the top with the described homologous TRAF6 binding motif VKEVEE at position 2152-2157 in the FAT domain depicted in red. In the active open conformation at the bottom, the region with the TRAF6 binding motif gets more accessible through monomerisation and conformational changes [393,394].

5.4 Regulation of the DSB mediated type I IFN induction by NF-κB and MAPKs

The activation of the E3 ubiquitin ligase TRAF6 is known to result in the recruitment of the E2 ubiquitin ligase UBC13 and its cofactor Uve1A. TRAF6 subsequently forms polyubiquitin chains with K63-linkages on itself [63,64]. This triggers the recruitment of TAB proteins and TAK1 (MAP3K7) to the polyubiquitin scaffold [396]. The activated TAK1-TAB complex mediates the phosphorylation of MAP2Ks as well as the activation of the IKK complex [397]. For the TOP2 inhibitor mediated type I IFN expression, we could show a strong dependency on TAK1. *MAP3K7^-/-* deficient cells displayed a complete loss of STAT1 phosphorylation for the stimulation with Doxorubicin as well as LPS and R848 stimulation as expected from the literature (Figure 4.8). This loss could also be shown in the production of IP-10 and the induction of IFNβ mRNA levels (Figure 4.8). Therewith, TAK1 completely abrogates DSB-induced as well as TLR4 or TLR7/8 mediated type I IFN induction. Interestingly, also the production of IP-10 in TAK1 deficient cells stimulated with IFNα was significantly reduced, which can be explained by the critical role of TAK1 in the activation of NF-κB (Figure 4.8). In addition, we could show that the adaptor protein of TAK1, TAB1, is needed for the signal transduction in cells stimulated with LPS and Doxorubicin, but not for R848 mediated signalling (Figure 4.8). This finding is in line with previously published studies indicating a stimuli dependent requirement of TAK1 adaptor proteins like TAB1, however, the detailed mechanism of TAB1 independent activation of TAK1 in R848 treated cells needs to be further investigated [398].

The activated TAK1-TAB complex subsequently triggers the recruitment of the IKK complex, consisting of the two kinases IKKα and IKKβ and the regulatory protein IKKγ. The regulatory subunit IKKγ senses K-63 polyubiquitin leading to the binding of the IKK complex to polyubiquitin chains at TRAF6 [399,400]. IKKγ itself has been shown to get ubiquitinated by LUBAC, a complex consisting of heme-oxidized IRP2 Ub ligase-1 (HOIL-1) and the HOIL-1-interacting protein (HOIP), leading to an optimized scaffold for signal transduction [401]. The binding of ubiquitin, as well as the ubiquitination of IKKγ, are both crucial for the activation of NF-κB [167,401]. In canonical NF-κB signalling, TAK1 mediates the phosphorylation and activation of IKKβ, while the MAP3K NIK triggers the phosphorylation and activation of IKKα in non-canonical NF-κB signalling [167]. The DSB induced type I IFN induction is dependent on the regulatory subunit IKKγ (Figure 4.9). Cells stimulated with LPS, and R848 demonstrated a complete dependency on the kinase subunit IKKβ, while IKKα deficiency did not negatively impact the signalling and even increased the response in the immunoblot for LPS stimulation (Figure 4.9). In contrast, the single knockouts of IKKα and IKKβ both only displayed a moderate reduction of STAT1 phosphorylation upon treatment with Doxorubicin (Figure 4.9). Only the double-knockout of IKKα and IKKβ depicted a complete loss of STAT1 phosphorylation (Figure 4.9). This stands in contrast to the sole dependency on IKKβ in the TLR4 and TLR7/8 mediated response and indicates a potentially redundant function of both kinase subunits in the DSB mediated antiviral immune response. IKKα and IKKβ have also been shown to be both necessary for the induction of IFNβ by IRF3 upon DNA damage and ATM activation in U2OSR cells [402]. Besides a redundant function with IKKβ in the activation of NF-κB, IKKα might also influence type I IFN signalling upon TOP2 inhibitor treatment differently. IKKα has been shown to be important for DDR activation upon DNA damage by triggering the phosphorylation and activation of ATM [403]. However, this would not explain the remaining STAT1 phosphorylation in the IKKβ single knockouts. To further validate the function of IKKα, the phosphorylation of RelA and the degradation

of IκBα in IKKβ deficient cells upon TOP2 inhibitor treatment need to be investigated. In addition, the generation of a kinase-dead IKKα mutant might help to elucidate the function of IKKα upon DNA damage. The activated IKK complex leads in the canonical NF-κB response to the phosphorylation of IκBα, an inhibitor protein, which is bound to the NF-κB transcription factors and prevents its translocation to the nucleus. Upon phosphorylation, IκBα is ubiquitinated and degraded, mediating the release of the NF-κB transcription factors [158,167]. In the non-canonical signalling, activated IKKα mediates the cleavage of p100, leading to the translocation of RelB/p52 to the nucleus [157]. We could show a complete dependence on RelA for the stimulation with Doxorubicin as well as for LPS and R848, while RelB deficiency did not impact one of these three activated signalling cascades (Figure 4.10). The second NF-κB family member, which forms an NF-κB heterodimer with RelA for the DSB mediated antiviral immune response, needs to be validated. Thus, the DSB mediated type I IFN induction relies on all three subunits of the IKK complex leading to the activation of RelA.

Besides TAK1, MAP3K3 has been shown to mediate the activation of the IKK complex and to trigger the activation of the p38 MAPK module in response to certain stimuli [167,404]. In addition, MAP3K3 has been reported to synergize with TAK1 for the activation of the IKK complex under certain conditions [405]. We also observed an impact of MAP3K3 on the induction of IFNβ mRNA levels in cells stimulated with Doxorubicin but not on R848 or LPS stimulation (Figure 4.11). In the immunoblot, STAT1 phosphorylation is only slightly reduced for LPS and Doxorubicin stimulation (Figure 4.11). These results suggest a minor role of MAP3K3 in the signalling cascade. However, its influence on p38 activation and interaction with the IKK complex needs to be further analysed. In addition, MAP3K3 functions in cell differentiation and thereby might influence the type I IFN signalling. This might also explain the missing induction of IFNβ mRNA levels, while the phosphorylation of STAT1 is only slightly reduced.

The TAK1-TAB complex further leads to the phosphorylation and activation of MAP2Ks. The signal transduction is mainly mediated by the four MAP2Ks (MKKs), MKK3, MKK4, MKK6 and MKK7 [406]. While MKK3, MKK6 and MKK4 have been described to mediate the activation of the p38 module, MKK4 and MKK7 regulate the activation of the JNK module [171,173]. However, MKK3, MKK4 or MKK6 deficient cells stimulated with Doxorubicin displayed no reduction of STAT1 or p38 phosphorylation (Figure 4.12). Since MAP2Ks have been reported to be redundant in their functions, double-knockouts of all three previously tested MAP2Ks were generated and analysed. The MKK3/6 double knockout displayed a complete loss of STAT1 and p38 phosphorylation upon stimulation with LPS and Doxorubicin (Figure 4.13). The MKK3/6 double knockout only affected the levels of phosphorylated p38 in cells stimulated with R848, not the phosphorylation of STAT1 (Figure 4.13). MKK4/6 deficient cells exhibit a slightly reduced STAT1 phosphorylation and a substantial reduction in JNK phosphorylation upon Doxorubicin treatment, while LPS and R848 stimulated cells and the phosphorylation of p38 was not affected (Figure 4.13). For MKK3/4 deficient cells, an almost complete loss of JNK phosphorylation was detectable for all three stimuli while the phosphorylation of STAT1 was reduced (Figure 4.13). This data points to signal transduction mediated by MKK3 and MKK6 for the activation of the p38 module and STAT1, while for the JNK activation, which is activated some hours later, MKK4 is crucial. In addition, this data shows the importance of a functional p38 response for the induction of type I IFNs upon LPS and Doxorubicin treatment.

Activated MAP2Ks trigger the phosphorylation and activation of MAPKs. Here, mainly, p38α, JNK1 and JNK2 have been described to impact the induction of type I IFN signalling in human macrophages [173]. As expected from the MAP2Ks knockout data, only the knockout of p38α resulted in a loss of STAT1 phosphorylation for the stimulation with LPS and Doxorubicin, while JNK1 and JNK2 knockouts only impact the phosphorylation of their corresponding protein bands (Figure 4.14). However, JNK2 deficient cells depicted increased phosphorylation of p38, which might indicate a negative feedback loop initiated to decrease p38α activity. Interestingly the activation of p38α subsequently leads to the activation of MSK2, which is displayed in the complete loss of STAT1 phosphorylation upon stimulation with Doxorubicin and LPS in MSK2 deficient cells (Figure 4.15). MSK2 has previously been described as a negative regulator of a TLR signalling [195]. Here, MSK1 and MSK2 have been reported to trigger the activation of the transcription factors CREB and ATF1 leading to the expression of the anti-inflammatory cytokine IL-10 and dual specific protein phosphatase 1 (DUSP1) [195]. However, also pro-inflammatory roles of MSK2 have been proposed. As a nuclear kinase, MSK2 has been shown to mediate histone H3 phosphorylation, enabling transcriptional activation of immediate early genes like AP-1 family members Jun and Fos [407,408]. Therefore, MSK2 might regulate the expression of AP-1 transcription factors necessary for the induction of type I IFNs, mediate the phosphorylation of histone H3 or directly trigger the activation of transcription factors independent of MSK1 in BLaER1 cells treated with TOP2 inhibitors. The activation of p38α eventually leads directly to the activation of transcription factors. The AP-1 transcription factor family has been described as a key mediator for pro-inflammatory cytokine expression partially regulated by p38α [200]. However, the double knockout of Jun and Fos indicates no difference in STAT1 phosphorylation (Figure 4.15). To further investigate the role of AP-1 transcription factors in the DSB mediated type I IFN response, combinations of AP-1 transcription factors need to be knocked out and analysed by immunoblotting.

5.5 IRF signalling in the context of DSB induced antiviral immune response

The expression of type I IFNs not only requires NF-κB and AP-1 transcription factors activation but is also critically dependent on IRFs. Together, these three groups of transcription factors form an enhanceosome, which mediates transcriptional activation [264,265]. Antiviral IRF activation is mainly controlled by pLxIS motif-containing proteins such as MAVS, TRIF, STING, and TASL, which have been described to regulate IRF3, IRF5 and IRF7 [73]. Interestingly, previous work in our laboratory showed that TOP2 inhibition leads to a type I IFN induction independent of these three IRFs. Therefore, quadruple knockouts were generated deficient for IRF1 in addition to IRF3, IRF5 and IRF7 deficiency. IRF1 is upregulated upon infections through NF-κB and has been reported to mediate the regulation of a basal antiviral state due to the lack of an auto-inhibitory domain [409,410]. However, the IRF1/3/5/7 quadruple knockout displayed only a slight reduction of STAT1 phosphorylation compared to WT cells upon stimulation with Doxorubicin (Figure 4.16). In addition, a quadruple knockout deficient for IRF3, IRF4, IRF5 and IRF7 was generated and analysed. The IR3/4/5/7 deficient cells showed no change in STAT1 phosphorylation upon stimulation with Doxorubicin (Figure 4.16). Interestingly, cells deficient for all five IRFs displayed a complete loss of STAT1 phosphorylation also upon stimulation with Doxorubicin (Figure 4.16). To validate this observation, single knockouts for IRF1 and IRF4 were generated and tested for their ability to induce STAT1 phosphorylation upon treatment with Doxorubicin. As expected from the quadruple knockouts, both IRF1 and IRF4 single knockouts displayed no complete loss of

STAT1 phosphorylation (Figure 4.17). However, a reduction of STAT1 phosphorylation in LPS and Doxorubicin stimulated single knockout cells compared to the WT cells could be observed (Figure 4.17). We then generated IRF1/4 deficient cells and analysed these for STAT1 phosphorylation by immunoblotting. These double knockouts displayed a complete loss of STAT1 phosphorylation for Doxorubicin treatment and surprisingly also for LPS stimulation, while the stimulation with R848 was not altered (Figure 4.17). The knockouts were also validated by immunoblotting to control for residual protein levels in the knockout cells (Figure 4.17). In addition, an upregulation of IRF1 protein levels was detected upon stimulation with LPS, Doxorubicin, and R848 (Figure 4.17). Since IRF1 can be transcriptionally regulated by AP-1 and NF-κB, these transcription factors might also trigger the upregulation and activation of IRF1 in our setting. However, the activation of IRF1 alone is not sufficient to drive type I IFN production as depicted by only a slight reduction in STAT1 phosphorylation levels in IRF1 deficient cells. For the type I IFN induction upon Doxorubicin treatment only the double knockout of IRF1 and IRF4 displayed a complete loss of STAT1 phosphorylation. The activation of IRF4 is more complex, since IRF4 is controlled by an AR and has been described to be activated only upon binding of an interaction partner [204]. This interaction leads to a conformational change in the protein structure, enabling DNA binding. Therefore, IRF1 and IRF4 could be involved in the regulation of the DSB mediated type I IFN response in different ways. Firstly, given previous reports on their consensus binding sites, it is conceivable that both transcription factors bind to the same regions within the promoter and thereby could act redundantly. To validate this function of the two IRFs in DSB mediated type I IFN response, a ChIP-sequencing or side specific ChIP-PCR needs to be performed to analyse the binding of IRF1 and IRF4 to the promotor region of the IFNβ gene. However, the different described activation mechanisms of IRF1 and IRF4 also could indicate the formation of an IRF1/4 heterodimer similar to the IRF1/IRF8 regulome. Therefore, a direct interaction of IRF1 and IRF4 needs to be assessed by a Co-IP experiment. In addition, possible known interaction partners like PU.1 should be tested as well, especially since PU.1 has been reported to be part of the IRF1/IRF8 regulome [211]. Nevertheless, since both single knockouts depicted only a slight reduction in STAT1 phosphorylation levels, these two IRFs do not seem to act as IRF1/4 heterodimers. Another possibility, which also could explain the loss of STAT1 phosphorylation in LPS stimulated IRF1/4 double knockout cells, is the regulation of an important signalling factor downstream of ATM by IRF1 and IRF4 instead of the direct activation of type I IFN expression. In addition, LPS induced type I IFN signalling has been described to be dependent on IRF3 and IRF7 and to be mediated by the adaptor protein TRIF, which also can be seen in previous work conducted in our lab and in the IRF quadruple knockouts depicting no STAT1 phosphorylation for LPS stimulated cells when IRF3 and IRF7 are knocked out (Figure 4.16) [346,411]. Therefore, the regulation of type I IFNs upon LPS stimulation by IRF1 and IRF4 indicates the regulation of a signalling factor needed for the type I IFN response rather than the direct regulation of IFN expression, which is already performed by IRF3 and IRF7. Since cells stimulated with R848 depicted no change in STAT1 phosphorylation in IRF1/4 deficient cells, this regulation might only affect components needed for LPS or Doxorubicin induced type I IFN signalling. To further investigate this hypothesis, the nuclear translocation of IRF1 and IRF4 needs to be analysed in a time-dependent manner, and the expression of signalling components as well as their regulation by IRF1 and IRF4 should be examined. Overall, the exact mechanism of IRF1 and IRF4 activation and their involvement in regulating type I IFN expression upon TOP2 inhibitor treatment need to be further examined and clarified.

5.6 The physiological relevance of the DSB induced type I IFN induction

Several links between DNA damage and the innate immune system's activation have been reported and uncovered over the past decades. In these studies, different DDR proteins have also been found to trigger or regulate innate immune signalling cascades upon DNA damage [326]. The signalling cascade we examined in this work adds another connection between the DDR machinery and the induction of an innate immune response, which helps further to understand the crosstalk between these two important defence mechanisms. However, the question concerning the relevance and function of this signalling cascade remains unclear, especially regarding the relatively weak induction of IFNβ and ISGs versus the activation of TLRs, RLRs or cGAS-STING signalling.

The DSB mediated immune response analysed in this work is triggered by the TOP2 inhibitors Doxorubicin and Etoposide, which are both commonly used in cancer therapy. Doxorubicin is a hydroxylated form of the anthracycline daunorubicin, which was firstly isolated from *Streptomyces peucetius* in the 1950s and deployed in the therapy of acute leukaemia and lymphoma. Due to strong side effects, Doxorubicin was developed and modified. In the following years, more than 2000 known analogues of Doxorubicin were found and described, highlighting its importance for cancer therapy [412]. However, several side effects are still associated with chemotherapy and the treatment with Doxorubicin, including disorders like cardiomyopathy or tumour formation and tumour recurrence [413]. Therefore, strategies to increase tumour cytotoxicity and to limit the development of resistances are intensively investigated. The uncovered signalling cascade and the immunogenic capacity of Doxorubicin and Etoposide might be of interest here for developing new chemotherapeutics. In addition, this work provides new insights for the proposed use of DDR cascade inhibitors together with chemotherapeutic drugs to increase their tumour cytotoxicity since blocking DDR components might reduce the immune response. Especially since the activation of an anthracycline-mediated immune response, which is similar to an antiviral immune response, is important for the success of chemotherapy, as shown in previous studies [414,415]. Chemotherapy associated immune responses can trigger tumour immunity in two different ways: On the one hand, chemotherapeutic drugs can induce immunostimulatory cell death of tumour cells and, on the other hand, can directly trigger the activation of immune responses, as shown in this study [415]. The unveiling of the signalling cascades behind these effects could provide new insights for the further understanding of the immunomodulatory effects of chemotherapy and could enable personalized and more effective treatment of cancer.

The source of DSB formation is not limited to chemotherapeutics drugs and non-ionising or ionising radiation. Viruses also can cause DNA damage and modify DDR components for their advantage. Since viruses developed several strategies to circumvent the detection by PRRs like RLRs or cGAS to begin protein production and replication, an additional line of defence against viral replication could be represented by DDR components. However, the DDR acts here in a double-edged fashion. On the one side, DDR components lead to cell-cycle arrest and inhibit viral replication upon DNA damage, but on the other side, DDR components also enable the viral integration into the host genome. To prevent the negative consequences of DDR activation, several viruses developed evasion mechanisms, oncoproteins and inhibitors [416]. For instance, these evasion strategies can trigger the mislocalisation of DDR proteins like ATM or mediate their degradation, as shown for MRN complex members [417–419]. On the contrary, some viruses like Epstein Barr virus (EBV), adeno-associated virus (AAV) or retroviruses

like human immunodeficiency virus 1 (HIV1) induce DNA damage in order to integrate their viral genome into the host genome, which leads to the activation of DDR proteins like ATM [420]. These DDR proteins can also be activated already upon entry of viral DNA shortly after infection [421]. Viruses have also been shown to form replication centres upon nuclear translocation, which are closely located to depots of DDR machinery components to take advantage of the proofreading or resolving abilities [422]. These links already indicate the importance of DDR components for viral infections and for the prevention of replication. Even a weak induction of antiviral immune responses by DDR components would be beneficial to activate and attract other immune cells. This was also shown by Mboko et al. in 2012 in murine gammaherpesvirus (MHV68) infections, where ISG production induced by irradiation is blocked upon viral infection, but in pre-irradiated cells, the replication of MHV68 was inhibited [387]. Therefore, even the weak induction of IFNβ in Doxorubicin stimulated cells could inhibit viral replication and be beneficial for the attraction of further immune cells. The interplay between DDR components as well as DDR mediated immune signalling, and viral infections could provide an additional layer in the innate immune response to viral infections.

The DSB-mediated expression of type I IFNs described in this work could also overlap with what previous have referred to as a homeostatic IFN production. The homeostatic IFN expression, in contrast to the PRR-induced IFN expression, is mainly mediated by AP-1 and NF-κB transcription factors [272]. We also could show a strong dependence of DSB mediated type I IFN expression on MAPK and NF-κB signalling, while classically strong type I IFN regulators like IRF3 and IRF7 were not required for ATM-dependent type I IFN production. In addition, the production of ISGs and IFNβ was several folds lower than for cells stimulated with LPS or R848. This weak induction of IFN expression could, for instance, regulate the activity of macrophages, maintenance of NK cells or the proliferation of immune cells [272]. Such a priming function could enable a fast and effective immune response, which would be in line with a possible role of the DSB mediated type I IFN induction in the detection and defence of viral infections. In addition, the induction of type I IFN could also influence the tissue homeostasis mediated by macrophages [423]. Here, the constitutive expression of type I IFN has been described to increase the phagocytic potential and reparative functions of macrophages and thereby is beneficial for tissue homeostasis [272,424].

The DDR and its components are also involved in other signalling cascades linked to senescence, ageing and apoptosis. DSBs and their repair pathways have been shown to not only affect signalling cascades in their own cell but also to generate extracellular alarm signals influencing bystander cells. This activation of neighbouring cells leads to DNA damage foci formation, activation of DDR signalling and senescence. These bystander effects can be subdivided into two time-specific waves, the first response acts early within hours upon DNA damage, while the second response acts several days later and is characterised by apoptosis or permanent-growth arrest, also referred to as cell senescence [425]. The early bystander effect has first been described in Chinese hamster ovary cells irradiated with low doses of α-particles leading to chromosomal changes even in cells that were not traversed by these particles [426]. The generation of this bystander signal has been shown to be dependent on the activation of the effector kinases ATM and DNA-PK, however, both kinases are not needed for the signal reception [427]. In addition, the signal transduction was proposed to be through direct cell-cell interaction or mediated by paracrine signal transduction [425]. The signal transduction through cell-cell contacts is mediated by

gap junctions leading to ROS transfer and to the activation of ATR [425,428]. The paracrine signalling was validated by supernatant transfer experiments, in which the supernatant of irradiated cells was transferred to non-irradiated cells and could induce a DDR activation.[429,430] Several mechanisms and signalling pathways like IL-6, IL-33 and TGF-β mediate this paracrine activation in different cell lines [431,432]. This is also important for the tumour microenvironment since it affects tissue repair and local immune responses [425]. Interestingly, the production and secretion of IFNβ mediated by DSBs could also affect this radiation-induced bystander effect in a paracrine manner. This could suggest a new function for IFNβ as a warning or priming signal produced by cells with damaged DNA, mediated by irradiation, chemotherapy or viral infections. However, severe persistent DNA damage can also result in a second response to DDR activation, which is activated several days later than the first response, leading either to apoptosis or senescence. In senescent cells, the DDR machinery stays permanently activated [433]. Senescent cells, which are stressed, for instance, by further DDR activation, can also trigger a pro-inflammatory SASP. The resulting secretome composition is strongly dependent on the cell type, tissue, and type of stress but involves cytokines like IL-6, growth factors, proteases, and other soluble proteins. This secretome generates a microenvironment that is beneficial for tissue repair or for age-related diseases and cancer [425]. The induction of DSBs in an ATM and type I IFN dependent fashion has been shown to trigger senescence and telomere shortening [402]. In addition, NF-κB has been described to regulate the SASP and to trigger senescence and enhanced chemosensitivity [434]. ATM-dependent activation of NF-κB and type I IFNs in cells treated with certain chemotherapeutics could mediate the SASP and thus could lead to senescence or impact chemoresistance.

Besides the possible functions in viral defence, homeostatic IFN production, radiation-induced bystander effect and senescence, TOP2 inhibitor mediated type I IFN induction could also be involved in ageing and age-related autoimmunity. Especially since premature ageing was found in patients treated for cancer in their childhood with chemotherapeutics or irradiation [435]. The treatment of cancer with Doxorubicin has also been shown to trigger an accelerated ageing-like state in patients [436]. Age-associated increased levels of IFN have been reported to reduce brain functions in humans and mice, which was partially reversible in mice by treatment with neutralizing antibodies against the type I IFN receptors [437]. Therefore, the treatment with chemotherapeutic drugs and the associated increase of type I IFN expression might be linked to premature ageing. However, mutations or defects in genes of the DSB repair machinery have also been described to trigger premature ageing. Patients with Werner Syndrome, which is caused by a mutation in RecQ helicases acting in the NHEJ and HR repair, display several clinical signs of premature ageing like greying hair, skin atrophy or osteoporosis, and show an increased cancer risk [438,439]. In addition, truncations in ATM described in the rare autosomal recessive disorder Ataxia-Telangiectasia are linked to premature ageing and immunodeficiency [440]. Nevertheless, these mutations could lead to increased levels of DNA damage mediating the activation of the cGAS-STING pathway and thereby to an increased type I IFN expression. Therefore, the role of DSB and its repair components in ageing and senescence might be connected to the type I IFN response upon chemotherapeutic drug treatment or irradiation.

Overall, the induction of DSBs through treatment with chemotherapeutic drugs like Doxorubicin or Etoposide mediates the activation of the HR components ATM and the MRN complex. Subsequently, ATM activates TRAF6 in the cytosol and promotes activation of MAPK, NF-κB signalling cascades and

IRF transcription factors. This triggers the induction of a type I IFN response, which could impact in combination with the activation of NF-κB the host on several levels ranging from viral defence and tissue homeostasis to senescence and premature ageing. The remaining above addressed open questions that need to be investigated to understand further these links and their effects on cell survival, homeostasis, and ageing. The role of the two transcription factors IRF1 and IRF4, could especially give new insights into the regulation of type I IFN expression.

5.7   SMRV RT knockout generation and integration site mapping

The infection of BLaER1 cells with SMRV could be detected during the analysis of supernatants of BLaER1 cells for RT activity coupled to the analysis of RNAseq data sets. This was validated with SMRV specific PCRs and supernatant transfer assays. Since the BLaER1 system is an important model cell line for human monocytes and macrophages in our laboratory, a possibility to enable SMRV-free handling was searched. In order to block the propagation of SMRV, we targeted the SMRV RT for knockout generation since the RT is essential for the integration of lenti- or retroviral genomes into the host genome and, therefore, for viral replication. The generation of such knockout cells was successful, despite a very low knockout efficiency (Figure 4.18). The generated RT knockout cells were subsequently tested for their response to different stimuli and assayed with different read-outs. BLaER1 WT cells, as well as viral RT knockout cells, showed similar responses with the exception of LPS stimulation, which increased in the knockout cells. In addition, we could show that the knockout cells exhibited no RT activity in the supernatant. Moreover, cells incubated with the supernatant from RT knockouts showed no RT activity even after 16 days, while cells transduced with the supernatant from WT cells depicted an induction of RT activity already after eight days (Figure 4.19). Additional analysis of Gag and Env proteins in the supernatant of infected cells and RT knockout cells might show if cells carrying RT deficient provirus are still capable of producing virus particles. On the other hand, the generation of a new BLaER1 cell line from the original B-cell clone could offer a possibility of a new cell system without viral integration sites.

To analyse where SMRV integrated into the BLaER1 genome, an inverse PCR was performed, analysed by agarose gel electrophoresis and subjected to Illumina sequencing. The primary analysis of the inverse PCR products on an agarose gel already revealed several integration sites, visible as multiple bands on the agarose gel (Figure 4.20). This also explained the difficulties and low efficiency during the RT knockout generation. The FastQ file obtained after Illumina sequencing was analysed, and reads containing viral sequences were kept for further analysis. In the next step, the viral sequence part of the reads was removed, and the remaining human sequences were mapped to the human genome to find the integration sites. After the mapping, all the hits with less than ten reads were excluded. To visualize the integration sites, a circos plot was used. An overlap of viral integration sites with euchromatin regions was noticeable. However, we found no overlap between integration sites from other viruses such as HIV and SMRV [441]. Due to the experimental procedure, DNA fragments with a length over 400 bp had to be excluded from the Illumina sequencing. Therefore, SMRV might have additional integrations sites, which are not yet uncovered. Additionally, the here-discovered SMRV integration sites should be validated by PCR. Since the inverse PCR was conducted in a polyclonal pool of WT cells, the same experiment repeated with monoclonal samples might lead to more accurate detection and localization of integration sites in BLaER1 cells. To add to our understanding of the virus,

a screening for its receptor could also be of interest since SMRV is able to infect several different human cell lines. This could lead to a better understanding of the viral entry and the infection process. In addition, this might enable the use of SMRV as a retroviral vector system in research and could represent an alternative to frequently applied vector system.

Contaminations of cell lines with SMRV and other viruses have already been described in the past [363], and several tests have been developed and employed to detect these infections. During a large scale analysis of cell lines used in laboratories initiated by the Central Committee on Biological Safety only around three percent of all tested cell lines have been shown to be SMRV positive [442]. Due to the low abundance of SMRV positive cells, extensive testing of risk group 1 cell lines has been discontinued. However still, SMRV contaminated cell lines, which have not been covered by large scale screenings, are used in laboratories. A possibility to ensure safe handling in the laboratory and detect these viral infections early on would be the testing of cell lines with an SG-PERT Assay on a regular basis.

6 Summary

Our organism is confronted on a daily basis with a broad spectrum of different threats ranging from pathogen infection to DNA damage and genomic instability. Several complex systems, such as the innate immune system or the DNA damage response (DDR) cascades, have evolved over time to maintain physiological functions. While the innate immune system senses nucleic acids from viruses or bacteria and subsequently mediates an antiviral immune response leading to the expression of type I IFNs and pro-inflammatory cytokines, the DDR machinery has evolved to repair the host DNA and maintain genomic stability. The DDR is composed of several highly specialized repair cascades activated by different kinds of DNA damage. The most severe form of DNA damage is represented by DNA double-strand breaks (DSBs), which are repaired either by HR or NHEJ. In the last decades, several links between the DDR and the innate immune system have been revealed. Several proteins from the DDR have been described to mediate or activate immune signalling cascades or the induction of cytokine expression. However, not all links between the DDR and the innate immune system are uncovered. In this thesis, a connection between the formation of DSBs by chemotherapeutic drugs like Doxorubicin and subsequent induction of a type I IFN response was investigated. Previous work conducted in our group showed a dependency of the type I IFN induction by Doxorubicin on the DDR protein ATM, as well as the subsequent induction of IFN stimulated genes (ISGs) by IFNAR and the transcription factor STAT1. This signalling cascade has been shown to be independent of nucleic acid-sensing PRRs like TLRs, cGAS or RLRs and their adaptor proteins.

In this thesis, we were able to reveal an undiscovered link between the DSB repair machinery and the induction of a type I IFN response. Besides the activation of ATM, we could demonstrate that the MRN complex protein NBS1 and therewith likely also the MRN complex is necessary for the detection of the DSB and subsequent activation of antiviral immune responses. Activated ATM leads to the activation and ubiquitination of TRAF6, which serves as a scaffold for the recruitment and activation of TAK1 and its adaptor protein TAB1. TAK1 mediates the phosphorylation and activation of MAP2Ks and the IKK complex, enabling the activation of AP-1 and canonical NF-κB transcription factors. In addition, the DSB mediated type I IFN expression was shown to be independent of IRF3, IRF5, and IRF7, instead relied on IRF1 and IRF4. In summary, we could describe a novel mechanism for type I IFN activation upon DNA damage independent of known PRRs. With these findings at hand, it should now be possible to study the importance of this signalling cascade in crucial physiological processes such as homeostatic IFN regulation, senescence, ageing, and cellular reactions to viral infections.

7 Bibliography

1. Acheson, N. H. Fundamentals of molecular virology. *Fundam. Mol. Virol.* (2011).

2. Köhler, J. R., Casadevall, A. & Perfect, J. The spectrum of fungi that infects humans. *Cold Spring Harb. Perspect. Med.* 5, (2015).

3. Prusiner, S. B. Novel proteinaceous infectious particles cause scrapie. *Science (80-.).* 216, 136–144 (1982).

4. Colby, D. W. & Prusiner, S. B. Prions. *Cold Spring Harb. Perspect. Biol.* 3, 1–22 (2011).

5. Gazzinelli-Guimaraes, P. H. & Nutman, T. B. Helminth parasites and immune regulation [version 1; peer review: 2 approved]. *F1000Research* 7, (2018).

6. Maizels, R. M. & McSorley, H. J. Regulation of the host immune system by helminth parasites. *J. Allergy Clin. Immunol.* 138, 666–675 (2016).

7. Murphy, K. & Weaver, C. *Janeway Immunologie*. *Janeway Immunologie* (Springer Berlin Heidelberg, 2018). doi:10.1007/978-3-662-56004-4

8. Janeway, C. A. & Medzhitov, R. Innate immune recognition. *Annual Review of Immunology* 20, 197–216 (2002).

9. Janeway, C. A. Approaching the asymptote? Evolution and revolution in immunology. in *Cold Spring Harbor Symposia on Quantitative Biology* 54, 1–13 (Cold Spring Harb Symp Quant Biol, 1989).

10. Matzinger, P. Tolerance, Danger, and the Extended Family. *Annu. Rev. Immunol.* 12, 991–1045 (1994).

11. Chen, G. Y. & Nuñez, G. Sterile inflammation: Sensing and reacting to damage. *Nature Reviews Immunology* 10, 826–837 (2010).

12. Gong, T., Liu, L., Jiang, W. & Zhou, R. DAMP-sensing receptors in sterile inflammation and inflammatory diseases. *Nature Reviews Immunology* 20, 95–112 (2020).

13. Lythe, G., Callard, R. E., Hoare, R. L. & Molina-París, C. How many TCR clonotypes does a body maintain? *J. Theor. Biol.* 389, 214–224 (2016).

14. Doria, A. *et al.* Autoinflammation and autoimmunity: Bridging the divide. *Autoimmunity Reviews* 12, 22–30 (2012).

15. Brogden, K. A. Antimicrobial peptides: Pore formers or metabolic inhibitors in bacteria? *Nature Reviews Microbiology* 3, 238–250 (2005).

16. Gallo, R. L. & Hooper, L. V. Epithelial antimicrobial defence of the skin and intestine. *Nature Reviews Immunology* 12, 503–516 (2012).

17. Bottazzi, B., Doni, A., Garlanda, C. & Mantovani, A. An Integrated View of Humoral Innate Immunity: Pentraxins as a Paradigm. *Annu. Rev. Immunol.* 28, 157–183 (2010).

18. Dunkelberger, J. R. & Song, W. C. Complement and its role in innate and adaptive immune responses. *Cell Res.* 20, 34–50 (2010).

19. Ross, G. D. Complement and complement receptors. *Curr. Opin. Immunol.* 2, 50–62 (1989).

20. Adinolfi Zenthon, M. J. *Complement and disease: a review*. *Journal of the Royal Society of Medicine* 75, (1982).

21. Flannagan, R. S., Jaumouillé, V. & Grinstein, S. The Cell Biology of Phagocytosis. (2011). doi:10.1146/annurev-pathol-011811-132445

22. Mandell, G. L. Cytokines, phagocytes, and pentoxifylline. *J. Cardiovasc. Pharmacol.* 25, S20–S22 (1995).

23. Wolf, S. A., Boddeke, H. W. G. M. & Kettenmann, H. Microglia in Physiology and Disease. *Annu. Rev. Physiol.* 79, 619–643 (2017).

24. Dale, D. C., Boxer, L. & Conrad Liles, W. The phagocytes: Neutrophils and monocytes. *Blood* 112, 935–945 (2008).

25. Abel, A. M., Yang, C., Thakar, M. S. & Malarkannan, S. Natural killer cells: Development, maturation, and clinical utilization. *Frontiers in Immunology* 9, 1 (2018).

26. Huntington, N. D., Cursons, J. & Rautela, J. The cancer–natural killer cell immunity cycle. *Nature Reviews Cancer* 20, 437–454 (2020).

27. Kerr, J. F. R., Wyllie, A. H. & Currie, A. R. Apoptosis: A basic biological phenomenon with wide-ranging implications in tissue kinetics. *Br. J. Cancer* 26, 239–257 (1972).

28. Tang, D., Kang, R., Berghe, T. Vanden, Vandenabeele, P. & Kroemer, G. The molecular machinery of regulated cell death. *Cell Research* 29, 347–364 (2019).

29. Holler, N. *et al.* Fas triggers an alternative, caspase-8-independent cell death pathway using the kinase RIP as effector molecule. *Nat. Immunol.* 1, 489–495 (2000).

30. Dhuriya, Y. K. & Sharma, D. Necroptosis: A regulated inflammatory mode of cell death. *Journal of Neuroinflammation* 15, 1–9 (2018).

31. Fink, S. L. & Cookson, B. T. Apoptosis, pyroptosis, and necrosis: Mechanistic description of dead and dying eukaryotic cells. *Infection and Immunity* 73, 1907–1916 (2005).

32. Man, S. M., Karki, R. & Kanneganti, T. D. Molecular mechanisms and functions of pyroptosis, inflammatory caspases and inflammasomes in infectious diseases. *Immunological Reviews* 277, 61–75 (2017).

33. Medzhitov, R., Preston-Hurlburt, P. & Janeway, C. A. A human homologue of the Drosophila toll protein signals activation of adaptive immunity. *Nature* 388, 394–397 (1997).

34. Poltorak, A. *et al.* Defective LPS signaling in C3H/HeJ and C57BL/10ScCr mice: Mutations in Tlr4 gene. *Science (80-.).* 282, 2085–2088 (1998).

35. Beutler, B. Inferences, questions and possibilities in Toll-like receptor signalling. *Nature* 430, 257–263 (2004).

36. Rock, F. L., Hardiman, G., Timans, J. C., Kastelein, R. A. & Bazan, J. F. A family of human receptors structurally related to Drosophila Toll. *Proc. Natl. Acad. Sci. U. S. A.* 95, 588–593 (1998).

37. McDonald, D. R. & Levy, O. Innate immunity. in *Clinical Immunology: Principles and Practice: Fourth Edition* 35–46 (Elsevier Inc., 2013). doi:10.1016/B978-0-7234-3691-1.00027-1

38. Kawasaki, T. & Kawai, T. Toll-like receptor signaling pathways. *Frontiers in Immunology* 5, (2014).

39. Kumar, V. The complement system, toll-like receptors and inflammasomes in host defense: three musketeers' one target. *International Reviews of Immunology* 38, 131–156 (2019).

40. Dolasia, K., Bisht, M. K., Pradhan, G., Udgata, A. & Mukhopadhyay, S. TLRs/NLRs: Shaping the landscape of host immunity. *International Reviews of Immunology* 37, 3–19 (2018).

41. Kranzusch, P. J., Lee, A. S. Y., Berger, J. M. & Doudna, J. A. Structure of Human cGAS Reveals a Conserved Family of Second-Messenger Enzymes in Innate Immunity. *Cell Rep.* 3, 1362–1368 (2013).

42. Choe, J., Kelker, M. S. & Wilson, I. A. Structural biology: Crystal structure of human toll-like receptor 3 (TLR3) ectodomain. *Science (80-.).* 309, 581–585 (2005).

43. Botos, I., Segal, D. M. & Davies, D. R. The structural biology of Toll-like receptors. *Structure* 19, 447–459 (2011).

44. Akira, S., Uematsu, S. & Takeuchi, O. Pathogen recognition and innate immunity. *Cell* 124, 783–801 (2006).

45. Kawai, T. & Akira, S. The role of pattern-recognition receptors in innate immunity: Update on

toll-like receptors. *Nature Immunology* 11, 373–384 (2010).

46.   Kim, H. M. *et al.* Crystal Structure of the TLR4-MD-2 Complex with Bound Endotoxin Antagonist Eritoran. *Cell* 130, 906–917 (2007).

47.   Płóciennikowska, A., Hromada-Judycka, A., Borzęcka, K. & Kwiatkowska, K. Co-operation of TLR4 and raft proteins in LPS-induced pro-inflammatory signaling. *Cell. Mol. Life Sci.* 72, 557–581 (2015).

48.   Wu, Z., Zhang, Z., Lei, Z. & Lei, P. CD14: Biology and role in the pathogenesis of disease. *Cytokine and Growth Factor Reviews* 48, 24–31 (2019).

49.   Kumar, H., Kawai, T. & Akira, S. Pathogen recognition by the innate immune system. *Int. Rev. Immunol.* 30, 16–34 (2011).

50.   Bell, J. K., Askins, J., Hall, P. R., Davies, D. R. & Segal, D. M. The dsRNA binding site of human Toll-like receptor 3. *Proc. Natl. Acad. Sci. U. S. A.* 103, 8792–8797 (2006).

51.   Zhang, Z. *et al.* Structural Analysis Reveals that Toll-like Receptor 7 Is a Dual Receptor for Guanosine and Single-Stranded RNA. *Immunity* 45, 737–748 (2016).

52.   Zhang, Z. *et al.* Structural Analyses of Toll-like Receptor 7 Reveal Detailed RNA Sequence Specificity and Recognition Mechanism of Agonistic Ligands. *Cell Rep.* 25, 3371-3381.e5 (2018).

53.   Tanji, H. *et al.* Toll-like receptor 8 senses degradation products of single-stranded RNA. *Nat. Struct. Mol. Biol.* 22, 109–116 (2015).

54.   Greulich, W. *et al.* TLR8 Is a Sensor of RNase T2 Degradation Products. 179, 1264–1275

55.   Kumagai, Y., Takeuchi, O. & Akira, S. TLR9 as a key receptor for the recognition of DNA. *Advanced Drug Delivery Reviews* 60, 795–804 (2008).

56.   Bowie, A. & O'Neill, L. A. J. The interleukin-1 receptor/Toll-like receptor superfamily: Signal generators for pro-inflammatory interleukins and microbial products. *Journal of Leukocyte Biology* 67, 508–514 (2000).

57.   Kawai, T. & Akira, S. Toll-like Receptors and Their Crosstalk with Other Innate Receptors in Infection and Immunity. *Immunity* 34, 637–650 (2011).

58.   Deguine, J. & Barton, G. M. MyD88: A central player in innate immune signaling. *F1000Prime Rep.* 6, (2014).

59.   Motshwene, P. G. *et al.* An Oligomeric Signaling Platform formed by the toll-like receptor signal transducers MyD88 and IRAK-4. *J. Biol. Chem.* 284, 25404–25411 (2009).

60.   Lin, S. C., Lo, Y. C. & Wu, H. Helical assembly in the MyD88-IRAK4-IRAK2 complex in TLR/IL-1R signalling. *Nature* 465, 885–890 (2010).

61.   Ferrao, R. *et al.* IRAK4 Dimerization and trans-Autophosphorylation Are Induced by Myddosome Assembly. *Mol. Cell* 55, 891–903 (2014).

62.   Lomaga, M. A. *et al.* TRAF6 deficiency results in osteopetrosis and defective interleukin-1, CD40, and LPS signaling. *Genes Dev.* 13, 1015–1024 (1999).

63.   Deng, L. *et al.* Activation of the Iκb kinase complex by TRAF6 requires a dimeric ubiquitin-conjugating enzyme complex and a unique polyubiquitin chain. *Cell* 103, 351–361 (2000).

64.   Fukushima, T. *et al.* Ubiquitin-conjugating enzyme Ubc13 is a critical component of TNF receptor-associated factor (TRAF)-mediated inflammatory responses. *Proc. Natl. Acad. Sci. U. S. A.* 104, 6371–6376 (2007).

65.   Chen, Z. J. Ubiquitin signalling in the NF-κB pathway. *Nature Cell Biology* 7, 758–765 (2005).

66.   Takaesu, G. *et al.* TAB2, a novel adaptor protein, mediates activation of TAK1 MAPKKK by linking TAK1 to TRAF6 in the IL-1 signal transduction pathway. *Mol. Cell* 5, 649–658 (2000).

67.   Wang, C. *et al.* TAK1 is a ubiquitin-dependent kinase of MKK and IKK. *Nature* 412, 346–351

(2001).

68.   Ninomiya-Tsuji, J. *et al.* The kinase TAK1 can activate the NIK-IκB as well as the MAP kinase cascade in the IL-1 signalling pathway. *Nature* 398, 252–256 (1999).

69.   Kawai, T. *et al.* Interferon-α induction through Toll-like receptors involves a direct interaction of IRF7 with MyD88 and TRAF6. *Nat. Immunol.* 5, 1061–1068 (2004).

70.   Honda, K. *et al.* Role of a transductional-transcriptional processor complex involving MyD88 and IRF-7 in Toll-like receptor signaling. *Proc. Natl. Acad. Sci. U. S. A.* 101, 15416–15421 (2004).

71.   Schoenemeyer, A. *et al.* The interferon regulatory factor, IRF5, is a central mediator of toll-like receptor 7 signaling. *J. Biol. Chem.* 280, 17005–17012 (2005).

72.   Takaoka, A. *et al.* Integral role of IRF-5 in the gene induction programme activated by Toll-like receptors. *Nature* 434, 243–249 (2005).

73.   Schmacke, N. A. & Hornung, V. Fourth defence molecule completes antiviral line-up. *Nature* 581, 266–267 (2020).

74.   Ban, T., Sato, G. R. & Tamura, T. Regulation and role of the transcription factor IRF5 in innate immune responses and systemic lupus erythematosus. *International Immunology* 30, 529–536 (2018).

75.   Heinz, L. X. *et al.* TASL is the SLC15A4-associated adaptor for IRF5 activation by TLR7–9. *Nature* 581, 316–322 (2020).

76.   Yamamoto, M. *et al.* TRAM is specifically involved in the Toll-like receptor 4-mediated MyD88-independent signaling pathway. *Nat. Immunol.* 4, 1144–1150 (2003).

77.   Zanoni, I. *et al.* CD14 controls the LPS-induced endocytosis of toll-like receptor 4. *Cell* 147, 868–880 (2011).

78.   Kagan, J. C. *et al.* TRAM couples endocytosis of Toll-like receptor 4 to the induction of interferon-β. *Nat. Immunol.* 9, 361–368 (2008).

79.   Tanimura, N., Saitoh, S., Matsumoto, F., Akashi-Takamura, S. & Miyake, K. Roles for LPS-dependent interaction and relocation of TLR4 and TRAM in TRIF-signaling. *Biochem. Biophys. Res. Commun.* 368, 94–99 (2008).

80.   Anwar, M. A., Shah, M., Kim, J. & Choi, S. Recent clinical trends in Toll-like receptor targeting therapeutics. *Med. Res. Rev.* 39, 1053–1090 (2019).

81.   Meylan, E. *et al.* RIP1 is an essential mediator of Toll-like receptor 3-induced NF κB activation. *Nat. Immunol.* 5, 503–507 (2004).

82.   Ermolaeva, M. A. *et al.* Function of TRADD in tumor necrosis factor receptor 1 signaling and in TRIF-dependent inflammatory responses. *Nat. Immunol.* 9, 1037–1046 (2008).

83.   Kim, Y. K., Shin, J. S. & Nahm, M. H. NOD-like receptors in infection, immunity, and diseases. *Yonsei Medical Journal* 57, 5–14 (2016).

84.   Motta, V., Soares, F., Sun, T. & Philpott, D. J. Nod-like receptors: Versatile cytosolic sentinels. *Physiol. Rev.* 95, 149–178 (2015).

85.   Zhong, Y., Kinio, A. & Saleh, M. Functions of NOD-Like Receptors in Human Diseases. *Front. Immunol.* 4, (2013).

86.   Nickerson, K. *et al.* Dendritic Cell-specific MHC Class II Transactivator Contains a Caspase Recruitment Domain That Confers Potent Transactivation Activity. *J. Biol. Chem.* 276, 19089–19093 (2001).

87.   Kofoed, E. M. & Vance, R. E. Innate immune recognition of bacterial ligands by NAIPs determines inflammasome specificity. *Nature* 477, 592–597 (2011).

88.   Man, S. M. & Kanneganti, T. D. Regulation of inflammasome activation. *Immunological*

Reviews 265, 6–21 (2015).

89.   Bauernfeind, F. & Hornung, V. Of inflammasomes and pathogens - sensing of microbes by the inflammasome. *EMBO Molecular Medicine* 5, 814–826 (2013).

90.   Heim, V. J., Stafford, C. A. & Nachbur, U. NOD Signaling and Cell Death. *Frontiers in Cell and Developmental Biology* 7, 208 (2019).

91.   Platnich, J. M. & Muruve, D. A. NOD-like receptors and inflammasomes: A review of their canonical and non-canonical signaling pathways. *Archives of Biochemistry and Biophysics* 670, 4–14 (2019).

92.   Girardin, S. E. *et al.* Nod2 is a general sensor of peptidoglycan through muramyl dipeptide (MDP) detection. *J. Biol. Chem.* 278, 8869–8872 (2003).

93.   Girardin, S. E. *et al.* Nod1 detects a unique muropeptide from gram-negative bacterial peptidoglycan. *Science (80-.).* 300, 1584–1587 (2003).

94.   Tattoli, I., Travassos, L. H., Carneiro, L. A., Magalhaes, J. G. & Girardin, S. E. The nodosome: Nod1 and Nod2 control bacterial infections and inflammation. *Seminars in Immunopathology* 29, 289–301 (2007).

95.   Downs, K. P., Nguyen, H., Dorfleutner, A. & Stehlik, C. An overview of the non-canonical inflammasome. *Molecular Aspects of Medicine* 76, 100924 (2020).

96.   Gross, O. *et al.* Syk kinase signalling couples to the Nlrp3 inflammasome for anti-fungal host defence. *Nature* 459, 433–436 (2009).

97.   Allen, I. C. *et al.* The NLRP3 Inflammasome Mediates In Vivo Innate Immunity to Influenza A Virus through Recognition of Viral RNA. *Immunity* 30, 556–565 (2009).

98.   Thomas, P. G. *et al.* The Intracellular Sensor NLRP3 Mediates Key Innate and Healing Responses to Influenza A Virus via the Regulation of Caspase-1. *Immunity* 30, 566–575 (2009).

99.   Bauernfeind, F. *et al.* Inflammasomes: Current understanding and open questions. *Cellular and Molecular Life Sciences* 68, 765–783 (2011).

100.   Davis, B. K., Wen, H. & Ting, J. P. Y. The Inflammasome NLRs in immunity, inflammation, and associated diseases. *Annu. Rev. Immunol.* 29, 707–735 (2011).

101.   Agostini, L. *et al.* NALP3 forms an IL-1β-processing inflammasome with increased activity in Muckle-Wells autoinflammatory disorder. *Immunity* 20, 319–325 (2004).

102.   Kufer, T. A. & Sansonetti, P. J. NLR functions beyond pathogen recognition. *Nature Immunology* 12, 121–128 (2011).

103.   Shi, J. *et al.* Cleavage of GSDMD by inflammatory caspases determines pyroptotic cell death. *Nature* 526, 660–665 (2015).

104.   Man, S. M., Karki, R. & Kanneganti, T. D. Molecular mechanisms and functions of pyroptosis, inflammatory caspases and inflammasomes in infectious diseases. *Immunological Reviews* 277, 61–75 (2017).

105.   D'Arcy, M. S. Cell death: a review of the major forms of apoptosis, necrosis and autophagy. *Cell Biology International* 43, 582–592 (2019).

106.   Rogers, C. *et al.* Cleavage of DFNA5 by caspase-3 during apoptosis mediates progression to secondary necrotic/pyroptotic cell death. *Nat. Commun.* 8, 1–14 (2017).

107.   Brown, G. D., Willment, J. A. & Whitehead, L. C-type lectins in immunity and homeostasis. *Nature Reviews Immunology* 18, 374–389 (2018).

108.   Weis, W. I., Taylor, M. E. & Drickamer, K. The C-type lectin superfamily in the immune system. *Immunological Reviews* 163, 19–34 (1998).

109.   Zelensky, A. N. & Gready, J. E. The C-type lectin-like domain superfamily. *FEBS Journal* 272, 6179–6217 (2005).

110. Hou, H. *et al.* C-type Lectin Receptor: Old Friend and New Player. *Med. Chem. (Los. Angeles).* 13, (2017).

111. Mócsai, A., Ruland, J. & Tybulewicz, V. L. J. The SYK tyrosine kinase: A crucial player in diverse biological functions. *Nature Reviews Immunology* 10, 387–402 (2010).

112. Schlee, M. & Hartmann, G. Discriminating self from non-self in nucleic acid sensing. *Nature Reviews Immunology* 16, 566–580 (2016).

113. Takeuchi, O. & Akira, S. Pattern Recognition Receptors and Inflammation. *Cell* 140, 805–820 (2010).

114. Yoneyama, M. & Fujita, T. Structural Mechanism of RNA Recognition by the RIG-I-like Receptors. *Immunity* 29, 178–181 (2008).

115. Hornung, V. *et al.* 5′-Triphosphate RNA is the ligand for RIG-I. *Science (80-.).* 314, 994–997 (2006).

116. Pichlmair, A. *et al.* RIG-I-mediated antiviral responses to single-stranded RNA bearing 5′-phosphates. *Science (80-.).* 314, 997–1001 (2006).

117. Schlee, M. *et al.* Recognition of 5′ Triphosphate by RIG-I Helicase Requires Short Blunt Double-Stranded RNA as Contained in Panhandle of Negative-Strand Virus. *Immunity* 31, 25–34 (2009).

118. Schmidt, A. *et al.* 5′-triphosphate RNA requires base-paired structures to activate antiviral signaling via RIG-I. *Proc. Natl. Acad. Sci. U. S. A.* 106, 12067–12072 (2009).

119. Kato, H. *et al.* Differential roles of MDA5 and RIG-I helicases in the recognition of RNA viruses. *Nature* 441, 101–105 (2006).

120. Duic, I. *et al.* Viral RNA recognition by LGP2 and MDA5, and activation of signaling through step-by-step conformational changes. *Nucleic Acids Res.* 48, 11664–11674 (2020).

121. Loo, Y. M. & Gale, M. Immune Signaling by RIG-I-like Receptors. *Immunity* 34, 680–692 (2011).

122. Scott, I. The role of mitochondria in the mammalian antiviral defense system. *Mitochondrion* 10, 316–320 (2010).

123. Dixit, E. *et al.* Peroxisomes Are Signaling Platforms for Antiviral Innate Immunity. *Cell* 141, 668–681 (2010).

124. Quicke, K. M., Diamond, M. S. & Suthar, M. S. Negative regulators of the RIG-I-like receptor signaling pathway. *Eur. J. Immunol.* 47, 615–628 (2017).

125. Abe, T., Marutani, Y. & Shoji, I. Cytosolic DNA-sensing immune response and viral infection. *Microbiology and Immunology* 63, 51–64 (2019).

126. Gray, E. E. *et al.* The AIM2-like receptors are dispensable for the interferon response to intracellular DNA. *Immunity* 45, 255 (2016).

127. Hornung, V. *et al.* AIM2 recognizes cytosolic dsDNA and forms a caspase-1-activating inflammasome with ASC. *Nature* 458, 514–518 (2009).

128. Fernandes-Alnemri, T., Yu, J. W., Datta, P., Wu, J. & Alnemri, E. S. AIM2 activates the inflammasome and cell death in response to cytoplasmic DNA. *Nature* 458, 509–513 (2009).

129. Unterholzner, L. *et al.* IFI16 is an innate immune sensor for intracellular DNA. *Nat. Immunol.* 11, 997–1004 (2010).

130. Hornung, V., Hartmann, R., Ablasser, A. & Hopfner, K. P. OAS proteins and cGAS: Unifying concepts in sensing and responding to cytosolic nucleic acids. *Nat. Rev. Immunol.* 14, 521–528 (2014).

131. Sun, L., Wu, J., Du, F., Chen, X. & Chen, Z. J. Cyclic GMP-AMP synthase is a cytosolic DNA sensor that activates the type I interferon pathway. *Science (80-.).* 339, 786–791 (2013).

132. Ablasser, A. *et al.* CGAS produces a 2′-5′-linked cyclic dinucleotide second messenger that

activates STING. *Nature* 498, 380–384 (2013).

133.   Civril, F. *et al.* Structural mechanism of cytosolic DNA sensing by cGAS. *Nature* 498, 332–337 (2013).

134.   Wu, J. *et al.* Cyclic GMP-AMP is an endogenous second messenger in innate immune signaling by cytosolic DNA. *Science (80-.).* 339, 826–830 (2013).

135.   Burdette, D. L. *et al.* STING is a direct innate immune sensor of cyclic di-GMP. *Nature* 478, 515–518 (2011).

136.   Sauer, J. D. *et al.* The N-ethyl-N-nitrosourea-induced Goldenticket mouse mutant reveals an essential function of sting in the in vivo interferon response to Listeria monocytogenes and cyclic dinucleotides. *Infect. Immun.* 79, 688–694 (2011).

137.   Ergun, S. L., Fernandez, D., Weiss, T. M. & Li, L. STING Polymer Structure Reveals Mechanisms for Activation, Hyperactivation, and Inhibition. *Cell* 178, 290-301.e10 (2019).

138.   Shang, G., Zhang, C., Chen, Z. J., Bai, X. chen & Zhang, X. Cryo-EM structures of STING reveal its mechanism of activation by cyclic GMP–AMP. *Nature* 567, 389–393 (2019).

139.   Ishikawa, H., Ma, Z. & Barber, G. N. STING regulates intracellular DNA-mediated, type i interferon-dependent innate immunity. *Nature* 461, 788–792 (2009).

140.   Sun, W. *et al.* ERIS, an endoplasmic reticulum IFN stimulator, activates innate immune signaling through dimerization. *Proc. Natl. Acad. Sci. U. S. A.* 106, 8653–8658 (2009).

141.   Zhong, B. *et al.* The Adaptor Protein MITA Links Virus-Sensing Receptors to IRF3 Transcription Factor Activation. *Immunity* 29, 538–550 (2008).

142.   Zierhut, C. *et al.* The Cytoplasmic DNA Sensor cGAS Promotes Mitotic Cell Death. *Cell* 178, 302-315.e23 (2019).

143.   Yang, H., Wang, H., Ren, U., Chen, Q. & Chena, Z. J. CGAS is essential for cellular senescence. *Proc. Natl. Acad. Sci. U. S. A.* 114, E4612–E4620 (2017).

144.   Hopfner, K. P. & Hornung, V. Molecular mechanisms and cellular functions of cGAS–STING signalling. *Nature Reviews Molecular Cell Biology* 21, 501–521 (2020).

145.   Jiang, H. *et al.* Chromatin-bound cGAS is an inhibitor of DNA repair and hence accelerates genome destabilization and cell death . *EMBO J.* 38, (2019).

146.   Michalski, S. *et al.* Structural basis for sequestration and autoinhibition of cGAS by chromatin. *Nature* 587, 678–682 (2020).

147.   Volkman, H. E., Cambier, S., Gray, E. E. & Stetson, D. B. Tight nuclear tethering of cGAS is essential for preventing autoreactivity. *Elife* 8, (2019).

148.   Gentili, M. *et al.* The N-Terminal Domain of cGAS Determines Preferential Association with Centromeric DNA and Innate Immune Activation in the Nucleus. *Cell Rep.* 26, 2377-2393.e13 (2019).

149.   Barnett, K. C. *et al.* Phosphoinositide Interactions Position cGAS at the Plasma Membrane to Ensure Efficient Distinction between Self- and Viral DNA. *Cell* 176, 1432-1446.e11 (2019).

150.   Ablasser, A. *et al.* RIG-I-dependent sensing of poly(dA:dT) through the induction of an RNA polymerase III-transcribed RNA intermediate. *Nat. Immunol.* 10, 1065–1072 (2009).

151.   Chiu, Y. H., MacMillan, J. B. & Chen, Z. J. RNA Polymerase III Detects Cytosolic DNA and Induces Type I Interferons through the RIG-I Pathway. *Cell* 138, 576–591 (2009).

152.   Kim, T. *et al.* Aspartate-glutamate-alanine-histidine box motif (DEAH)/RNA helicase a helicases sense microbial DNA in human plasmacytoid dendritic cells. *Proc. Natl. Acad. Sci. U. S. A.* 107, 15181–15186 (2010).

153.   Zhang, Z. *et al.* The helicase DDX41 senses intracellular DNA mediated by the adaptor STING in dendritic cells. *Nat. Immunol.* 12, 959–965 (2011).

154. Takeda, K. Toll-like receptors in innate immunity. *Int. Immunol.* 17, 1–14 (2004).

155. Karin, M. & Greten, F. R. NF-κB: Linking inflammation and immunity to cancer development and progression. *Nature Reviews Immunology* 5, 749–759 (2005).

156. Sen, R. & Baltimore, D. Multiple nuclear factors interact with the immunoglobulin enhancer sequences. *Cell* 46, 705–716 (1986).

157. Zhang, Q., Lenardo, M. J. & Baltimore, D. 30 Years of NF-κB: A Blossoming of Relevance to Human Pathobiology. *Cell* 168, 37–57 (2017).

158. Sun, S. C., Chang, J. H. & Jin, J. Regulation of nuclear factor-κB in autoimmunity. *Trends in Immunology* 34, 282–289 (2013).

159. Chen, F. E., Huang, D. Bin, Chen, Y. Q. & Ghosh, G. Crystal structure of p50/p65 heterodimer of transcription factor NF-κb bound to DNA. *Nature* 391, 410–412 (1998).

160. Taniguchi, K. & Karin, M. NF-B, inflammation, immunity and cancer: Coming of age. *Nature Reviews Immunology* 18, 309–324 (2018).

161. Liu, T., Zhang, L., Joo, D. & Sun, S. C. NF-κB signaling in inflammation. *Signal Transduction and Targeted Therapy* 2, 17023 (2017).

162. Zhang, H. & Sun, S. C. NF-KB in inflammation and renal diseases. *Cell and Bioscience* 5, (2015).

163. Sato, S. *et al.* Essential function for the kinase TAK1 in innate and adaptive immune responses. *Nat. Immunol.* 6, 1087–1095 (2005).

164. Shim, J. H. *et al.* TAK1, but not TAB1 or TAB2, plays an essential role in multiple signaling pathways in vivo. *Genes Dev.* 19, 2668–2681 (2005).

165. Senftleben, U. *et al.* Activation by IKKα of a second, evolutionary conserved, NF-κB signaling pathway. *Science (80-.).* 293, 1495–1499 (2001).

166. Xiao, G., Harhaj, E. W. & Sun, S. C. NF-κB-inducing kinase regulates the processing of NF-κB2 p100. *Mol. Cell* 7, 401–409 (2001).

167. Israël, A. The IKK complex, a central regulator of NF-kappaB activation. *Cold Spring Harbor perspectives in biology* 2, (2010).

168. Ben-Neriah, Y. Regulatory functions of ubiquitination in the immune system. *Nature Immunology* 3, 20–26 (2002).

169. Hayden, M. S. & Ghosh, S. Shared Principles in NF-κB Signaling. *Cell* 132, 344–362 (2008).

170. Sun, S. C. The noncanonical NF-κB pathway. *Immunological Reviews* 246, 125–140 (2012).

171. Arthur, J. S. C. & Ley, S. C. Mitogen-activated protein kinases in innate immunity. *Nature Reviews Immunology* 13, 679–692 (2013).

172. Newton, K. & Dixit, V. M. Signaling in innate immunity and inflammation. *Cold Spring Harb. Perspect. Biol.* 4, (2012).

173. Plotnikov, A., Zehorai, E., Procaccia, S. & Seger, R. The MAPK cascades: Signaling components, nuclear roles and mechanisms of nuclear translocation. *Biochimica et Biophysica Acta - Molecular Cell Research* 1813, 1619–1633 (2011).

174. Wei, Z. & Liu, H. T. MAPK signal pathways in the regulation of cell proliferation in mammalian cells. *Cell Research* 12, 9–18 (2002).

175. Sun, W. *et al.* MEKK2 Associates with the Adapter Protein Lad/RIBP and Regulates the MEK5-BMK1/ERK5 Pathway. *J. Biol. Chem.* 276, 5093–5100 (2001).

176. Wang, X. & Tournier, C. Regulation of cellular functions by the ERK5 signalling pathway. *Cellular Signalling* 18, 753–760 (2006).

177. Nishimoto, S. & Nishida, E. MAPK signalling: ERK5 versus ERK1/2. *EMBO Reports* 7, 782–786 (2006).

178. Rincón, M. & Davis, R. J. Regulation of the immune response by stress-activated protein kinases. *Immunol. Rev.* 228, 212–224 (2009).

179. Morrison, D. K. MAP kinase pathways. *Cold Spring Harb. Perspect. Biol.* 4, (2012).

180. Cargnello, M. & Roux, P. P. Activation and Function of the MAPKs and Their Substrates, the MAPK-Activated Protein Kinases. *Microbiol. Mol. Biol. Rev.* 75, 50–83 (2011).

181. Sabio, G. *et al.* p38γ regulates the localisation of SAP97 in the cytoskeleton by modulating its interaction with GKAP. *EMBO J.* 24, 1134–1145 (2005).

182. Remy, G. *et al.* Differential activation of p38MAPK isoforms by MKK6 and MKK3. *Cell. Signal.* 22, 660–667 (2010).

183. Risco, A. & Cuenda, A. New Insights into the p38 γ and p38 δ MAPK Pathways . *J. Signal Transduct.* 2012, 1–8 (2012).

184. Escós, A., Risco, A., Alsina-Beauchamp, D. & Cuenda, A. p38γ and p38δ Mitogen Activated Protein Kinases (MAPKs), New Stars in the MAPK Galaxy. *Front. Cell Dev. Biol.* 4, 31 (2016).

185. Cuevas, B. D., Abell, A. N. & Johnson, G. L. Role of mitogen-activated protein kinase kinase kinases in signal integration. *Oncogene* 26, 3159–3171 (2007).

186. Morrison, D. K. & Davis, R. J. Regulation of MAP Kinase Signaling Modules by Scaffold Proteins in Mammals. in *Annual Review of Cell and Developmental Biology* 19, 91–118 (Annual Reviews 4139 El Camino Way, P.O. Box 10139, Palo Alto, CA 94303-0139, USA , 2003).

187. Good, M. C., Zalatan, J. G. & Lim, W. A. Scaffold proteins: Hubs for controlling the flow of cellular information. *Science* 332, 680–686 (2011).

188. Gaestel, M. MAPKAP kinases - MKs - Two's company, three's a crowd. *Nature Reviews Molecular Cell Biology* 7, 120–130 (2006).

189. Soni, S., Anand, P. & Padwad, Y. S. MAPKAPK2: The master regulator of RNA-binding proteins modulates transcript stability and tumor progression. *Journal of Experimental and Clinical Cancer Research* 38, 1–18 (2019).

190. Ehlting, C. *et al.* Distinct functions of the Mitogen-activated Protein Kinase-activated Protein (MAPKAP) kinases MK2 and MK3: MK2 mediates lipopolysaccharide-induced Signal Transducers and Activators of Transcription 3 (STAT3) activation by preventing negative regulatory effects of MK3. *J. Biol. Chem.* 286, 24113–24124 (2011).

191. Ehlting, C. *et al.* Cooperative and distinct functions of MK2 and MK3 in the regulation of the macrophage transcriptional response to lipopolysaccharide. *Sci. Rep.* 9, 1–14 (2019).

192. Vermeulen, L., Berghe, W. Vanden, Beck, I. M. E., De Bosscher, K. & Haegeman, G. The versatile role of MSKs in transcriptional regulation. *Trends in Biochemical Sciences* 34, 311–318 (2009).

193. Pierrat, B., Da Silva Correia, J., Mary, J. L., Tomás-Zuber, M. & Lesslauer, W. RSK-B, a novel ribosomal S6 kinase family member, is a CREB kinase under dominant control of p38α mitogen-activated protein kinase (p38α(MAPK)). *J. Biol. Chem.* 273, 29661–29671 (1998).

194. Deak, M., Clifton, A. D., Lucocq, J. M. & Alessi, D. R. Mitogen- and stress-activated protein kinase-1 (MSK1) is directly activated by MAPK and SAPK2/p38, and may mediate activation of CREB. *EMBO J.* 17, 4426–4441 (1998).

195. Ananieva, O. *et al.* The kinases MSK1 and MSK2 act as negative regulators of Toll-like receptor signaling. *Nat. Immunol.* 9, 1028–1036 (2008).

196. Atsaves, V., Leventaki, V., Rassidakis, G. Z. & Claret, F. X. AP-1 transcription factors as regulators of immune responses in cancer. *Cancers* 11, (2019).

197. Karin, M., Liu, Z. G. & Zandi, E. AP-1 function and regulation. *Curr. Opin. Cell Biol.* 9, 240–246 (1997).

198. Shaulian, E. & Karin, M. AP-1 as a regulator of cell life and death. *Nature Cell Biology* 4, E131–E136 (2002).

199. Eferl, R. & Wagner, E. F. AP-1: A double-edged sword in tumorigenesis. *Nature Reviews Cancer* 3, 859–868 (2003).

200. Qiao, Y. *et al.* AP-1 is a key regulator of proinflammatory cytokine TNFα-mediated triple-negative breast cancer progression. *J. Biol. Chem.* 291, 5068–5079 (2016).

201. Fujita, T. *et al.* Evidence for a nuclear factor(s), IRF-1, mediating induction and silencing properties to human IFN-beta gene regulatory elements. *EMBO J.* 7, 3397–3405 (1988).

202. Miyamoto, M. *et al.* Regulated expression of a gene encoding a nuclear factor, IRF-1, that specifically binds to IFN-β gene regulatory elements. *Cell* 54, 903–913 (1988).

203. Antonczyk, A. *et al.* Direct inhibition of IRF-dependent transcriptional regulatory mechanisms associated with disease. *Front. Immunol.* 10, 1176 (2019).

204. Remesh, S. G., Santosh, V. & Escalante, C. R. Structural studies of IRF4 reveal a flexible autoinhibitory region and a compact linker domain. *J. Biol. Chem.* 290, 27779–27790 (2015).

205. Bonelli, M. *et al.* IRF1 is critical for the TNF-driven interferon response in rheumatoid fibroblast-like synoviocytes: JAKinibs suppress the interferon response in RA-FLSs. *Exp. Mol. Med.* 51, 1–11 (2019).

206. Yanai, H., Negishi, H. & Taniguchi, T. The IRF family of transcription factors inception, impact and implications in oncogenesis. *OncoImmunology* 1, 1376–1386 (2012).

207. Schwartz, J. L., Shajahan, A. N. & Clarke, R. The Role of Interferon Regulatory Factor-1 (IRF1) in Overcoming Antiestrogen Resistance in the Treatment of Breast Cancer. *Int. J. Breast Cancer* 2011, 1–9 (2011).

208. Yarilina, A., Park-Min, K. H., Antoniv, T., Hu, X. & Ivashkiv, L. B. TNF activates an IRF1-dependent autocrine loop leading to sustained expression of chemokines and STAT1-dependent type I interferon-response genes. *Nat. Immunol.* 9, 378–387 (2008).

209. Lohoff, M. & Mak, T. W. Roles of interferon-regulatory factors in T-helper-cell differentiation. *Nature Reviews Immunology* 5, 125–135 (2005).

210. Schaefer, B. C., Paulson, E., Strominger, J. L. & Speck, S. H. Constitutive activation of Epstein-Barr virus (EBV) nuclear antigen 1 gene transcription by IRF1 and IRF2 during restricted EBV latency. *Mol. Cell. Biol.* 17, 873–886 (1997).

211. Langlais, D., Barreiro, L. B. & Gros, P. The macrophage IRF8/IRF1 regulome is required for protection against infections and is associated with chronic inflammation. *J. Exp. Med.* 213, 585–603 (2016).

212. Han, K. J., Jiang, L. & Shu, H. B. Regulation of IRF2 transcriptional activity by its sumoylation. *Biochem. Biophys. Res. Commun.* 372, 772–778 (2008).

213. DREW, P. D. *et al.* NFκB and Interferon Regulatory Factor 1 Physically Interact and Synergistically Induce Major Histocompatibility Class I Gene Expression. *J. Interf. Cytokine Res.* 15, 1037–1045 (1995).

214. Minamino, K. *et al.* IRF-2 regulates B-cell proliferation and antibody production through distinct mechanisms. *Int. Immunol.* 24, 573–581 (2012).

215. Kayagaki, N. *et al.* IRF2 transcriptionally induces GSDMD expression for pyroptosis. *Sci. Signal.* 12, (2019).

216. Takahasi, K. *et al.* X-ray crystal structure of IRF-3 and its functional implications. *Nat. Struct. Biol.* 10, 922–927 (2003).

217. Qin, B. Y. *et al.* Crystal structure of IRF-3 reveals mechanism of autoinhibition and virus-induced phosphoactivation. *Nat. Struct. Biol.* 10, 913–921 (2003).

218. Schmid, S., Sachs, D. & Ten Oever, B. R. Mitogen-activated protein kinase-mediated licensing of interferon regulatory factor 3/7 reinforces the cell response to virus. *J. Biol. Chem.* 289, 299–311 (2014).

219. Wang, Z. *et al.* Complex Regulation Pattern of IRF3 Activation Revealed by a Novel Dimerization Reporter System. *J. Immunol.* 196, 4322–4330 (2016).

220. Barnes, B. J. *et al.* Global and distinct targets of IRF-5 and IRF-7 during innate response to viral infection. *J. Biol. Chem.* 279, 45194–45207 (2004).

221. Li, Q. *et al.* Interferon regulatory factors IRF5 and IRF7 inhibit growth and induce senescence in immortal Li-Fraumeni fibroblasts. *Mol. Cancer Res.* 6, 770–784 (2008).

222. Andrilenas, K. K. *et al.* DNA-binding landscape of IRF3, IRF5 and IRF7 dimers: Implications for dimer-specific gene regulation. *Nucleic Acids Res.* 46, 2509–2520 (2018).

223. Oberbeck, N. *et al.* The RIPK4–IRF6 signalling axis safeguards epidermal differentiation and barrier function. *Nature* 574, 249–253 (2019).

224. Taniguchi, T., Ogasawara, K., Takaoka, A. & Tanaka, N. IRF family of transcription factors as regulators of host defense. *Annual Review of Immunology* 19, 623–655 (2001).

225. Pongubala, J. M. *et al.* PU.1 recruits a second nuclear factor to a site important for immunoglobulin kappa 3' enhancer activity. *Mol. Cell. Biol.* 12, 368–378 (1992).

226. Eisenbeis, C. F., Singh, H. & Storb, U. Pip, a novel IRF family member, is a lymphoid-specific, PU.1-dependent transcriptional activator. *Genes Dev.* 9, 1377–1387 (1995).

227. Eklund, E. A., Jalava, A. & Kakar, R. PU.1, Interferon regulatory factor 1, and interferon consensus sequence- binding protein cooperate to increase gp91(phox) expression. *J. Biol. Chem.* 273, 13957–13965 (1998).

228. Levy, D. E., Kessler, D. S., Pine, R. & Darnell, J. E. Cytoplasmic activation of ISGF3, the positive regulator of interferon-alpha-stimulated transcription, reconstituted in vitro. *Genes Dev.* 3, 1362–1371 (1989).

229. Turner, M. D., Nedjai, B., Hurst, T. & Pennington, D. J. Cytokines and chemokines: At the crossroads of cell signalling and inflammatory disease. *Biochimica et Biophysica Acta - Molecular Cell Research* 1843, 2563–2582 (2014).

230. Berraondo, P. *et al.* Cytokines in clinical cancer immunotherapy. *British Journal of Cancer* 120, 6–15 (2019).

231. Dinarello, C. A., Goldin, N. P. & Wolff, S. M. Demonstration and characterization of two distinct human leukocytic pyrogens. *J. Exp. Med.* 139, 1369–1381 (1974).

232. Dinarello, C. A. Immunological and inflammatory functions of the interleukin-1 family. *Annual Review of Immunology* 27, 519–550 (2009).

233. Dinarello, C. A. Overview of the IL-1 family in innate inflammation and acquired immunity. *Immunological Reviews* 281, 8–27 (2018).

234. O'Neill, L. A. J. The interleukin-1 receptor/Toll-like receptor superfamily: 10 Years of progress. *Immunological Reviews* 226, 10–18 (2008).

235. Carswell, E. A. *et al.* An endotoxin induced serum factor that cuases necrosis of tumors. *Proc. Natl. Acad. Sci. U. S. A.* 72, 3666–3670 (1975).

236. Tracey, D., Klareskog, L., Sasso, E. H., Salfeld, J. G. & Tak, P. P. Tumor necrosis factor antagonist mechanisms of action: A comprehensive review. *Pharmacology and Therapeutics* 117, 244–279 (2008).

237. Stow, J. L., Ching Low, P., Offenhäuser, C. & Sangermani, D. Cytokine secretion in macrophages and other cells: Pathways and mediators. *Immunobiology* 214, 601–612 (2009).

238. Pinci, F. *et al.* C-tag TNF: A reporter system to study TNF shedding. *J. Biol. Chem.* 295, 18065–

18075 (2020).

239.   Rose-John, S., Scheller, J. & Schaper, F. 'Family reunion' - A structured view on the composition of the receptor complexes of interleukin-6-type and interleukin-12-type cytokines. *Cytokine and Growth Factor Reviews* 26, 471–474 (2015).

240.   Cameron, M. J. & Kelvin, D. J. Cytokines, Chemokines and Their Receptors. (2013).

241.   Hirano, T. *et al.* Complementary DNA for a novel human interleukin (BSF-2) that induces B lymphocytes to produce immunoglobulin. *Nature* 324, 73–76 (1986).

242.   Kishimoto, T. IL-6: from its discovery to clinical applications. *Int. Immunol.* 22, 347–352 (2010).

243.   Hurst, S. M. *et al.* IL-6 and its soluble receptor orchestrate a temporal switch in the pattern of leukocyte recruitment seen during acute inflammation. *Immunity* 14, 705–714 (2001).

244.   Kany, S., Vollrath, J. T. & Relja, B. Cytokines in inflammatory disease. *International Journal of Molecular Sciences* 20, (2019).

245.   Heinrich, P. C. *et al.* Principles of interleukin (IL)-6-type cytokine signalling and its regulation. *Biochemical Journal* 374, 1–20 (2003).

246.   Radtke, S. *et al.* Cross-regulation of cytokine signalling: Pro-inflammatory cytokines restrict IL-6 signalling through receptor internalisation and degradation. *J. Cell Sci.* 123, 947–959 (2010).

247.   Bachmann, M. F., Kopf, M. & Marsland, B. J. Opinion: Chemokines: More than just road signs. *Nature Reviews Immunology* 6, 159–164 (2006).

248.   Zlotnik, A. & Yoshie, O. Chemokines: A new classification system and their role in immunity. *Immunity* 12, 121–127 (2000).

249.   Luster, A. D. Chemokines — Chemotactic Cytokines That Mediate Inflammation. *N. Engl. J. Med.* 338, 436–445 (1998).

250.   Levy, D. E., Marié, I. J. & Durbin, J. E. Induction and function of type i and III interferon in response to viral infection. *Current Opinion in Virology* 1, 476–486 (2011).

251.   A, I. & J, L. Virus interference. I. The interferon. *Proc. R. Soc. London. Ser. B - Biol. Sci.* 147, 258–267 (1957).

252.   A, I., J, L. & RC, V. Virus interference. II. Some properties of interferon. *Proc. R. Soc. London. Ser. B - Biol. Sci.* 147, 268–273 (1957).

253.   Stanifer, M. L., Pervolaraki, K. & Boulant, S. Differential regulation of type I and type III interferon signaling. *International Journal of Molecular Sciences* 20, (2019).

254.   Alspach, E., Lussier, D. M. & Schreiber, R. D. Interferon γ and its important roles in promoting and inhibiting spontaneous and therapeutic cancer immunity. *Cold Spring Harb. Perspect. Biol.* 11, a028480 (2019).

255.   Stetson, D. B. *et al.* Constitutive cytokine mRNAs mark natural killer (NK) and NK T cells poised for rapid effector function. *J. Exp. Med.* 198, 1069–1076 (2003).

256.   Mah, A. Y. & Cooper, M. A. Metabolic regulation of natural killer cell IFN-γ production. *Crit. Rev. Immunol.* 36, 131–147 (2016).

257.   Kotenko, S. V. *et al.* IFN-λs mediate antiviral protection through a distinct class II cytokine receptor complex. *Nature Immunology* 4, 69–77 (2003).

258.   Sheppard, P. *et al.* IL-28, IL-29 and their class II cytokine receptor IL-28R. *Nature Immunology* 4, 63–68 (2003).

259.   Prokunina-Olsson, L. *et al.* A variant upstream of IFNL3 (IL28B) creating a new interferon gene IFNL4 is associated with impaired clearance of hepatitis C virus. *Nat. Genet.* 45, 164–171 (2013).

260.   Pott, J. *et al.* IFN-λ determines the intestinal epithelial antiviral host defense. *Proc. Natl. Acad. Sci. U. S. A.* 108, 7944–7949 (2011).

261. Mahlakõiv, T., Hernandez, P., Gronke, K., Diefenbach, A. & Staeheli, P. Leukocyte-Derived IFN-α/β and Epithelial IFN-λ Constitute a Compartmentalized Mucosal Defense System that Restricts Enteric Virus Infections. *PLoS Pathog.* 11, (2015).

262. Odendall, C. & Kagan, J. C. The unique regulation and functions of type III interferons in antiviral immunity. *Current Opinion in Virology* 12, 47–52 (2015).

263. Odendall, C. *et al.* Diverse intracellular pathogens activate type III interferon expression from peroxisomes. *Nat. Immunol.* 15, 717–726 (2014).

264. Thanos, D. & Maniatis, T. Virus induction of human IFNβ gene expression requires the assembly of an enhanceosome. *Cell* 83, 1091–1100 (1995).

265. Panne, D. The enhanceosome. *Current Opinion in Structural Biology* 18, 236–242 (2008).

266. Thomson, S. J. P. *et al.* The role of transposable elements in the regulation of IFN-λ1 gene expression. *Proc. Natl. Acad. Sci. U. S. A.* 106, 11564–11569 (2009).

267. De Weerd, N. A., Samarajiwa, S. A. & Hertzog, P. J. Type I interferon receptors: Biochemistry and biological functions. *Journal of Biological Chemistry* 282, 20053–20057 (2007).

268. De Weerd, N. A. & Nguyen, T. The interferons and their receptors-distribution and regulation. *Immunology and Cell Biology* 90, 483–491 (2012).

269. Barrat, F. J., Crow, M. K. & Ivashkiv, L. B. Interferon target-gene expression and epigenomic signatures in health and disease. *Nature Immunology* 20, 1574–1583 (2019).

270. Ng, C. T., Mendoza, J. L., Garcia, K. C. & Oldstone, M. B. A. Alpha and Beta Type 1 Interferon Signaling: Passage for Diverse Biologic Outcomes. *Cell* 164, 349–352 (2016).

271. McNab, F., Mayer-Barber, K., Sher, A., Wack, A. & O'Garra, A. Type I interferons in infectious disease. *Nature Reviews Immunology* 15, 87–103 (2015).

272. Gough, D. J., Messina, N. L., Clarke, C. J. P., Johnstone, R. W. & Levy, D. E. Constitutive Type I Interferon Modulates Homeostatic Balance through Tonic Signaling. *Immunity* 36, 166–174 (2012).

273. Balachandran, S. & Beg, A. A. Defining Emerging Roles for NF-κB in Antivirus Responses: Revisiting the Interferon-β Enhanceosome Paradigm. *PLoS Pathog.* 7, e1002165 (2011).

274. Hata, N. *et al.* Constitutive IFN-α/β signal for efficient IFN-α/β gene induction by virus. *Biochem. Biophys. Res. Commun.* 285, 518–525 (2001).

275. Lazear, H. M., Schoggins, J. W. & Diamond, M. S. Shared and Distinct Functions of Type I and Type III Interferons. *Immunity* 50, 907–923 (2019).

276. Lindahl, T. Instability and decay of the primary structure of DNA. *Nature* 362, 709–715 (1993).

277. Cadet, J., Berger, M., Douki, T. & Ravanat, J. L. Oxidative damage to DNA: formation, measurement, and biological significance. *Reviews of physiology, biochemistry and pharmacology* 131, 1–87 (1997).

278. De Bont, R. & van Larebeke, N. Endogenous DNA damage in humans: A review of quantitative data. *Mutagenesis* 19, 169–185 (2004).

279. Hoeijmakers, J. H. J. DNA Damage, Aging, and Cancer. *N. Engl. J. Med.* 361, 1475–1485 (2009).

280. Iyama, T. & Wilson, D. M. DNA repair mechanisms in dividing and non-dividing cells. *DNA Repair (Amst.)* 12, 620–636 (2013).

281. Jackson, S. P. & Bartek, J. The DNA-damage response in human biology and disease. *Nature* 461, 1071–1078 (2009).

282. Jackson, S. P. & Bartek, J. The DNA-damage response in human biology and disease. *Nature* 461, 1071–1078 (2009).

283. Dizdaroglu, M., Coskun, E. & Jaruga, P. Repair of oxidatively induced DNA damage by DNA glycosylases: Mechanisms of action, substrate specificities and excision kinetics. *Mutat. Res.*

Mutat. Res. 771, 99–127 (2017).

284. Shibutani, S., Takeshita, M. & Grollman, A. P. Insertion of specific bases during DNA synthesis past the oxidation-damaged base 8-oxodG. *Nature* 349, 431–434 (1991).

285. Brégeon, D. & Doetsch, P. W. Transcriptional mutagenesis: Causes and involvement in tumour development. *Nature Reviews Cancer* 11, 218–227 (2011).

286. Iyama, T., Abolhassani, N., Tsuchimoto, D., Nonaka, M. & Nakabeppu, Y. NUDT16 is a (deoxy)inosine diphosphatase, and its deficiency induces accumulation of single-strand breaks in nuclear DNA and growth arrest. *Nucleic Acids Res.* 38, 4834–4843 (2010).

287. Taghizadeh, K. *et al.* Quantification of DNA damage products resulting from deamination, oxidation and reaction with products of lipid peroxidation by liquid chromatography isotope dilution tandem mass spectrometry. *Nat. Protoc.* 3, 1287–1298 (2008).

288. Wilson, D. M. & Bohr, V. A. The mechanics of base excision repair, and its relationship to aging and disease. *DNA Repair (Amst).* 6, 544–559 (2007).

289. Chatterjee, N. & Walker, G. C. Mechanisms of DNA damage, repair, and mutagenesis. *Environmental and Molecular Mutagenesis* 58, 235–263 (2017).

290. Jacobs, A. L. & Schär, P. DNA glycosylases: In DNA repair and beyond. *Chromosoma* 121, 1–20 (2012).

291. Lord, C. J. & Ashworth, A. The DNA damage response and cancer therapy. *Nature* 481, 287–294 (2012).

292. Li, G. M. Mechanisms and functions of DNA mismatch repair. *Cell Research* 18, 85–98 (2008).

293. Pećina-Šlaus, N., Kafka, A., Salamon, I. & Bukovac, A. Mismatch Repair Pathway, Genome Stability and Cancer. *Frontiers in Molecular Biosciences* 7, 122 (2020).

294. Gillet, L. C. J. & Schärer, O. D. Molecular mechanisms of mammalian global genome nucleotide excision repair. *Chemical Reviews* 106, 253–276 (2006).

295. Fousteri, M. & Mullenders, L. H. F. Transcription-coupled nucleotide excision repair in mammalian cells: Molecular mechanisms and biological effects. *Cell Research* 18, 73–84 (2008).

296. Stingele, J., Bellelli, R. & Boulton, S. J. Mechanisms of DNA-protein crosslink repair. *Nature Reviews Molecular Cell Biology* 18, 563–573 (2017).

297. Wang, J. C. Cellular roles of DNA topoisomerases: A molecular perspective. *Nature Reviews Molecular Cell Biology* 3, 430–440 (2002).

298. Hegde, M. L., Hazra, T. K. & Mitra, S. Early steps in the DNA base excision/single-strand interruption repair pathway in mammalian cells. *Cell Research* 18, 27–47 (2008).

299. Caldecott, K. W. Single-strand break repair and genetic disease. *Nature Reviews Genetics* 9, 619–631 (2008).

300. Caldecott, K. W. DNA single-strand break repair. *Experimental Cell Research* 329, 2–8 (2014).

301. Hossain, M. A., Lin, Y. & Yan, S. Single-strand break end resection in genome integrity: Mechanism and regulation by APE2. *International Journal of Molecular Sciences* 19, (2018).

302. Lord, C. J. & Ashworth, A. The DNA damage response and cancer therapy. *Nature* 481, 287–294 (2012).

303. Nitiss, J. L. DNA topoisomerase II and its growing repertoire of biological functions. *Nature Reviews Cancer* 9, 327–337 (2009).

304. Rothenberg, M. L. Topoisomerase I inhibitors: Review and update. *Annals of Oncology* 8, 837–855 (1997).

305. Nitiss, J. L. Targeting DNA topoisomerase II in cancer chemotherapy. *Nature Reviews Cancer* 9, 338–350 (2009).

306. Soulas-Sprauel, P. *et al.* V(D)J and immunoglobulin class switch recombinations: A paradigm to study the regulation of DNA end-joining. *Oncogene* 26, 7780–7791 (2007).

307. Lam, I. & Keeney, S. Mechanism and regulation of meiotic recombination initiation. *Cold Spring Harb. Perspect. Biol.* 7, (2015).

308. Jinek, M. *et al.* A programmable dual-RNA-guided DNA endonuclease in adaptive bacterial immunity. *Science (80-.).* 337, 816–821 (2012).

309. Cong, L. *et al.* Multiplex genome engineering using CRISPR/Cas systems. *Science (80-.).* 339, 819–823 (2013).

310. Scully, R., Panday, A., Elango, R. & Willis, N. A. DNA double-strand break repair-pathway choice in somatic mammalian cells. *Nature Reviews Molecular Cell Biology* 20, 698–714 (2019).

311. Stracker, T. H. & Petrini, J. H. J. The MRE11 complex: Starting from the ends. *Nature Reviews Molecular Cell Biology* 12, 90–103 (2011).

312. Lavin, M. F. & Kozlov, S. ATM activation and DNA damage response. *Cell Cycle* 6, 931–942 (2007).

313. Maréchal, A. & Zou, L. DNA damage sensing by the ATM and ATR kinases. *Cold Spring Harb. Perspect. Biol.* 5, (2013).

314. Falck, J., Coates, J. & Jackson, S. P. Conserved modes of recruitment of ATM, ATR and DNA-PKcs to sites of DNA damage. *Nature* 434, 605–611 (2005).

315. You, Z., Chahwan, C., Bailis, J., Hunter, T. & Russell, P. ATM Activation and Its Recruitment to Damaged DNA Require Binding to the C Terminus of Nbs1. *Mol. Cell. Biol.* 25, 5363–5379 (2005).

316. Ball, H. L., Myers, J. S. & Cortez, D. ATRIP binding to replication protein A-single-stranded DNA promotes ATR-ATRIP localization but is dispensable for Chk1 phosphorylation. *Mol. Biol. Cell* 16, 2372–2381 (2005).

317. Savic, V. *et al.* Formation of Dynamic γ-H2AX Domains along Broken DNA Strands Is Distinctly Regulated by ATM and MDC1 and Dependent upon H2AX Densities in Chromatin. *Mol. Cell* 34, 298–310 (2009).

318. Holloman, W. K. Unraveling the mechanism of BRCA2 in homologous recombination. *Nature Structural and Molecular Biology* 18, 748–754 (2011).

319. DeFazio, L. G., Stansel, R. M., Griffith, J. D. & Chu, G. Synapsis of DNA ends by DNA-dependent protein kinase. *EMBO J.* 21, 3192–3200 (2002).

320. Ma, Y., Pannicke, U., Schwarz, K. & Lieber, M. R. Hairpin opening and overhang processing by an Artemis/DNA-dependent protein kinase complex in nonhomologous end joining and V(D)J recombination. *Cell* 108, 781–794 (2002).

321. Jeggo, P. & O'Neill, P. The Greek Goddess, Artemis, reveals the secrets of her cleavage. *DNA Repair (Amst.)* 1, 771–777 (2002).

322. Ramadan, K., Shevelev, I. V., Maga, G. & Hübscher, U. De Novo DNA synthesis by human DNA polymerase λ, DNA polymerase μ and terminal deoxyribonucleotidyl transferase. *J. Mol. Biol.* 339, 395–404 (2004).

323. Roberts, S. A. *et al.* Ku is a 5'-dRP/AP lyase that excises nucleotide damage near broken ends. *Nature* 464, 1214–1217 (2010).

324. Grawunder, U. *et al.* Activity of DNA ligase IV stimulated by complex formation with XRCC4 protein in mammalian cells. *Nature* 388, 492–495 (1997).

325. Nakad, R. & Schumacher, B. DNA damage response and immune defense: Links and mechanisms. *Front. Genet.* 7, 1–10 (2016).

326. Pateras, I. S. *et al.* The DNA damage response and immune signaling alliance: Is it good or bad? Nature decides when and where. *Pharmacology and Therapeutics* 154, 36–56 (2015).

327. Takaoka, A. *et al.* Integration of interferon-α/β signalling to p53 responses in tumour suppression and antiviral defence. *Nature* 424, 516–523 (2003).

328. Kim, K. S., Kang, K. W., Seu, Y. B., Baek, S. H. & Kim, J. R. Interferon-γ induces cellular senescence through p53-dependent DNA damage signaling in human endothelial cells. *Mech. Ageing Dev.* 130, 179–188 (2009).

329. Glück, S. *et al.* Innate immune sensing of cytosolic chromatin fragments through cGAS promotes senescence. *Nat. Cell Biol.* 19, 1061–1070 (2017).

330. Dou, Z. *et al.* Cytoplasmic chromatin triggers inflammation in senescence and cancer. *Nature* 550, (2017).

331. MacKenzie, K. J. *et al.* CGAS surveillance of micronuclei links genome instability to innate immunity. *Nature* 548, 461–465 (2017).

332. Harding, S. M. *et al.* Mitotic progression following DNA damage enables pattern recognition within micronuclei. *Nature* 548, 466–470 (2017).

333. Liu, S. *et al.* Nuclear envelope assembly defects link mitotic errors to chromothripsis. *Nature* 561, 551–555 (2018).

334. Hatch, E. M., Fischer, A. H., Deerinck, T. J. & Hetzer, M. W. Catastrophic Nuclear Envelope Collapse in Cancer Cell Micronuclei. *Cell* 154, 47 (2013).

335. Lan, Y. Y., Londoño, D., Bouley, R., Rooney, M. S. & Hacohen, N. Dnase2a deficiency uncovers lysosomal clearance of damaged nuclear DNA via autophagy. *Cell Rep.* 9, 180–192 (2014).

336. Lan, Y. Y. *et al.* Extranuclear DNA accumulates in aged cells and contributes to senescence and inflammation. *Aging Cell* 18, (2019).

337. Ragu, S., Matos-Rodrigues, G. & Lopez, B. S. Replication stress, DNA damage, inflammatory cytokines and innate immune response. *Genes* 11, (2020).

338. Diamond, J. M. *et al.* Exosomes Shuttle TREX1-Sensitive IFN-Stimulatory dsDNA from Irradiated Cancer Cells to DCs. *Cancer Immunol. Res.* 6, 910–920 (2018).

339. Nastasi, C., Mannarino, L. & D'incalci, M. DNA damage response and immune defense. *International Journal of Molecular Sciences* 21, 1–28 (2020).

340. Ferguson, B. J., Mansur, D. S., Peters, N. E., Ren, H. & Smith, G. L. DNA-PK is a DNA sensor for IRF-3-dependent innate immunity. *Elife* 2012, (2012).

341. Zhang, X. *et al.* Cutting Edge: Ku70 Is a Novel Cytosolic DNA Sensor That Induces Type III Rather Than Type I IFN. *J. Immunol.* 186, 4541–4545 (2011).

342. Roth, S. *et al.* Rad50-CARD9 interactions link cytosolic DNA sensing to IL-1β production. *Nat. Immunol.* 15, 538–545 (2014).

343. Miyamoto, S. Nuclear initiated NF-κB signaling: NEMO and ATM take center stage. *Cell Res.* 21, 116–130 (2011).

344. McCool, K. W. & Miyamoto, S. DNA damage-dependent NF-κB activation: NEMO turns nuclear signaling inside out. *Immunol. Rev.* 246, 311–326 (2012).

345. Dunphy, G. *et al.* Non-canonical Activation of the DNA Sensing Adaptor STING by ATM and IFI16 Mediates NF-κB Signaling after Nuclear DNA Damage. *Mol. Cell* 71, 745-760.e5 (2018).

346. Höning, K. Cell autonomous type I interferon induction by DNA damage. (Rheinische Friedrich-Wilhelms-Universtiät Bonn, 2017).

347. Bald, T. *et al.* Ultraviolet-radiation-induced inflammation promotes angiotropism and metastasis in melanoma. *Nature* 507, 109–113 (2014).

348. Gao, D. *et al.* Activation of cyclic GMP-AMP synthase by self-DNA causes autoimmune

diseases. *Proc. Natl. Acad. Sci. U. S. A.* 112, E5699–E5705 (2015).

349. Ciccia, A. & Elledge, S. J. The DNA Damage Response: Making It Safe to Play with Knives. *Molecular Cell* 40, 179–204 (2010).

350. Soriani, A. *et al.* ATM-ATR-dependent up-regulation of DNAM-1 and NKG2D ligands on multiple myeloma cells by therapeutic agents results in enhanced NK-cell susceptibility and is associated with a senescent phenotype. *Blood* 113, 3503–3511 (2009).

351. Gasser, S., Orsulic, S., Brown, E. J. & Raulet, D. H. The DNA damage pathway regulates innate immune system ligands of the NKG2D receptor. *Nature* 436, 1186–1190 (2005).

352. Coppé, J.-P. *et al.* Senescence-Associated Secretory Phenotypes Reveal Cell-Nonautonomous Functions of Oncogenic RAS and the p53 Tumor Suppressor. *PLoS Biol.* 6, e301 (2008).

353. Muñoz-Espín, D. & Serrano, M. Cellular senescence: From physiology to pathology. *Nature Reviews Molecular Cell Biology* 15, 482–496 (2014).

354. Xue, W. *et al.* Senescence and tumour clearance is triggered by p53 restoration in murine liver carcinomas. *Nature* 445, 656–660 (2007).

355. Gaidt, M. M., Rapino, F., Graf, T. & Hornung, V. Modeling primary human monocytes with the trans–differentiation cell line BLaER1. in *Methods in Molecular Biology* 1714, 57–66 (Humana Press Inc., 2018).

356. Rapino, F. *et al.* Article C/EBPa Induces Highly Efficient Macrophage Transdifferentiation of B Lymphoma and Leukemia Cell Lines and Impairs Their Tumorigenicity. *CellReports* 3, 1153–1163 (2013).

357. Rapino, F. *et al.* C/EBPα Induces Highly Efficient Macrophage Transdifferentiation of B Lymphoma and Leukemia Cell Lines and Impairs Their Tumorigenicity. *Cell Rep.* 3, 1153–1163 (2013).

358. Colcher, D., Heberling, R. L., Kalter, S. S. & Schlom, J. *Squirrel Monkey Retrovirus: an Endogenous Virus of a New World Primate*. (1977).

359. Schochetman, G., Fine, D., Arthur, L., Gilden, R. & Heberling, R. *Characterization of a Retravirus Isolated from Squirrel Monkeys. JOURNAL OF VIROLOGY* (1977).

360. Baillie, G. J., van de Lagemaat, L. N., Baust, C. & Mager, D. L. Multiple Groups of Endogenous Betaretroviruses in Mice, Rats, and Other Mammals. *J. Virol.* 78, 5784–5798 (2004).

361. Lerche, N. W. *et al. AIDS RESEARCH AND HUMAN RETROVIRUSES Expanded Search for Human Infection with Simian Type D Retrovirus*. 11, (1995).

362. T. Oda, S. Ikeda, S. Watanabe, M. Hatsushika, K. Akiyama, F. M. Molecular cloning, complete nucleotide sequence, and gene structure of the provirus genome of a retrovirus produced in a human lymphoblastoid cell line. *Virology* 167, 468–476 (1988).

363. Uphoff, C. C., Denkmann, S. A., Steube, K. G. & Drexler, H. G. Detection of EBV, HBV, HCV, HIV-1, HTLV-I and-II, and SMRV in human and other primate cell lines. *J. Biomed. Biotechnol.* 2010, (2010).

364. Middleton, P. G., Miller, S., Ross, J. A., Steel, C. M. & Guy, K. Insertion of SMRV-H viral DNA at the c-myc gene locus of a BL cell line and presence in established cell lines. *Int. J. Cancer* 52, 451–454 (1992).

365. MacDonald, K. M., Benguerfi, S. & Harding, S. M. Alerting the immune system to DNA damage: Micronuclei as mediators. *Essays in Biochemistry* 64, 753–764 (2020).

366. Tsuchiya, S. *et al.* Establishment and characterization of a human acute monocytic leukemia cell line (THP-1). *Int. J. Cancer* 26, 171–176 (1980).

367. Schmidt, T., Schmid-Burgk, J. L. & Hornung, V. Synthesis of an arrayed sgRNA library targeting the human genome. *Sci. Rep.* 5, 14987 (2015).

368. Labun, K. *et al.* CHOPCHOP v3: Expanding the CRISPR web toolbox beyond genome editing. *Nucleic Acids Res.* 47, W171–W174 (2019).

369. Montague, T. G., Cruz, J. M., Gagnon, J. A., Church, G. M. & Valen, E. CHOPCHOP: A CRISPR/Cas9 and TALEN web tool for genome editing. *Nucleic Acids Res.* 42, 401–407 (2014).

370. Labun, K., Montague, T. G., Gagnon, J. A., Thyme, S. B. & Valen, E. CHOPCHOP v2: a web tool for the next generation of CRISPR genome engineering. *Nucleic Acids Res.* 44, W272–W276 (2016).

371. Schmid-Burgk, J. L. *et al.* Rapid hierarchical assembly of medium-size DNA cassettes. *Nucleic Acids Res.* 40, e92 (2012).

372. Fisher, S. *et al.* A scalable, fully automated process for construction of sequence-ready human exome targeted capture libraries. *Genome Biol.* 12, R1 (2011).

373. Pizzato, M. *et al.* A one-step SYBR Green I-based product-enhanced reverse transcriptase assay for the quantitation of retroviruses in cell culture supernatants. *J. Virol. Methods* 156, 1–7 (2009).

374. Schmid-Burgk, J. L. *et al.* OutKnocker: A web tool for rapid and simple genotyping of designer nuclease edited cell lines. *Genome Res.* 24, 1719–1723 (2014).

375. Martínez-Gil, L. *et al.* Identification of Small Molecules with Type I Interferon Inducing Properties by High-Throughput Screening. *PLoS One* 7, e49049 (2012).

376. Härtlova, A. *et al.* DNA Damage Primes the Type I Interferon System via the Cytosolic DNA Sensor STING to Promote Anti-Microbial Innate Immunity. *Immunity* 42, 332–343 (2015).

377. Israël, A., Staudt, L. M., Dea, E. O., Hoffmann, A. & Lawrence, T. The IKK Complex , a Central Regulator of NF-kB Activation. 1–14 (2014). doi:10.1101/cshperspect.a000158

378. Uhlik, M. T. *et al.* Rac-MEKK3-MKK3 scaffolding for p38 MAPK activation during hyperosmotic shock. *Nat. Cell Biol.* 5, 1104–1110 (2003).

379. Drew, B. A., Burow, M. E. & Beckman, B. S. MEK5/ERK5 pathway: The first fifteen years. *Biochimica et Biophysica Acta - Reviews on Cancer* 1825, 37–48 (2012).

380. Takayanagi, H. *et al.* RANKL maintains bone homeostasis through c-fos-dependent induction of interferon-β. *Nature* 416, 744–749 (2002).

381. Fornes, O. *et al.* JASPAR 2020: Update of the open-Access database of transcription factor binding profiles. *Nucleic Acids Res.* 48, D87–D92 (2020).

382. Li, T. *et al.* Phosphorylation and chromatin tethering prevent cGAS activation during mitosis. *Science (80-.).* eabc5386 (2021). doi:10.1126/science.abc5386

383. Burleigh, K. *et al.* Human DNA-PK activates a STING-independent DNA sensing pathway. *Sci. Immunol.* 5, 4219 (2020).

384. Kondo, T. *et al.* DNA damage sensor MRE11 recognizes cytosolic double-stranded DNA and induces type I interferon by regulating STING trafficking. *Proc. Natl. Acad. Sci.* 110, 2969–2974 (2013).

385. You, Z., Chahwan, C., Bailis, J., Hunter, T. & Russell, P. ATM Activation and Its Recruitment to Damaged DNA Require Binding to the C Terminus of Nbs1. *Mol. Cell. Biol.* 25, 5363–5379 (2005).

386. Pamment, J., Ramsay, E., Kelleher, M., Dornan, D. & Ball, K. L. Regulation of the IRF-1 tumour modifier during the response to genotoxic stress involves an ATM-dependent signalling pathway. *Oncogene* 21, 7776–7785 (2002).

387. Mboko, W. P. *et al.* Coordinate Regulation of DNA Damage and Type I Interferon Responses Imposes an Antiviral State That Attenuates Mouse Gammaherpesvirus Type 68 Replication in Primary Macrophages. *J. Virol.* 86, 6899–6912 (2012).

388. Pépin, G. *et al.* Topoisomerase 1 inhibition promotes cyclic GMP-AMP synthase-dependent antiviral responses. *MBio* 8, (2017).

389. Pépin, G. *et al.* Cre-dependent DNA recombination activates a STING-dependent innate immune response. *Nucleic Acids Res.* 44, 5356–5364 (2016).

390. Wu, Z. H. *et al.* ATM- and NEMO-dependent ELKS ubiquitination coordinates TAK1-Mediated IKK activation in response to genotoxic stress. *Mol. Cell* 40, 75–86 (2010).

391. Yang, Y. *et al.* A Cytosolic ATM/NEMO/RIP1 Complex Recruits TAK1 To Mediate the NF- B and p38 Mitogen-Activated Protein Kinase (MAPK)/MAPK-Activated Protein 2 Responses to DNA Damage. *Mol. Cell. Biol.* 31, 2774–2786 (2011).

392. Mansell, A., Brint, E., Gould, J. A., O'Neill, L. A. & Hertzog, P. J. Mal interacts with tumor necrosis factor receptor-associated factor (TRAF)-6 to mediate NF-κB activation by Toll-like receptor (TLR)-2 and TLR4. *J. Biol. Chem.* 279, 37227–37230 (2004).

393. Hinz, M. *et al.* A cytoplasmic ATM-TRAF6-cIAP1 module links nuclear DNA damage signaling to ubiquitin-mediated NF-κB activation. *Mol. Cell* 40, 63–74 (2010).

394. Baretic, D. *et al.* Structures of closed and open conformations of dimeric human ATM. *Sci. Adv.* 3, (2017).

395. Armstrong, S. A., Schultz, C. W., Azimi-Sadjadi, A., Brody, J. R. & Pishvaian, M. J. ATM dysfunction in pancreatic adenocarcinoma and associated therapeutic implications. *Molecular Cancer Therapeutics* 18, 1899–1908 (2019).

396. Kanayama, A. *et al.* TAB2 and TAB3 activate the NF-κB pathway through binding to polyubiquitin chains. *Mol. Cell* 15, 535–548 (2004).

397. Sato, S. *et al.* Essential function for the kinase TAK1 in innate and adaptive immune responses. *Nat. Immunol.* 6, 1087–1095 (2005).

398. Aashaq, S., Batool, A. & Andrabi, K. I. TAK1 mediates convergence of cellular signals for death and survival. *Apoptosis* 24, 3–20 (2019).

399. Wu, C. J., Conze, D. B., Li, T., Srinivasula, S. M. & Ashwell, J. D. NEMO is a sensor of lys 63-linked polyubiquitination and functions in NF-κB activation. *Nat. Cell Biol.* 8, 398–406 (2006).

400. Ea, C. K., Deng, L., Xia, Z. P., Pineda, G. & Chen, Z. J. Activation of IKK by TNFα Requires Site-Specific Ubiquitination of RIP1 and Polyubiquitin Binding by NEMO. *Mol. Cell* 22, 245–257 (2006).

401. Haas, T. L. *et al.* Recruitment of the Linear Ubiquitin Chain Assembly Complex Stabilizes the TNF-R1 Signaling Complex and Is Required for TNF-Mediated Gene Induction. *Mol. Cell* 36, 831–844 (2009).

402. Yu, Q. *et al.* DNA-Damage-Induced Type I Interferon Promotes Senescence and Inhibits Stem Cell Function. *Cell Rep.* 11, 785–797 (2015).

403. Colomer, C. *et al.* IKKα Kinase Regulates the DNA Damage Response and Drives Chemo-resistance in Cancer. *Mol. Cell* 75, 669-682.e5 (2019).

404. Sun, W. *et al.* MEKK3 is required for lysophosphatidic acid-induced NF-κB activation. *Cell. Signal.* 21, 1488–1494 (2009).

405. Sokolova, O., Maubach, G. & Naumann, M. MEKK3 and TAK1 synergize to activate IKK complex in Helicobacter pylori infection. *Biochim. Biophys. Acta - Mol. Cell Res.* 1843, 715–724 (2014).

406. Hirata, Y., Takahashi, M., Morishita, T., Noguchi, T. & Matsuzawa, A. Post-translational modifications of the TAK1-TAB complex. *International Journal of Molecular Sciences* 18, (2017).

407. Reyskens, K. M. S. E. & Arthur, J. S. C. Emerging roles of the mitogen and stress activated kinases MSK1 and MSK2. *Frontiers in Cell and Developmental Biology* 4, 56 (2016).

408. Wiggin, G. R. *et al.* MSK1 and MSK2 Are Required for the Mitogen- and Stress-Induced Phosphorylation of CREB and ATF1 in Fibroblasts. *Mol. Cell. Biol.* 22, 2871–2881 (2002).

409. Watanabe, N., Sakakibara, J., Hovanessian, A. G., Taniguchi, T. & Fujita, T. Activation of IFN-β element by IRF-1 requires a post-translational event in addition to IRF-1 synthesis. *Nucleic Acids Res.* 19, 4421–4428 (1991).

410. Feng, H., Zhang, Y. B., Gui, J. F., Lemon, S. M. & Yamane, D. Interferon regulatory factor 1 (IRF1) and anti-pathogen innate immune responses. *PLoS Pathogens* 17, e1009220 (2021).

411. Ciesielska, A., Matyjek, M. & Kwiatkowska, K. TLR4 and CD14 trafficking and its influence on LPS-induced pro-inflammatory signaling. *Cellular and Molecular Life Sciences* 78, 1233–1261 (2021).

412. Rivankar, S. An overview of doxorubicin formulations in cancer therapy. *J. Cancer Res. Ther.* 10, 853 (2014).

413. Roychoudhury, S., Kumar, A., Bhatkar, D., Nilesh, & & Sharma, K. Molecular avenues in targeted doxorubicin cancer therapy. *Futur. Oncol* 687–700 (2020). doi:10.2217/fon-2019-0458

414. Sistigu, A. *et al.* Cancer cell–autonomous contribution of type I interferon signaling to the efficacy of chemotherapy. *Nat. Med.* 20, 1301–1309 (2014).

415. Emens, L. A. & Middleton, G. The interplay of immunotherapy and chemotherapy: Harnessing potential synergies. *Cancer Immunol. Res.* 3, 436–443 (2015).

416. McFadden, K. & Luftig, M. A. Interplay between DNA tumor viruses and the host DNA damage response. *Curr. Top. Microbiol. Immunol.* 371, 229–257 (2013).

417. Stracker, T. H., Carson, C. T. & Weilzman, M. D. Adenovirus oncoproteins inactivate the Mre11-Rad50-NBs1 DNA repair complex. *Nature* 418, 348–352 (2002).

418. Gaspar, M. & Shenk, T. Human cytomegalovirus inhibits a DNA damage response by mislocalizing checkpoint proteins. *Proc. Natl. Acad. Sci. U. S. A.* 103, 2821–2826 (2006).

419. Zhao, X. *et al.* Ataxia Telangiectasia-Mutated Damage-Signaling Kinase- and Proteasome-Dependent Destruction of Mre11-Rad50-Nbs1 Subunits in Simian Virus 40-Infected Primate Cells. *J. Virol.* 82, 5316–5328 (2008).

420. Xiaofei, E. & Kowalik, T. F. The DNA Damage Response Induced by Infection with Human Cytomegalovirus and Other Viruses. *Viruses* 6, 2155–2185 (2014).

421. Lilley, C. E., Chaurushiya, M. S., Boutell, C., Everett, R. D. & Weitzman, M. D. The Intrinsic Antiviral Defense to Incoming HSV-1 Genomes Includes Specific DNA Repair Proteins and Is Counteracted by the Viral Protein ICP0. *PLoS Pathog.* 7, e1002084 (2011).

422. Luftig, M. A. Viruses and the DNA Damage Response: Activation and Antagonism. *Annu. Rev. Virol.* 1, 605–625 (2014).

423. Okabe, Y. & Medzhitov, R. Tissue biology perspective on macrophages. *Nature Immunology* 17, 9–17 (2016).

424. Wynn, T. A., Chawla, A. & Pollard, J. W. Macrophage biology in development, homeostasis and disease. *Nature* 496, 445–455 (2013).

425. Malaquin, N., Carrier-Leclerc, A., Dessureault, M. & Rodier, F. DDR-mediated crosstalk between DNA-damaged cells and their microenvironment. *Front. Genet.* 5, 12 (2015).

426. Nagasawa, H. & Little, J. B. Induction of Sister Chromatid Exchanges by Extremely Low Doses of α-Particles. *Cancer Res.* 52, (1992).

427. Hagelstrom, R. T. *et al.* DNA-PKcs and ATM influence generation of ionizing radiation-induced bystander signals. *Oncogene* 27, 6761–6769 (2008).

428. Kirolikar, S. *et al.* Prevention of radiation-induced bystander effects by agents that inactivate

cell-free chromatin released from irradiated dying cells. *Cell Death Dis.* 9, 1–16 (2018).

429. Sokolov, M. V. *et al.* Ionizing radiation induces DNA double-strand breaks in bystander primary human fibroblasts. *Oncogene* 24, 7257–7265 (2005).

430. Shao, C., Folkard, M. & Prise, K. M. Role of TGF-B1 and nitric oxide in the bystander response of irradiated glioma cells. *Oncogene* 27, 434–440 (2008).

431. Morgan, W. F. & Sowa, M. B. Non-targeted effects induced by ionizing radiation: Mechanisms and potential impact on radiation induced health effects. *Cancer Letters* 356, 17–21 (2015).

432. Ivanov, V. N. *et al.* Radiation-induced bystander signaling pathways in human fibroblasts: A role for interleukin-33 in the signal transmission. *Cell. Signal.* 22, 1076–1087 (2010).

433. Rodier, F. *et al.* DNA-SCARS: Distinct nuclear structures that sustain damage-induced senescence growth arrest and inflammatory cytokine secretion. *J. Cell Sci.* 124, 68–81 (2011).

434. Chien, Y. *et al.* Control of the senescence-associated secretory phenotype by NF-κB promotes senescence and enhances chemosensitivity. *Genes Dev.* 25, 2125–2136 (2011).

435. Ness, K. K. *et al.* Physiologic frailty as a sign of accelerated aging among adult survivors of childhood cancer: A report from the st jude lifetime cohort study. *J. Clin. Oncol.* 31, 4496–4503 (2013).

436. Cupit-Link, M. C. *et al.* Biology of premature ageing in survivors of cancer. *ESMO Open* 2, (2017).

437. Baruch, K. *et al.* Aging-induced type I interferon response at the choroid plexus negatively affects brain function. *Science (80-.).* 346, 89–93 (2014).

438. Goto, M. Hierarchical deterioration of body systems in Werner's syndrome: Implications for normal ageing. *Mech. Ageing Dev.* 98, 239–254 (1997).

439. White, R. R. & Vijg, J. Do DNA Double-Strand Breaks Drive Aging? *Molecular Cell* 63, 729–738 (2016).

440. Shiloh, Y. & Ziv, Y. The ATM protein kinase: Regulating the cellular response to genotoxic stress, and more. *Nature Reviews Molecular Cell Biology* 14, 197–210 (2013).

441. Doolittle-Hall, J., Cunningham Glasspoole, D., Seaman, W. & Webster-Cyriaque, J. Meta-Analysis of DNA Tumor-Viral Integration Site Selection Indicates a Role for Repeats, Gene Expression and Epigenetics. *Cancers (Basel).* 7, 2217–2235 (2015).

442. ZKBS. *Bericht der Geschäftsstelle der ZKBS zu SMRV*. (2008).

8 List of abbreviations

3BP1	SH3 Domain Binding Protein 1
3p-dsRNA	5'-triphosphate dsRNA
8-oxo-dG	8-Oxo-2'-deoxyguanosine
AAV	adeno-associated virus
AD	activation domain
ADAM17	disintegrin and metalloproteinase 17
AIM2	Absent in melanoma 2
ALRs	AIM2-like receptors
AMP	adenosine monophosphate
AP-1	activator protein-1
APC	antigen-presenting cells
APE1	apurinic/apyrimidinic endonuclease 1
AR	auto-inhibitory region
ASC	apoptosis-associated speck-like protein containing a CARD
ASK1	apoptosis signal-regulating kinase 1
A-T	ataxia-telangiectasia
ATF	activating transcription factor
ATM	ataxia-telangiectasia mutated
ATP	adenosine triphosphate
ATR	ATM- and Rad3-Related
ATRIP	ATR interacting protein
BCA	bicinchoninic acid assay
BCL-10	B cell lymphoma/leukaemia 10
BCR	B-cell receptor
BER	base excision repair
BIR	baculovirus inhibitor of apoptosis protein repeats
BPE	bovine pituitary extract
BRCA2	breast cancer associated gene 2
BSA	bovine serum albumin
CARD9	caspase-recruitment domain protein 9
CD	cluster of differentiation
cDCs	convential dendritic cells
cDNA	complementary DNA
CDNs	cyclic dinucleotides
CETN2	Centrin 2
cGAMP	2'-3'-cyclic GMP-AMP
cGAS	cyclic GMP-AMP synthase
CIITA	class II major histocompatibility complex transactivatior
Cas9	CRISPR associated protein 9

CLRs	C-type lectin receptors
CRD	carbohydrate recognition domain
CRISPR	clustered regularly interspaced palindromic repeats
Ct	threshold cycle
CtBP	C-terminal binding protein
CTD	C-terminal domain
CtIP	CtBP-interacting protein
CTKD	C-terminal kinase domain
CTLD	C-type lectin domain
CXCL10	C-X-C motif chemokine 10
DAMPs	damage-associated molecular patterns
DD	death domain
DDR	DNA damage response
DDX41	DEAD-Box Helicase 41
DHX36	DEAH-Box Helicase 36
DHX9	DExH-Box Helicase 9
DMSO	dimethyl sulfoxide
DNA	deoxyribonucleic acid
DNA2	DNA replication helicase/nuclease 2
DNAM1	DNAX Accessory Molecule-1
DNA-PK	DNA-dependent protein kinase
Doxo	Doxorubicin
DPC	DNA-protein crosslink
DSB	double-strand break
dsDNA	double-stranded DNA
dsRNA	double-stranded RNA
DTT	1,4-dithiothreitol
DUSP1	dual specific protein phosphatase 1
EBV	Epstein Baar virus
EDTA	ethylenediaminetetraacetic acid
EGF	epidermal growth factor
ELISA	enzyme linked immunosorbent assay
ER	endoplasmic reticulum
ERCC1	excision repair 1, endonuclease non-catalytic subunit
ERK1/2	extracellular signal-regulated kinase ½
Exo1	exonuclease 1
FACS	fluorescence-activated cell sorting
FAK	focal adhesion kinase
FAT	FAK focal adhesion targeting
FcRγ	Fc receptor γ-chain

FCS	foetal calf serum
FEN1	flap endonuclease 1
GAS	γ-activated sequence
GMP	guanosine monophosphate
gp130	glycoprotein 130 kDa
gRNA	guide RNA
GSDMD	gasdermin D
GTP	guanosine triphosphate
H2AX	histone H2AX
HEAT	Huntington-elongation factor 3-protein phosphatase 2A-TOR1
HEPES	4-(2-hydroxyethyl)-1-piperazineethanesulfonic acid
HIN	H inversion
HIV1	human immunodeficiency virus 1
HMGB1	high mobility group box 1
HOIL-1	heme-oxidized IRP2 Ub ligase-1
HOIP	HOIL-1-interacting protein
HR	homologous recombination
HT DNA	herring testis DNA
IAD	IRF-association domain
ICE	IL-1-converting enzyme
IFI16	IFN-inducible protein 16
IFIT1	interferon-induced protein with tetratricopeptide repeats 1
IFN	interferon
IFNAR	interferon-α receptor
IFNGR	interferon-γ receptor
IFNLR	interferon-λ receptor
IKK	IκB kinase
IL	interleukin
IL10R	interleukin 10 receptor
IL-1R1	IL-1 family receptors 1
IL-1RAP	IL-1 family receptors accessory protein
iNOS	inducible NO synthase
IR	ionizing radiation
IRAK	Interleukin-1 receptor associated kinase
IRE	IFN regulatory element
IRF	IFN regulatory factor
ISG	interferon stimulated genes
ISGF3	IFN stimulated gene factor 3
ISRE	IFN-stimulated response elements
ITAMs	immunoreceptor tyrosine-based activation motifs

IκB	inhibitor of κB
JAK	Janus family tyrosine kinase
JNK1/2/3	Jun N-terminal kinase 1/2/3
KO	knock-out
LB	lysogenic broth
LGP2	laboratory of genetics and physiology 2
LPS	lipopolysaccharide
LRR	leucine-rich repeat
LTGC	long-tract gene conversion
LUBAC	linear ubiquitin chain assembly complex
MAC	membrane-attack complex
Maf	masculoaponeurotic fibrosarcoma
MALT1	mucosa-associated lymphoid tissue lymphoma translocation protein 1
MAPK	mitogen-activated protein kinase
MKK	MAP2K
MAPKAPK	MAPK-activated protein kinase
mbIL6R	membrane-bound IL-6 receptor
MD-2	myeloid Differentiation factor 2
MDA5	melanoma differentiation-associated gene 5
MDM	monocyte dervied macrophages
MEKK3	MAPK/ERK kinase kinase 3
MHC	major histocompatibility complex
MHL1	MutL homolog 1
MK2/3/5	MAPKAPK2/3/5
MKK	MAPK kinase
MMEJ	microhomology-mediated end joining
MMR	mismatch repair
MNK1/2	MAPK interacting protein kinase 1/2
MOMP	mitochondrial outer membrane permeabilization
MPMV	Mason-Pfizer monkey virus
MRE11	meiotic recombination 11
MRN	MRE11-RAD50-NBS1
mRNA	messenger RNA
MSH2	MutS homolog 2
MSK1/2	mitogen- and stress-activated kinases ½
MHV68	murine gamma herpes virus
MyD88	myeloid differentiation primary response 88
NACHT	nucleotide-binding and oligomerization
NADPH	nicotinamide adenine dinucleotide phosphate
NAIP	NLR family apoptosis inhibitory protein

NBS1	Nijmegen breakage syndrome 1
NER	nucleotide excision repair
NF- κB	nuclear factor κB
NHEJ	non-homologous end joining
NIK	NF-κB-inducing kinase
NK cells	natural killer cells
NKG2D	natural killer group 2 member
NLRs	NOD-like receptors
NLS	nuclear localisation sequence
NO	nitric oxide
NOD	nucleotide oligomerization domain
NP-40	Nonidet P-40
NTKD	N-terminal kinase domain
OAS	oligoadenylate synthase
OLRs	OAS-like second-messenger receptors
PAMPs	pathogen-associated molecular patterns
PARP1/2	poly ADP-ribose-polymerase-1/2
PBS	phosphate buffered saline
pDCs	plasmacytoid dendritic cells
pDNA	plasmid DNA
PI3K	phosphoinositide 3-kinase
PKC	protein kinase C
PNKP	polynucleotide kinase/phosphatase
poly(I:C)	polyinosinic-polycytidylic acid
PRR	pattern recognition receptor
PYD	pyrin domain
RAD	UV excision repair protein
RAD23B	UV excision repair protein Radiation sensitive 23B
RHD	Rel homology domain
RIG-I	retinoic acid-inducible gene I
RIPK1	receptor-interacting serine/threonine-protein kinase 1
RIPK2	receptor-interacting serine/threonine kinase 2
RLRs	RIG-I-like receptors
RNA	ribonucleic acid
ROS	reactive oxygen species
RPA	replication protein A
RSKs	ribosomal s6 kinases
RT	reverse transcriptase
RTEL1	regulator of telomere length 1
SASP	senescence-associated secretory phenotype

SDS	sodium dodecyl sulphate
SDSA	synthesis-dependent strand annealing
SEM	standard error of the mean
sIL6R	soluble IL-6 receptor
SMRV	squirrel monkey retrovirus
SOD	superoxide dismutase
SPRTN	Spartan
SSA	single strand annealing
SSB	single-strand break
ssDNA	single-stranded DNA
ssRNA	single-stranded RNA
STAT	signal transducers and activators of transcription
STING	stimulator of interferon genes
SYK	spleen recruitment tyrosine kinase
TAB	TGF-beta-activated kinase 1 and MAP3K7-binding protein
TADs	transactivation domains
TAE	tris, acetic acid and EDTA
TAK1	transforming growth factor-β-activated kinase 1
TASL	TLR adaptor interacting with SCL15A4 on the lysosome
TBK1	TANK-binding kinase 1
TBS	tris buffered saline
TCR	T-cell receptor
TDPs	tyrosyl-DNA phosphodiesterases
TGFβ	transforming growth factor-β
TIR	Toll/IL-1-receptor
TIRAP	Toll/interleukin-1 receptor domain-containing adapter protein
TLRs	Toll-like receptors
TNF	tumour necrosis factor
TOP	topoisomerase
TPL2	tumour progression locus 2
TRAF6	tumour necrosis factor receptor-associated factor 6
TRAM	translocating chain-associated membrane protein
TRIF	TIR-domain-containing adapter-inducing interferon-β
TYK2	tyrosine kinase 2
U	units
UBC13	ubiquitin-conjugating enzyme 13
UV	ultraviolet
Uve1a	ubiquitin-conjugating enzyme E2 variant 1A
WT	wildtype
XPC	Xeroderma Pigmentosum, complementation group C

XRCC1	X-ray repair cross-complementing protein 1
α-	anti-
μ-	micro-

9 Acknowledgements

10 Appendix

10.1 R script for the detection of viral sequences in FASTQ files

```
library(ShortRead)
#FASTQ files for in1 primer #
in1_primer="CATGTCTTGCCCGTGATCAG"
virus_seq="CATGTCTTGCCCGTGATCAGGTCCTCCATTGGTGGCCCGCCACCACGCCCGGGGCATGCTTTTGG
CGGGGAGGGCTGATGCAACCTTTTGTTCCAATAGCATCAGCTTAGCCTGGGTTCCCAACATCTCCTCCCTTTTTC
TTTAAAAAAAGAGGAGGCGGACCTTAACCAGCTAGGGGAGGTAGAGGCTGTGCTCCTCCTGAGCCTTAATTTT
CAGGCTTACAGGTACCTT"

#for the in2 primer:
#in2_primer="GTTCCCAACATCTCCTCCCT"
#virus_seq="GTACCTGTAAGCCTGAAAATTAAGGCTCAGGAGGAGCACAGCCTCTACCTCCCCTAGCTGGTTA
AGGTCCGCCTCCTCTTTTTTTAAAGAAAAAGGGAGGAGATGTTGGGAAC"

#set location
dirPath=" C:/Users/…/Data/02.Fastq/In1/"
fastqPath=list.files(dirPath, pattern = "_L001_R1_001.fastq", full = TRUE)
fastqPath
#Read in all files together
reads_in1=readFastq(fastqPath)
reads_in1
sread(reads_in1)
#read in 1 or more files at a time #
#only sequences that do not contain full virus sequences #
filter=agrep(virus_seq,sread(reads_in1),max.distance = 0.05)
length(filter)
filter
#kept_reads=reads[-filter]
" No intact viral sequences were found! "

#reads that contain the first three MseI cutting sites
seq="CATGTCTTGCCCGTGATCAGGTCCTCCATTGGTGGCCCGCCACCACGCCCGGGGCATGCTTTTGGCGGG
GAGGGCTGATGCAACCTTTTGTTCCAATAGCATCAGCTTAGCCTGGGTTCCCAACATCTCCTCCCTTTTTCTTTAA
AAAAAGAGGAGGCGGACCTTAACCAGCTAGGGGAGGTAGAGGCTGTGCTCCTCCTGAGCCTTA"
#for the in2 primer
#seq="GTTCCCAACATCTCCTCCCTTTTTCTTTAAAAAAAGAGGAGGCGGACCTTAACCAGCTAGGGGAGGTAG
AGGCTGTGCTCCTCCTGAGCCTTA "

filter=grep(seq,sread(reads_in1))
length(filter)
in1_kept_reads1=reads_in1[filter]
reads_in1=reads_in1[-filter] # remove the found sequences
sread(in1_kept_reads1)
in1_kept_reads1=as.character(sread(in1_kept_reads1))
length(in1_kept_reads1)
in1_kept_reads1=c(paste0("Matched sequence: ",seq),sort(in1_kept_reads1))
write.csv(in1_kept_reads1," C:/Users/…/Data/in1 primer/first_3_MseI_sites.csv")

#reads that contain the first two MseI sites
```

```
seq="CATGTCTTGCCCGTGATCAGGTCCTCCATTGGTGGCCCGCCACCACGCCCGGGGCATGCTTTTGGCGGG
GAGGGCTGATGCAACCTTTTGTTCCAATAGCATCAGCTTAGCCTGGGTTCCCAACATCTCCTCCCTTTTTCTTTAA
AAAAAGAGGAGGCGGACCTTA"
```
#for the in2 primer
```
#seq="GTTCCCAACATCTCCTCCCTTTTTCTTTAAAAAAAGAGGAGGCGGACCTTA"
```

```
filter=grep(seq,sread(reads_in1))
length(filter)
in1_kept_reads2=reads_in1[filter]
reads_in1=reads_in1[-filter] # Remove the found sequences
sread(in1_kept_reads2)
in1_kept_reads2=as.character(sread(in1_kept_reads2))
length(in1_kept_reads2)
in1_kept_reads2=c(paste0("Matched sequence: ",seq),sort(in1_kept_reads2))
write.csv(in1_kept_reads2,"C:/Users/…//Data/in1 primer/first_2_MseI_sites.csv")
```

#reads that contain only the first MseI cutting site
```
seq="CATGTCTTGCCCGTGATCAGGTCCTCCATTGGTGGCCCGCCACCACGCCCGGGGCATGCTTTTGGCGGG
GAGGGCTGATGCAACCTTTTGTTCCAATAGCATCAGCTTAGCCTGGGTTCCCAACATCTCCTCCCTTTTTCTTTA"
```
#for the in2 primer
```
#seq="GTTCCCAACATCTCCTCCCTTTTTCTTTA"
```

```
filter=grep(seq,sread(reads_in1))
length(filter)
in1_kept_reads3=reads_in1[filter]
in1_kept_reads3=as.character(sread(in1_kept_reads3))
length(in1_kept_reads3)
in1_kept_reads3=c(paste0("Matched sequence: ",seq),sort(in1_kept_reads3))
write.csv(in1_kept_reads3,"C:/Users/…//Data/in1 primer/first_1_MseI_sites.csv ")
```

10.2 Clean-up R script for viral sequence removal from obtained reads

```
options(stringsAsFactors = F)
library(tidyverse)
library(gtools)
library(tictoc)
```

```
" In1 primer"
# For in2, in1 files were replaced by in2 files in the code
# Read in the matched sequences
cleaned1=read.csv("C:/Users/…//Data/in1 primer/first_1_MseI_sites.csv ")
tail(cleaned1,3)
```
 # Removing row numbers and the very first element (matched sequence)
```
cleaned1=cleaned1$x[-49956]
tail(cleaned1,3)
```
#A sliding window approach list of sequences to match from this main sequence.
```
rada="GACCATAGTTAGCAACAGCAGTTTTAATTTTTTCTATGGTCTTTAGATTTAGCCGCTTATAGGAATGGGT
GTAGGTAGGCTCGGTGGGCTCTGAGCTTTCCTCCTCCTCATCCTCTGAGTCAGATTCTCCGGAGTCTGCTTCCTC
CTCCTCAGGGATGGTGTGTGTGTCAGGGTGAGGAGACGCTCGGCCCGTGGTATTGGAGCTAACCTGTCCCTGA
CTTCTGGTAACGGGAAAAGCCATAACTCCCGCGGGAGGTAGAAGGGCCAAATCGGACAGTTTTGTGACTAAG
GTTTTAACCCCATCAAGAAGAGAAACAGTCTCATCAATGGGACCGGAGGGTTTGGCTAGGGCTACACCGGGCA
AGTTTGGGGCCGTGGGGGAACCAGGAACGCCTGAAGTAGGGGCATGCAAAACAGGAGCCGCAACTGCCACT
```

GGGGGCACTGCTGTAGAAACATAGGACGGTGGCCGGAAAGGTGGCAATGCCGGGGTGTTAGTTAATTGGGG
CCAATCAGGGTTGTTATATTGGGCAGCTGCCTCTTCCAGATCTGCTTGATCGGCGGGATTTAGTTGATCATCCT
GACTACCCGAGTTATGCAAGGTTTTAGAATTAGCAAGCAAGGGCAAATGTTGGGGCGGAGTATGCGCTCGAG
AATGAGGACTTTGAATGGGGGGGTCCGTAAGGGTTGCAAGGTTGGGGTACAGTGAAGACTGCCCTGTATCAT
CTGAACCAATGTCAATTGCAACCGAGGGGCAGGTAGAAGGGGCCCTAGAGGGAGGGCGAGAGGAGGCCTTT
TCAGAGGTGGTAATTGTTACAGGGGCTTGTCTAGATGGAGGTCGGGAGTGGCTAATAAGAATTTTGTGACCCT
CCTTGCAGAGGCGTTGAATGTCAGGGGAGTCGCTCTGATTAGTAAGGACGTCCCTTATTAAATTATAATAATTA
AAAGTGGTGATCGGAATAGTCTCAGGACCAAAAACACGGTAATAGTCGTTCAGACAATCACCAACACGTCCCC
AAACACGGGAGTCAATAGACCCTTCCTGGGGGAACCATGGACATGTTTTAAAAATGAAACTAAAAAAGGAGA
CAAGGTCTTTCTTGCGAACCCGAATTCTACGCACCTTGAGAGATTCCTTTAACTGACTTATAAAGAGATCATTTT
CACTGTGTGAAGATGCTTGTCCCATGATTGGGTCTTACCTGAGTAATGCCGCCGTCGAAATGAGGAACGAACT
CCAGGAGTCGGCTCGCGGTCGGGTGGTCCGCGGTGCTCCGTGCGGGGAATCGGTTAATCGGGACAGCCGTGC
AGGGAACCGGTTACAGGGGACGGCGGTCCACGGAGGCCGGCATCGAGCCCCACGTCTGGGCGCCACTTGCTC
TGTCCCGCAGAGCAACAAACAGGAACCCGAGCAAGCCTGTCGTGGATGAGAAAGGGATGGGACAAGAGGCG
CGAAGAATGGCAGCAAGACAAAAGTTCTGATCATTCTTTTTTTTCTGATCAAGCTGCAAAGTTTATTTCAAAATG
GGTTCCTTATATAGGGAGGGGAGCGGGTAGAGAGGGGAAAGGGGAAGTAGTTCTGATAGGCTGGGAGACG
AGTGTTTAGCTCATGATCAGCTACCCCATTGGTGCAGCCATGCATGTTCTGTGCGTGATCAGGTCCTTTATTGGT
GGCCCTGAGGCATGTCTTGCCCGTGATCAGGTCCTCCATTGGTGGCCCGCCACCACGCCCGGGGCATGCTTTTG
GCGGGGAGGGCTGATGCAACCTTTTGTTCCAATAGCATCAGCTTAGCCTGGGTTCCCAACATCTCCTCCCTTTTT
CTTTAAAAAAAGAGGAGGCGGACCTTAACCAGCTAGGGGAGGTAGAGGCTGTGCTCCTCCTGAGCCTTAATTT
TCAGGCTTACAGGTACCTTTTTGGGAGGAGAGGATTTTTCGAGTACCAACCTCTATGCAAGCCAGCTTACCTCT
CAGGAGACTCGACAGTAGCCTTAGTAAGGCCTCTCCTTGCAGTGCCTTGCCTTGCACCTAGCGGTGTCCATTAC
CTTCGTAAAGCATAGTGTCGAGCGGTATGCTGCTCCCGTAGGAGGGGAACCGGCTACAGTCTGCCATATTCTA
GATCACGCGTTGCTAGTTGGTGATAGTGGATTTGTATGGGCTTTCCCAGTAGGGAATTGAGCTGATCCCTGATT
AACGCTGTTACTCGTTTTAGGATCCAAGGGGCAAAAGAGAAGAACAGGATGATAGCGAATAAGGGTCCAAGG
AAGGGGAGGAGGTAAGGGAGAAGTCCATTGAGGCCGGTGAGGAAGGGATTGTCTGCAAGTGCCTTGCGTCT
TTGTTCGAGGTCTTCTTGTAGATTTTTTATTTTATCTCGGACAATTCCTGACTTGTTGGCATAAAAGCAGCAACG
TTCCTGTAGAGCCAAACAGATACCTCCCTGTTCTGCAGTGAGTAGGTCTAAGCCTCTTCTGTTTTGGAGGACTA
CTTCGGCTAGGGAATCTAGTTGGTCCTGTAAGTCATTAATGGTGCTAGACAAGGCTTGGACGTCGTTAATAAGT
TGATGGGAAAGTTTTGTGTAAGATTGAACAGCCACCCCGAGTCCTGCTGTACCGGTAGCGACTGCTGTAGAGA
CACCCAATCCTACTAGCAGGGGAATCAGTGTAACGGCTCGTTTCTGCCGCCCTGCAATATAGTCAAAGGTAGG
TATAGGGACAGGGTCATCACCAGAAATAATGTCTATATCTGGCAGGAGGGCGGCTAACACACATGACCCTGTC
CAGTTTGCAGGCAGAGCAGTAAA"

#Generation of a custom function
windows=function (data, window, step)
#Data is a string, window is integer (how many characters long is the window) and step is the distance between each window
{
  window=window-1
  total <- nchar(data)
  spots <- seq(from = 1, to = (total - window), by = step)
  result <- vector(length = length(spots))
  for (i in 1:length(spots)) {
    result[i] <- substr(data,spots[i],(spots[i]+window))
  }
  return(result)
}
# Outputs a vector of sequences 20 letters long after every 10 letters
list_of_sequences=windows(rada,20,10)
list_of_sequences
window_size=nchar(list_of_sequences[1])
results=""

```
#tictoc to measure the time it runs
tic()
for (i in seq_along(cleaned1)) {
 text=cleaned1[i]
 for (j in list_of_sequences) {
   match=aregexec(j,text,max.distance = 0.01)
   match=as.numeric(match[[1]][1])
     if (match>0) {
       substr(text,match,(match+window_size))=paste0(rep("X",window_size),collapse = "")}
  }
 results[i]=text
 }
toc()

Results_in1=results
Results_in1a=Results_in1
Results_in1b=Results_in1
#now substituting the Xs with placeholders
Results_in1a=gsub(pattern="XXXXXXXXXXXXXXXXXXXX",replacement="_",Results_in1a)# 20 xs
Results_in1a=gsub(pattern="XXXXXXXXXXXXXXXXXXX",replacement="_",Results_in1a)# 19 xs
Results_in1a=gsub(pattern="XXXXXXXXXXXXXXXXXX",replacement="_",Results_in1a)# 18 xs
#check if any Xs are left
Results_in1a[grep(pattern="X",Results_in1a)]
Results_in1a
res_df=as.data.frame(Results_in1a)
#breaking all the reads apart now from where the placeholders were.
long_df=res_df %>% separate(Results_in1a, c("a", "b", "c" ,"d","e","f","g","h","i","j"))
dim(long_df)
#putting all the columns into one long column
long_df2=data.frame(a=unlist(long_df, use.names = FALSE))
dim(long_df2)
#Removal of all the reads that are shorter than 10 bases
long_df2=long_df2[nchar(long_df2$a)>10,]
long_df2=long_df2[!is.na(long_df2)]
length(long_df2)
max(nchar(long_df2))
#table(nchar(results2))
#results2
#making a fasta file from these reads
res_in1=as.data.frame(long_df2)
head(res_in1)
res_in1$V1=paste0(">",rownames(res_in1),"_",res_in1$long_df2)
head(res_in1)
res_in1=res_in1[-1]
head(res_in1)
write.csv(res_in1,"C:/Users/…/Data/in1 primer/after_cleanup_separated.csv")
## Shortening reads if needed
over100=long_df2[nchar(long_df2)>100]
under100=long_df2[nchar(long_df2)<100]
length(over100)
halved=""
for (i in over100) {
```

```
   halved=c(halved,substring(i, c(1, 90), c(91, 200)))
}
halved=halved[-1]
length(halved)
nchar(halved)
shortened=c(under100,halved)
short_in1=as.data.frame(shortened)
head(short_in1)
short_in1$V1=paste0(">",rownames(short_in1),"_",short_in1$shortened)
head(short_in1)
short_in1=short_in1[-1]
head(short_in1)
write.csv(short_in1,"C:/Users/…/Data/in1 primer/after_cleanup_separated_shortened.csv")

together_short=rbind(short_in1,short_in2)
head(together_short)
together_short$V1=paste0(">",rownames(together_short),"_",together_short$shortened)
head(together_short)
together_short=together_short[-1]
head(together_short)
dim(together_short)
tail(together_short)
write.csv(together_short,"/C:/Users/…/Data/in_both/after_cleanup_separated_shortened_together.
csv")


# Generation of a sam table
#user_sam=read.table,("C:/Users/…/Data/results/Fuzzy
matches/together_reads_mapped_bowtie.sam",header = T)
user_sam=read.csv("C:/Users/…/Data/in1 primer/in1.sam.csv",header = T)
#user_sam=read.csv ("C:/Users/…/Data/in2 primer/in2.sam.csv", header = T)
head(user_sam)
tail(user_sam)
#
colnames(user_sam)=c("QNAME","FLAG","RNAME","POS","MAPQ","CIGAR","MRNM","MPOS","ISIZE
","SEQ","QUAL","OPT1","OPT2","OPT3")
# table(user_sam$QNAME)
table(user_sam$FLAG) # 0 is mapped to FWD, 16 is mapped to REV and 4 is unmapped
# Keep only mapped
user_sam=user_sam[user_sam$FLAG!=4,]
#1 table(user_sam$QNAME)
#2 table(user_sam$FLAG)
table(user_sam$RNAME)
table(user_sam$POS)
table(user_sam$RNAME)
#5 table(user_sam$MAPQ)
#6 table(user_sam$CIGAR)
#7 table(user_sam$MRNM)
# table(user_sam$MPOS)
#9 table(user_sam$ISIZE)
table(user_sam$SEQ)
#11 table(user_sam$QUAL)
```

```
table(user_sam$OPT)

colnames(user_sam)
head(user_sam,3)
user_sam=user_sam[-c(1,2,5,6,7,8,9,11,12,13,14)]
# NEW TABLE
user_sam=user_sam[order(user_sam$POS),]
head(user_sam)
new_table=data.frame(pos=as.numeric(names(table(user_sam$POS))),Hits=as.numeric(table(user_sa
m$POS)))
unique(user_sam$POS)
identical(as.numeric(unique(user_sam$POS)),new_table$pos)

user_sam$RNAME
uniik=user_sam[!duplicated(user_sam$POS),]
head(uniik)
rownames(uniik)=NULL
uniik=as.data.frame(cbind(uniik$RNAME,uniik$POS,new_table$Hits,uniik$SEQ))
colnames(uniik)=c("Chr_name","Chr_pos","Num_hits","Seq")
uniik=uniik[mixedorder(uniik$Chr_name),]
head(uniik,3)
dim(uniik)
uniik=uniik[nchar(uniik$Seq)>15,]
dim(uniik)
uniik$Num_hits=as.numeric(uniik$Num_hits)
uniik=uniik[uniik$Num_hits>10,]
dim(uniik)
uniik=uniik[uniik$Num_hits>100,]
uniik=uniik[uniik$Num_hits>1000,]

write.csv(table(user_sam$RNAME),"C:/Users/…/Data in1 primer/in1_chromosome_table.csv")
write.csv(uniik,"C:/Users/…/Data /in1 primer/in1_hits_table.csv")
```

10.3 R script for circos plot generation

Data obtained from the clean-up R script was mapped using one of the following tools:
Bowtie: http://bowtie-bio.sourceforge.net/index.shtml (1.2.3 - 07/05/2019)
STAR: https://github.com/alexdobin/STAR (2.7.8a_2021-03-08)

```
options(stringsAsFactors = F)
library("ggrepel")
library("tidyr")
library("RCircos")
library("ggplot2")
library("dplyr")
library("gtools")
library("RColorBrewer")
library("cowplot")
library("BioCircos")

" Bowtie mapped file"
```

```
# in1=read.csv("C:/Users/Second Plotting/in1_after_ cleanup.csv")
" Star mapped file"
in1=read.delim("C:/Users/Data/05.Mapped SAM files/after_star_in1_cleaned-up.csv")
head(in1)
in1$Length=nchar(in1$Seq)
# First plot
new_data=as.data.frame(table(in1$Seq))
head(new_data)
new_data$Var1=as.character(new_data$Var1)
new_data$Length=nchar(new_data$Var1)
head(new_data)
summary(new_data$Length)
new_data[which.max(new_data$Freq),]
#Barplot(log10(new_data$Freq)) # Simple base barplot
new_data=new_data[order(new_data$Length,decreasing = T),]
new_data$order=1:nrow(new_data)
new_data$order=factor(new_data$order,levels = 1:nrow(new_data))
colodata=data.frame(num=unique(new_data$Length)[1:5],colo=as.character(unique(new_data$Length)[1:5]))
new_data$color=NA
new_data$color=colodata[match(new_data$Length,colodata$num),"colo"]
in1p=ggplot(new_data,aes(x=order,y=log10(Freq),color=Length))+geom_bar(stat =
"identity")+theme_classic()+theme(axis.text.x=element_blank())+ggtitle("In1 primer")+xlab("Size")

#RCIRCOS

# Reading in data, same for in2 primer
"Mapped with bowtie"
# in1=read.csv("C:/Users/…/data/Second Plotting/in1_after_bowtie_and_cleanup.csv")
#########################
"Mapped with STAR"
in1=read.delim("C:/Users/…/data /05.Mapped SAM files/after_Star_in1_cleaned-up.csv")
in1$Chr=paste0("chr",in1$Chr)
table(in1$Chr)  #how many times each chromosome was found
in1$toto=paste0(in1$Chr,"_",in1$Pos)
new_in1=as.data.frame(table(in1$toto)) #Count the identical sequences (based on chromosome and
location, so if the same number comes up twice it gets freq=2, e.g. chr1_100000)
new_in1=new_in1 %>% separate(Var1, c("Chr", "Pos"))
head(new_in1)
#get rid of low counts
new_in1=new_in1[new_in1$Freq>10,]
summary(new_in1$Freq)
#take away everything lower than 3rd quantile
new_in1=new_in1[new_in1$Freq>67,]
#
#run this line if you use bowtie mapped files instead
# new_in1=new_in1[new_in1$Freq>7,]
#

new_in1$Pos=as.numeric(new_in1$Pos)
new_in1$chromStart=new_in1$Pos
new_in1$chromEnd=new_in1$Pos+1000
```

```
new_in1$Data=log2(new_in1$Freq)
new_in1$Chromosome=new_in1$Chr
head(new_in1)
```

```
in1_histo=new_in1[,c(7,4,5,6)] # either re-organise columns or just keep the ones you actually need
for plotting
#remove mitochondrial chromosome
in1_histo=in1_histo[in1_histo$Chromosome!="chrMT",]
table(in1_histo$Chromosome) # How many times each chromosome comes up but this time same
location is only counted once and "data" column gives the bar the height or how many times this one
specific sequence came up
rownames(in1_histo)=NULL
head(in1_histo)
```

```
data(UCSC.HG19.Human.CytoBandIdeogram) # Load the ideograms - giemsa stain
head(UCSC.HG19.Human.CytoBandIdeogram)
```

To remove individually values too large (UCSC, where the cytobands are from uses slightly different
numbers than ensemble, which was used for both Bowtie and STAR)

```
max18=max(UCSC.HG19.Human.CytoBandIdeogram$ChromEnd[UCSC.HG19.Human.CytoBandIdeogr
am$Chromosome=="chr18"])
```

```
in1_histo$chromEnd[in1_histo$Chromosome=="chr18"][in1_histo$chromEnd[in1_histo$Chromosom
e=="chr18"]>max18]=max18
```

```
in1_histo$chromStart[in1_histo$Chromosome=="chr18"][in1_histo$chromStart[in1_histo$Chromoso
me=="chr18"]>max18]=(max18-1000)
```

```
UCSC.HG19.Human.CytoBandIdeogram$Chromosome=as.character(UCSC.HG19.Human.CytoBandIde
ogram$Chromosome)
# nimed=unique(in1_histo$Chromosome)
# for (i in seq_along(nimed)) {
#filter=in1_histo$chromEnd[in1_histo$Chromosome==nimed[i]]>max(UCSC.HG19.Human.CytoBandI
#deogram$ChromEnd[UCSC.HG19.Human.CytoBandIdeogram$Chromosome==nimed[i]])
#   if (sum(filter)>0) {
#in1_histo$chromEnd[in1_histo$Chromosome==nimed[i]][filter]=max(UCSC.HG19.Human.CytoBandI
deogram$ChromEnd[UCSC.HG19.Human.CytoBandIdeogram$Chromosome==nimed[i]])
#   }}
```

Now the actual circos plotting starts

```
chr.exclude <- NULL # Which chromosomes to exclude
cyto.info <- UCSC.HG19.Human.CytoBandIdeogram # Any ideograms?
tracks.inside <- 1 # How many tracks inside
tracks.outside <- 0 # How many tracks outside
RCircos.Set.Core.Components(cyto.info, chr.exclude, tracks.inside, tracks.outside) # initializes circos
```

```
out.file <- "C:/Users/…/RCircos_in1_star.pdf" # filename where to write
pdf(file=out.file, height=8, width=8, compress=TRUE) # type and size
RCircos.Set.Plot.Area() # start a new image, if you run it in between then each "circle/track" will be
on their own page
```

```
data.col <- 4 # how many data columns in histogram file
track.num <- 1 # where to plot it
side <- "in" # in or out?
RCircos.Histogram.Plot(in1_histo,data.col, track.num, side) # actual histogram plotting
RCircos.Chromosome.Ideogram.Plot() # ideogram plotting
dev.off() # finish writing

#Plot both histograms but onto different tracks (for in1 and in1)

chr.exclude <- NULL
cyto.info <- UCSC.HG19.Human.CytoBandIdeogram
tracks.inside <- 2
tracks.outside <- 0
RCircos.Set.Core.Components(cyto.info, chr.exclude, tracks.inside, tracks.outside)

out.file <- "C:/Users/data/…/RCircos_in_both.pdf"
pdf(file=out.file, height=8, width=8, compress=TRUE)

RCircos.Set.Plot.Area()
data.col <- 4
track.num <- 1
side <- "in"
RCircos.Histogram.Plot(in1_histo,data.col, track.num, side)
data.col <- 4
track.num <- 2
side <- "in"
RCircos.Histogram.Plot(in1_histo,data.col, track.num, side)
RCircos.Chromosome.Ideogram.Plot()
dev.off()
```